2021-12-14

Death-associated Protein Kinase 3 (DAPK3), Identified as a Potential Key Factor for the Progression of Ulcerative Colitis (UC), Regulates Intestinal Epithelial Repair

Chen, Tina Huey-Miin

UNIVERSITY OF CALGARY

Death-associated Protein Kinase 3 (DAPK3), Identified as a Potential Key Factor for the Progression of Ulcerative Colitis (UC), Regulates Intestinal Epithelial Repair

by

Tina Huey-Miin Chen

A THESIS

SUBMITTED TO THE FACULTY OF GRADUATE STUDIES

IN PARTIAL FULFILMENT OF THE REQUIREMENTS FOR THE

DEGREE OF DOCTOR OF PHILOSOPHY

GRADUATE PROGRAM IN BIOCHEMISTRY AND MOLECULAR BIOLOGY

CALGARY, ALBERTA

DECEMBER, 2021

Abstract

Ulcerative colitis (UC) is a progressive disorder that elevates the risk of cancer development through a colitis-dysplasia-carcinoma sequence. Recent evidence demonstrates the necessity of Yes-associated protein (YAP) signaling, interceded by cytoskeletal remodeling, for intestinal regeneration. Death-associated protein kinase 3 (DAPK3) is a regulator of actin-cytoskeleton reorganization that controls proliferation and apoptosis. In this thesis, *DAPK3* was identified as a candidate gene involved in UC progression. Gene ontology (GO) enrichment analysis revealed a shift in transcriptome landscape as UC progressed from left-sided colitis to pancolitis to colitis-associated dysplasia (CAD), from being immune-centric to being cytoskeleton-dependent. Molecular interaction network analysis of genes differentially expressed in left-sided colitis, pancolitis, and CAD revealed one pairwise line or *edge* that was topologically important to the network structure. This edge was found to be highly enriched in actin-based processes, and DAPK3 was the sole protein kinase associated with this edge. Pharmacological inhibition of DAPK3 in Caco-2 human intestinal epithelial cells (IECs) with the HS38 compound augmented cell proliferation to enhance wound closure. This phenotype corresponded with the increased colocalization of YAP with F-actin, which is indicative of YAP activation. In mice recovering from dextran sodium sulfate (DSS-) induced UC, pharmacological inhibition of DAPK3 increased YAP nuclear localization in IECs, another indicator of YAP activation. However, IEC proliferation was repressed, and mice exhibited increased disease severity when DAPK3 was inhibited with the HS38 compound. It is yet unclear if the incongruous phenotype between the cell and animal studies was the consequence of DAPK3 function on other cell types (e.g., macrophages). In summary, this thesis established DAPK3 as a key factor in intestinal epithelial regeneration and UC progression

by way of YAP signaling. Nevertheless, the role that DAPK3 play in different cell types will need further investigation to decipher the full consequence of DAPK3 inhibition on UC progression.

Preface

This thesis is original, unpublished, independent work by the author, H.-M. Chen. The mice experiments reported in **Chapter 4** were covered by the University of Calgary Animal Care Committee Protocol #AC16-0046 (4-May-2016), entitled "Examining novel molecular contributors to immune regulation in murine models of colitis". Human samples for the quantitative real-time polymerase chain reaction experiments reported in **Chapter 4** were obtained through the Intestinal Inflammation Tissue Bank and were covered by Protocol #18142, Ethics #REB14-2430, which was issued by the University of Calgary Conjoint Health Ethic Board for the project "Changes in barrier function and apoptotic pathways associated with intestinal inflammation" (7-May-2007).

Portions of this thesis have been presented at conferences. Results shown under **Section 3.3.1** and **Section 4.3.2** were presented as a poster at The Gastrointestinal Tract XVIII Conference: Integrated Biology of the GI Super-Organ (July 2019). Results shown under **Sections 2.3.3, 2.3.4, 2.3.5, 2.3.6** and **Sections 4.3.1, 4.3.2, 4.3.3** were presented as an e-poster at the Crohn's and Colitis Congress 2021 (January 2021), and were published in abstract form in Gastroenterology (https://doi.org/10.1053/j.gastro.2021.01.133), as well as in Inflammatory Bowel Diseases (https://doi.org/10.1093/ibd/izaa347.087). **Figure 1** was modified from Figure 1A in Yu et al. (2012). **Table 3** was created with data extracted from Figure 2A in Carlson et al. (2018).

The research work was guided by my supervisor, Dr. Justin MacDonald. Microscope image acquisition was supported by the Snyder Institute Live Cell Imaging Resource Laboratory. Tissue processing for histology was supported by the Libin Cardiovascular Institute Core Pathology Laboratory.

Acknowledgement

I would first like to thank my supervisor Dr. Justin MacDonald for the opportunities, insightful suggestions, and stable working environment that he has provided me. I would also like to thank my supervisor committee members, Dr. Robin Yates and Dr. Humberto Jijon for their guidance and advice over the course of my graduate studies. Special thank you to Mona Chappellaz for her technical support.

I would like to acknowledge the Cumming School of Medicine (CSM) for funding my CSM Graduate Scholarship. I am also grateful to the Canadian Institutes of Health Research (CIHR) for the Graduate Scholarship Master's award and to the Government of Alberta/University of Calgary for the Alberta Graduate Excellence Scholarship and for the Queen Elizabeth II Graduate Scholarship.

Finally, I would like to express the deepest gratitude to my husband, Stef, who has been continually supportive of my education. You have been patient with me when I am unable to put into words my frustrations, and you celebrated with me on the tiniest victories. I am lucky to have you in my life.

Peer Reviewed Publications

Chen, H.-M., & MacDonald, J. A. (2021). Network analysis identifies DAPK3 as a potential biomarker for lymphatic invasion and colon adenocarcinoma prognosis. iScience, 24(8), 102831. https://doi.org/10.1016/J.ISCI.2021.102831

Platnich, J., Chung, H., Lau, A., Sandall, C., Bondzi-Simpson, A., **Chen, H.-M.**, Komada, T., Trotman-Grant, A., Brandelli, J., Chun, J., Beck, P. L., Philpott, D. J., Girardin, S., Ho, M., Johnson, R., MacDonald, J. A., Armstrong, G., & Muruve, D. (2018). Shiga Toxin/Lipopolysaccharide Activates Caspase-4 and Gasdermin D to Trigger Mitochondrial Reactive Oxygen Species Upstream of the NLRP3 Inflammasome. Cell Reports, 25(6), 1525-1536.e7. https://doi.org/10.1016/J.CELREP.2018.09.071

Chappellaz, M., Segboer, H., Ulke-Lemée, A., Sutherland, C., **Chen, H.-M.**, & MacDonald, J. A. (2018). Quantitation of myosin regulatory light chain phosphorylation in biological samples with multiple reaction monitoring mass spectrometry. Biochimica et Biophysica Acta. Proteins and Proteomics, 1866(5–6), 608–616. https://doi.org/10.1016/J.BBAPAP.2018.03.008

Published Abstracts

Chen, H.-M., & MacDonald, J. A. (2021). Inhibition of DAPK3, pinpointed as a key factor in the development of colitis-associated dysplasia, increases severity of DSS-induced colitis via Hippo signaling. Gastroenterology, 160(3), S48–S49. https://doi.org/10.1053/j.gastro.2021.01.133

Chen, H.-M., & MacDonald, J. A. (2021). Inhibition of DAPK3, pinpointed as a key factor in the development of colitis-associated dysplasia, increases severity of DSS-induced colitis via Hippo signaling. Inflammatory Bowel Diseases, 27(1), S36. https://doi.org/10.1093/ibd/izaa347.087

Preprint Server (non-peer reviewed) Publications

Chen, H.-M., Carlson, D.A., Haystead, T.A.J., MacDonald, J.A. (2021). Death-associated protein kinase 3 (DAPK3) contributes to intestinal epithelial wound healing and the resolution of experimental colitis in mice. 2021, Repository: bioRxiv. https://doi.org/10.1101/2021.12.03.471118

Chen, H.-M., MacDonald, J.A. (2021). Molecular network analyses implicate death-associated protein kinase 3 (DAPK3) as a key factor in colitis-associated dysplasia progression. 2021, Repository: medRxiv. https://doi.org/10.1101/2021.09.21.21263916

Chen, H.-M., MacDonald, J.A. (2021). Network analysis identifies DAPK3 as a potential biomarker for lymphovascular invasion and prognosis of colon adenocarcinoma. 2021, Repository: medRxiv. https://doi.org/10.1101/2021.02.03.21251102

Table of Contents

List of Tables

List of Figures

List of Abbreviations

aa	Amino acid
ABP	Actin binding protein
AJ	Adherens junctions
ANCA	Anti-neutrophil cytoplasmic antibodies
ANKRD1	Ankyrin repeat domain 1
ANOVA	Analysis of variance
AOM	Azoxymethane
APC/C	Anaphase promoting complex/cyclosome
AR	Androgen receptor
ARHGAP29	Rho GTPase Activating Protein 29
ATF4	Activating transcription factor 4
ATG	Autophagy-related
BP	Biological process
BSA	Bovine serum albumin
CAC	Colitis-associated colorectal cancer
CAD	Colitis-associated dysplasia
CaM	Calmodulin
CD	Crohn's disease
CDC14A	Cell-division cycle 14A
CDK	Cyclin-dependent kinase
CHOP	CCAAT-enhancer-binding protein homologous protein
Clu	Clusterin
CPI-17	C-kinase potentiated protein phosphatase-1 inhibitor
CRC	Sporadic colorectal cancer
CTGF	Connective tissue growth factor
CYR61	Cysteine-rich angiogenic inducer 61
DAI	Disease activity index
DAPI	4’,6-diamidino-2-phenylindole
DAPK	Death-associated protein kinase
DEG	Differentially expressed gene
DMEM	Dulbecco’s Modified Eagle Medium
DMSO	Dimethyl sulfoxide
DSS	Dextran sodium sulfate
ECM	Extracellular matrix
EDTA	Ethylenediaminetetraacetic acid
EdU	5-Ethynyl-2’-deoxyuridine
ELC	Essential light chain
Eph	Ephrin receptors
ER	Endoplasmic reticulum
FAK	Focal adhesion kinase
FBS	Fetal bovine serum
FDR	False discovery rate

GEO	Gene Expression Omnibus
GFP	Green fluorescent protein
GO	Gene ontology
GPCR	G protein-coupled receptor
H&E	Hematoxylin and eosin
HC	Healthy control
HLA	Human leukocyte antigen
IBD	Inflammatory bowel disease
IDT	Integrated DNA Technologies
IEC	Intestinal epithelial cell
IFN	Interferon
IHC	Immunohistochemistry
IKB	Ingenuity Knowledge Base
IL	Interleukin
ILK	Integrin-linked protein kinase
IPA	Ingenuity Pathway Analysis
ISC	Intestinal stem cells
KIBRA	Kidney- and brain-expressed protein
LATS	Large tumor suppressor kinase
LIMK	LIM domain kinase
LINC	Linker of nucleoskeleton and cytoskeleton
LMO7	LIM domain only 7
LPS	Lipopolysaccharide
LZ	Leucine-zipper
MAPK	Mitogen-activated protein kinase
MAPKAPK	MAPK-activated protein kinase
MDM2	Murine double minute 2
MLCK	Myosin light chain kinase
MLCP	Myosin light chain phosphatase
MOB1	Mps one binder 1
MST	Mammalian Ste20-like kinase
MUC2	Mucin-2
MYPT1	Myosin phosphatase target subunit 1
NFκB	Nuclear factor kappa-light-chain-enhancer of activated B cells
NLK	Nemo-like kinase
NLS	Nuclear localization signal
NM-II	Non-muscle myosin II
OR	Odds ratio
PAGE	Polyacrylamide gel electrophoresis
PAK	p21-activated protein kinase
PBS	Phosphate-buffered saline
PBST	PBS containing Tween-20
PCA	Primary component analysis
PFA	Paraformaldehyde
PIM3	Proviral integration of Moloney virus 3

PML	Promyelocytic leukemia
POD	PML oncogenic domain
PPP1CB	Protein phosphatase PP1-β catalytic subunit
qRT-PCR	Quantitative real-time reverse transcription polymerase chain reaction
RLC	Regulatory light chain
ROCK	Rho-associated coiled-coil containing protein kinase
RT	Room temperature
RTK	Receptor tyrosine kinase
SAV1	Salvador 1
SCFA	Short-chain fatty acid
SDS	Sodium dodecyl sulfate
siRNA	Silencing RNA
STAT	Signal transducer and activator of transcription
STING	Stimulator of interferon genes
TA	Transit amplifying
TAZ	Transcriptional co-activator with PDZ-binding motif
TBST	Tris-buffered saline containing Tween-20
TCF4	Transcription factor 4
TGF	Transforming growth factor
Th	T helper
TJ	Tight junctions
TLR	Toll-like receptor
TM	Tunicamycin
TNF	Tumor necrosis factor
UC	Ulcerative colitis
ULK1	Unc-51 like autophagy activating kinase
VSMC	Vascular smooth muscle cells
WASP	Wiskott-Aldrich syndrome protein
WAVE	WASP-family verprolin-homologous protein
WGCNA	Weighted gene co-expression analysis
Wnt	Wingless-related integration site
YAP	Yes-associated protein
ZIPK	Zipper-interacting protein kinase
β-TrCP	β-transducin repeat-containing protein

Chapter 1 . Introduction

1.1. Ulcerative Colitis (UC).

Ulcerative colitis (UC) is a chronic, inflammatory bowel disease (IBD) that is confined to the mucosal layer of the large bowel, most commonly the rectum, and may extend proximally in a continuous fashion. This is a heterogeneous and progressive disorder that has seen a substantial increase in global prevalence. A 2017 review of population-based studies shows that the highest prevalence of UC was observed in Europe and North America: 505 per 100,000 in southeast Norway and 286 per 100,000 in Olmsted County, USA (S. C. Ng et al., 2017). In Canada, the prevalence of UC is high and continues to rise. In 2012, the number of Canadians estimated to be afflicted with UC was 104,000 (Rocchi et al., 2012); This number rose to 120,000 as of 2018, with predicted prevalence of 0.41% by 2030 (Coward et al., 2019). Importantly, the incidence of UC has been growing globally with increases observed mainly in newly industrialized countries. Of note are Brazil and Taiwan, where the annual percentage change in incidence were +14.9% and +4.8% respectively (S. C. Ng et al., 2017). IBD places great burdens on the individuals, the health care system, as well as society at large. Indeed, a Canadian study revealed direct medical costs and indirect costs carried by individuals and society (e.g., work-place loss) to total $2.8 billion in 2012 (Rocchi et al., 2012). Furthermore, UC patients can experience reduced quality of life with respect to career, family, and personal well-being. Rising incidence and prevalence rates mean that the impact of UC on society will only increase, emphasizing the need to better understand the cause and treatment of this disorder.

1.2. UC Heterogeneity.

The current framework of UC pathogenesis comprises environmental, genetic, immune, and microbiome factors that culminate at the perturbation of the mucosal barrier and prolonged mucosal inflammatory response (Porter et al., 2020). Consequently, UC is a clinically-, molecularly-, and genetically- heterogeneous disease that fosters varied disease course and mixed response to therapy. Among UC patients, the extent of disease, the severity of disease, and age at diagnosis had been cited as the main determinants of disease course (Torres & Colombel, 2016). An example of molecular heterogeneity is the anti-neutrophil cytoplasmic antibodies (ANCAs), which was suggested as a viable marker for distinguishing UC from Crohn's disease (i.e., another inflammatory bowel disease (Mahler et al., 2013), and for assessing UC severity (Pang et al., 2020). However, not all UC patients are ANCA-positive – a discrepancy that had been linked to genetic differences in the human leukocyte antigen (HLA) region (H. Yang et al., 1993). With regards to genetic heterogeneity, the analysis of 75,000 IBD cases and controls by Jostins and colleagues identified 23 UC-specific risk loci that are primarily involved in the regulation of epithelial barrier function and immune pathways (Jostins et al., 2012). Genetic studies such as this promote the concept of strength in number, i.e., UC disease susceptibility is a compilation of small effects/gene-alterations that is not shared by all patients. The genetic variant *HLA-DRB1*0103* is one example. The HLA region has one of the strongest associations with UC-specific loci (Jostins et al., 2012), and *HLA-DRB1*0103* was linked to the need for colectomy on multiple occasions (Ahmad et al., 2003; Goyette et al., 2015; Silverberg et al., 2003). However, the rarity of the *HLA-DRB1*0103* variant precludes this linkage from broad clinical application. Nevertheless, HLA allelic association with UC implies errors in antigen presentation to T cells and the consequent dysregulation of host T-cell responses. This ties into the conventional acceptance of UC as a Th-

2-mediated immune disorder (i.e., elevated interleukin (IL)-4, IL-5, and IL-13; (Bouma & Strober, 2003). Interestingly, therapeutics that block IL-13 (e.g., anrukinzumab and tralokinumab) were shown to be ineffective against UC (Danese et al., 2015; Reinisch et al., 2015). The newly discovered importance of Th-17 (Kobayashi et al., 2008), Th-9 (Nalleweg et al., 2015), and innate lymphoid cells (Geremia & Arancibia-Cárcamo, 2017) in UC, and the demonstrated effectiveness of IL-23R antagonist (e.g., ustekinumab and mirikizumab) for UC treatment (Sandborn et al., 2020; Sands et al., 2019) despite opposing consequences of IL-23 signaling on innate and adaptive compartments (Cox et al., 2012) provides further confirmation for the molecular complexity of this disease. Genetic heterogeneity was also reported among endoscopically similar UC biopsies, from which three transcriptionally distinct archetypes were discovered, that may be used to predict endoscopic remission (Madill-Thomsen et al., 2018).

1.3. Differential Response to UC Treatments.

Resistance to treatment accentuates the stress that UC place on patients and society. Common treatments for UC include 5-aminosalicylates, corticosteroids and azathioprine/6-mercaptopurine. For patients with refractory UC, anti-tumor necrosis factor (TNF)-α (e.g., infliximab) may be prescribed to avoid colectomy (Feuerstein et al., 2020); however, approximately one-in-four UC patients treated with infliximab do not acquire appreciable benefits from treatment (Ford et al., 2011; Yamada et al., 2014). The molecular mechanisms driving effective response to treatment is unclear, although patients with higher baseline disease severity are less likely to respond to current therapeutic approaches (Hyams et al., 2017; Romberg-Camps et al., 2009). To address the issue of differential response to treatments, several UC gene array studies have derived gene signatures that can predict responsiveness to treatment by examining transcriptomic data obtained from responders vs. non-responders. In one such study, gene expression changes showed that the top

three most significantly enriched biological processes associated with **non**-responsiveness to infliximab were cellular movement, cellular growth and proliferation, and hematological system development and function; immune response came fifth in the order of significance (Arijs et al., 2009). Another transcriptome study that endeavored to stratify infliximab responders vs. non-responders opted to focus on differential enrichment of immunological processes (Pavlidis et al., 2019). This study showed higher enrichment score of inflammatory signatures in non-responders vs. responders at baseline. And whereas the significant differences (in enrichment score) with healthy controls were lost post-treatment in responders, the non-responders maintained significant differences with respect to the healthy controls. The authors rationalized the results identified for non-responders by suggesting an effective therapeutic dosage could not be reached to achieve inflammatory resolution and/or attenuation of the disease activity index score. Nevertheless, it is possible that for non-responders, the disease-driving pathways are not immuno-centric. This notion is supported by Haberman and colleagues' 2019 paper, in which gene signatures associated with UC disease severity and/or responsiveness to corticosteroid treatment were described (Haberman et al., 2019). This study revealed: 1) mitochondrial dysfunction, previously described in UC (Santhanam et al., 2012; Sifroni et al., 2010), to be specific to epithelial cells of active UC as opposed to $CD45^+$ leucocytes, 2) down- and up- regulated genes associated with UC severity to be profoundly enriched in processes known to drive epithelial transformation, 3) upregulated severity genes to be associated with innate immunity and chemokine signaling, and 4) corticosteroid response gene signatures to be tied to innate immunity and chemokine signaling, although they were not significantly associated with epithelial transformation.

Over the last 25 years, a more refined understanding of UC has emerged. Following the discovery of Th-17, Th-9, and innate lymphoid cell involvement in UC as well as the effectiveness of IL-23

blockade therapies, we realize that the immune component of UC is not restricted to a Th-2 response. Furthermore, our comprehension of UC pathophysiology has expanded to encompass the importance of epithelial dysfunction on the genesis and perpetuation of UC. It is pertinent however, to emphasize that current approaches in UC therapies largely target the immune component rather than the epithelial component of the disease (Feuerstein et al., 2020).

1.4. The Intestinal Epithelium.

The large intestine is lined by a monolayer of polarized epithelial cells that are organized into invaginations called crypts. The integrity and barrier properties of the epithelium are regulated by three main types of intercellular junctional complexes – tight junctions (TJ), adherens junctions (AJ), and desmosomes that are connected to the intracellular actin cytoskeletal network (Turner, 2009). Layers of mucus film containing mucins and antimicrobial peptides cover the epithelial monolayer to complete the intestinal epithelium (Antoni et al., 2014). There are four main types of intestinal epithelial cells (IECs) in the colon: absorptive enterocytes, goblet cells, enteroendocrine cells, and a small population of Paneth cells in the proximal colon. In mammals, IECs have a turnover time of five days, the fastest among all tissues (Schepers et al., 2011). The continuous renewal of IECs is fueled by crypt-resident pluripotent intestinal epithelial stem cells that undergo (a)symmetric divisions to produce progenitor or transit amplifying (TA) cells (Schepers et al., 2011; Tomasetti & Bozic, 2015). The TA cells divide rapidly before differentiating into mature IECs that migrate upwards along the crypt axis to replace aged, apoptotic IECs. An exception is for Paneth cells, which migrates toward the crypt base. (**Figure 1**) Within the apoptotic IECs and in the IECs surrounding it, intracellular actomyosin rearrangement allow for apical extrusion of the apoptotic cell without leaving gaps in the monolayer (Kuipers et al., 2014; Rosenblatt et al., 2001). In addition to the physiological shedding of apoptotic cells,

epithelial integrity can be weakened by inflammation or minor physical trauma. Re-establishment of the epithelial barrier is dependent on the precise regulation and synchronization of three processes. First, IECs adjacent to the damaged area lose their polarity, flatten, and migrate into the wound to cover the denuded area. This process is termed epithelial restitution and is independent of cell proliferation (Dignass & Podolsky, 1993). Next, IEC proliferation increases to replenish the pool of enterocytes necessary to encase the sub-epithelial compartment (Iizuka & Konno, 2011). Finally, IECs mature and differentiate to restore the functional activities of the intestinal epithelium (Iizuka & Konno, 2011).

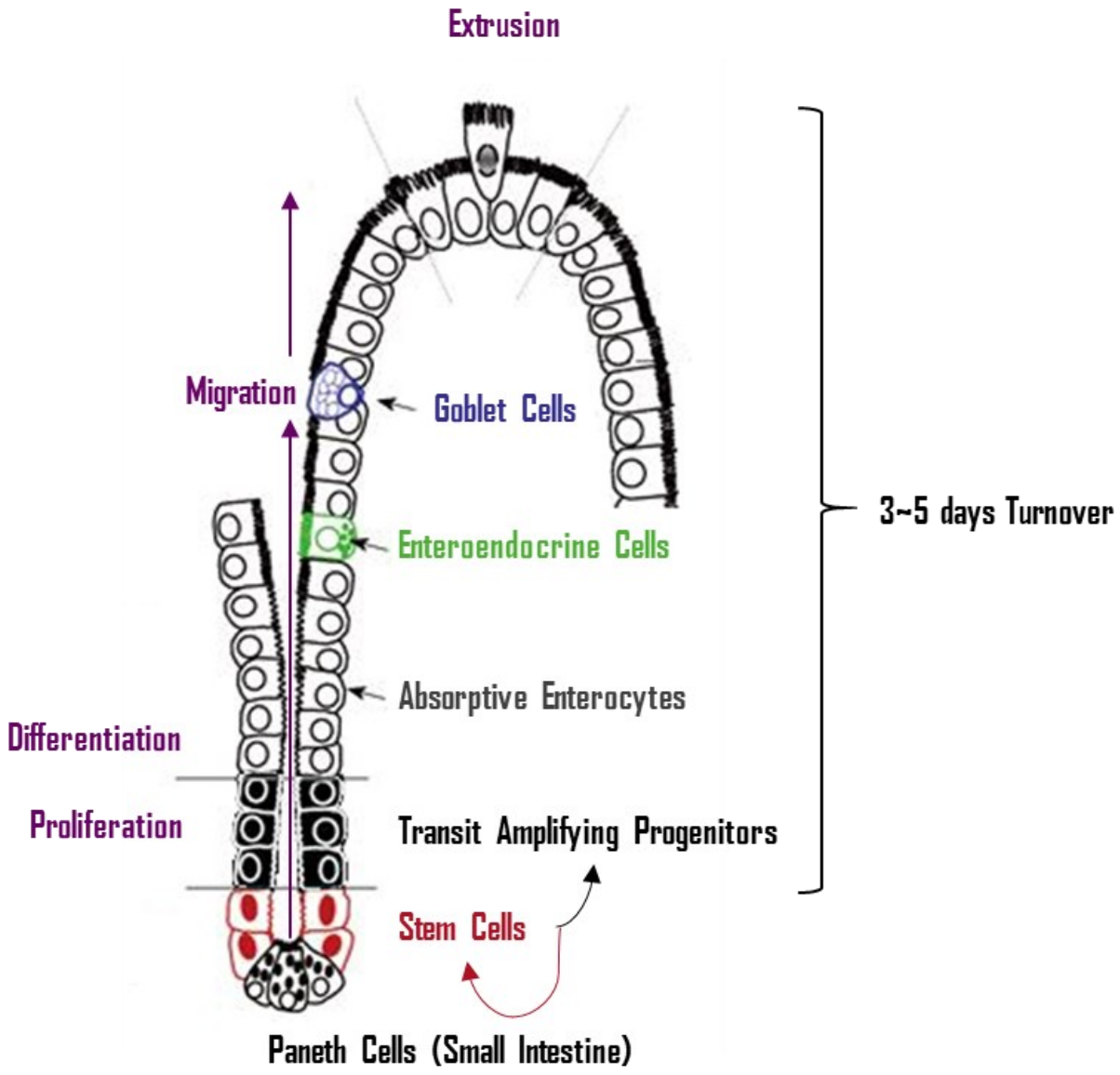

Figure 1. Schematic diagram of the major intestinal epithelial cell types and their regeneration from crypt-resident pluripotent stem cells. Diagram modified from Figure 1A of 'Host-microbial interactions and regulation of intestinal epithelial barrier function: From physiology to pathology' (World J Gastrointest Pathophysiol. 2012 Feb 15;3(1):27-43).

1.5. Epithelial Dysfunction in UC.

Epithelial cells that line the gastrointestinal tract provide a physical and biochemical barrier that separate the host's internal milieu from foreign antigens and microbial pathogens present in the lumen (Peterson & Artis, 2014). Moreover, the epithelium serves as a communication hub for the intestinal mucosa by disseminating luminal events to the sub-epithelial immune compartment and participating in the coordination of mucosal defense and homeostasis (Kagnoff, 2014). Not surprisingly, altered epithelial cell function is frequently detected in UC patients (Büning et al., 2012; Chang et al., 2017; Haberman et al., 2019; Issenman et al., 1993), and has been proposed as a potential etiologic factor for UC (Pastorelli et al., 2013). Epithelial integrity may be provisionally weakened by physiological inflammation or minor trauma (Fiocchi, 1997). But, as the balance between pro- and anti-inflammatory stimuli is perpetually disturbed in UC (Strober & Fuss, 2011), epithelial regeneration may be altered so that normal epithelial barrier function is not restored. Inefficacious wound healing can give rise to altered epithelial architecture, impaired barrier function, and intestinal neoplasia which further aggravate the inflammatory state. (Koch & Nusrat, 2012; Leoni et al., 2015) Therefore, rapid, and complete wound healing is essential for intestinal health and resolution of UC.

Various signaling molecules affecting epithelial restitution and wound healing were found to be dysregulated in UC, examples include: 1) elevated expression of Wnt5a, a noncanonical Wingless-related integration site (Wnt) ligand that facilitates crypt regeneration in wound-associated epithelia (Miyoshi et al., 2012; Moparthi & Koch, 2019) and paradoxically imparts susceptibility to experimental murine colitis (A. Sato et al., 2015); 2) increased production of transforming growth factor-β1 (TGF-β1), an anti-inflammatory cytokine and inducer of TJ protein and collagen expression (Del Zotto et al., 2003; Howe et al., 2005; Nigdelioglu et al., 2016) was observed to

have diminishing effect on IBD cells, partly due to the concurrent increase of TGF-β1-inhibitory molecule Smad7 (Monteleone et al., 2004; Troncone et al., 2018); and 3) constitutive activation of signal transducer and activator of transcription (STAT)-3, a pro-proliferative, anti-apoptotic factor essential for the regeneration of epithelium in response to injury, can perpetuate and worsen UC despite its protective attributes (Nguyen et al., 2015). In recent years, increasing research has brought forward the Hippo pathway as a potential therapeutic target for UC. Dysregulation of the Hippo pathway was found in UC patients as well as multiple models of experimental colitis (F. Deng et al., 2018; Nterma et al., 2020; Xie et al., 2021). Evidence suggests that the major effectors of Hippo pathway, the Yes-associated protein (YAP) and the transcriptional co-activator with PDZ-binding motif (TAZ), link inflammation to epithelial regeneration through their integration of mechanical cues with growth factor signaling (Piccolo et al., 2014). Notably, crosstalk between the Hippo/Wnt and the TGF-β1/STAT3 pathways (Gruber et al., 2016; Park et al., 2015; Qin et al., 2018) exposes an inherently complex role for Hippo signaling in intestinal regeneration that requires further investigation in UC (Xie et al., 2021).

While several conserved signaling pathways have been identified that lead to intestinal epithelial dysfunction in UC (Koch & Nusrat, 2012; Leoni et al., 2015; Xie et al., 2021), the intricacies of effector networks that are involved in the restoration of epithelium homeostasis after injury and/or inflammation is not fully understood. The identification of specific molecular factors that are pivotal in mending intestinal epithelial defects may therefore assist in the design of UC therapeutics.

1.6. Intestinal Mucus Barrier Defects and Gut Dysbiosis in UC.

Adjacent to the monolayer of colonic IECs is the mucus layer, that is primarily composed of the glycoprotein mucin-2 (MUC2), which is constitutively produced by the intestinal epithelial goblet cells (Allen et al., 1998). The mucus layer serves as habitat and a source of nutrient for the commensal and pathogenic microbial populations. At 10^{11} to 10^{12} bacterial cells per milliliter, the colon is considered one of the most densely populated habitats for microorganisms (Rinninella et al., 2019). Bidirectional signaling between these microorganisms and the intestinal epithelium, mediated through changes in mucus layer homeostasis, modulates the development and physiology of the gastrointestinal tract (Fang et al., 2021; Schroeder, 2019). Disruption to the mutualistic relationship between microbial populations and the intestinal epithelium elicits the development of colitis in mice and humans (Fang et al., 2021; Schroeder, 2019).

The intestinal microbial community, termed the gut microbiota, acts as a metabolic organ (Oliphant & Allen-Vercoe, 2019), and contributes to human health by inhibiting pathogenic bacterial colonization (Sommer et al., 2017), modulating the host immune system (Belkaid & Hand, 2014), and promoting intestinal epithelial integrity; Short-chain fatty acids (SCFAs) produced by the commensal bacteria are utilized by the IECs as an energy source (Oliphant & Allen-Vercoe, 2019) and were shown to promote epithelial barrier function by inducing assembly of TJs (Venegas et al., 2019) and by stimulating mucin production in goblet cells (Barcelo et al., 2000; Gaudier et al., 2004; Willemsen et al., 2003). The healthy human gut microbiota is composed of >160 bacterial species, of which ~90% belong to the phyla *Firmicutes* and *Bacteroidetes* (Rinninella et al., 2019). In general, the gut dysbiosis associated with UC involves decreased amounts of *Firmicutes* and *Bacteroidetes*, increased amounts of *Fusobacteria* and *Proteobacteria*, and an overall decrease in microbial diversity (Pittayanon et al., 2020). However, inconsistent

methods and results among studies hinders the association between specific common microbial taxa and UC pathogenesis (Pittayanon et al., 2020). Nevertheless, studies that investigated the interplay between isolated pathogens and the mucus layer have established the mucus interface as an important factor in maintaining homeostasis of the gut microenvironment. For example, Desai and colleagues showed that dietary fiber deficiency increased the utilization of colonic mucus glycoprotein by gut microbiota as nutrient source, which compromised the integrity of the mucus barrier, and increased access to the epithelium by *Citrobacter rodentium*, a colitis-causing attaching/effacing pathogen (Collins et al., 2014; Desai et al., 2016). Moreover, Ng and colleagues showed that the expansion of *Salmonella typhimurium*, a pathogen that elicit susceptibility of mice to DSS-induced colitis (Schultz et al., 2018), is aided by the consumption of sialic acids that were liberated from mucin molecules (e.g., MUC2) by *Bacteroides thetatiotaomicron* (i.e., a model gut symbiont) (K. M. Ng et al., 2013). With regard to the replenishment of the mucus layer, the central effectors of Hippo signaling, YAP and TAZ, were found to be essential for the maintenance of lung epithelial homeostasis by their deterrence of goblet cell metaplasia and mucin hypersecretion (Hicks-Berthet et al., 2021). Interestingly, YAP/TAZ was inactivated in intestinal stem cells (ISCs)/progenitor cells destined for differentiation. Upon differentiation into secretory precursors, YAP/TAZ cooperate with the transcription factor Klf4 to promote terminal differentiation of secretory precursors into goblet cells, thereby increasing production of the mucin MUC2 (Imajo et al., 2014). These findings further emphasize the complex role that YAP/TAZ plays in intestinal homeostasis and regeneration.

The symbiotic relationship between human and their gut microbiota is in large part communicated via the mucus interface. Impairment in the degradation and replenishment of the mucus layer can negatively impact the homeostasis of the gut microbiota and vice versa. As such, mechanisms

underlying the transference of information between the gut microbiota and the intestinal epithelium, via the mucus interface, has been recognized as an important aspect of UC research.

1.7. UC Progression – The Colitis-Dysplasia-Carcinoma Sequence.

Ulcerative colitis is a progressive disorder. In a Swiss IBD study of UC patients with disease limited to proctitis (i.e., limited to the rectum) at diagnosis, approximately 30% of patients had disease expansion into left-sided colitis (i.e., inflammation and architectural distortion that extends from the rectum into the colon, but not beyond the splenic flexure) with 16% exhibiting pancolitis (i.e., disease activity that begins at the rectum and extends beyond the splenic flexure) development within nine years. Additionally, 17% of patients with left-sided colitis had further disease advancement to pancolitis after nine years (Safroneeva et al., 2015). The extent of colonic involvement has implications on the rate of hospitalization, cancer development, and mortality. Earlier meta-analysis conducted by Eaden and colleague estimated that 18% of UC patients will develop colitis-associated colorectal cancer (CAC) within 30 years of UC diagnosis (Eaden et al., 2001). More recent meta-analysis of population-based cohort studies reported a reduction in cumulative risks of CAC, to 5% after >20 years of UC disease duration (Lutgens et al., 2013). Although the probability of developing CAC appears to have declined over time, perhaps due to advancements in medical therapies or optimization of endoscopic surveillance, CAC remains a dire consequence of long-standing UC (Dulai et al., 2016; Kabir et al., 2020). Risk factors that have consistently been identified for CAC development include disease extent, disease duration, disease severity, and family history of colorectal cancer (Eaden et al., 2001; Lakatos et al., 2006; Q. Zhou et al., 2019). The extent of colitis was identified as the most significant risk factor (Q. Zhou et al., 2019).

CAC progresses through a colitis-dysplasia-carcinoma sequence (Itzkowitz & Yio, 2004) and has a mortality rate of around 35% (Ananthakrishnan et al., 2015; Kunovszki et al., 2020). One may reason that as the area affected by UC grows, so too does the inflammatory load which could in turn accelerate dysplasia and CAC tumorigenesis (Grivennikov, 2013). However, among patients or animals with similar inflammatory status, some develop CAC while others do not (Van Der Kraak et al., 2015). Additionally, whole-exome sequence analysis of IBD-associated colorectal cancer showed that, apart from the rare cases of mutations in DNA proofreading or repair pathways, supra-IBD inflammation alone does not compel greater mutation rates – when compared with sporadic colorectal cancer (CRC) of non-inflammatory origin (Robles et al., 2016). This suggests a role for non-inflammatory factors in mediating colitis-dysplasia-carcinoma progression.

While there had been a plethora of CRC-related studies (Farooqi et al., 2019), those that specifically examined CAC were decidedly scarce. Nevertheless, these limited studies on CAC revealed some distinct features on the mutational landscapes of CAC vs. CRC. These include: 1) the higher prevalence and earlier acquisition of *TP53* mutation (Itzkowitz & Yio, 2004), 2) the lower prevalence and later acquisition of *APC* mutation (Itzkowitz & Yio, 2004), 3) the enrichment of mutations in genes responsible for cell motility and cytoskeleton remodeling (Grivennikov & Cominelli, 2016; Robles et al., 2016), and 4) the evolutionary divergence between CAC and CRC that begin in non-dysplastic colitic mucosa (Baker et al., 2019).

While frequent surveillance can reduce CAC incidence and mortality in patients with IBD (Ananthakrishnan et al., 2015), surveillance programs in IBD patient cohort are challenged by concomitant inflammation, scarring, and flat dysplasia with indistinct margins (Ullman et al., 2009). The burden of colonoscopy surveillance may be eased with the discovery of biomarkers that can be routinely used to identify patients at high risk of developing dysplasia or CAC.

Likewise, newly discovered biomarkers may one day be exploited in the development of precision prophylactics for UC patients in the high-risk category.

1.8. The Hippo-YAP/TAZ Signaling Pathway.

The Hippo pathway (**Figure 2**) is an evolutionarily conserved serine/threonine kinase signaling cascade that ultimately phosphorylates and inhibits the activity of transcriptional co-activators YAP and TAZ. By and large, YAP and TAZ are functionally redundant (Varelas, 2014). However, YAP has greater influence on cell morphology, cell proliferation and cell migration (Plouffe et al., 2018). Most Hippo research carried out in the mouse intestine has focused on YAP, perhaps due to the short half-life of TAZ (C. Y. Liu et al., 2010) relative to that of YAP (i.e., < 2 hours vs. 15-21 hours, respectively) (Hein et al., 2019). It was suggested that TAZ abundance is mainly regulated through proteostasis (Piccolo et al., 2014). YAP was demonstrated to negatively regulate TAZ abundance by way of proteosomal degradation, whereas TAZ does not appear to control YAP abundance in the same manner (Finch-Edmondson et al., 2015). Given the redundancy in cellular activities, the two co-activators are generally classified as a functional pairing YAP/TAZ.

Best known as the pathway for organ-size regulation, Hippo controls cell growth, cell proliferation, and cell survival by relaying biochemical and mechanical inputs such as G protein-coupled receptor (GPCR) engagement (Yu et al., 2012), extracellular matrix (ECM) stiffness (Dupont et al., 2011), cell-cell adhesion (Schlegelmilch et al., 2011), and cell morphology (Wada et al., 2011) to YAP/TAZ to regulate expression of target genes (e.g. connective tissue growth factor; *CTGF*, cysteine-rich angiogenic inducer 61; *CYR61*, ankyrin repeat domain 1; *ANKRD1*, and others). As YAP/TAZ do not bind DNA directly, the main transcriptional output of YAP/TAZ is mediated through the TEAD transcription factor family (TEAD1–4) (Piccolo et al., 2014). The core Hippo kinase cascade include the mammalian Ste20-like kinases 1/2 (MST1/2) and the large tumor

suppressor kinases 1/2 (LATS1/2). MST1/2 are known to undergo auto-activation through dimerization-initiated autophosphorylation (Y. Deng et al., 2003; Praskova et al., 2004). Active MST1/2 binds to the adaptor protein salvador 1 (SAV1) to initiate phosphorylation of the scaffolding protein Mps one binder 1 (MOB1A/B). The subsequent MOB1A/B-dependent recruitment of MST1/2 enables phosphorylation of LATS1/2 (Callus et al., 2006; Chan et al., 2005; Praskova et al., 2008). Activated LATS1/2 recognize the consensus sequence HXRXXS/T, of which there are five on YAP (Ser61, Ser109, Ser127, Ser164, and Ser397) and four on TAZ (Ser66, Ser89, Ser117, and Ser311) that are phosphorylated by LATS1/2 (Hao et al., 2008; Lei et al., 2008). The most relevant of these residues are Ser127 and Ser397. The phosphorylation of Ser127 specifically primes YAP's binding to 14-3-3 and lead to its cytoplasmic retention (Zhao et al., 2007), whereas the phosphorylation of Ser397 generates a phosphodegron that is recognized by β-transducin repeat-containing protein (β-TrCP, adaptor for the SCF E3 ubiquitin ligases) to initiate proteasomal degradation of YAP (Zhao et al., 2010).

Though regulation of YAP/TAZ was first identified to occur downstream of the Hippo kinase cascade, subsequent studies indicate that mechanical signaling via the actin cytoskeleton may play a bigger part in controlling YAP/TAZ activity. Wada and colleagues published one of the first studies that demonstrated the regulation of YAP/TAZ by actin remodeling (Wada et al., 2011). The disruption of actin polymerization with cytochalasin D or latrunculin A resulted in cytoplasmic retention of YAP. Likewise, inhibition of myosin II ATPase or myosin light chain kinase (MLCK) with blebbistatin or ML-7 respectively, reduced nuclear accumulation of YAP. Subsequently, Aragona and colleagues revealed that F-actin organization was essential for the responsiveness of YAP/TAZ to the core Hippo kinase cascade under multicellular contexts (Aragona et al., 2013). Interestingly, F-actin can influence YAP/TAZ activity through both Hippo

kinase cascade-dependent (Aragona et al., 2013; Zhao et al., 2012) and -independent (Das et al., 2016; Elosegui-Artola et al., 2017) mechanisms. Importantly, the relationship between actin cytoskeleton and Hippo-YAP/TAZ is not unidirectional. Several studies have demonstrated the regulation of actin dynamics by various Hippo elements. These include MST1-dependent regulation of the actin-bundling protein L-plastin (Xu et al., 2016), the capacity of LATS1 to bind F-actin and inhibit actin polymerization (Visser-Grieve et al., 2011), and YAP-associated transcriptional upregulation of Rho GTPase Activating Protein 29 (ARHGAP29) to suppress the RhoA-LIM Kinase (LIMK)-cofilin pathway in favor of actin depolymerization (Qiao et al., 2017). Despite recent progress made on the mutual regulation between Hippo-YAP/TAZ and the cytoskeleton, the mechanisms by which Hippo-YAP/TAZ signaling operates within the mechanotransduction circuitry remain largely unanswered.

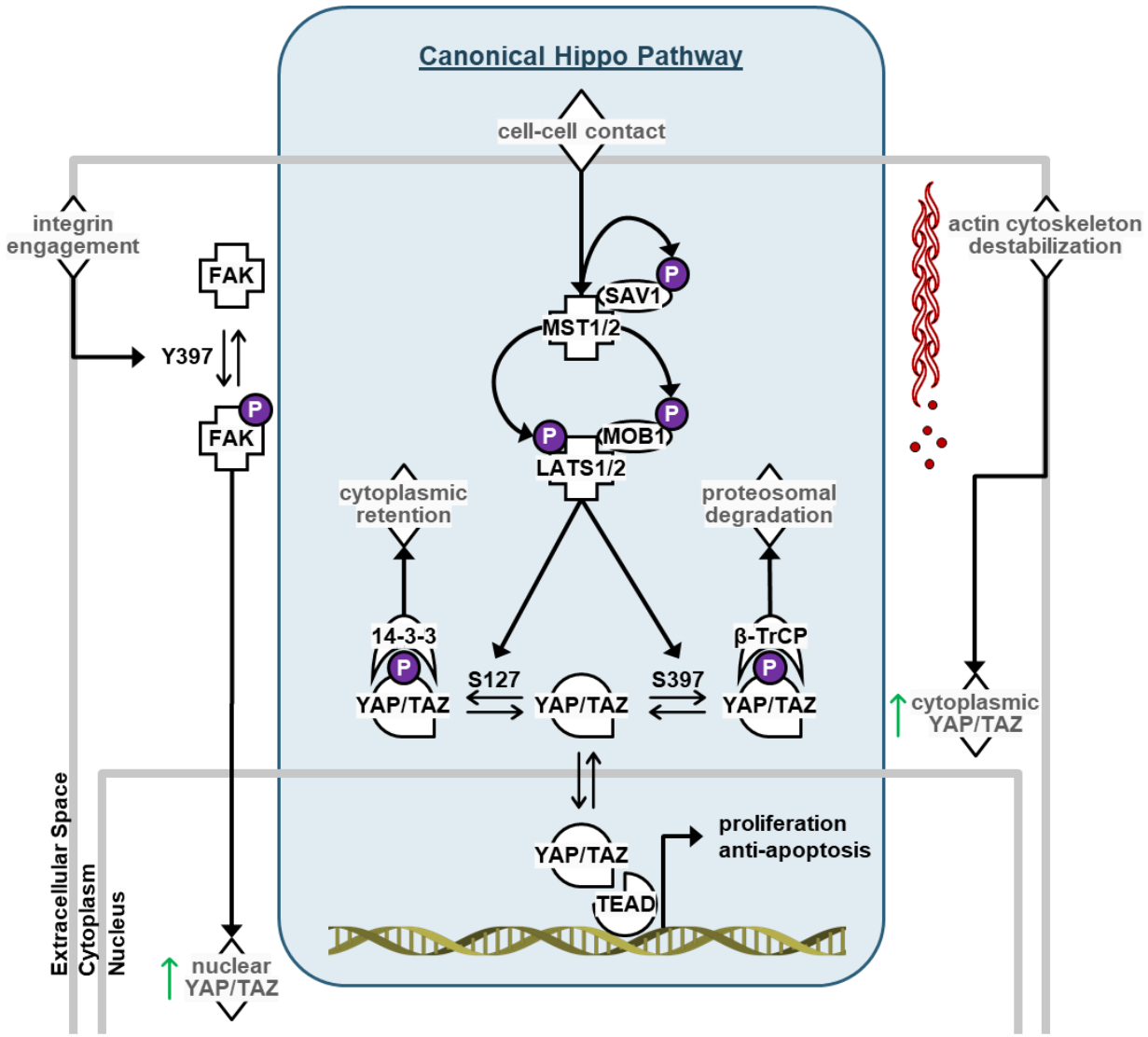
Canonical Hippo Pathway
cell-cell contact
integrin engagement
FAK
Y397
FAK
P
SAV1
MST1/2
P
P
P
(MOB1)
LATS1/2
actin cytoskeleton destabilization
cytoplasmic retention
proteosomal degradation
14-3-3
P
YAP/TAZ
S127
YAP/TAZ
S397
β-TrCP
P
YAP/TAZ
cytoplasmic YAP/TAZ
YAP/TAZ
TEAD
proliferation anti-apoptosis
Extracellular Space
Cytoplasm
Nucleus
nuclear YAP/TAZ

Figure 2. The Hippo-YAP/TAZ signaling pathway. Hippo signaling is an evolutionarily conserved pathway that regulates cell proliferation and apoptosis. The canonical Hippo pathway is a kinase cascade, wherein MST1/2 (mammalian Ste20-like kinases 1/2) and SAV1 (salvador 1) form a complex to phosphorylate MOB1 (Mps one binder 1) and LAT1/2 (large tumor suppressor kinases 1/2) and activate LAT1/2. LATS1/2 in turn phosphorylates and inhibits the transcription co-activators YAP (Yes-associated protein) and TAZ (transcriptional co-activator with PDZ-binding motif), the essential downstream effectors of the Hippo pathway. When dephosphorylated, YAP/TAZ translocate into the nucleus and interact with the TEAD transcription factor family (TEAD1–4) to induce the expression of genes that promote cell proliferation and inhibit apoptosis. Phosphorylation of YAP at Ser127 retains YAP in the cytoplasm, whereas phosphorylation of YAP at S397 promotes YAP degradation. Outside of the core Hippo pathway (enclosed by the blue box), YAP/TAZ is also regulated by actin cytoskeleton and ECM mechanical signaling. Disruption of actin cytoskeleton organization promotes cytoplasmic retention of YAP/TAZ whereas integrin engagement increases nuclear translocation of YAP/TAZ by way of activated focal adhesion kinase (FAK).

1.9. The Role of Hippo-YAP/TAZ in UC and Epithelial Repair.

Immunohistochemical analysis of intestine samples revealed elevated LAT1/2 abundance in UC patients (Nterma et al., 2020), and lower YAP expression and abundance in patients with acute UC (F. Deng et al., 2018). Moreover, YAP abundance correlates positively with IEC proliferation and negatively with UC severity (F. Deng et al., 2018), which suggests that Hippo-YAP/TAZ signaling may mediate intestinal regeneration within the context of UC. Epithelial repair in the intestine is supported by a unique population of cells at the crypt base expressing clusterin (Clu). Clu^+ cells rarely proliferate or differentiate under homeostatic conditions but can replace lost $Lgr5^+$ ISC to reconstitute the entire epithelial structure upon injury (Ayyaz et al., 2019). Remarkably, the YAP-associated gene signature overlaps that of the Clu^+ cluster in damaged crypts, indicating the dependence of Clu^+ cell activation, thus epithelial repair, on YAP activation (Gregorieff et al., 2015; Seo et al., 2020).

During dextran sodium sulfate (DSS)- induced murine colitis, YAP abundance increases early during IEC regeneration, then decreases toward baseline as the epithelium approaches full histological recovery (J. Cai et al., 2010; F. Deng et al., 2018). This upregulation of YAP abundance was attributed to post-transcriptional control rather than increased transcription (J. Cai et al., 2010; F. Deng et al., 2018; D. Zhou et al., 2011). *Yap*-deficient mice experience increased crypt loss, have fewer proliferating IECs, and display more apoptotic IECs after DSS treatment (J. Cai et al., 2010). Likewise, overexpression of YAP enhances IEC regeneration in the DSS model of colitis (F. Deng et al., 2018). However, overexpression of YAP also increases susceptibility to CAC in the azoxymethane (AOM)/DSS murine model of CAC (F. Deng et al., 2018). Interestingly, while YAP is essential for crypt regeneration post-DSS-induced injury, IEC-specific *Yap* knockout mice develop normally with no visible defects along the crypt axis (J. Cai et al., 2010). Nonetheless,

conditional knockout of Hippo components that normally restrict YAP activity elicit adverse phenotypes, such as enlarged crypts and formation of colon polyps in S*av1* knockouts (J. Cai et al., 2010), and dysplastic epithelia with expansion of undifferentiated IECs and loss of goblet cells in *Mst1* and *Mst2* knockouts (D. Zhou et al., 2011). These data suggest that the Hippo pathway is constitutively active during homeostasis to restrict YAP/TAZ activity when injury-induced regeneration is not required.

It is then relevant to highlight that DSS-induced injury and subsequent repair in *Sav1* deficient mice bring about accelerated malignant transformation, which speaks to the importance of restraining the oncogenic potential intrinsic to the regenerative function of YAP/TAZ. Beyond the canonical Hippo kinase cascade, DSS-induced IL-6 upsurge in the colon elicits the activation of YAP that is required for reconstitution of the epithelium. This activation is independent of the Hippo cascade and is mediated by the Src family of tyrosine kinases (Taniguchi et al., 2015). As well, crosstalk between the Hippo and Wnt signaling pathways plays a key role in coordinating tissue regeneration after injury. Mechanistically, *Yap* expression is enhanced by Wnt signaling (Konsavage et al., 2012), and while cytoplasmic YAP antagonizes Wnt signaling by restricting nuclear translocation of β-catenin (Imajo et al., 2012), nuclear YAP interacts with β-catenin to promote transcription of Wnt targets (F. Deng et al., 2018). As such, a distinction between YAP abundance and localization needs to be made as the two events may result in different phenotypes by way of Wnt signaling. Lastly, during the restitution phase of mucosal healing, remodeling of the ECM augments focal adhesion kinase (FAK)-Src signaling to enhance YAP activation by way of actin cytoskeleton reorganization (N. G. Kim & Gumbiner, 2015; Yui et al., 2018). This activation of YAP potentially induces the obligatory de-differentiation of committed IECs back to

a progenitor state, to support the heightened IEC proliferation necessary for replenishment of lost IECs (Gregorieff et al., 2015; Yui et al., 2018).

1.10. The Actin Cytoskeleton.

The cytoskeleton includes a dynamic network of actin filaments that undergoes constant remodeling by regulatory proteins to provide the structural framework and mechanical forces necessary for cellular, and ultimately, tissue morphogenesis. Biochemical and mechanical stimuli induce reorganization of the actin cytoskeleton, which in turn regulates cytoskeleton-anchored functions such as cell migration, cell-cell interaction, cell-substratum interaction, and cell division that are vital for the maintenance of tissue homeostasis (Merino et al., 2020). There is a vast research literature dedicated to the understanding of the cytoskeletal structure and the molecular elements that govern its dynamic control. Although appreciable advances in understanding of the actin cytoskeleton have been achieved (Brito & Sousa, 2020; Merino et al., 2020; Schwayer et al., 2016), there still remain many regulatory aspects that require continued investigation.

The intracellular orientation of the actin cytoskeleton is well described. Lamellipodia and filopodia, composed of quasi-two-dimensional branched actin networks and cross-linked bundles of parallel actin filaments respectively, are the main structures responsible for cell migration, while anti-parallel focal adhesion-anchored stress fibers and junction-associated cortical actin belt enable the transduction of environmental cues and the coordination of movements across multiple cells. (Schwayer et al., 2016) The coupling of actin cytoskeleton to the nucleus occurs through the linker of nucleoskeleton and cytoskeleton (LINC) complex, which has been implicated in the regulation of nucleus shape, cell division, and gene expression. (Bouzid et al., 2019)

Remodeling of the actin cytoskeleton is driven by mechanisms of actin turnover. F-actin is an assembly of monomeric G-actin that forms double-stranded helix with a right-handed twist (Holmes et al., 1990). At the barbed (+) end, F-actin polymerizes by the incorporation of ATP-bound G-actin (Merino et al., 2020). In lamellipodia and filopodia, the barbed end faces the plasma membrane, where elongation of F-actin underscores leading edge protrusion in migrating cells (Small, 1988). At the pointed (–) end of the filament, the release of P_i from ADP-P_i-bound actin triggers structural changes in terminal actin protomers, which promote release of ADP-bound actin protomers from the actin filament (Merino et al., 2020). Newly released ADP-G-actin undergo nucleotide exchange with assistance from the actin binding protein (ABP) profilin to replenish the pool of polymerization-competent ATP-G-actin (Selden et al., 1999). Actin turnover is ATP hydrolysis-dependent, but ATP hydrolysis is not required for polymerization per se. Rather, the turnover is regulated by various ABPs that possess actin-binding affinity dependent upon the nucleotide-specific conformational states of actin (Merino et al., 2020). Spontaneous polymerization of ATP-bound G-actins into filament is blocked by profilin, which binds the barbed end of G-actin while leaving the pointed end free to interact with filaments that have had their barbed ends adorned with formins (Merino et al., 2020; Rottner et al., 2017). Formins comprise a group of ABPs that facilitate the dissociation of capping proteins from, and the recruitment of profilin/actin complex to the barbed end of F-actin to promote linear extension of filaments (Merino et al., 2020). To create the branched actin networks seen in lamellipodia, Arp2/3 protein complex binds to the flank of an F-actin and nucleate a new filament that branch out at an angle of ~70° relative to the existing filament. Activation of the Arp2/3 complex by nucleation-promoting Wiskott–Aldrich syndrome protein (WASP)/WASP-family verprolin-homologous protein (WAVE) induces structural changes in ABPs Arp2 and Arp3 that generate pseudo-barbed

end, to which profilin/actin complex binds (Merino et al., 2020). To hasten actin turnover, the ABP cofilin creates new barbed ends for polymerization through its actin-severing activity and builds up the reserve of actin monomers by increasing P_i dissociation from ADP-P_i actin (Merino et al., 2020). Phosphorylation of cofilin on Ser3 is inhibitory and is carried out by LIMK, among others (N. Yang et al., 1998). Dephosphorylation of Ser3 promotes the binding of cofilin to actin filament and activates the severing function of cofilin (Moriyama et al., 1996). The synergy between cofilin and Arp2/3 complex is in part coordinated by the ABP coronin 1B, which interact with Arp2/3 on younger ATP-actin filaments to impede cofilin-mediated disassembly while activating cofilin on older ADP-P_i-actin filaments to enhance disassembly (Campellone & Welch, 2010). Apart from cofilin, activation of non-muscle myosin II (NM-II) can cause fragmentation of actin filaments and thus contribute to the recovery of polymerization-competent G-actin (Medeiros et al., 2006).

Myosins are motor proteins that utilize energy derived from ATP hydrolysis for movement along actin filaments (Syamaladevi et al., 2012). Highly expressed in non-muscle cells, NM-II is a hexameric ABP composed of two heavy chains, two essential light chains (ELC) and two regulatory light chains (RLC), and associate with actin filaments to form the actomyosin contractile fibers required for mechanical force generation. The heavy chains interact through their coiled-coil tail domains and binds actin with their head domains, which also house the ATPase (Brito & Sousa, 2020). The essential and regulatory light chains bind to the necks of heavy chains, where the ELCs can stabilize the myosin structure and RLCs can regulate the ATPase activity of myosin. Bipolar arrays of NM-II that walk towards the barbed ends of antiparallel or off-angled actin filaments generate the pulling force that underwrites functions specified at the opening of this subsection (Brito & Sousa, 2020). Monophosphorylation of RLC on Ser19 increase the actin-activated ATPase activity and assembly of NM-II, and diphosphorylation of RLC on both Ser19

and Thr18 further enhance the increase. (Adelstein & Anne Conti, 1975; Craig et al., 1983; Umemoto et al., 1989; Walsh, 2011). Monophosphorylation of RLC on Ser19 is carried out in Ca^{2+}-dependent manner by MLCK and in Ca^{2+}-independent manner by Rho-associated coiled-coil containing protein kinase (ROCK), p21-activated protein kinase (γ-PAK), citron kinase, integrin-linked protein kinase (ILK), death-associated protein kinase 3 (DAPK3), MAPK-activated protein kinase 1b (MAPKAPK-1b or RSK-2) and MAPKAPK-2; of which, ILK and DAPK3 are also responsible for diphosphorylation of RLC on both Ser19 and Thr18 (Ulke-Lemée & MacDonald, 2010). NM-II activity is terminated when RLC dephosphorylation of Ser19 and Thr18 is completed by myosin light chain phosphatase (MLCP), the activity of which is attenuated by the phosphorylation of its subunit myosin phosphatase target subunit 1 (MYPT1) on Thr697 by ROCK, ILK, or DAPK3 (Grassie et al., 2011; MacDonald & Walsh, 2018).

1.11. The Role of Actin Cytoskeleton in UC and Epithelial Repair.

Epithelial permeability defect is a hallmark of UC (Chang et al., 2017; Gitter et al., 2001). It remains unsettled whether barrier dysfunction is the cause or consequence of UC inflammation, but the efficient restoration of epithelial integrity is essential to prevent additional aggravation of the inflammatory state. The actin cytoskeleton is an important component of epithelial repair, and is required for cell migration, wound contraction, and propagation of injury signals. Actin cytoskeletal functions are partially mediated through RLC phosphorylation (Turner et al., 1997; Yuhan et al., 1997). With respect to UC, elevated colonic epithelial MLCK accompanying increased RLC phosphorylation correlate positively with disease activity (Blair et al., 2006) However, despite the availability of an MLCK-specific inhibitor molecule, MLCK inhibition is ill-suited for treating UC as it can bring about systemic toxicity with concurrent inhibition of the smooth muscle MLCK isoform that is transcribed from the same gene *MYLK1* as the epithelial

MLCK isoforms (Cunningham & Turner, 2012; Y. Jin & Blikslager, 2020). As such, contemplation of MLCK as a therapeutic target for UC has evolved from inhibition of enzymatic activity to prevention of subcellular translocation, which can be accomplished in an isoform-specific manner. To this end, Graham and colleagues examined usage of a molecular tool, the *Divertin* compound, that blocks recruitment of the epithelial MLCK1 isoform to the junction-associated cortical actin belt without inhibiting enzymatic function and showed attenuation of experimental murine colitis (Graham et al., 2019). Also, while the curtailment of RLC phosphorylation at Ser19 is not feasible from the perspective of directly targeting MLCK enzymatic activity, there remains multiple additional prospects such as ROCK, ILK, or DAPK3 that may be worthy of examination under pathological conditions.

An investigation into proteomic changes associated with risk of UC progression was conducted by May and colleagues and showed enrichment of actin cytoskeletal dysregulation in dysplastic samples of UC patients at high risk of CAC (May et al., 2011). Notably, the cytoskeletal changes were also observed in nondysplastic samples from patients at high risk of CAC, which suggests that alteration of actin cytoskeleton may be an important factor in early UC neoplastic progression (May et al., 2011). In a separate gene expression study, the progression of nondysplastic tissue toward CAC phenotype was associated with dysregulation of the actin cytoskeleton pathway, involving significant downregulation of *DIAPH1* (the formin mDia1) and significant upregulation of *PFN2* (profilin-2) (Kanaan et al., 2010). Studies conducted on human colorectal cancer cell lines showed that enhanced self-renewal and motility coincide with increased profilin-2 abundance (M. J. Kim et al., 2015), and decreased level of strain-induced RLC phosphorylation and wound closure follow siRNA-mediated reduction of mDia1 (Chaturvedi et al., 2011). Interestingly, in the absence of strain, mDia1 knockdown increases basal epithelial wound closure (Chaturvedi et al.,

2011). Activation of the ABP cofilin was shown to increased epithelial permeability (Nagumo et al., 2008), whereas LIMK-mediated inhibition of cofilin was suggested to regulate chemokine-mediated epithelial restitution (Moyer et al., 2007). Intriguingly, though the suppression of the LIMK-cofilin pathway by YAP promotes cell migration in 3D Matrigel invasion assays, no difference was observed in 2D wound healing assays (Qiao et al., 2017). This discrepancy might be guided by a yet unexplored coordination of activity between cofilin and Arp2/3. Recently, arpin, an Arp2/3 inhibitory protein, was found downregulated in acutely inflamed UC tissues and in murine colitis (Chánez-Paredes et al., 2021). And, small-molecule inhibition of Arp2/3 attenuated murine colitis severity, likely through modification of F-actin integrity and actomyosin contractility (Chánez-Paredes et al., 2021). Paradoxically, loss of Arp2/3 complex activity brings about YAP activation and causes proliferation, differentiation, and barrier defects in the epidermis that was rescued by pharmacologic inhibition of YAP activity (K. Zhou et al., 2013). It has been recognized that YAP responds to increasing applied forces by adjusting its cytoplasmic to nuclear localization (Panciera et al., 2017). Forces exerted through focal adhesions reach the nucleus by way of stress fibers, that act on nuclear pores to increase YAP nuclear import (Elosegui-Artola et al., 2017). Accordingly, matrix stiffness-induced colocalization of YAP with stress fibers accompany nuclear translocation of YAP which can be disrupted by knockdown of integrins (Lee et al., 2019) or impairment of LINC complex components (Driscoll et al., 2015; Guilluy et al., 2014).

Altered structure and dynamics of the actin cytoskeleton have been consistently demonstrated to impact intestinal epithelial repair within the context of UC. Although recent studies have extended our understanding of the relationship between actin cytoskeleton remodeling and epithelial repair, the exact mechanism by which forces transmitted across the actin cytoskeleton influence specific

cellular functions such as epithelial proliferation, differentiation, and apoptosis remains ambiguous. More research is also needed to resolve the association of actin cytoskeleton with UC neoplastic progression.

1.12. The Death-Associated Protein Kinase (DAPK) Family.

The death-associated protein kinase family (DAPKs) is composed of five members: DAPK1, DAPK2 (a.k.a. DAPK-related protein kinase 1; DRP1), DAPK3 (a.k.a. zipper-interacting protein kinase; ZIPK), DRAK1 (a.k.a. STK17A), and DRAK2 (a.k.a. STK17B) (Farag & Roh, 2019). DAPKs belong to the Ca^{2+}/calmodulin (CaM)-dependent family of Ser/Thr kinases and share a highly conserved kinase domain; however, beyond this catalytic domain, the five members of DAPKs differ substantially in terms of size, overall structure, and subcellular distribution (Bayer & Schulman, 2019; Farag & Roh, 2019). DAPK1 is the largest member of the family with six extra-catalytic subdomains in addition to the kinase domain; these extra-catalytic subdomains include the Ca^{2+}/CaM regulatory domain, a feature shared with DAPK2 but not DAPK3, DRAK1, or DRAK2. Both DAPK1 and DAPK2 lack nuclear localization signal (NLS) sequence, whereas DAPK3 contains four NLS sequences and each of DRAK1 and DRAK2 contains two (Farag & Roh, 2019).

Functionally, all DAPKs demonstrate the capacity to regulate RLC phosphorylation and to trigger apoptosis (Farag & Roh, 2019). Individually, the DAPKs have been linked to a broad spectrum of biological processes, including response to oxidative stress, response to viral infection, regulation of synaptic plasticity, and regulation of muscle contraction (Farag & Roh, 2019). Within the context of UC, DAPK1 is the most oft reported DAPK. Localizing to the cytoskeleton through its ankyrin repeats, DAPK1 has several cytoskeleton-associated substrates (Bialik & Kimchi, 2014; Shani et al., 2004) and acts as a scaffold to the LIMK/cofilin complex (Ivanovska et al., 2013). It

was shown that *DAPK1* silencing via promoter hypermethylation correlates with a decrease in DAPK1 abundance and an increase in the severity of UC-associated inflammation (Kuester et al., 2010). Furthermore, pharmacological inhibition of DAPK1 was reported to augment susceptibility to DSS-induced colitis in mice, with concomitant increase in bacterial translocation that was ascribed to barrier defects (Lopes et al., 2018). Among the remaining DAPKs, direct linkages to UC have not been made, but are likely to be established given their individual influence on cytoskeleton-related cellular functions and biological processes.

1.13. The Death-Associated Protein Kinase 3 (DAPK3).

DAPK3 was discovered in a yeast two-hybrid assay that identified it as a binding partner of activating transcription factor 4 (ATF4) (Kawai et al., 1998). Encoded by the *DAPK3* gene that is located on chromosome 19, DAPK3 consists of 454 a.a. with an approximate mass of 52.5 kDa. (**Figure 3**) DAPK3 is ubiquitously expressed in various human and mouse tissues, including thymus, spleen, and the small intestine (Kawai et al., 1998; Saito et al., 1998). On the cellular level, localization of human DAPK3 is in part regulated through (de)phosphorylation, as Thr299 phosphorylation was shown to promote cytoplasmic retention of DAPK3 (Weitzel et al., 2011). The N-terminal catalytic kinase domain of DAPK3 carries ~80% a.a. sequence identity to that of DAPK1. The sequence similarity between DAPK3 and DAPK1, in addition to functional overlap in cell death processes, categorize the kinase within the DAPK family of Ser/Thr-kinases where DAPK3 is also known as zipper-interacting protein kinase (ZIPK) due to the presence of a C-terminal leucine-zipper (LZ) domain (Kawai et al., 1998). Although DAPK3 is closely related to the other DAPK family members, it is distinct in its lack of the Ca^{2+}/CaM regulatory domain (Kawai et al., 1998) and Ca^{2+}-independent activity (Borman et al., 2002; Niiro & Ikebe, 2001). As well, in place of the ankyrin repeats and the death domain found on the C-terminus of DAPK1,

DAPK3 has instead the LZ domain, a dimerization module that mediates self-association with other DAPK3 molecules or with ATF4 via homotypic LZ-LZ interactions (Kawai et al., 1998). The stability of DAPK3 is regulated by the ubiquitin proteasome system and involves interaction of the kinase domain with the heat-shock protein HSP90 (Citri et al., 2006). Three sites (Thr180, Thr225, and Thr265) within the kinase domain of DAPK3 have been shown to undergo autophosphorylation, resulting in its activation (Graves et al., 2005). DAPK3 is also activated through DAPK1-induced and ROCK-induced multisite phosphorylation (Hagerty et al., 2007; Shani et al., 2004). Four putative NLS motif were identified in the human DAPK3: one in the N-terminal kinase domain, one immediately downstream of the kinase domain, and two near the C-terminus (Weitzel et al., 2011). The predominantly nuclear localization of DAPK3 was thought to be the effect of the extreme C-terminal NLS (NLS4) (Kögel et al., 1999). However, there remains an unresolved debate over the species-specific localization and shuttling of DAPK3 (Shoval et al., 2007; Weitzel et al., 2011). In humans, the subcellular localization of DAPK3 is partly regulated by the phosphorylation status of the Thr299 residue. Phosphorylation of Thr299 or phosphomimetic substitution (Thr→Asp) at this position resulted in cytoplasmic localization of DAPK3 (Graves et al., 2005). It was proposed that Thr299 phosphorylation blocked the functionality of an immediately adjacent NLS (NLS2) to enable the cytoplasmic retention of DAPK3. In rat and mouse orthologs of human DAPK3, the Thr to Ala divergence at position 299 was thought to be partially responsible for the predominantly nuclear localization of rodent DAPK3 (Shoval et al., 2007). Nevertheless, phosphomimetic conversion of Ala299Asp and the introduction of NLS2 to murine DAPK3 did not alter the predominantly nuclear localization of this DAPK3 ortholog (Weitzel et al., 2011). This suggests that NLS4 may be the functional NLS of murine DAPK3, as originally proposed by Kögel and colleagues (Kögel et al., 1999) . The

differential regulation of DAPK3 subcellular localization will influence the transferability of knowledge gained from studies of DAPK3 in mice. However, the basic biological functions of DAPK3 are conserved between species. Thus, insights may still be gained from mouse models of diseases – such as the DSS-model of UC employed in this study.

DAPK3 acts as a molecular switch for a multitude of cellular processes, one of which is its induction of apoptotic and autophagic cell death. The pro-apoptotic effects of DAPK3 depend on its catalytic activity, which was first demonstrated in NIH 3T3 fibroblasts with the use of catalytic inactive or "kinase-dead" mutant (i.e., DAPK3-K42A) (Kawai et al., 1998). DAPK3 was found to tightly associate with promyelocytic leukemia (PML) oncogenic domains (PODs) – nuclear structures implicated in transcription and regulation of apoptotic factors (Seeler & Dejean, 1999). It was suggested that DAPK3 promoted apoptosis via its cooperative recruitment of Daxx to the PODs, and its subsequent phosphorylation of the pro-apoptotic protein Par-4 (prostate apoptosis response gene 4) (Kawai et al., 2003). Co-expression of DAPK3 and Par-4 led to translocation of DAPK3 from the nucleus to the cytoplasm, which was followed by cytoskeleton perturbation and morphological changes indicative of apoptosis (Page et al., 1999). With regards to autophagy, an interaction of DAPK3 with autophagy-related (Atg)-1 protein kinase generated a kinase cascade that mediated autophagosome formation via myosin II activation during starvation-induced autophagy (Tang et al., 2011). DAPK3 was also found to increase the activity of Unc-51 like autophagy activating kinase (ULK1; mammalian Atg1 homologs) through direct phosphorylation of ULK1, thereby induced autophagy upon starvation (G. M. Li et al., 2021). Furthermore, DAPK3 contributes to autophagy via the direct phosphorylation of Beclin 1, which is a key regulator of autophagosome formation (Fujiwara et al., 2016). As well, the interaction of DAPK3 with the human cell-division cycle 14A (hCDC14A) was reported to activate high glucose-induced

autophagy in mouse pancreatic β cells (Hu et al., 2020). Interestingly, hCDC14A is a cytoskeleton-associated phosphatase; its colocalization with the Hippo component KIBRA (kidney- and brain-expressed protein) was shown to regulate epithelial cell migration and cell adhesion (N.-P. Chen et al., 2016).

In both smooth muscle and non-muscle cells, DAPK3 phosphorylates RLC at Ser19/Thr18 in a Ca^{2+}-independent manner (Borman et al., 2002; Moffat et al., 2011; Murata-Hori et al., 1999; Niiro & Ikebe, 2001). DAPK3 was also found to phosphorylate the inhibitory site (Thr697) on MYPT1 (MacDonald, Borman, et al., 2001) and the activation site (Thr38) of the protein kinase C-activated inhibitor of MLCP (CPI-17) (MacDonald, Eto, et al., 2001). Through either the direct phosphorylation of RLC, or the inhibition of MLCP, DAPK3 promotes actomyosin cytoskeleton remodeling, which has a broad range of effects: including contraction (Ihara & MacDonald, 2007), autophagic cell death (Tang et al., 2011), cell migration (Komatsu & Ikebe, 2004; Newell-Litwa et al., 2015), and cell adhesion (Nehru et al., 2013). The regulation of RLC phosphorylation by DAPK3 is also important for cytokinesis (Hosoba et al., 2015); Colon cancer-associated loss-of-function DAPK3 mutant D161N was shown to cause cytokinesis failure and induce multinucleation via decreased RLC phosphorylation at the contractile ring (Ono et al., 2020). This suggests that downregulation of DAPK3 may play a role in carcinogenesis through cytokinetic defects.

DAPK3 plays a regulatory role in transcriptional and translational programs that are tightly connected to cell survival, proliferation, and growth. Interaction of DAPK3 with the DNA-binding androgen receptor (AR) enhances its transcriptional activity (Felten et al., 2013; Leister et al., 2008). As well, DAPK3 binds to Nemo-like kinase (NLK) to downregulate NLK-mediated repression of β-catenin signaling (Togi et al., 2011). Likewise, DAPK3 was demonstrated to

decrease E-cadherin expression levels, while increasing β-catenin and its nuclear translocation (J. Li et al., 2015). Lastly, DAPK3 was shown to interact with STAT3 and could enhance STAT3-mediated transcription in an IL-6-dependent manner (N. Sato et al., 2005, 2006).

DAPK3 displays diverse biological impact. With regards to cell growth, the regulation of β-catenin signaling by DAPK3 via interaction with NLK altered colon carcinoma cell growth (Togi et al., 2011). In terms of proliferation, phosphorylation of STAT3 by DAPK3, which enhances the transcriptional activity of STAT3 (N. Sato et al., 2005, 2006), has the potential to confer resistance to colitis and colitis-associated tumorigenesis by promoting IEC proliferation following epithelial damage (Bollrath et al., 2009). Augmentation of RLC phosphorylation by DAPK3 stimulates actomyosin contraction (Hosoba et al., 2015; Ihara & MacDonald, 2007), which is important for cytokinesis during cell division (Ono et al., 2020), and is essential in the "purse-string" mechanism of epithelial restitution (Bement et al., 1993; Nusrat et al., 1992; Russo et al., 2005). Moreover, DAPK3 has the potential to alter the dynamics of collective sheet migration via E-cadherin downregulation during epithelial restitution (D. Cai et al., 2014; Hwang et al., 2012). Lastly, the reduction of FAK activity by the ectopic expression of DAPK3 (Nehru et al., 2013), may play a part in cell adhesion regulation during epithelial wound repair, to influence IEC proliferation and survival during UC progression (Owen et al., 2011).

Given that DAPK3 had been shown to regulate key signaling pathways that coordinate epithelial regeneration after injury, it is tempting to speculate that DAPK3 may play a role in epithelial repair and/or UC progression. However, the significance of DAPK3 within these contexts has yet been directly assessed.

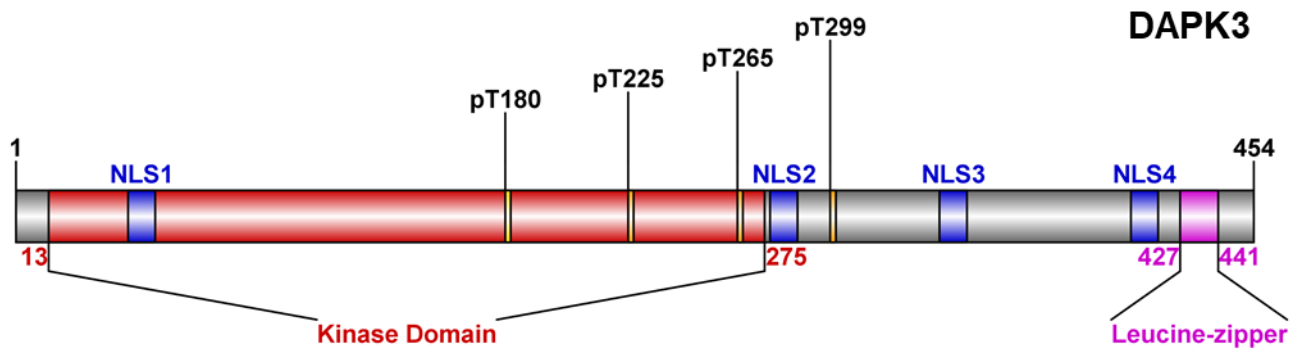

Figure 3. Structural features of the human DAPK3. DAPK3 (NCBI Reference Sequence: NP_001339.1) possesses an N-terminal kinase domain, a leucine-zipper domain, and four nuclear localization signals (NLS). DAPK3 is autophosphorylated at T180, T225 and T265. DAPK3 is also phosphorylated by ROCK at T265 and T299, and by DAPK1 at T299. The recent domain information on human DAPK3 was collected from www.nextprot.org. Graphic was generated with IBS: Illustrator for Biological Sequences (W. Liu et al., 2015).

1.14. Hypothesis and Objectives.

I hypothesize that DAPK3 is an important effector in the reparative intestinal epithelium and plays a key role in the development of colitis-associated dysplasia-carcinoma. Furthermore, I posit that DAPK3 contributes to UC progression through its regulation of colonic epithelial restitution and cell proliferation.

The following three chapters give a detailed account of the way by which I came to identify DAPK3 as key factor in colitis-dysplasia progression. As well, these chapters report the findings of cell and animal studies that demonstrate the propensity of DAPK3 to regulate wound repair and augment colitis disease severity.

For ***Bioinformatic Studies***, my objective was to answer the follow three questions:

1) How does the extent of colitis impact biological functions and regulatory pathways?
2) What are the key molecular factors that bridge the colitis-dysplasia progression?
3) How do these key molecular factors relate to one another, and to DAPK3?

For ***Cell Studies***, my objective was to answer the follow three questions:

1) Does DAPK3 inhibition affect epithelial wound closure?
2) How does DAPK3 inhibition affect epithelial cell proliferation post-wounding?
3) How does DAPK3 inhibition affect Hippo signaling during epithelial wound closure?

For ***Animal Studies***, my objective was to answer the following three questions:

1) Does DAPK3 inhibition affect the severity of DSS-induced colitis?
2) How does DAPK3 inhibition affect epithelial cell proliferation post-DSS-induced injury?
3) How does DAPK3 inhibition affect Hippo signaling in the DSS-model of colitis?

Chapter 2 . Transcriptional Analysis of Left-sided Ulcerative Colitis, Pancolitis, and Ulcerative Colitis-associated Dysplasia to Identify Potential Biomarkers of Importance for UC Progression.

2.1. Introduction.

UC patients are at greater risks of developing colorectal cancer through the colitis-dysplasia-carcinoma sequence of transformation (Van Der Kraak et al., 2015). Mutational signature analysis of tissue and blood samples from CAC patients showed that the evolutionary trajectory of CAC is initiated early in the colitis-dysplasia-carcinoma sequence (Baker et al., 2019). Furthermore, the extent of colitis has been recognized as an independent and most significant risk factor for CAC (Eaden et al., 2001; Q. Zhou et al., 2019). This suggests that gene expression profiles of colitis-associated lesions obtained from patients with varied extent (i.e., area(s) of involvement) of UC can be mined to support the development of molecular panels that identify patients at high risk of developing dysplasia or CAC.

To derive key factors responsible for the progression of UC, I utilized the microarray dataset GSE47908, that was generated by Bjerrum and colleagues based on the GPL570 platform (Bjerrum et al., 2014). This dataset was selected because it comprises the transcriptional profiles of colonic mucosa from patients with varying extent of UC. Specifically, the dataset included microarray gene expression data of mucosal biopsies from the left colon of patients with left-sided colitis, pancolitis, or colitis-associated dysplasia (CAD), plus healthy controls (HC). In their 2014 paper, Bjerrum and colleagues reported results from their principal component analysis (PCA) that showed differential expression profiles of the UC-subtypes, which in turn, were not inferred by potential covariates in the clinical data (i.e., age, years with disease, Mayo score, and medication). The Bjerrum study presented a general view of the differentiation between pancolitis/CAD and

left-sided colitis and validated, by real-time reverse transcription polymerase chain reaction (RT-PCR) and immunohistochemistry (IHC), a panel of deregulated transcripts that were selected based on their known involvement in inflammatory and neoplastic processes. Additional network analyses and detailed interrogation of specific molecular participants were not provided by the Bjerrum study (Bjerrum et al., 2014).

Subsequently, the GSE47908 dataset was employed by multiple studies to investigate key genes and/or biological processes that contribute to UC. Most commonly, GSE47908 was combined with other datasets from the Gene Expression Omnibus (GEO) database to conduct differential expression comparison of UC vs. normal samples. As an example, Kaiko and colleagues included GSE47908 as part of their multi-institute retrospective cohort study which identified plasminogen activator inhibitor-1 as a key link between the epithelium and inflammation (Kaiko et al., 2019). Unfortunately, when these studies consolidated GSE47908 with other datasets from the GEO database, the key strength of GSE47908 was inadvertently lost. That is, the extent of disease, which may affect transcriptional profiles, was no longer accounted for. Several research groups capitalized on the clear distinction made on UC extent by Bjerrum and colleagues by undertaking weighted gene co-expression analysis (WGCNA) in search of genes that may play a part in the progression of UC. However, in my opinion, these studies contain methodological issues with WGCNA that puts into question the conclusions made.

The questions I aimed to answer with the GSE47908 dataset were: 1) How does the extent of colitis impact biological functions and regulatory pathways? 2) What are the key molecular factors that bridge the colitis-dysplasia progression? And 3) How do these key molecular factors relate to one another, and to DAPK3? To answer these questions, I performed differential expression analysis, pathway analysis, network analysis, and differential correlation analysis on the GSE47908 dataset.

Results from this exploratory study should provide insight into the molecular events associated with colitis-dysplasia progression, which could be exploited for the development of biomarkers in non-dysplastic mucosa that identify the risk of dysplasia for UC patients.

2.2. Methods.

2.2.1. Differential Gene Expression Analysis.

Log transformed microarray expression data for GSE47908 and microarray platform data for GPL570 (HG-U133_Plus_2; Affymetrix Human Genome U133 Plus 2.0 Array) was retrieved from the GEO database (https://www.ncbi.nlm.nih.gov/geo/) via R package GEOquery (Davis & Meltzer, 2007). The limma workflow (Ritchie et al., 2015) was used to detect differentially expressed transcripts between the UC-subtypes [left-sided colitis (n=20), pancolitis (n=19), CAD (n=6)], and HC samples (n=15). Specifically, the function |lmFit| was used to generate a linear model fit to the data matrix containing log expression values for GSE47908. Next, function |contrasts.fit| was used to compute estimated coefficients and standard error for a given set of contrasts (e.g., pancolitis vs. HC). Finally, function |eBayes| was used to compute log-odds of differential expression by empirical Bayes moderation of the standard errors towards a global value. All functions were operated with default settings.

Log-fold changes calculated by function |eBayes| for 54,675 transcripts, along with their false discovery rate (FDR) and p-values, were uploaded to the Ingenuity Pathway Analysis (IPA) software (Krämer et al., 2014). Some Affymetrix transcript identifiers remain unmapped by IPA; these transcripts were eliminated from the study, leaving 45,480 transcripts to be mapped by IPA. Due to redundancy of the GeneChip HG-U133 Plus 2.0 Array, this transcript pool included duplicate genes. To resolve duplicates, IPA Core Analyses were performed on the mapped

transcripts, and transcript identifiers were consolidated using their log_2FC measurement, by which, representative transcript was selected based on maximum absolute log_2FC. This returned 21,475 'analysis-ready' genes. To distinguish differentially expressed genes (DEGs), the combined application of a stringent FDR threshold ($q < 0.001$) and a moderate fold change threshold ($|log_2FC| > 0.75$) was used. This reduced the number of false positives while maintaining the 'ideal' dataset size (200-3,000 genes) for subsequent IPA Core Analysis from gene expression data (Krämer et al., 2014). Differential expression was then visualized via the EnhancedVolcano R package (Blighe et al., 2021)

2.2.2. Functional Analysis of DEGs of UC-Subtypes.

To compare lists of DEGs and illustrate possible relationships between left-sided colitis, pancolitis, and CAD, a Venn diagram was first used to visualize the overlap of DEGs found in the three UC-subtypes. The lists of overlapping DEGs derived from the comparison of UC-subtypes were then used as input data for gene ontology (GO) enrichment analysis, performed with the topGO R package (Alexa & Rahnenführer, 2021). topGO was chosen owing to its *'elim'* method, that take GO hierarchy into consideration when calculating enrichment. In brief, the algorithm accounts for the *'inheritance problem'* (i.e., where root terms inherit annotations from descendent terms, which can lead to generation of false positives) in GO enrichment analysis by disregarding genes that had already been annotated with significantly enriched descendant GO terms. For the enrichment analysis, the background consisted of all genes assessed by the microarray platform GPL570, and annotation was completed with the R package org.Hs.eg.db (M. Carlson, 2021); GO terms with <=10 annotations were excluded for interpretability. The degree of enrichment was reported as the odds ratio (OR), where I^A = # DEGs annotated with the GO term, I^B = # background genes annotated with the GO term, and OR = (I^A/size of DEG list) / (I^B/size of background list). Statistical

significance was defined with a Fisher's Exact Test. Data processing was completed using the R (v4.0.2) programming language, and all codes used in this thesis align with recommendations made by authors of R packages in their respective user's guide, which can be accessed at https://bioconductor.org.

2.2.3. Ingenuity Pathway Analyses.

To analyze changes in biological states across UC-subtypes, three sets of IPA Core Analyses were performed, followed by IPA Comparison Analysis. The IPA Comparison Analysis allows for side-by-side comparison of multiple Core Analyses, which facilitated the discovery of trends amongst the three datasets.

Core Analyses were performed on the three datasets (left-sided colitis vs. HC, pancolitis vs. HC, and CAD vs. HC) to assess the canonical pathways, upstream regulators, molecular and cellular functions, and molecular interaction networks that are most likely to be perturbed based on the changes of gene expression. Within IPA, canonical pathways were built with reference to literature prior to DEG input and did not undergo structural changes upon DEG input. Instead, IPA computes a z-score that assesses the directionality within a gene set (the DEG input) to infer the activation state of each canonical pathway or molecular and cellular function. Upstream regulators were identified by the observed differential regulation of known downstream effector(s). The z-score determines the activation state of an upstream regulator by the regulation direction associated with the relationship from the upstream regulator to the effector(s). A negative z-score indicates inhibition, and a positive z-score indicates activation. Significance was calculated with the right-tailed Fisher's Exact Test. Changes in activation state across UC-subtypes were assessed with Comparison Analysis (sort method = trend + z-score). In this study, I examined the correlation of

activation state as the extent of disease progressed from left-sided colitis to pancolitis to CAD (the trend) and reported the findings as trending towards activation or trending towards deactivation.

With regards to molecular interaction networks, DEGs from the three datasets were mapped to their corresponding gene objects in the Ingenuity Knowledge Base (IKB), and those that interacted with other molecules in the IKB were designated focus molecules. Focus molecules were then assembled into networks by maximizing their interconnectedness with each other (relative to non-focus molecules with which they are connected to in the IKB). While non-focus molecules from the IKB may be used to merge smaller networks into a larger network, networks are scored based on the number of focus molecules they contain. Network size, the total number of focus molecules analyzed, and the total number of molecules in the IKB that could be included in the networks also contribute to the network scores. The score is a test of significance using hypergeometric distribution and is calculated with the right-tailed Fisher's Exact Test (Score = -log (Fisher's p-value; score ≥ 2 equals $p \leq 0.01$). The higher the score, the lower the probability of finding the observed number of focus molecules in each network by random chance. For this study, networks were limited to 70 molecules each, and a maximum of 25 networks per UC-subtype were constructed. Individual networks (child networks, count = 75) were overlapped with one another to create a single parent network by virtue of common network molecules between child pairings; this was done with the RVenn R package (Akyol, 2019). Finally, the edge betweenness parameter for the parent network was computed via the NetworkAnalyzer app, included in Cytoscape 3.8.0 (Shannon et al., 2003).

2.2.4. Differential Correlation.

ggpubr, a ggplot2-based R package (Kassambara, 2020), was used to investigate the relationship between expression profiles of two genes *x* and *y*. A Shapiro-Wilk normality test was conducted

to resolve redundancies for the *YAP*, *DAPK3*, and *PPP1CB* probe-sets prior to completion of the parametric correlation analyses. Specifically, function |stat_cor| was used to calculate the Pearson correlation coefficient. The size of the concentration ellipse in normal probability was left at the default 0.95, which translates to a 95% confidence interval.

2.3. Results.

2.3.1. Genes Differentially Expressed in UC Subtypes.

The distribution of gene expression ratios (log-transformed) calculated between UC subtypes and HC is presented in **Figure 4**. For the left-sided colitis vs. HC comparison, 1,016 genes had $\log_2$FC greater than 0.75 ($q < 0.001$); of these DEGs, 614 were upregulated, and 402 were downregulated. Pancolitis returned 2,858 DEGs, half of which were upregulated. CAD returned 1,842 DEGs; 393 were upregulated, and 1,449 were downregulated.

2.3.2. Functional Analysis of DEGs of UC-Subtypes.

For functional predictions, a Venn diagram was first used to delineate genes with expression regulation observed in two or three UC subtypes (**Appendix A**). As can be seen in **Figure 5**, pancolitis straddled both left-sided colitis and CAD in terms of common DEGs. Of the 2,858 pancolitis DEGs, 651 shared similar expression regulation as left-sided colitis DEGs (465 common upregulation plus 159 common downregulation), and 1,194 shared similar expression regulations as CAD DEGs (209 common upregulation plus 985 common downregulation). This feature was not observed when comparing left-sided colitis and CAD. Less than 2% of the input DEGs appeared at the intersection of left-sided colitis ∩ pancolitis ∩ CAD. This analysis suggests pancolitis as the middle ground of UC subtypes that bridges the progression of UC from left-sided

colitis to CAD. Thus, the DEGs located at the intersection of pancolitis ∩ left-sided colitis or pancolitis ∩ CAD (**Appendix A**) were utilized for functional analysis.

To identify the potential biological processes associated with UC progression, two sets of DEGs at the intersection of 1) pancolitis ∩ left-sided colitis, or 2) pancolitis ∩ CAD were processed separately with the topGO R package for functional enrichment analysis. These enrichment analyses included both up-regulated and down-regulated genes. The top 10 terms from the Biological Process (BP) category of the GO enrichment analysis are presented in **Figure 6**. The DEGs at the intersection of pancolitis and left-sided colitis were enriched in inflammatory processes (**Appendix B**) while the pancolitis ∩ CAD overlapping DEGs were enriched in actin-based processes (**Appendix C**). Specifically, the pancolitis ∩ left-sided colitis DEGs showed significant enrichment for the regulation of IFN-γ mediated signaling pathways (GO:0060334), the antimicrobial humoral immune response mediated by antimicrobial peptide (GO:0061844), and the acute-phase response (GO:0006953) with 8.6-, 6.4-, and 6.0-fold enrichments, respectively. Across the pancolitis ∩ CAD DEGs, microvillus assembly (GO:0030033), Golgi to plasma membrane transport (GO:0006893), and actin cytoskeleton reorganization (GO:0031532) were found significantly over-represented with 6.3-, 3.1-, and 3.0-fold enrichments, respectively. Overall, the GO enrichment analysis suggests that as UC progressed from left-sided colitis to pancolitis to CAD, the transcriptome pattern shifted from being immune-centric to being cytoskeleton-dependent. Presumably, the regulation of actin cytoskeleton organization plays an important role in colitis-dysplasia progression.

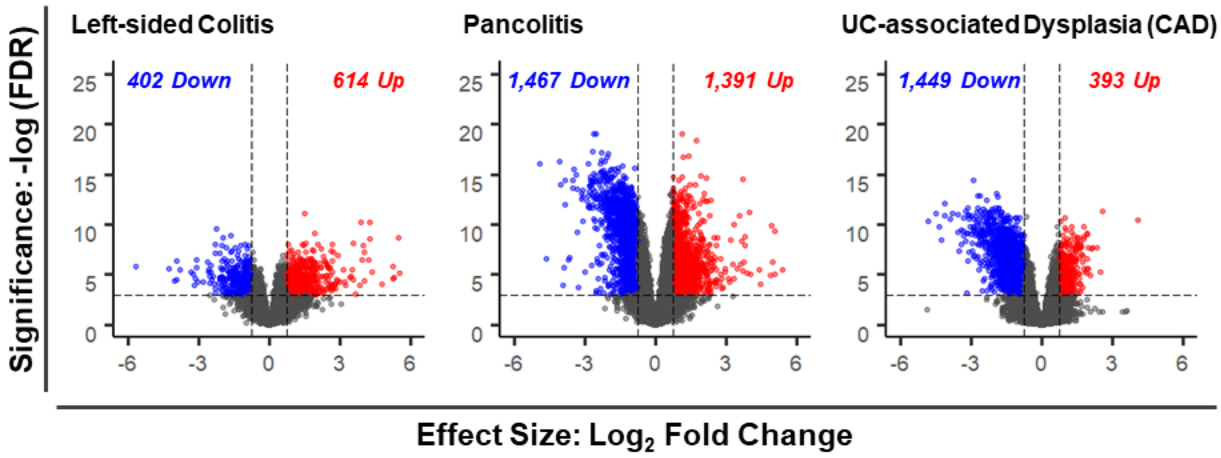

Figure 4. Differential gene expression of the three UC subtypes against healthy controls. Log_2FC calculated with limma R on GSE47908 [n = 15 (HC), 20 (Left-sided colitis), 19 (Pancolitis), and 6 (CAD)]. Threshold set for log_2FC was |0.75|. Significance was determined by FDR ($q<0.001$).

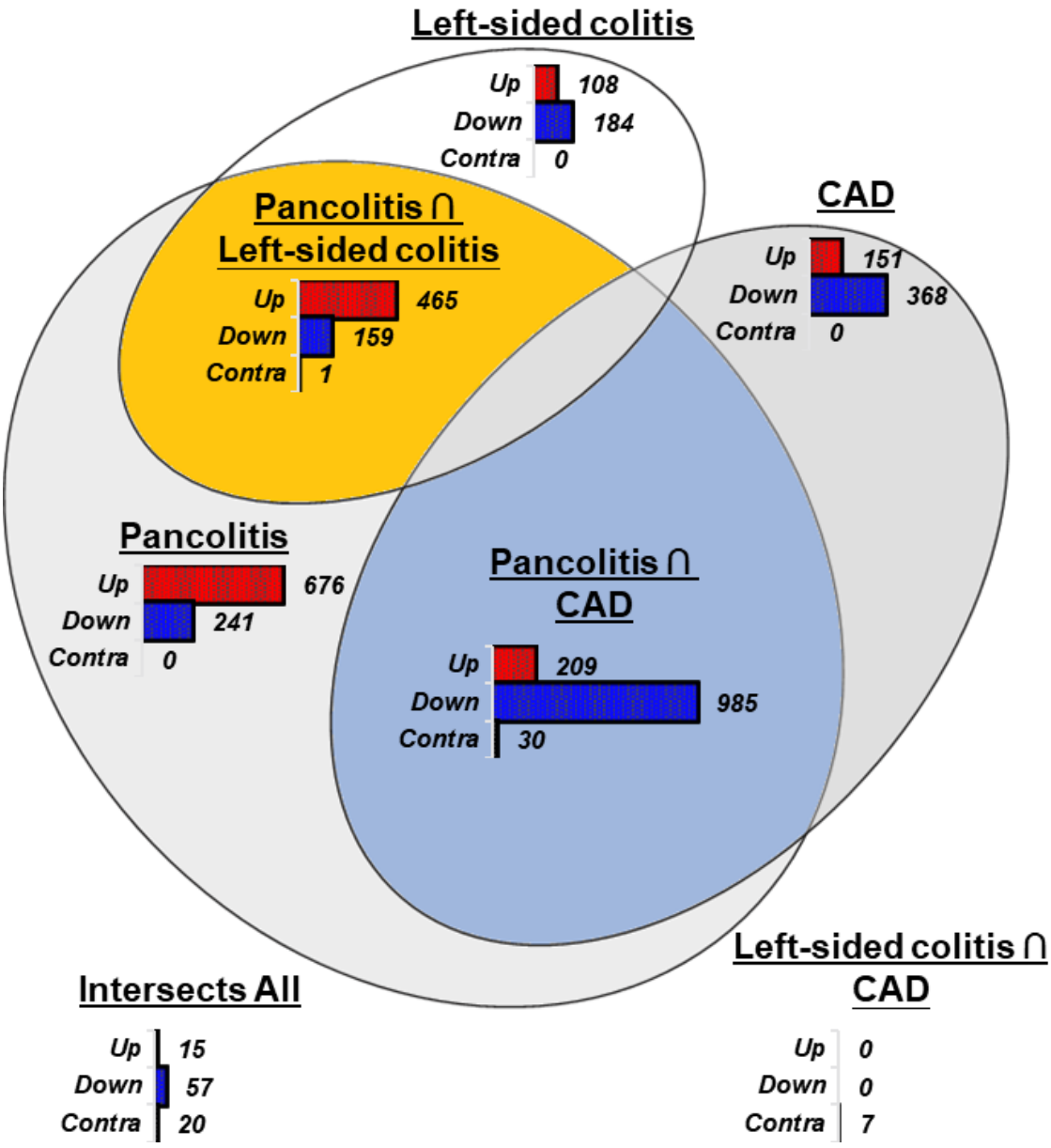

Figure 5. Overlap of shared differentially expressed genes (DEGs) between UC subtypes. Proportional Venn diagram was calculated with the BioVenn web application (https://www.biovenn.nl/), then optimized with the eulerAPE_3.0.0.jar. Complete gene lists can be found under **Appendix A**.

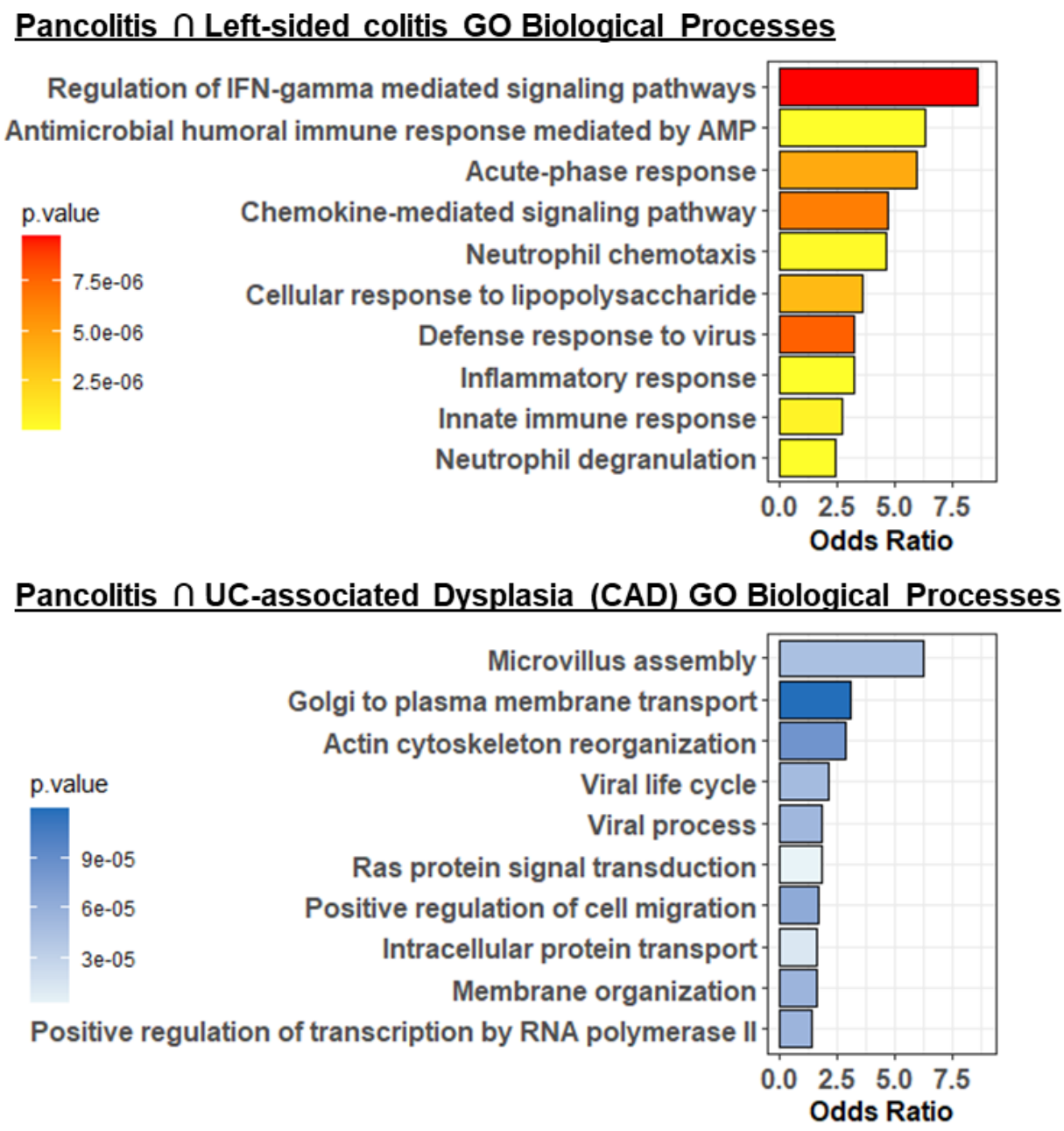

Figure 6. Gene ontology (GO) term enrichment analysis of common differentially expressed genes (DEGs) between colitis-subtypes. DEGs at the intersection of Pancolitis ∩ Left-sided colitis or Pancolitis ∩ CAD were subjected to GO term enrichment analysis for Biological Process categories. Enrichment was performed with topGO R ("*elim*" algorithm, "*fisher*" statistic). Statistical significance was defined with a Fisher's Exact Test. Complete gene lists can be found under **Appendix B** and **Appendix C**.

2.3.3. Association of Hippo Signaling Activation to Colitis-Dysplasia Progression.

To identify canonical pathways that are most relevant to the observed shift in gene expression profile (**Figure 5**), a comparison analysis heat map for canonical pathways significantly altered by UC-subtypes was constructed (**Figure 7**); This heatmap displays the trend of either activation or deactivation as the gene expression profile shift in response to UC extent, that is, from left-sided colitis to pancolitis to CAD. The heatmap revealed Hippo signaling and Ephrin receptor signaling as the top canonical pathways that were progressively altered in concert with the extent of UC. The Hippo signaling pathway displayed incremental activation, while the Ephrin receptor signaling pathway exhibited gradual deactivation as the UC extent broadened (**Figure 7**). Diagrammatic comparison of Hippo and Ephrin receptor analyses conducted on UC-subtype DEGs are located in **Appendix D** and **Appendix E**, respectively.

To obtain a basic view of the molecular mechanisms underlying the extent of colitis, trends of activation or deactivation were also probed on upstream regulators and biological functions. In terms of upstream regulators, IL10RA exhibited a trend of increased activity whereas IFN-γ exhibited a trend of decreased activity. Affected biological functions include apoptosis and cell movement, that underwent gradual activation and deactivation, respectively, as disease extended from left-sided colitis to pancolitis to CAD. (**Figure 8**)

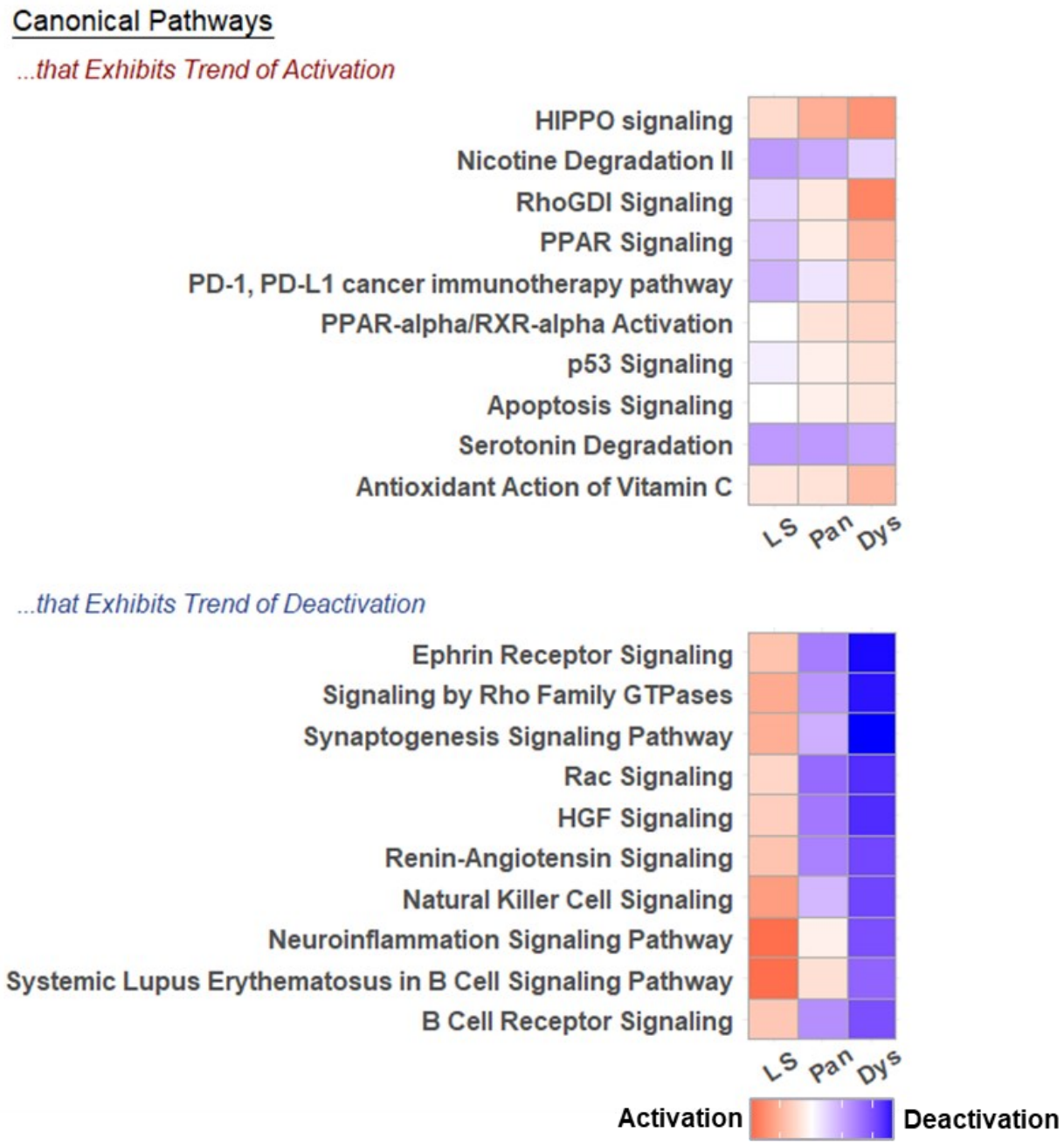

Figure 7. Ingenuity Pathway Analysis (IPA) heat map of canonical pathways differentially deregulated amongst colitis-subtypes. For each colitis subtype, the activation z-score calculated by IPA software predicts the activation (red) or inhibition (blue) potential for each canonical pathway. The pathways are sorted based on correlation of z-scores to extent of disease (Left-sided colitis to Pancolitis to CAD) with higher total scores across the colitis-subtypes ranked higher than those with lower total scores. LS: Left-sided colitis, Pan: Pancolitis, Dys: CAD.

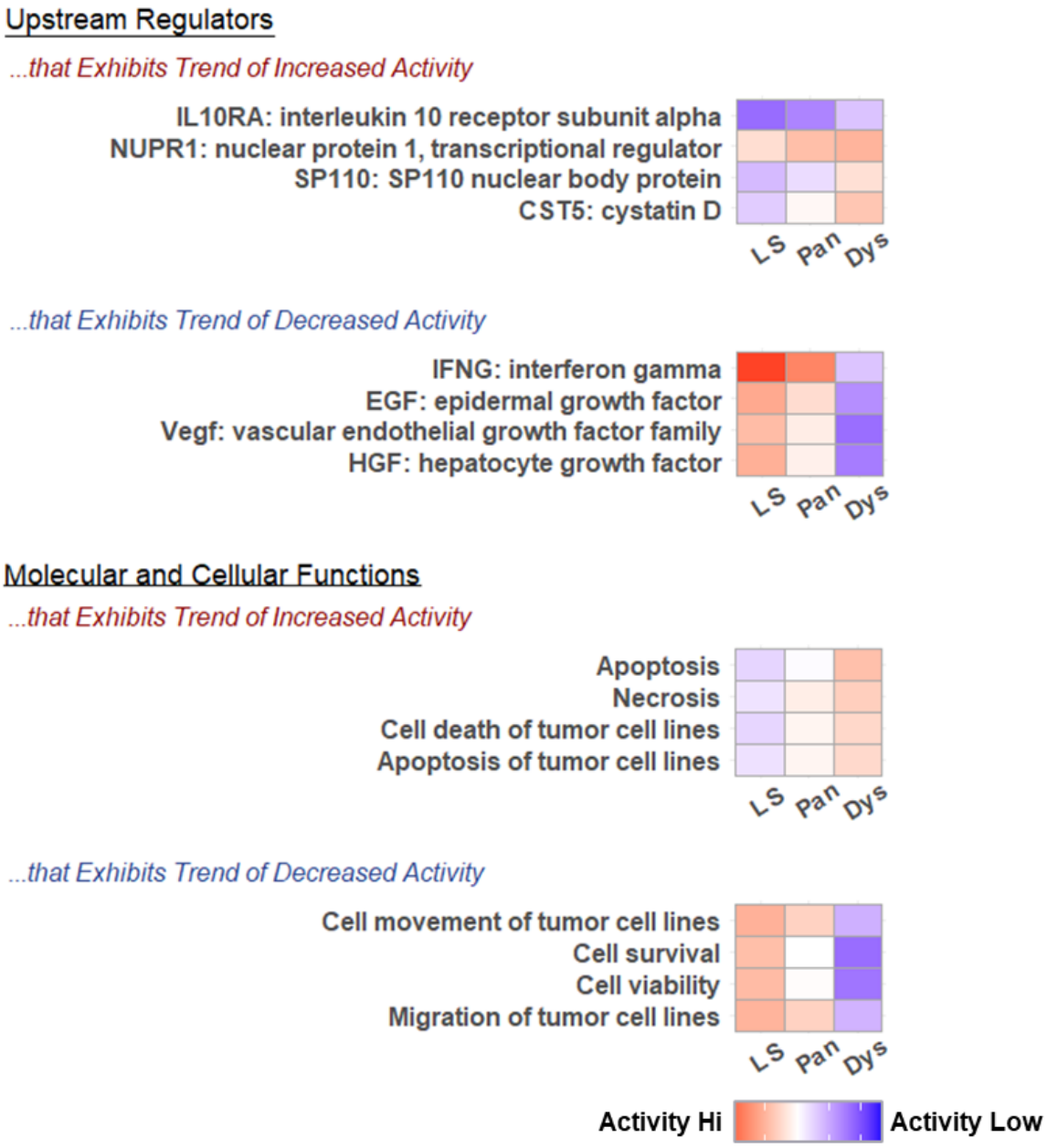

Figure 8. Ingenuity Pathway Analysis (IPA) heat map of upstream regulators and functions differentially deregulated amongst colitis-subtypes. For each colitis subtype, the activation z-score calculated by IPA software predicts the activation (red) or inhibition (blue) potential for each regulator/function. The regulators/functions are sorted based on correlation of z-scores to extent of disease (Left-sided colitis to Pancolitis to CAD) with higher total scores across the colitis-subtypes ranked higher than those with lower total scores. LS: Left-sided colitis, Pan: Pancolitis, Dys: CAD.

2.3.4. Actin Reorganization as a Potential Key Determinant for Colitis Progression.

By way of limma R-derived DEGs, the IPA software generated 25 networks for each of the three UC subtypes. Molecular network intersections, assembled with the RVenn R package, revealed a single parent network that connected all 75 child networks via 757 intersections/edges (**Figure 9A**). Among the 75 child networks, approximately two-third (48/75) were composed of less than 60 focus molecules (<85% focus molecules). The 757 intersections/edges that connected the child networks each comprise one to 24 common molecule overlaps. Nevertheless, over half (57%) of the interactions/edges were enabled by just one common molecule, and 87% of the edges involved less than four common molecules (<5% overlap). To reduce noise from the parent network depicted in **Figure 9A**, molecular network intersection was compiled once more, but with child networks that were built upon 60 or more focus molecules (>85% focus molecules) and preserving connections that were maintained by four or more common molecules (>5% overlap). This produced one core network of networks that connected 21 child networks with 21 edges; One intersection segment, though strongly connecting pancolitis network 6 to CAD network 10 with 24 common molecules (34% overlap), stood apart from the core network of networks (**Figure 9B**), so was excluded from subsequent analysis.

To pinpoint a network pairing that may be used to discern pathways or molecular processes bridging pancolitis to CAD, the measures 'count of overlapping molecules and 'value of edge betweenness' were utilized for edge evaluation. Edge betweenness reflects the amount of control that an edge exerts over the interactions of other child networks in the parent network; The edge betweenness of $e = (v, w)$ is defined as the number of shortest paths between two nodes s and t that go through e divided by the total number of shortest paths that go from s to t. Edge betweenness does not consider the number of overlapping molecules that contribute to the intrinsic strength of

each edge. Thus, additional consideration for this attribute was completed *post hoc*. As shown in **Figure 9B** and **Table 1**, the edge connecting pancolitis network 15 to CAD network 1 stood out from the remaining network associations by virtue of its 1) high count of overlapping molecules (20% overlap) and 2) high value of edge betweenness, which suggests that the removal of this edge may affect interactions between the remaining networks within network. Thus, the overlap between pancolitis network 15 and CAD network 1 was selected for detailed examination.

The intersection pancolitis 15 ∩ CAD 1 was formed by 14 gene products (13 focus molecules plus one IPA-derived molecule), which, when analyzed for GO term enrichment, was found to be highly enriched in actin-based processes (**Figure 10**). Specifically, the DEGs at this intersection showed significant enrichment for the ruffle organization (GO:0031529), the regulation of actin filament polymerization (GO:0030833), and the myofibril assembly (GO:0030239) GO terms with 66-, 33-, and 33- fold enrichments, respectively. However, within the confines of the IKB, none of the 13 focus molecules were directly linked to UC (**Appendix F**). All probable shortest paths by which the focus molecules were connected to UC required at least one IPA-derived intermediate molecules. For the majority of indirect connections, gene products CTNNB1 (β-catenin), CDH1 (E-Cadherin), and TNF (Tumor Necrosis Factor) functioned as the IPA-derived intermediate molecules (**Appendix F**).

2.3.5. Implication of DAPK3 as a Key Factor in Colitis-Dysplasia Progression.

Further dissection of pancolitis 15 and CAD 1 revealed two signal transduction gene products that reside in the overlap of these two networks (**Table 2**). Namely, DAPK3 as the sole protein kinase, and protein phosphatase PP1-β catalytic subunit (PPP1CB) as the sole protein phosphatase. The remaining 11 focus molecules were categorized as either mechanochemical enzymes (i.e., motors) or scaffolding proteins involving the cytoskeleton. Both DAPK3 and PPP1CB were downregulated

in pancolitis [log_2FC: -1.08 (DAPK3); -1.56 (PPP1CB)] and CAD [log_2FC: -0.98 (DAPK3); -1.52 (PPP1CB)] but showed no deregulation in left-sided colitis. Presumably, DAPK3 and PPP1CB act as key factors regulating the altered molecular pathways that bridge pancolitis to CAD.

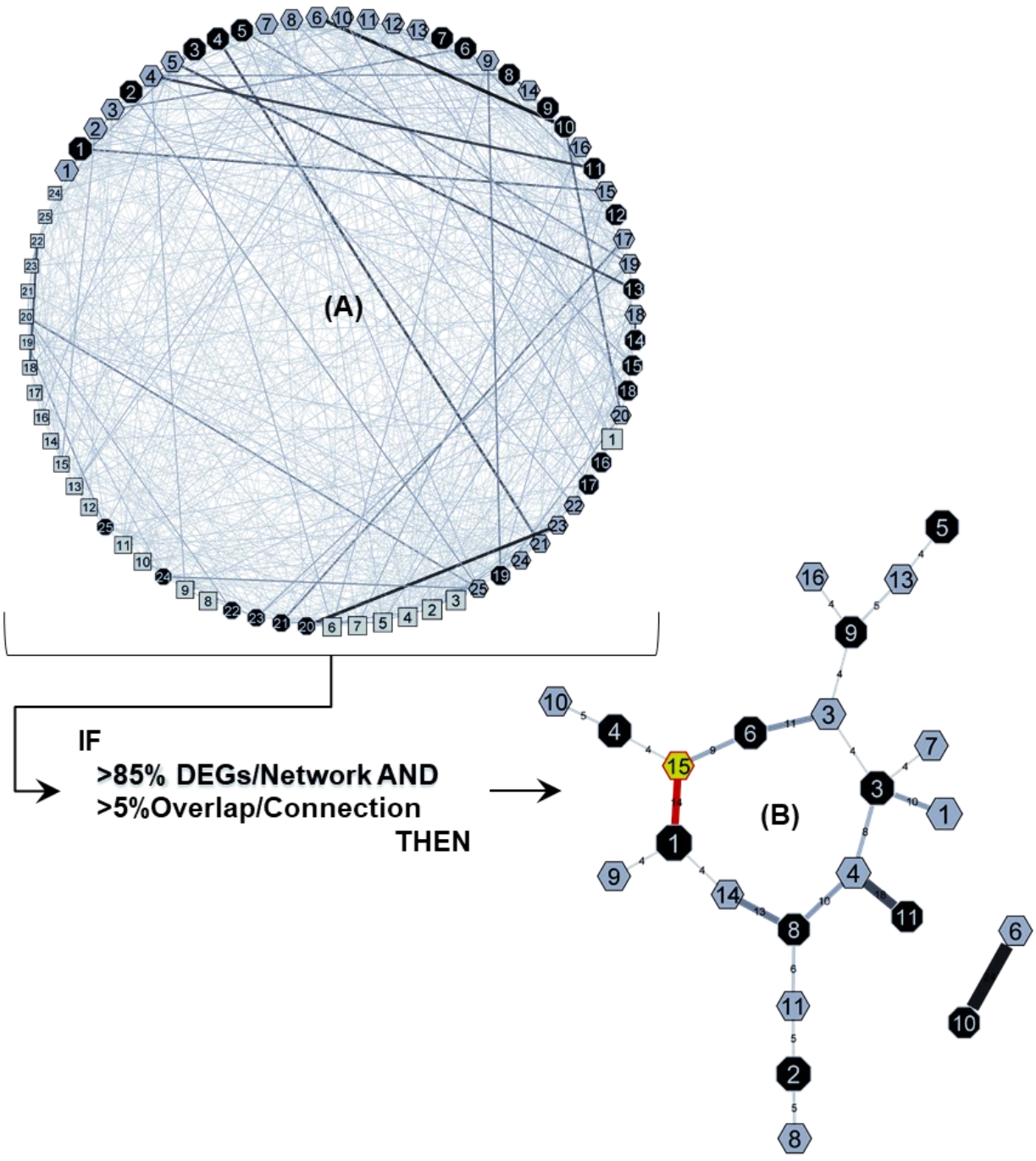
(A)
IF
>85% DEGs/Network AND
>5%Overlap/Connection
THEN
(B)

Figure 9. Intersections of UC-subtype molecular interactions. Molecular networks were constructed for each UC subtype. Octagons represent networks constructed with CAD DEGs, hexagons represent Pancolitis networks, and rectangles indicate Left-sided colitis networks. Shape size represents the relative number of DEGs used to build each network. The networks are connected to each other if there are any overlapping gene products, and line width represent the number of shared gene products. The serpentine network overlap **(A)** was detangled by focusing on networks that had >85% of DEG inputs and keeping edges that involved >5% overlap of gene products. This returned a core network of networks **(B)** that was heavily leveraged on the edge connecting CAD network 1 and Pancolitis network 15 (Red).

Table 1. Edge attributes of the core network of networks. The edge connecting CAD network 1 (CAD.1) and pancolitis network 15 (Pan.15) was selected based on the number of overlapping molecules and degree of betweenness. Edge betweenness was computed with Cytoscape (3.8.0) NetworkAnalyzer.

Edge	No. of Overlapping Molecules	Edge- Betweenness*
CAD.1 (Overlap) Pan.15	14	89
CAD.8 (Overlap) Pan.14	13	87
CAD.6 (Overlap) Pan.3	11	109
CAD.8 (Overlap) Pan.4	10	119
CAD.6 (Overlap) Pan.15	9	101
CAD.3 (Overlap) Pan.4	8	127
CAD.8 (Overlap) Pan.11	6	108
CAD.3 (Overlap) Pan.3	4	139
CAD.8 (Overlap) Pan.3	4	136
CAD.1 (Overlap) Pan.14	4	81

*Edge betweenness reflects the amount of control that an edge exerts over the interactions of other nodes in the network. This measure does not consider the number of overlapping molecules that contributes to the intrinsic strength of each edge. Consideration for the strength attribute was thus completed *post hoc*.

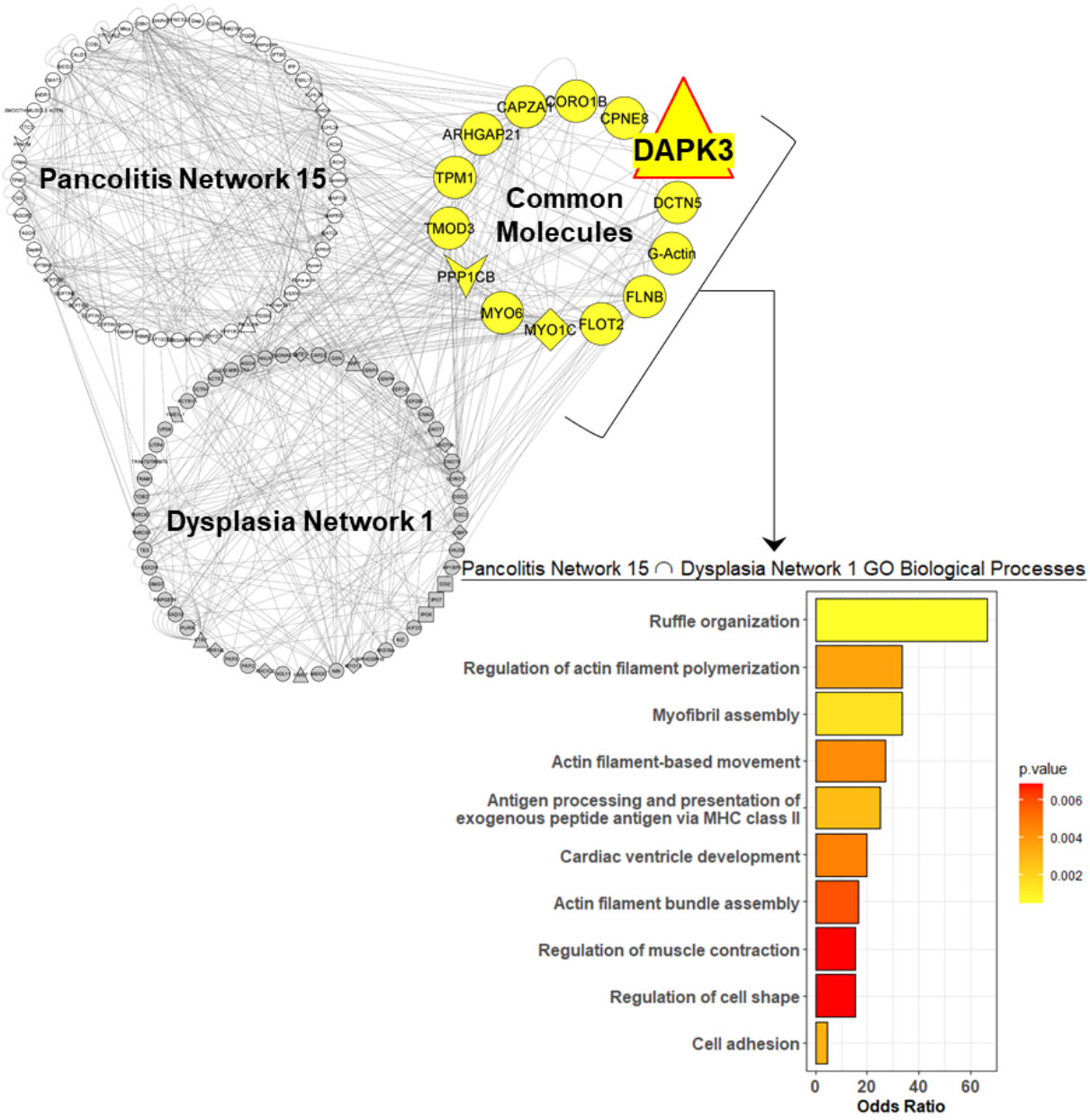

Figure 10. GO term enrichment analysis of the Pancolitis network 15 and CAD network 1 intersection. DEGs at the intersection of Pancolitis network 15 ∩ CAD (Dysplasia) network 1 were subjected to GO term enrichment analysis in the Biological Process categories. Network constructed by IPA software. Network intersection compiled with RVenn R. Edge betweenness computed with Cytoscape (3.8.0) NetworkAnalyzer. Enrichment performed with topGO R. Statistical significance was defined with a Fisher's Exact Test.

Table 2. List of overlapping gene products in the Pancolitis 15 ∩ CAD 1 intersection.

Gene	Protein	Molecular Function	Expression FC		
			L	P	D
DAPK3	Death-associated protein kinase 3	Kinase	-0.15	-1.08§	-0.98§
PPP1CB	Protein phosphatase PP1β subunit	Phosphatase	-0.12	-1.56§	-1.52§
MYO1C	Unconventional myosin IC	Motor	-0.18	0.77*	0.99*
MYO6	Unconventional myosin VI	Motor	-0.31	-0.88§	-1.36§
ARHGAP21	Rho GTPase-activating protein 21	GTPase	-0.48	-0.98§	-0.97§
CAPZA1	F-actin-capping protein α1	Actin Binding	0.18	-1.89§	-2.21§
CORO1B	Coronin 1B	Actin Binding	-0.08	0.88*	0.86*
CPNE8	Copine 8	Membrane Binding	-0.34	-1.55§	-1.93§
DCTN5	Dynactin 5	Scaffold	-0.20	-0.80§	-1.64§
FLNB	Filamin B	Actin Binding	-0.49	-0.76§	-1.20§
FLOT2	Flotillin 2	Scaffold	0.17	-0.78§	-0.95§
TMOD3	Tropomodulin 3	Actin Binding	-0.22	-1.36§	-2.15§
TPM1	Tropomyosin α1	Actin Binding	-0.61	-0.86§	1.01*
---	Monomeric (G) actin	Structural	Not a focus molecule		

FC=$\log_2$ fold-change. L = Left-sided colitis; P = Pancolitis; and D = UC-associated Dysplasia (CAD). A gene was deemed dysregulated when $|\log_2 FC|>0.75$ and FDR<0.001; * - significant upregulation, § - significant downregulation.

2.3.6. Correspondence of *DAPK3-YAP* Differential Correlation with UC-Extent.

Given the association of Hippo signaling activation with UC extent (**Figure 7**), and the implication of *DAPK3* and *PPP1CB* as key factors in colitis-dysplasia progression (**Figure 10** and **Table 2**), differential correlation analyses for the pairings *DAPK3-YAP* and *PPP1CB-YAP* were conducted to assess the difference in gene-gene regulatory relationships among the UC-subtypes.

The GSE47908 dataset was generated using the GeneChip HG-U133 Plus 2.0 Array, which included three probe sets for *YAP* (**Figure 11A**), three probe sets for *DAPK3* (**Figure 11B**) and four probe sets for *PPP1CB* (**Figure 11C**). Resolution of probe set redundancy with the IPA software returned one representative probe set each for *DAPK3* (203890_s_at) and *PPP1CB* (228222_at); however, two representative probe sets (213342_at and 224894_at) were resolved for *YAP*. To identify the *YAP* probe set that best satisfied the assumption of a Pearson correlation, namely, that the expression values represented by the probe sets are normally distributed, the Shapiro-Wilk test was performed separately for each probe set. Expression values represented by two of the three *YAP* probe sets (213342_at and 224894_at) conformed to a normal distribution (i.e., $p>0.05$ across all conditions, **Figure 11A**). Additionally, expression values represented by probe set 2133342_at returned higher mean W-value (0.948 vs. 0.940 for 213342_at and 224894_at, respectively). As such, expression values represented by probe set 213342_at was utilized for subsequent Pearson correlation analysis. The Shapiro-Wilk test was also performed for the *DAPK3* and *PPP1CB* probe sets. While the representative *DAPK3* probe set selected by IPA (203890_s_at) passed the test of normality (**Figure 11B**), the representative probe set selected by IPA for *PPP1CB* (228222_at) did not (i.e., with $p<0.05$ for Left-sided colitis, the null hypothesis of normality was rejected; **Figure 11C**). Because the *PPP1CB* expression values did not display a normal distribution, the Pearson's correlation test should not be used for population inferences.

However, a relationship between the expression of *PPP1CB* and *YAP* for this sample set could still be inferred. As such, for the sake of continuity, expression values derived from probe set 228222_at were used to study whether there was some association between the expression of *PPP1CB* and *YAP* and to estimate the strength of this relationship.

As shown in **Figure 12A**, the *DAPK3*-*YAP* correlation in HC (green) was negative but flipped to positive in left-sided colitis (blue). Moreover, as UC-extent progressed from left-sided colitis to pancolitis (yellow), then to CAD (red), the *DAPK3*-*YAP* correlation grew progressively more positive. The general direction of differential correlation for the *PPP1CB*-*YAP* pairing mirrors that of the *DAPK3*-*YAP* pairing (**Figure 12B**). However, the correspondence of *DAPK3*-*YAP* differential correlation with UC-extent, was less apparent for the *PPP1CB*-*YAP* pairing. This result suggests that changes in the potential regulatory relationship between *DAPK3* and *YAP*, conditioned on UC-extent, may contribute to UC progression.

(A)

	YAP.213342_at				YAP.224894_at				YAP.224895_at			
	Ctrl	*Left*	*Pan*	*CAD*	*Ctrl*	*Left*	*Pan*	*CAD*	*Ctrl*	*Left*	*Pan*	*CAD*
W	0.95	0.94	0.96	0.94	0.99	0.97	0.92	0.88	0.93	0.94	0.86	0.90
p-value	0.46	0.30	0.48	0.69	1.00	0.81	0.09	0.25	0.25	0.90	0.01	0.40

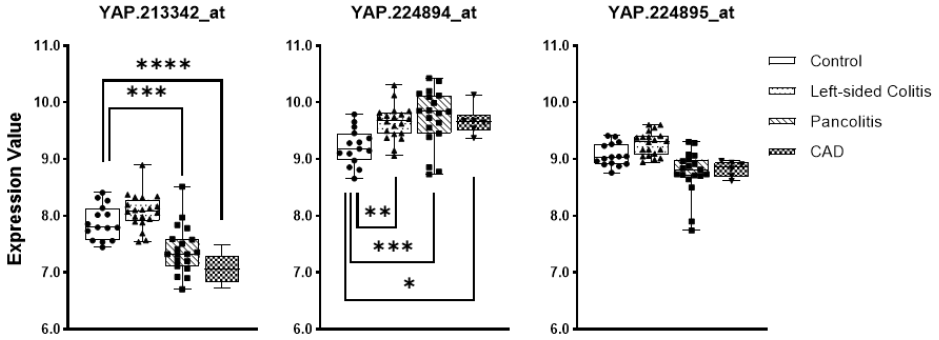

(B)

	DAPK3.203890_s_at				DAPK3.203891_s_at				DAPK3.228681_x_at			
	Ctrl	*Left*	*Pan*	*CAD*	*Ctrl*	*Left*	*Pan*	*CAD*	*Ctrl*	*Left*	*Pan*	*CAD*
W	0.95	0.96	0.95	0.87	0.96	0.96	0.80	0.97	0.94	0.97	0.96	0.86
p-value	0.56	0.49	0.40	0.25	0.69	0.50	0.00	0.90	0.39	0.85	0.52	0.19

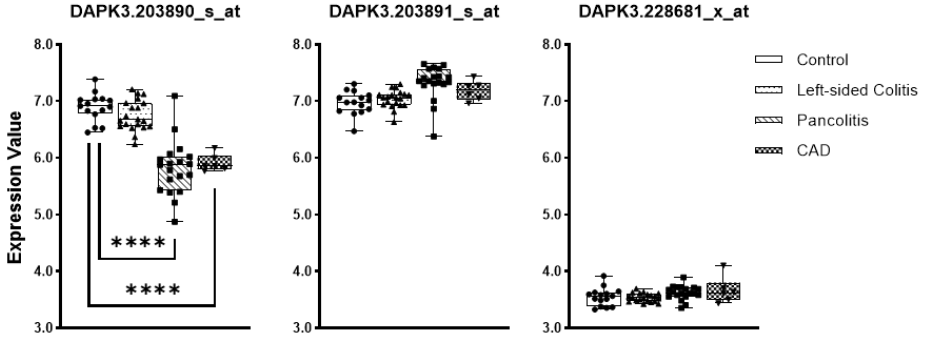

(C)

	PPP1CB.228222_at				PPP1CB.201407_s_at				PPP1CB.201408_at				PPP1CB.201409_s_at			
	Ctrl	*Left*	*Pan*	*CAD*	*Ctrl*	*Left*	*Pan*	*CAD*	*Ctrl*	*Left*	*Pan*	*CAD*	*Ctrl*	*Left*	*Pan*	*CAD*
W	0.96	0.87	0.91	0.89	0.97	0.87	0.98	0.92	0.97	0.95	0.94	0.94	0.95	0.92	0.95	0.83
p-value	0.70	0.01	0.08	0.32	0.87	0.01	0.93	0.55	0.82	0.38	0.22	0.69	0.60	0.10	0.47	0.12

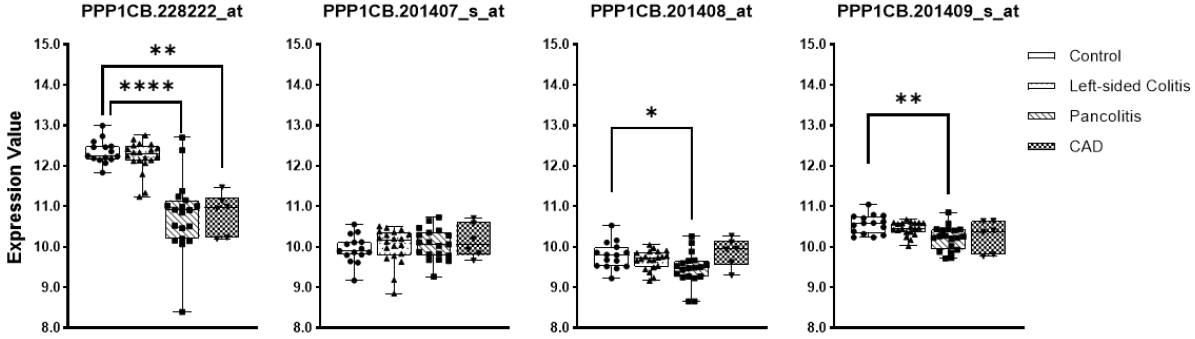

Figure 11. Test for normal distribution of *YAP*, *DAPK3*, and *PPP1CB* datasets. The data series GSE47908 was generated on the Affymetrix Human Genome U133 Plus 2.0 Array platform (Bjerrum et al., 2014), which included three probe sets for *YAP* (**A**), three probe sets for *DAPK3* (**B**), and four probe sets for *PPP1CB* (**C**). The IPA duplication resolution output returned one representative probe set for *DAPK3* (203890_s_at) and two representative probe sets for *YAP* (213342_at and 224894_at). To decide on a single representative *YAP*, *DAPK3*, and *PPP1CB* probe set for the parametric correlation analysis, the Shapiro-Wilk normality test was conducted. W- and p-values for the expression values represented by each of the unique probe sets are provided. Significant results suggest a deviation from normality. Boxplots of expression values represented by each of the probe sets are also provided. Error bars represent min/max. *p<0.05, **p<0.01, ***p<0.001, ****p<0.0001.

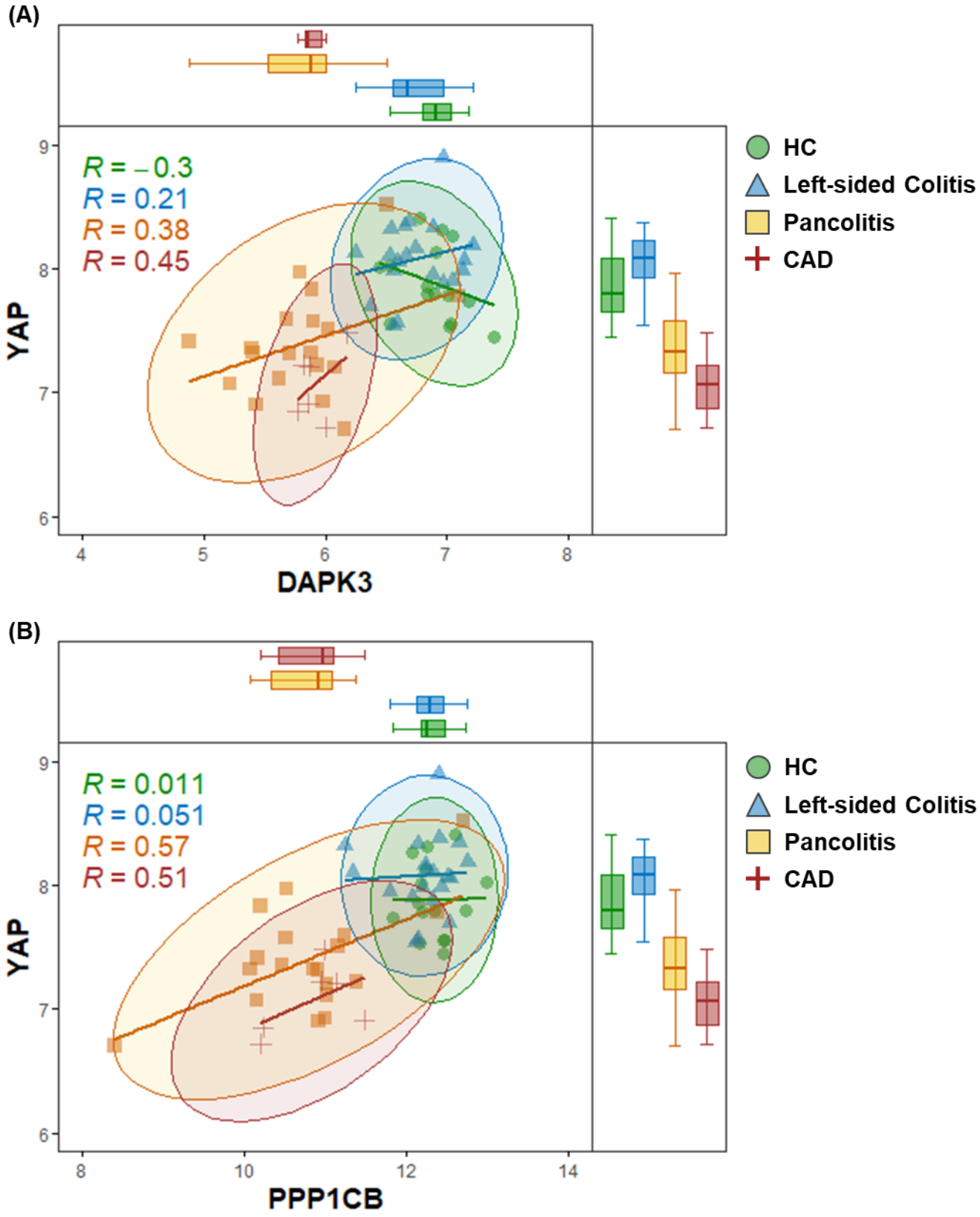
(A)
R = −0.3
R = 0.21
R = 0.38
R = 0.45
YAP
DAPK3
HC
Left-sided Colitis
Pancolitis
CAD
(B)
R = 0.011
R = 0.051
R = 0.57
R = 0.51
YAP
PPP1CB
HC
Left-sided Colitis
Pancolitis
CAD

Figure 12. Differential correlation of *DAPK3-YAP* and *PPP1CB-YAP*. The main panels display the relationship between the log-transformed expression profiles of *DAPK3* and *YAP* **(A)** or *PPP1CB* and *YAP* **(B)**. These scatterplots were overlayed with confidence ellipses of covariance, constructed for the 95% CI. In the marginal box plots of log-transformed gene expression, the lower whisker represents the lowest datum still within 1.5 interquartile range (IQR) of the lower quartile, and the upper whisker represent the highest datum still within 1.5 IQR of the upper quartile.

2.4. Discussion.

In UC, prolonged disease duration and extensive involvement (i.e., pancolitis) are associated with an increased risk for colorectal cancer (Q. Zhou et al., 2019). The progression of carcinogenesis in UC is thought to be driven by chronic inflammation and proceeds in a stepwise manner through a colitis-dysplasia-carcinoma sequence (Grivennikov, 2013; Itzkowitz & Yio, 2004). While one should not discount the impact that inflammation can have on carcinogenesis, evidence suggests that non-inflammatory factors also play a role in mediating the colitis-dysplasia-carcinoma progression (Grivennikov & Cominelli, 2016; Robles et al., 2016; Van Der Kraak et al., 2015). As an example, Arthur and colleagues found that while AOM-treated *IL10*$^{-/-}$ mice infected with colitogenic *E. coli* NC101 or *E. faecalis* OG1RF exhibited a similar degree of colitis and comparable levels of immune infiltrate, tumors were observed in only 10% of *E. faecalis* infected mice whereas 80% of *E. coli* infected mice showed tumor development. The authors then associated the polyketide synthase (*pks*) genotoxic island, found in *E. coli* NC101 but not *E. faecalis* OG1RF, with the DNA damage and subsequent tumorigenesis in their *E. coli* infected mice (Arthur et al., 2012). Meanwhile, gene mutation and gene expression analyses have associated cytoskeleton remodeling to colitis-dysplasia-carcinoma progression (Kanaan et al., 2010; Robles et al., 2016). Elucidation of the mechanisms of CAC carcinogenesis requires further investigation, and insight into the molecular events underpinning the progression of UC to CAC may be gained from the study of non-dysplastic colitic mucosa (Baker et al., 2019; Bjerrum et al., 2014).

The purpose of this bioinformatic study was to use publicly available gene expression profiles of colonic mucosal biopsies from healthy controls and patients with UC to identify variables associated with the carcinogenic behaviour of pancolitis. To this end, the dataset generated by

Bjerrum and colleagues (Bjerrum et al., 2014), composed of transcriptional profiles of colonic mucosa from patients with varying extent of UC, was utilized. Regrettably, while there exist other microarray datasets that incorporate the extent of disease as a variable, CAD does not form part of the variable selection. Furthermore, in these datasets, the anatomic location of biopsy collection was either not reported or varied across samples (Ouahed et al., 2018; Planell et al., 2013; Smith et al., 2014; Vinayaga-Pavan et al., 2019). To minimize subjective interpretation, a validation dataset was not included in this thesis.

Out of the Bjerrum dataset, 651 and 1,194 parallel dysregulated transcripts were identified at the intersection of pancolitis ∩ left-sided colitis and pancolitis ∩ CAD, respectively. GO term enrichment analysis showed that the parallelisms of pancolitis with CAD were rooted in dysregulation of actin-based processes, whereas the similarities between pancolitis and left-sided colitis were rooted in dysregulation of inflammatory processes. This finding substantiates results of a gene expression analysis of patients with CAC presented by Kanaan and colleagues, identifying actin cytoskeleton organization as the most significantly disrupted process in UC progression (Kanaan et al., 2010). Protein abundance analysis of UC progressors (UC patients with CAD or CAC) vs. UC non-progressors, carried out by May and colleagues, also identified enrichment of dysregulated cytoskeletal proteins in UC progressors (May et al., 2011). Drawbacks in the two aforementioned studies are 1) the evaluation of UC progression in a binary fashion (presence or absence of CAD/CAC), and 2) the small sample sizes (three unique patients in the study conducted by Kanaan and colleagues (Kanaan et al., 2010), and 15 unique patients in the study conducted by May and colleagues (May et al., 2011)). To provide insight into the molecular events associated with the stepwise progression of UC, it is necessary to demonstrate that the dysregulations observed in CAD or CAC were issued forth from some form of non-dysplastic UC.

The dataset generated by Bjerrum and colleagues provided an excellent opportunity to perform such analysis. Utilizing the Bjerrum dataset, this thesis verified pancolitis as a conduit for UC advancement from left-sided colitis to CAD, confirming dysregulation of actin reorganization as a key determinant for the progression of UC from non-dysplastic to dysplastic UC.

Signal transduction pathways regulate many cellular functions that were found altered in UC carcinogenesis, such as proliferation, growth, differentiation, metabolism, and survival. Studies that investigated the molecular alterations in CAC have previously associated STAT3, Wnt, TGF-β, and TLR4/NFκB signaling with the pathogenesis of CAC (Chandrasinghe et al., 2018; Muller et al., 2020; Shenoy et al., 2012). However, pathways most relevant to the gene expression changes observed during the progression of UC, before any histological evidence of dysplasia/carcinoma in UC, remain unknown. In my quest to answer how known signaling pathways conform to the extent of colitis to bring about dysplasia-inducing molecular changes, Hippo signaling and Ephrin receptor signaling were uncovered as the top canonical pathways that were progressively altered in concert with the extent of UC.

The Hippo pathway is a signaling cascade that negatively regulates the activity of YAP/TAZ to coordinate cell proliferation, apoptosis, and cell movement; as such, it is essential for tissue homeostasis, repair, and regeneration. Importantly, YAP/TAZ-mediated cell proliferation in epithelial monolayers is controlled by a cytoskeletal checkpoint, which in turn, is monitored by actin-processing factors (**Section 1.8**). The Ephrin pathway also controls intestinal homeostasis through cell proliferation and cell movement additionally to cell attachment and repulsion. However, deciphering functional outcomes by Ephrin pathway activation is circuitous due to the redundancy and idiosyncrasy of this pathway. The Ephrin receptors (Eph) comprise the largest family of receptor tyrosine kinase (RTK). But, unlike most RTKs whose ligands are generally

soluble, the cognate ligands of Eph receptors, the ephrins, are also membrane bound. This aspect of the Eph-ephrin receptor-ligand pairing consequently induces bidirectional signaling, where signaling through Eph is termed forward signaling and through ephrin is termed reverse signaling. Furthermore, there is a plethora of Ephs and ephrins (i.e., 14 Ephs, 8 ephrins) with promiscuous pairing options. Finally, Eph/ephrin also exhibits cis interaction to inhibit forwarding signaling (Darling & Lamb, 2019; Perez White & Getsios, 2014). Ephrin is therefore a more convoluted pathway to render, relative to the Hippo pathway.

Using the DSS-induced colitis mice model, the Hippo pathway was identified as a key factor for the compensatory regeneration of IECs in response to tissue injury (J. Cai et al., 2010). The recent emergence of YAP as a potential regulator of intestinal diseases involves elements beyond the canonical Hippo pathway. For one, YAP can be sequestered at AJs via interactions with α-catenin (Schlegelmilch et al., 2011), a molecule whose abundance is significantly altered in active UC (Karayiannakis et al., 1998). Secondly, nuclear translocation of YAP may be brought about via stimulation of gp130-associated Src family kinase Yes (Taniguchi et al., 2015). Finally, YAP was found to be a crucial pivot point of cellular reprograming during intestinal epithelial repair, coupling epithelial restitution to the proliferative phase of regeneration by way of FAK-Src signaling (Yui et al., 2018). In view of YAP as a mechanosensor and mechanotranducer amidst IEC regeneration of injured tissues, a comprehensive understanding of the interplay between YAP and the actin cytoskeleton is needed to make rational selections of therapeutic targets for patients at high risk of UC neoplastic progression.

The identification of DAPK3 as a potential key factor in UC progression is particularly interesting. Had the relevance of *DAPK3* to UC been judged solely by its differential expression in inflamed tissues from each UC-subtype, independently of one another, the analysis would come to naught.

Notably, the same statement also applies to the canonical pathway analysis done for this thesis (i.e., the importance of Hippo signaling would not be recognized). Be that as it may, DAPK3 and the Hippo pathway, two factors with known influence on cytoskeleton-related cellular functions that are altered in UC carcinogenesis, displayed significance in UC progression when UC-subtypes were overlayed with one another during bioinformatic analyses.

The role that DAPK3 plays in UC was unknown prior to this study. However, the upstream regulator of DAPK3, DAPK1, was previously associated with UC severity (Kuester et al., 2010). Further, pharmacological inhibition of DAPK1 was reported to augment susceptibility to DSS-induced colitis in mice, with concomitant increase in bacterial translocation that was ascribed to barrier defects (Lopes et al., 2018). It is interesting to note that DAPK6 (a.k.a. DI), the DAPK1 inhibitor employed by Lopes and colleagues for their study of tunicamycin (TM)-induced, ER-stress-dependent reduction of bacterial translocation, cross-inhibits DAPK3 (IC_{50}=225 nM) and ROCK (K_i=132 nM) (Al-Ghabkari et al., 2016; Okamoto et al., 2009). Although the Lopes et al. study included siRNA knockdown experiments to test whether DAPK1 signaling was needed for TM-induced ER-stress response, the potential impact of concurrent DAPK3 and ROCK inhibition, brought forth with DAPK6, was not examined. Ito and colleagues showed that ROCK activity increased in response to TM, and that treatment with Y27632 [a ROCK inhibitor: K_i=220 nM for ROCK1, K_i=300 nM for ROCK2 (Davies et al., 2000; Ishizaki et al., 2000)] completely reversed the TM-induced ER-stress response in the J774 macrophage cell line (Ito et al., 2020). The involvement of DAPK3 in ER-stress response was demonstrated in human aortic vascular smooth muscle cells (VSMCs), where shRNA-mediated silencing of *DAPK3* ablated the calcifying-media induced increase of CCAAT-enhancer-binding protein homologous protein (CHOP), a multifunctional transcription factor in ER-stress response (K.-X. Li et al., 2019). In the same study,

DAPK6 treatment attenuated vascular calcification in rats, alongside significant reduction in CHOP protein abundance in the aorta (K.-X. Li et al., 2019). It may be beneficial to learn whether DAPK3 and/or ROCK alter ER-stress-dependent autophagy in the context of DSS-induced colitis in mice.

The probability that DAPK3 plays a role in the progression of the pathological changes of UC is high. DAPK3 had been shown to influence growth of human colon carcinoma cell lines HCT-116 and Caoc-2 (Togi et al., 2011). In human, expression of *DAPK3* was highest in skeletal muscle, testis, lung, then colon and ovary; Moreover, the high expression of *DAPK3* in the colon was echoed in non-human primates (**Figure 13**). However, there has been no publication on *DAPK3* within the context of colitis or colitis-associated dysplasia-carcinoma. To substantiate the connection of DAPK3 to UC progression, the difference in correlation between *DAPK3* and *YAP* was studied in all UC-subtypes plus healthy control samples. Differential co-expression operates on the level of gene pairs and was suggested as an alternative approach to identifying disease-related genes (Lai et al., 2004; McKenzie et al., 2016). Results from the differential co-expression analyses demonstrate the correspondence of *DAPK3*-*YAP* correlation with UC-extent. This suggests that changes in the potential regulatory relationship between *DAPK3* and *YAP*, conditioned on UC-extent, may contribute to UC progression. Still, the driver(s) behind the differential *DAPK3–YAP* co-expression pattern is unclear. Better understanding of the DAPK3-YAP relationship may enable the discovery of targeted therapy for the prevention of UC neoplastic progression.

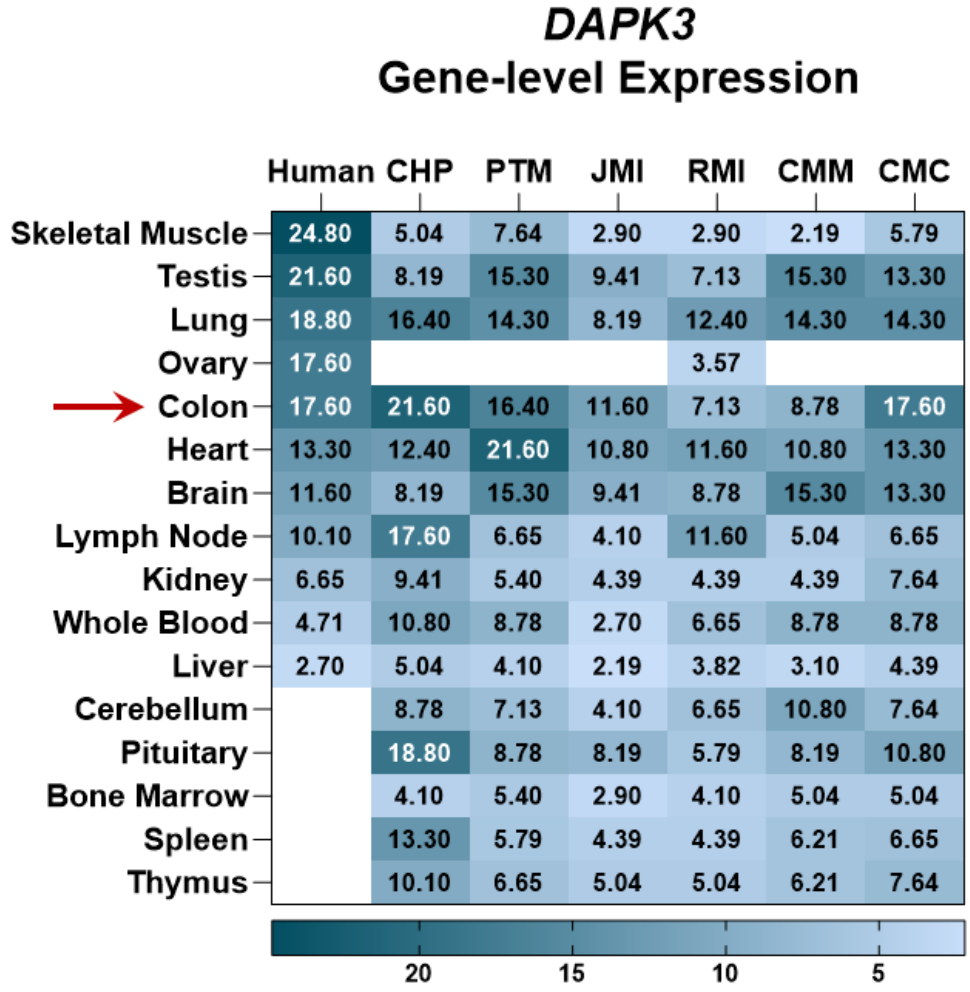

Figure 13. *DAPK3* RNA-Seq gene expression profile across 16 selected tissues. Human expression values are in significant fragments per kilobase of transcript per million mapped reads (sFPKM). Data were sorted by gene expression value (high to low). *DAPK3* expression was highest in skeletal muscle, testis, lung, then colon and ovary. The high expression of *DAPK3* in the colon was echoed in non-human primates. CHP: chimpanzee, PTM: pig-tailed macaque, JMI: Japanese macaque, RMI: rhesus macaque Indian, CMM: cynomolgus macaque Mauritian, CMC: cynomolgus macaque Chinese. Data retrieved from NHPRTR (Non-Human Primates Reference Transcriptome Resource) at:

https://www.ncbi.nlm.nih.gov/IEB/Research/Acembly/av.cgi?db=human&term=dapk3&submit=Go

Chapter 3 . Cell Studies of DAPK3 Contributions to Intestinal Epithelial Wound Closure and Intestinal Epithelial Cell Proliferation.

3.1. Introduction.

Mucosal healing in UC is essential to reduce the risk of dysplasia and CAC (Boal Carvalho & Cotter, 2017). Inefficacious wound healing can give rise to altered epithelial architecture, impaired barrier function, and malignant transformation of neoplastic tissues (Koch & Nusrat, 2012; Leoni et al., 2015). With DAPK3 identified to be a potential key factor in UC progression, and given reports that DAPK3 contributes to cell growth in colon carcinoma cell lines (Togi et al., 2011) and wound closure in gastric carcinoma cell lines (J. Li et al., 2015), I further examined how DAPK3 inhibition might affect IEC wound healing. This question was broken up into three parts: 1) How does DAPK3 inhibition affect IEC wound closure? 2) How does DAPK3 inhibition affect IEC cell proliferation post-wounding? And 3) How does DAPK3 inhibition affect Hippo signaling during IEC wound closure? To answer these questions, I performed wound-closure assays, cell proliferation assays, and immunofluorescence microscopy on the human epithelial cell line Caco-2.

3.1.1. DAPK3 Inhibitors.

To examine the involvement of DAPK3 in the regulation of IEC wound healing, I employed the small molecule inhibitors HS38, HS56, and HS94 that were developed and characterized by the MacDonald laboratory in collaboration with the Haystead laboratory (D. A. Carlson et al., 2013, 2018). The pyrazolo[3,4-*d*]pyrimidinone (HS38) ATP-competitive inhibitor of DAPK3 (**Figure 14**) was identified using the fluorescence-linked enzyme chemoproteomic strategy. HS38

demonstrated higher specificity and greater potency, while bypassing the chemical liabilities that are inherent to other DAPK3 inhibitors (D. A. Carlson et al., 2013).

In addition to DAPK3, HS38 exhibits high potency towards DAPK1 and the structurally related Proviral Integrations of Moloney virus 3 (PIM3) kinase. After the discovery of HS38, second-generation inhibitors HS56 and HS94 were synthesized via the introduction of diverse functional groups around the pyrazolo[3,4-*d*]pyrimidinone scaffold of HS38. The potency of HS56 and HS94 toward DAPK3 was maintained at a similar level, whereas their potency toward PIM3 increased or decreased by one order of magnitude, respectively (**Table 3**). Parallel *in vitro* experiments completed by treatment of Caco-2 cells with HS38, HS56, or HS94 facilitated the assignment of observed effects as being DAPK3-centric or PIM3-centric.

3.1.2. Caco-2.

Caco-2, HT-29, and T84 represent commonly employed IEC lines for *in vitro* studies. These cell lines were derived from adult colon adenocarcinoma and have been widely utilized in the study of intestinal epithelium physiology and pathophysiology (Jochems et al., 2018). While the abundance of DAPK3 in these cell lines has not been quantified, one study with Caco-2 cells did show a decline in cellular metabolism that roughly corresponded with the percentage of siRNA-induced mRNA knockdown (Togi et al., 2011). It is therefore likely that DAPK3 is expressed and has biological significance in Caco-2. As such, I initiated cellular studies with the use of the Caco-2 cell line.

(A)

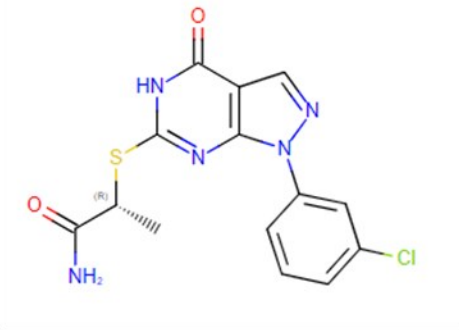
O
HN
N
S
N
N
O
(R)
NH2
Cl

(B)

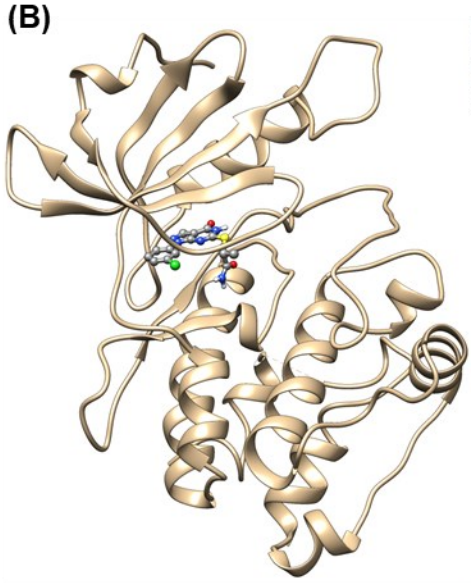

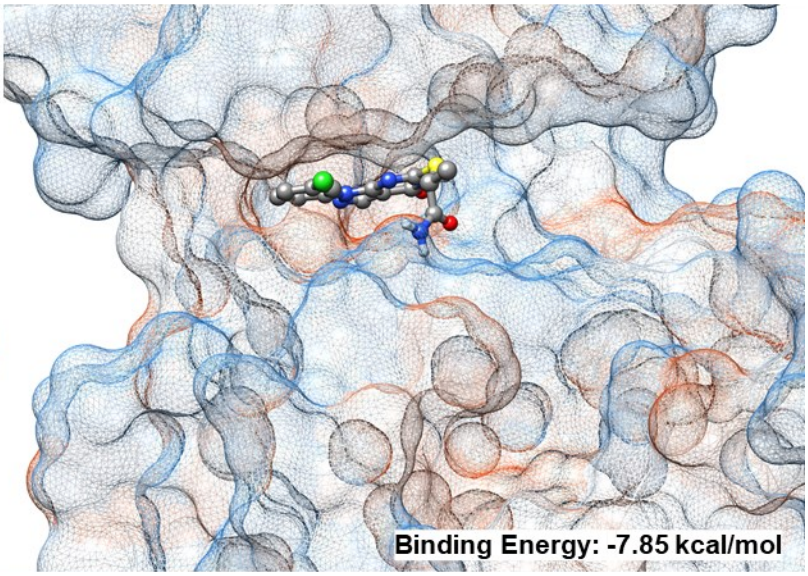
Binding Energy: -7.85 kcal/mol

(C)

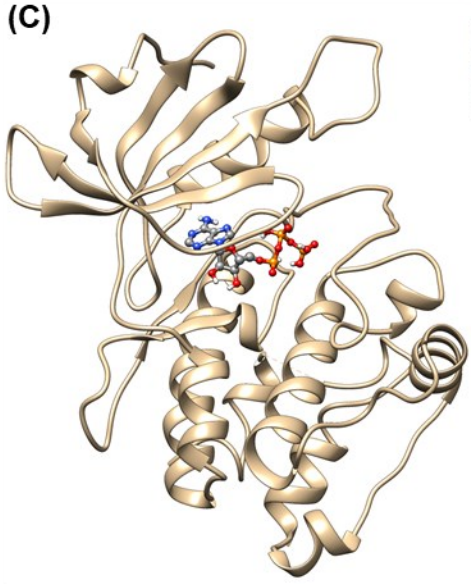

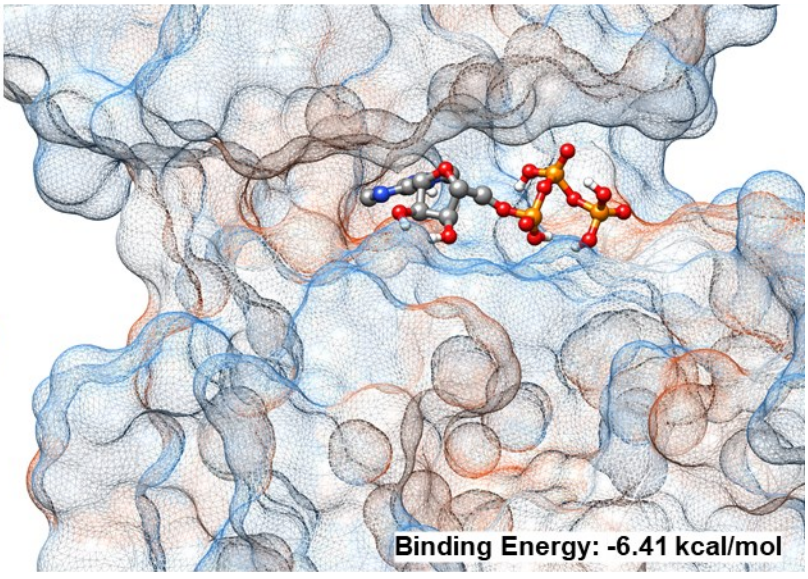
Binding Energy: -6.41 kcal/mol

Figure 14. Molecular docking simulations of HS38 or ATP to the ATP-binding site of DAPK3. **(A)** Chemical structure of the DAPK3 inhibitor HS38. **(B)** Docking of HS38 to the ATP-binding site of DAPK3 (left: ribbon, right: hydrophobic surface). **(C)** Docking of ATP to the ATP-binding site of DAPK3 (left: ribbon, right: hydrophobic surface). For docking simulations, the DAPK3 structure (PDB ID 1YRP, resolution 3.10 Å) and the ligand structures for HS38 and ATP were downloaded from www.rcsb.org. PDBQT files with appropriate atomic charges were generated for all ligands using Open Babel GUI (version 2.3.1, http://openbabel.org), and for DAPK3 using AutoDock Tools 1.5.6 (Morris et al., 2009). Docking simulations were performed using AutoDock 4.2 (Morris et al., 2009). Search space was defined by a 60 x 60 x 60 grid, centered at the centroid of the DAPK3 ATP-binding site with a grid spacing of 0.375 Å. 50 runs were carried out per ligand, each with 150 individuals in population. The Lamarckian genetic algorithm, with a maximum of 2.5 x 10^6 energy evaluation, was utilized for the docking simulation. From the ATP docking log, the conformation with the lowest binding energy was selected for this figure. From the HS38 docking log, the conformation with the lowest binding energy amongst the largest cluster (Cluster 3, where 50% of conformers reside) was selected for this figure.

Table 3. Inhibition constants for the HS compounds utilized.

	K_i (μM)		
	HS38	***HS56***	***HS94***
DAPK3	0.260	0.315	0.126
PIM3	0.208	0.072	2.50

Data extracted from Figure 2A in 'Targeting Pim Kinases and DAPK3 to Control Hypertension' (Cell Chem Biol. 2018;25(10):1195-1207.)

3.2. Methods.

3.2.1. Cell Line Maintenance and Subculturing Protocol.

Caco-2 human IECs (ATCC #HTB-37), gifted by the Hirota laboratory at the University of Calgary, were grown in Dulbecco's Modified Eagle Medium (DMEM; 11965, Gibco) supplemented with 10% (v/v) fetal bovine serum (FBS; F1051 Sigma), 100 U/mL penicillin and 100 µg/mL streptomycin (15140, Gibco), 1 mM sodium pyruvate (S8636, Sigma), and 1X MEM Non-Essential Amino Acids (11140, Gibco). Cells were maintained in a 37 °C humidified incubator with 5% CO_2 and were routinely passaged every four days at ~50% confluence (Natoli et al., 2012) using Trypsin-EDTA (0.25%-0.91 mM; 25200, Gibco) solution. Trypsin action was arrested with complete medium at a ratio of 4:1 (media: trypsin). Cell suspension was then centrifuged at 600 xg for 5 minutes to obtain the cell pellet, which was resuspended in complete medium for seeding at 5.0 x 10^3 cells/cm^2 (Natoli et al., 2012). Media was changed every two days. All experiments were performed using cells from passage 41-45.

3.2.2. Wound Closure Assays.

Caco-2 cells were seeded into Nunclon™ Delta 96-Well MicroWell (167008, Thermo Scientific) at a density of 1.5 x 10^4 cells/cm^2 and were maintained for seven days in complete medium. Under these conditions, cells reached confluence in 5-6 days. On day eight, the monolayers underwent overnight serum starvation in preparation for the wound closure assay. On day nine, circular wounds were made using the WoundMaker tool (Essen BioSciences). Wounded monolayers were washed twice with serum-free media to remove cellular debris. The wash media was then replaced with treatment media (HS compounds at various concentrations, or DMSO at 1% (v/v), diluted in complete medium, 150 µL/well). Plates were placed into the IncuCyte live-cell imaging system

(Essen BioSciences) and maintained in culture at 37 °C, 5% CO_2 while whole-well phase images were taken once every hour for 72 hours. Three independent experiments were conducted using separate passages of cells, each with at least three technical replicates.

The Fiji distribution of ImageJ (Schindelin et al., 2012) was used to batch compile overlay masks for images exported from the IncuCyte ZOOM software. Briefly, the steps undertaken were 1) background subtraction, 2) local contrast enhancement, 3) set threshold, 4) convert to mask, 5) analyze particles (i.e., wound area), then 6) overlay the boundary of the wound area. Parameters for each step were set based on stacked images from five random wells per experiment, then applied similarly to the entire experiment. Wound closure at endpoint was analyzed using one-way analysis of variance (ANOVA) with *post hoc* Tukey multiple comparison. Percentage wound closure was fitted to an exponential plateau model [$y = y_m - (y_m - y_0) * \exp^{-k*x}$; where y_0 is the starting % wound closure (0%), y_m is the maximum % wound closure (100%), and k is the rate constant (hr^{-1})]. The wound closure over time was analyzed using 2-way ANOVA.

3.2.3. EdU Cell Proliferation Assay.

Cell proliferation was determined using the 5-Ethynyl-2'-deoxyuridine (EdU) system, in which EdU, a nucleoside analog of thymidine, is incorporated into DNA during active DNA synthesis. EdU harbors a terminal alkyne group that can be detected by its covalent reaction with a fluorochrome-conjugated azide. Stoichiometric detection of EdU incorporated into DNA can thus be done via measurement of fluorescence intensity. Caco-2 cells were seeded into LabTekII 2-well chambered coverglass (155380, Thermo Fisher) pre-coated with 0.01% Poly-$_L$-lysine (P4707, Sigma), at a density of 1.0 x 10^4 cells/cm^2. On day eight, the monolayers underwent overnight serum starvation in preparation for wounding. Four scratch wounds per well were created on day nine using a sterile P200 pipette tip attached to an aspirator. The wounded monolayers were

washed twice with DMEM then replaced with treatment media (containing 100 μM HS38 or 1% (v/v) DMSO in complete media, 2 mL/well) for 10- or 22-hour incubation in a 37 °C humidified incubator with 5% CO_2.

The Click-iT EdU Cell Proliferation Kit for Imaging, Alexa Fluor™ 488 (C10337, Invitrogen) was used for labeling and detection. Briefly, EdU (10 μM) was added to the treatment media then applied to the wounded monolayers for two-hour incubation at 37 °C and 5% CO_2. At 12- and 24-hours, the monolayers were washed with phosphate-buffered saline (PBS), then fixed with 4% (v/v) paraformaldehyde (PFA; 50-980-487, Fisher Scientific) in PBS for 15 minutes. The fixed monolayers were washed twice with 3% (w/v) bovine serum albumin (BSA) in PBS, then permeabilized via 20-minute incubation with 0.5% (w/v) Triton-X in PBS, followed by two more washes of 3% BSA. EdU detection was completed following a 30-minute incubation with the Click-iT reaction cocktail. Post-incubation, wells were washed with 3% BSA then PBS, then counterstained with Hoechst 33342 for 30 minutes. After which, the monolayers were washed twice with PBS, then mounted with ProLong™ Glass Antifade Mountant (P36980, Invitrogen). Images were taken using the Nikon A1R laser scanning confocal microscope on 20X objective. One representative image per wound was saved for subsequent analyses.

Image analysis was done using the CellProfiler software (McQuin et al., 2018). Briefly, the Hoechst stain was used for the identification of individual cells, and the EdU stain was used to mark cells undergoing proliferation. Objects defined by the EdU overlay were required to overlap with objects defined by the Hoechst stain to ensure that all EdU-positive objects were true. Cells were then classified as EdU-positive or EdU-negative by count of object-EdU per object-Hoechst. To determine the percentage of EdU-positive nuclei, roll-up summation was done on count of

EdU-positive and count of nuclei for wounds within a single well. In essence, each data point provided in the results were acquired from 3-4 unique wounds.

3.2.4. Immunofluorescence Microscopy.

Cell culture and cell wounding were conducted as described in **Section 3.2.3.** However, only the 24-hour time point was selected for immunofluorescence microscopy. In total, seven wounds were observed for the DMSO control group, and 15 wounds were observed for the HS38-treatment group. The YAP (D8H1X) XP® rabbit mAb (14074, Cell Signaling), diluted 1:100 in PBS (containing 1% (w/v) BSA and 0.3% (v/v) Triton X-100) was used to detect endogenous levels of total YAP protein. The Cy3-conjugated AffiniPure donkey anti-rabbit IgG (711-165-152, Jackson ImmunoResearch) was used as the secondary antibody and was applied to samples at 1:200 dilution in conjunction with the Phalloidin-iFluor 647 reagent (176759, abcam), used at 1:1,000 dilution in PBS (with 1% (w/v) BSA). 4',6-diamidino-2-phenylindole (DAPI; 62248, Thermo Scientific) was used at 10 μg/mL to mark nuclei.

A standard immunofluorescence protocol was followed. Monolayers were rinsed twice with PBS prior to a 10-minute incubation with 4% (v/v) PFA. The fixative was removed with two PBS washes. Then, cells were permeabilized with 0.5% (v/v) Tween-20 PBS for 10 minutes. Tween-20 was washed off with PBS (3X, 5 min/wash). Blocking of non-specific binding was completed with 5% (v/v) normal donkey serum in PBS for one hour at room temperature (RT). The blocking solution was replaced by primary antibody for overnight incubation at 4 °C. Prior to incubation with secondary antibody and phalloidin (one hour at RT), monolayers were washed three times with PBST (PBS containing 0.1% (v/v) Tween-20). Three more PBST washes followed, after which DAPI was added for a 3-minute-long incubation at RT. Two final PBS washes were carried out before samples were mounted with ProLong™ Glass Antifade Mountant. Images were taken

using the Nikon A1R laser scanning confocal microscope on 40X objective (oil) at Nyquist (xy-plane). For image deconvolution, stacks of seven equidistant (1 μm) z-planes were evaluated.

For image and statistical analysis of YAP-F-actin colocalization, the toolbox '*Colocalization GUI*', developed by Villalta and colleagues (Villalta et al., 2011) for MATLAB (MathWorks, Natick, MA) was used. The algorithm that underlies *Colocalization GUI* generates a colocalization mask for the calculation of Manders coefficients *m*1 and *m*2 (Manders et al., 1993), which allows for the construction of the *m*1 and *m*2 MAPs. The mask represents pixels that display true (i.e., non-random) colocalization in a pair of images. The *m*1 and *m*2 parameters represent the percentage of image 1 (YAP) or image 2 (F-actin) intensity that is colocalized with matched pixels on image 2 (F-actin) or image 1 (YAP), respectively. MAPs are the visual representation of the contribution of each pixel to the colocalization coefficients *m*1 or *m*2. Two *z*-slices per stack (of seven equidistant z-planes) were selected for colocalization analysis based on the broad presence of distinct cortical actin belt across the full image.

3.2.5. Molecular Cloning.

Human *Cdc14A* from pcDNA3.1+/C-(K)DYK-Cdc14A (OHu05407D, GenScript) was subcloned into pAcGFP1-N1 (632426, Clontech) using the FastCloning method (C. Li et al., 2011). The insert was amplified with forward primer 5'-CGAGTCTGGGAGGCGAAAGCTTGGTACCGAGCTCG-3' and reverse primer 5'-GCCAGTGGTGAGAACCCTTATCGTCGTCATCCTTGTAATCGG-3'. The vector was amplified with forward primer 5'-GGTTCTCACCACTGGCCACCGGTCATGGTGAG-3' and reverse primer 5'-TCGCCTCCCAGACTCGAGATCTGAGTCCGGTA-3'. All primers used in this study were synthesized by Integrated DNA Technologies (IDT). The PCR reaction components were: 50 μL total volume, 0.5 μL Phusion DNA polymerase (New England Biolabs), 10 μL 5x buffer, 4 μL of 2.5 mM dNTPs, 20 ng of plasmid DNA template, 500 nM of each primer,

and 1.5 µL of DMSO. The PCR cycling parameters were 98 °C 30 seconds, (98 °C 10 seconds, 70 °C 30 seconds, 72 °C 30 seconds/kb) x 20 cycles, 72 °C 10 minutes, and 4 °C infinite. After confirmation of PCR products, 1.5 µL of *Dpn*I enzyme (New England Biolabs) was added to the unpurified PCR reactions (45 µL) for vector or insert separately. The vector and insert (10 µL each) were then mixed and digested at 37 °C for 1 hour. Two microliters of the digested vector-insert mixture were added to 40 µL of chemically competent *E. coli* cells (NEB5α, C2987H). The mixture was then incubated for 30 minutes on ice. After heat shock at 42 °C for 45 seconds, 350 µL of pre-warmed SOC medium was added to the mixture. After 60 minutes shaking at 37 °C and 350 rpm with an Eppendorf Thermomixer, the entire content was plated onto a LB agar plate supplemented with 50 µg/mL kanamycin. Colony PCR was conducted with orientation-specific primers. DNA mini prep was performed using QIAprep® Spin Miniprep Kit (QIAGEN), and final confirmation of insertion was done via sequencing at the DNA lab of the University of Calgary. The resulting construct carries FLAG- and GFP- tags downstream of Cdc14A, and a SNAC-tag (Dang et al., 2019) sandwiched between the FLAG- and GFP- tags (i.e., Cdc14A-FLAG-SNAC-GFP). Truncated Cdc14A was generated from the Cdc14A-FLAG-SNAC-GFP construct by using the FastCloning method. Briefly, for a.a. 1-43 deletion (V44), forward primer 5'-AGAAATTTTCATAGACCATGGTGGCGGATCCGAG-3' and reverse primer 5'-GTCTATGAAAATTTCTATGCAGATTTTGGACCGC-3' were used; for a.a. 1-79 deletion (K80), forward primer 5'-TGTAGTGCACTATTTTCATGGTGGCGGATCCGAG-3' and reverse primer 5'-AAAATAGTGCACTACACCTGTTTTGACCAAC-3' were used; for a.a. 1-99 deletion (G100), forward primer 5'-TTACTGCATAGGCACCCATGGTGGCGGATCCGAG-3' and reverse primer 5'-GGTGCCTATGCAGTAATCTATTTAAAGAAGACAC-3' were used. Apart from the primers used, all other steps taken mirrored what was done for the generation of the Cdc14A-FLAG-SNAC-GFP

construct. The Myc-DAPK3-HA construct was previously generated by a past member of the MacDonald lab.

3.2.6. Cell Culture, Transfection, and Live Cell Imaging.

HEK293T human embryonic kidney 293 cells (ATCC #CRL-3216), gifted by the Muruve laboratory at the University of Calgary, were maintained in DMEM (11965, Gibco), supplemented with 10% FBS (F1051 Sigma) and 100 U/mL penicillin and 100 µg/mL streptomycin (15140, Gibco). One day prior to transfection, HEK293T was seeded into a 10 cm culture dish at a density of 5.0 x 10^5 cells/cm^2. On the day of transfection, 15 µL of PolyJet (SL100688, SignaGen) was added to 235 µL DMEM, and 2.5 µg plasmid DNA (per construct) was added to 250 µL DMEM. The diluted PolyJet was added to the diluted plasmid DNA then incubated at RT for 15 minutes. The lipid-DNA complex was introduced dropwise to HEK293T, then cells were returned to the incubator. Standard epi-fluorescent microscope was used to detect GFP-tagged Cdc14A in live cells at 24-hour post-transfection.

3.2.7. Immunoprecipitation and Immunoblotting.

HEK293T cells were lysed at 24-hour post-transfection. Briefly, cells were washed with ice-cold PBS (x2) then pelleted at 500 xg for 3 minutes at 4 °C. NP-40 (0.5% v/v) was added to Dilution Buffer, composed of 10 mM Tris-HCl (pH 8.0), 150 mM NaCl, 0.5 mM EDTA, and cOmplete™ Protease Inhibitor Cocktail for cell lysis, which was completed on ice for 30 minutes. After lysis, the cell suspension was centrifuged at 14,000 rpm for 10 min at 4 °C to retrieve the cell lysate. Then, 600 µL of ice-cold Dilution Buffer was added to 400 µL of lysate in preparation for immunoprecipitation (IP). The GFP-Trap®_A (Chromotek), small recombinant Alpaca antibody fragments covalently coupled to agarose beads, was used for the IP of GFP-tagged Cdc14A.

Briefly, GFP-Trap bead slurry was washed with dilution buffer (x3). Diluted lysate (800 µL) was added to equilibrated beads (135 µL), then tumbled end-over-end for one hour at 4 °C. Beads were washed with high-salt wash buffer (500 mM), then with Triton-X-100 (0.5% v/v) wash buffer prior to elution at 98 °C for 10 min with 100 µL of 2X SDS-sample buffer. The immunoprecipitants from cell lysates were resolved by SDS-PAGE (10%) gel electrophoresis then transferred onto 0.2 µm nitrocellulose membranes. Blocking was done with 5% BSA (w/v) in TBST, then membranes were incubated overnight in primary antibodies at 4 °C. Primary antibodies used included the HA-Tag (C29F4) rabbit mAb (3724, Cell Signaling), diluted 1:1,000 in TBST (containing 5% (w/v) BSA), the FLAG-Tag (9A4) mouse mAb (8146, Cell Signaling), diluted 1:1,000 in TBST (containing 5% (w/v) BSA), the GAPDH (14C10) rabbit mAb (2118, Cell Signaling), diluted 1:1,000 in TBST (containing 5% (w/v) BSA), and the Cdc14A (DCS-291) mouse mAb (NB120-10536, Novus Biological), diluted 1:2,000 in PBST (containing 5% (w/v) BSA). Immunoreactive proteins were visualized using the ChemiDoc Imaging System (Bio-Rad).

3.3. Results.

3.3.1. Caco-2 Monolayer Wound Closure is Enhanced with Application of the DAPK3 Inhibitor HS38.

To investigate the effects of DAPK3 inhibition on IEC wound healing, circular wounds were made on Caco-2 monolayers. The size of wound areas was measured once per hour as the monolayers healed over the next 72 hours, in the presence or absence of DAPK3 inhibitor HS38 (at 1, 5, 25, or 100 µM). As shown in **Figure 15**, application of the DAPK3 inhibitor HS38 significantly enhanced Caco-2 wound closure in a concentration-dependent manner. At 36-hour post-wounding, treatment with 100 µM HS38 increased the percentage of wound closure by 46% when compared to the DMSO vehicle control. Because of enhanced wound closure, many wounds treated with

HS38 became segmented following the 36-hour time point and created multiple (smaller) wound areas in one single well. The presence of segmented wounds obstructed the ability to complete effective data processing and analyses. Consequently, the time frame for percentage wound closure was reduced to 36 hours.

With regards to wound closure analyses, prior studies have suggested that: 1) when using the percentage of initial wound area to assess wound closure efficiency, the data will bias small wounds, 2) when using the absolute wound area to assess wound closure efficiency, the data will bias large wounds, and 3) the calculation of rate of wound closure may be the best approach when analyzing wound closure data (Arciero & Swigon, 2013; Jonkman et al., 2014). Given such, the percentage wound closure data was fitted onto the exponential plateau model [$y = plateau – (plateau – y_0) * exp^{-k*x}$] to evaluate rate of wound closure. The wound closure rate constant, expressed in reciprocal of the *x*-axis time units, was derived based on the assumption that during each time interval, a certain fraction of the wound area would become occupied by cells. As time advanced, the wound area would decrease in size. Consequently, fewer cells would migrate to occupy the (now smaller) wound area so the curve levels off as the monolayer approaches 100% wound closure. The goodness of fit statistics confirmed suitability of the input model (**Table 4**). In all instances, the modeling took on an R^2 value that was >0.85, and in most instances, the R^2 value was found to be >0.95. **Figure 16A** shows the percentage wound closure over time, overlayed with the fitted curves. Rate constants derived from the modeling exercise are presented in **Figure 16B** and supports the notion that pharmacological inhibition of DAPK3 with HS38 increases the rate of wound closure in a concentration-dependent manner.

Visual examination of the fitted curve (**Figure 16A**) suggests that at higher [HS38], the rate of wound closure might not be restrained by the parameters set forth for the modeling exercise (i.e.,

plateau ≠ 100). To investigate, the first derivative of the percentage wound closure curve was computed. As shown in **Figure 16C**, the rate of wound closure decreased over time for all wounded monolayers. However, monolayers treated with HS38 experienced a smaller decrease in rate of wound closure than the control monolayers (Media and DMSO), irrespective of their greater percentage of closure at 36 hours. Presumably, DAPK3 inhibition via application of HS38 interfered with the sensing of chemical and/or mechanical environmental cues that would otherwise inform the collective behaviour of the reparative monolayer.

To differentiate the DAPK3-mediated phenotype from the PIM3-mediated phenotype, parallel experiments were conducted by treating wounded Caco-2 monolayers with HS38, HS56 (more inhibitory activity towards PIM3), or HS94 (less inhibitory activity towards PIM3). As can be seen in **Figure 17A**, HS94 treatment resulted in a similar phenotype as HS38, whereas HS56 treatment produced an opposite phenotype. That is, monolayers treated with HS94 experienced enhanced wound closure (19% increase vs. DMSO vehicle control), and monolayers treated with HS56 yielded a reduction in percentage wound closure (21% decrease vs. DMSO vehicle control) at the 36-hour mark. It should be noted that wound closure in monolayers treated with HS56 plateaued at around 40% (**Figure 17B**). In all independent experiments, wound closure in monolayers treated with HS56 halted at about 36 hours post-wounding and failed to achieve 100% wound closure (data not shown). The rate constants derived from modeling exhibited the same trend as what was reflected by the 36-hour end-point measurement of percentage wound closure. That is, HS94 produced greater rate constant whereas HS56 produced lower rate constant (**Figure 17C)**. Interestingly, in the early phase of wound closure, treatment with HS56 increased the rate of wound closure (**Figure 17D**); however, this was not sustained, and a rapid deceleration in wound repair was observed as time advanced.

(A)

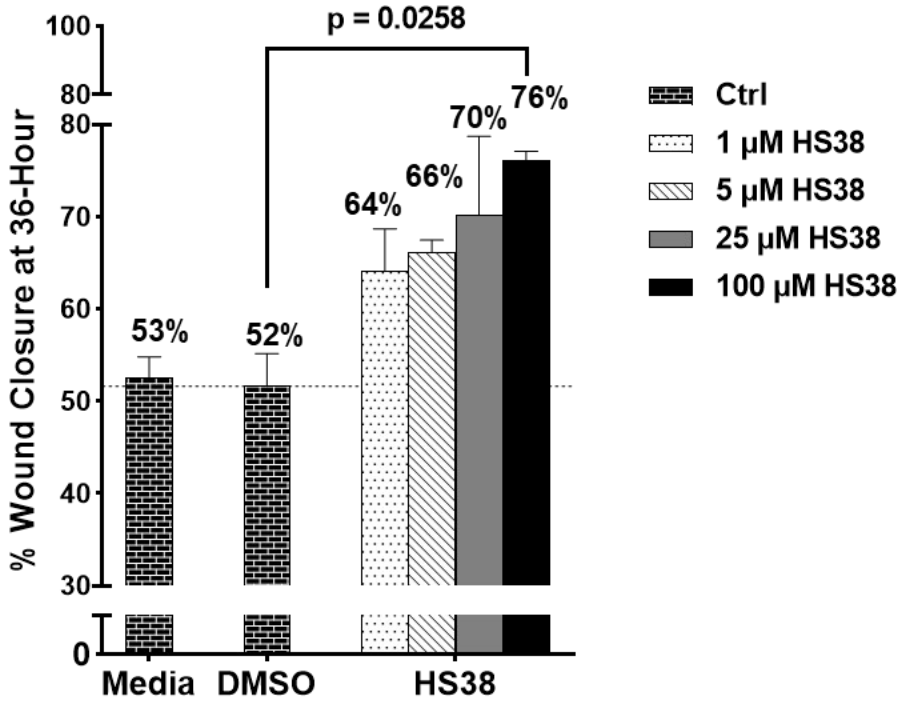
p = 0.0258
% Wound Closure at 36-Hour
100
80
80
70
60
50
40
30
0
53%
52%
64%
66%
70%
76%
Media
DMSO
HS38
Ctrl
1 μM HS38
5 μM HS38
25 μM HS38
100 μM HS38

(B)

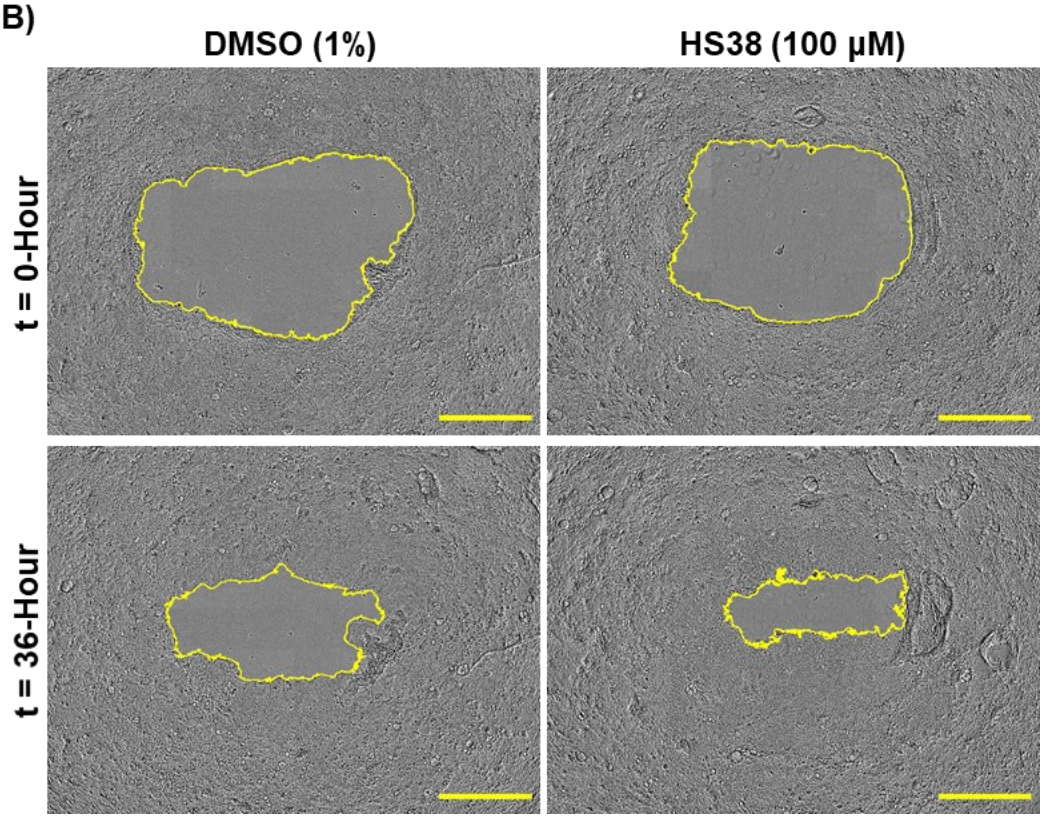
DMSO (1%)
HS38 (100 μM)
t = 0-Hour
t = 36-Hour

Figure 15. Application of the DAPK3 inhibitor HS38 increased percentage wound closure in a concentration-dependent manner. (A) Percent wound closure was calculated at 36-hour against initial wound size. One-way ANOVA comparing the five treatment types (DMSO and HS38 at various concentrations) indicate significant difference among means ($p = 0.0396$). Tukey test was used for *post hoc* multiple comparisons, which showed that percent wound closure was significantly different between DMSO and the 100 μM HS38 condition. Error bars represent ± SEM. **(B)** Representative images for the 36-hour time point. Figures are representative of three independent experiments, each containing 3-9 technical replicates. Scale bars = 800 μm.

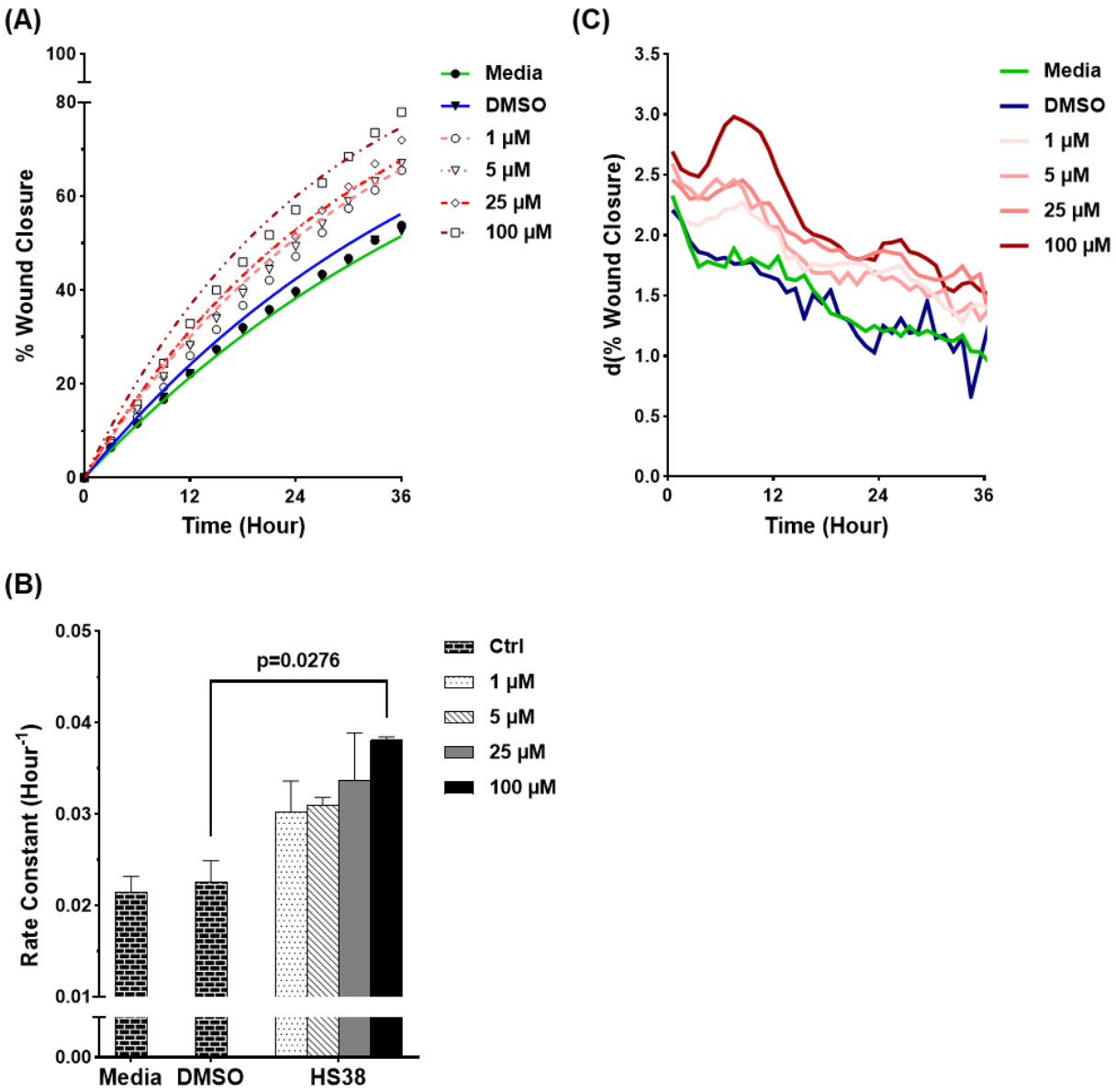
(A)
% Wound Closure
Time (Hour)
Media
DMSO
1 μM
5 μM
25 μM
100 μM
(C)
d(% Wound Closure)
Time (Hour)
Media
DMSO
1 μM
5 μM
25 μM
100 μM
(B)
Rate Constant (Hour-1)
p=0.0276
Ctrl
1 μM
5 μM
25 μM
100 μM
Media
DMSO
HS38

Figure 16. Application of the DAPK3 inhibitor HS38 augmented rate of wound closure. (A) Percentage wound closure over time, data plotted at 3-hour intervals. **(B)** Rate constants derived by fitting the % wound closure curve to an exponential plateau model [$y = y_m - (y_m - y_0) * exp^{-k*x}$], where y_0 is the starting % wound closure (constrained to 0), y_m is the maximum % wound closure (constrained to 100), and k is the rate constant (no constraints). One-way ANOVA comparing the five treatment types (DMSO and HS38 at various concentrations) indicate significant difference among means ($p = 0.0456$). Tukey test was used for *post hoc* multiple comparisons, which showed that wound closure rate constant was significantly different between DMSO and the 100 μM HS38 condition. Error bars represent ± SEM. **(C)** First derivative of the % wound closure curve. The first derivative is the steepness of the % wound closure curve **(A)** at every *x*-value. Smoothness of the curve was adjusted by averaging four neighboring *x*-values and by adopting the second order of the smoothing polynomial. Figures are representative of three independent experiments, each containing 3-9 technical replicates.

Table 4. Goodness of fit statistics for the exponential plateau modeling of wound closure. GraphPad Prism built-in XY analysis: Nonlinear regression (curve fit) was used to derive the presented values. **Figure 16A** exemplifies the abridged source data.

			HS38			
	Media	**DMSO**	**1 µM**	**5 µM**	**25 µM**	**100 µM**
Best-fit values						
Y_m: max % wound closure	100	100	100	100	100	100
Y_0: starting % wound closure	0	0	0	0	0	0
k: rate of wound closure	0.020	0.023	0.030	0.031	0.031	0.038
Goodness of Fit						
Degree of Freedom	172	183	203	186	157	144
R squared	0.9934	0.9476	0.9444	0.9785	0.8948	0.9752

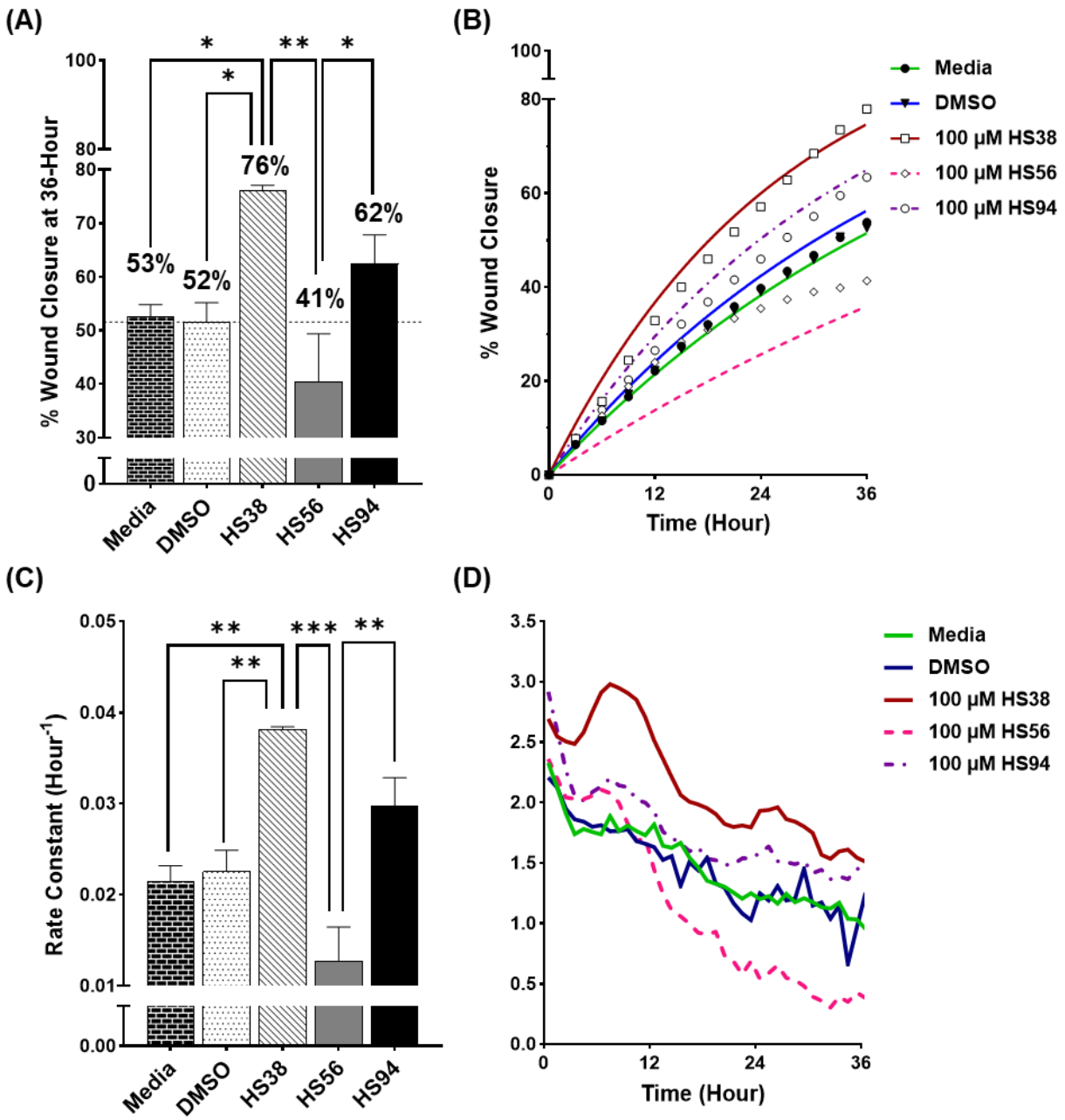
(A)
% Wound Closure at 36-Hour
53%
52%
76%
41%
62%
Media
DMSO
HS38
HS56
HS94
(B)
% Wound Closure
Time (Hour)
Media
DMSO
100 µM HS38
100 µM HS56
100 µM HS94
(C)
Rate Constant (Hour-1)
Media
DMSO
HS38
HS56
HS94
(D)
Time (Hour)
Media
DMSO
100 µM HS38
100 µM HS56
100 µM HS94

Figure 17. *In vitro* wound closure effects obtained with HS38 can be ascribed to DAPK3 inhibition. (A) Comparison of % wound closure at 36-hour post-wounding for monolayers treated with 100 μM of HS38, HS56, or HS94. Bars represent ±SEM. *p<0.05, **p<0.01. **(B)** % wound closure over time; data are plotted at 3-hour intervals. **(C)** Rate constants derived by fitting the % wound closure curve to an exponential plateau model [$y = y_m – (y_m – y_0) * exp^{-k*x}$], where y_0 is the starting % wound closure (constrained to 0), y_m is the maximum % wound closure (constrained to 100), and k is the rate constant (no constraints). One-way ANOVA comparing the five treatment types indicate significant difference among means (p = 0.0005). Tukey test was used for *post hoc* multiple comparisons. Error bars represent ± SEM. **p<0.01, ***p<0.001. **(D)** First derivative of the % wound closure curve. The first derivative is the steepness of the % wound closure curve **(A)** at every *x*-value. To see the trends, smoothness of the curve was adjusted by averaging four neighboring *x*-values and by adopting the second order of the smoothing polynomial. Figures are representative of three independent experiments, each containing 3-9 technical replicates.

3.3.2. Caco-2 Cell Proliferation is Augmented with Application of the DAPK3 Inhibitor HS38.

Closure of epithelial wounds involves epithelial cell proliferation and migration. To examine the effects of DAPK3 inhibition on cellular proliferation in wounded monolayers, EdU-coupled fluorescence was used to evaluate cell proliferation around wound edges at 12- and 24-hours post-wounding. As shown in **Figure 18A**, treatment with HS38 did not alter the percentage of EdU-positive cells at 12 hours post-wounding. However, at 24 hours post-wounding, cell proliferation in HS38-treated monolayers was significantly greater than in the control monolayer (**Figure 18B**; HS38: 38% EdU-positive, DMSO: 18% EdU-positive; $p<0.01$). This finding suggests that the enhanced rate of wound closure seen on HS38-treated monolayers (**Figure 15**) is owed, in part, to an augmentation of cell proliferation following the administration of HS38.

Although the percentage of EdU-positive cells did not change in response to HS38 treatment at the 12-hour time point, an interesting observation was made when EdU intensity levels were transformed from nominal (i.e., positive, or negative) to interval scale. When cells in the EdU-positive population were partitioned based on relative intensity, it was apparent that most EdU-positive cells in the HS38-treated monolayers exhibited maximal-intensity (>0.9), whereas the opposite was true for cells in the control monolayer (**Figure 19A**; EdU-positive cells showing maximal-intensity: HS38, 56%, Control, 16%, $p=0.024$). Similar bias was detected for monolayers treated for 24 hours with HS38; among the EdU-positive cells exposed to HS38, 57% were found to have reached maximum intensity, whereas only 5% of the EdU-positive cells in control monolayers achieved maximum intensity ($p=0.012$) (**Figure 19B)**.

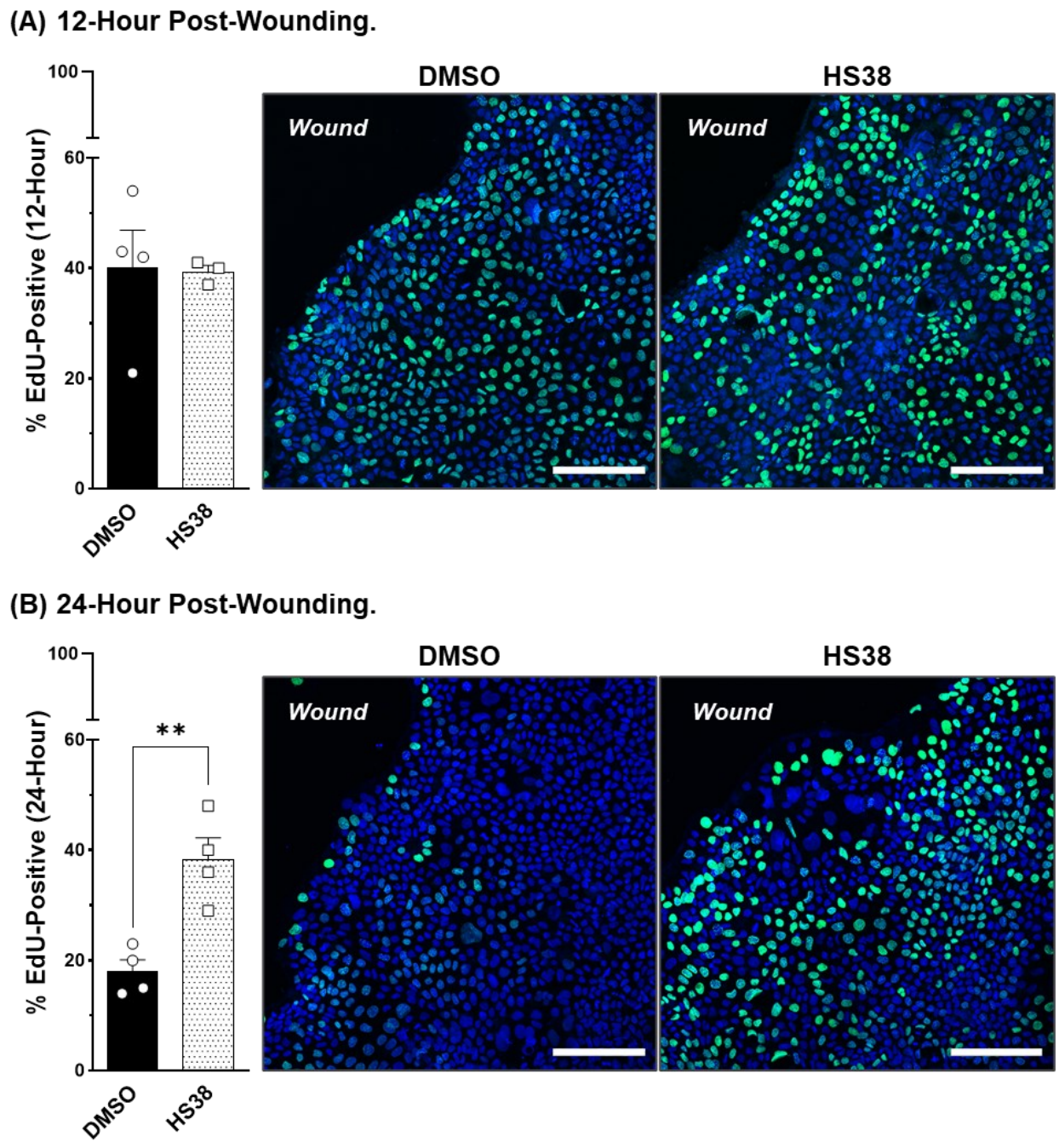

Figure 18. HS38 treatment augmented Caco-2 cell proliferation during *in vitro* wound closure. EdU-labeled proliferation of Caco-2 cells after treatment with HS38 at 100 μM for 12 hours **(A)** or 24 hours **(B)**. Statistical significance was determined via unpaired t-test. **p<0.01. Error bars represent ± SEM. N=3-4. Scale bars=300 μm.

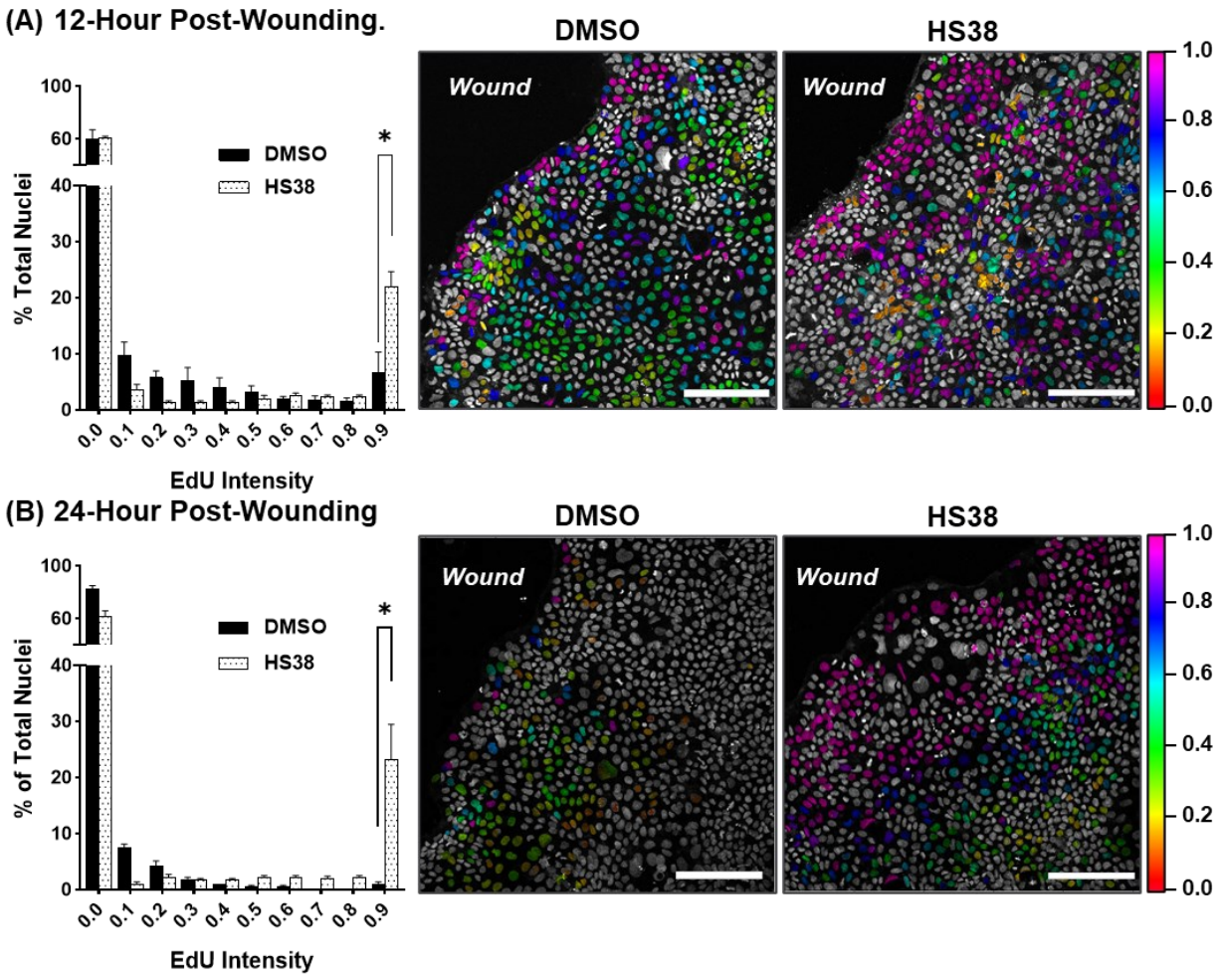

Figure 19. HS38 treatment altered cell cycle progression during *in vitro* wound closure. Distribution of EdU-coupled fluorescence intensity after 12 hours **(A)** or 24 hours **(B)** of treatment with HS38 (100 μM) or DMSO (1%) showed increased percentage of EdU-positive cells reached maximal intensity at experimental end points. Statistical significance was determined via unpaired t-test. *$p<0.05$. Error bars represent ± SEM. N=3-4. Scale bars=300 μm.

3.3.3. Treatment of Caco-2 Monolayers with HS38 Increased Co-localization of YAP with F-actin during Wound Closure.

Given the effects seen on cell proliferation and cell cycle kinetics with the use of HS38 for DAPK3 inhibition, I next investigated the effects that HS38 may have on the colocalization of YAP with F-actin. Factors influencing this decision were: 1) Studies that associated DAPK3 expression and/or activity with perturbed cell cycle kinetics (Hu et al., 2020; Ono et al., 2020; Wu et al., 2015), 2) Studies that associated YAP expression and/or activity with S-phase shortening and promotion of G1/S transition (Cabochette et al., 2015; J. Cai et al., 2010), 3) The colocalization of YAP with F-actin under YAP-activating conditions (Lee et al., 2019), 4) The regulation of actomyosin cytoskeleton remodeling by DAPK3 (**Section 1.13**), and 5) The potential regulatory relationship identified for DAPK3 and YAP (**Section 2.3.6**).

Caco-2 monolayers were stained with YAP antibodies as well as phalloidin at 24-hour post-wounding. Immunofluorescence in the YAP channel showed few instances of nuclear localization in both HS38-treated and control monolayers (**Figure 20**), suggesting that treatment with HS38 did not influence nuclear translocation of YAP. The colocalization of YAP with F-actin was evaluated at the wound edges of Caco-2 monolayers at 24 hours post-wounding via 1) computation of a colocalization mask with algorithm written by Villalta and colleagues (Villalta et al., 2011), 2) calculation of the $m1$ coefficient value, which represent the percentage of YAP-positive pixels that are colocalized with matched pixels on the F-actin channel, and 3) generation of the $m1$ MAP, that provide visual representation of the contribution of each pixel to the colocalization coefficients $m1$. **Figure 21A** showed that the $m1$ value for HS38-treated monolayers was significantly greater than for the control monolayers ($+0.253 \pm 0.0792$, $p=0.0064$). Since $m1$ values represent the percentage of YAP-positive pixels that also display non-random fluorescence in the Phalloidin

channel, this result suggests that DAPK3 inhibition increased colocalization of YAP with F-actin. Even though the difference in $m1$ value between treatment types was significant, several control monolayers exhibited similar $m1$ values as HS38 treated monolayers (**Figure 21A**). Potentially, the $m1$ results for the control monolayers included data points that were driven by high, but focused, YAP staining at defined subcellular compartment/components. Qualitative analysis of $m1$ MAPs generated for HS38-treated and control monolayers supported this hypothesis. As shown in **Figure 21B**, monolayers treated with HS38 displayed a qualitative difference in dispersion of $m1$ signal intensity throughout the entire cell cytoplasm, whereas the $m1$ signal intensity are localized to the cortical actin ring on the cell periphery in the control monolayer. The visual phenotype displayed in **Figure 21B** is representative of the general trend observed for the two treatment types. One interpretation of these data is that the inhibition of DAPK3 via HS38 initiated YAP activation via dispersion of YAP from the cell membrane. Continued association of YAP with F-actin in the cytoplasm might facilitate the transport of YAP from cell periphery to the nuclear membrane.

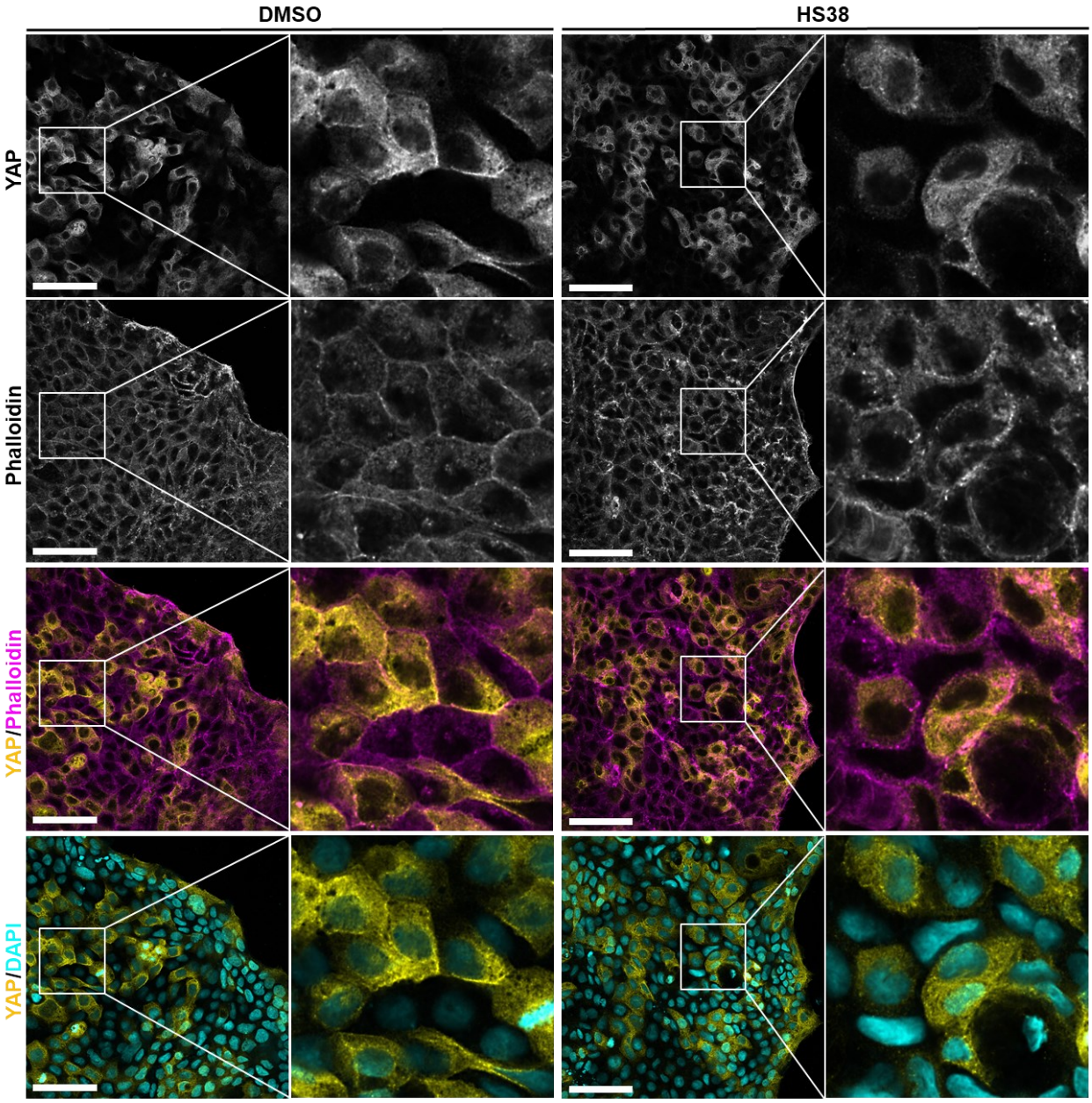

Figure 20. Immunofluorescence staining of YAP and F-actin. Immunofluorescence in the YAP channel showed few instances of nuclear localization in both HS38-treated and control monolayers, suggesting that treatment with HS38 did not influence nuclear translocation of YAP. The images displayed serve as source material for the generation of *m*1 maps shown in **Figure 21B**. Images were taken on Nikon A1R laser scanning confocal microscope on 40X objective (oil) at Nyquist (xy-plane). For image deconvolution, stacks of seven equidistant (1 µm) z-planes were evaluated. Scale bars=300 µm.

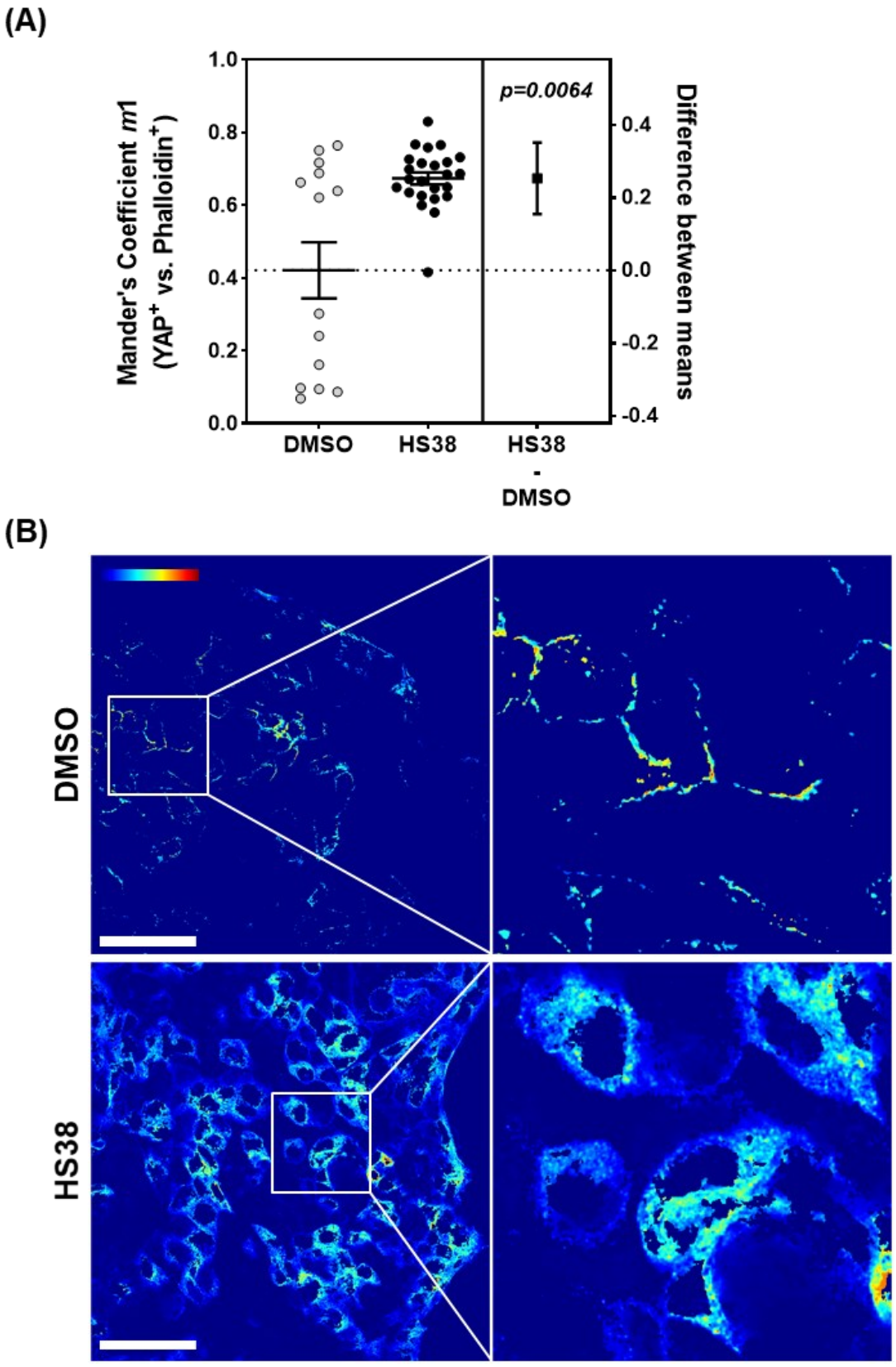
(A)
Mander's Coefficient m1
(YAP+ vs. Phalloidin+)
1.0
0.8
0.6
0.4
0.2
0.0
p=0.0064
0.4
0.2
0.0
-0.2
-0.4
Difference between means
DMSO
HS38
HS38
-
DMSO
(B)
DMSO
HS38

Figure 21. YAP colocalization with F-actin increased following *in vitro* treatment of wounded Caco-2 monolayers with HS38. (A) Comparison of *m*1 coefficient values between HS38-treated (100 μM) and control (1% DMSO) monolayers showed significant increase in YAP-F-actin colocalization. Datapoints represent z-slices analyzed for colocalization; Error bars represent ± SEM. The dotted line represents the mean *m*1 value for the control (1% DMSO) monolayers. **(B)** *m*1 MAPs of representative images from the HS38-treated and control groups. Jet color bar: contribution of each pixel to the m*1* coefficient. Scale bars=300 μm.

3.3.4. Candidate Intermediary Molecules for the DAPK3-YAP Connection.

The dual-specificity phosphatase Cdc14A is a conduit through which DAPK3 may exert its influence on YAP activity. Cdc14A controls mitotic exit by dephosphorylating CDK1-phosphorylated YAP, a mechanism that had demonstrated importance in the control of discordant cell proliferation (S. Yang et al., 2015). Moreover, the anaphase promoting complex/cyclosome (APC/C) activator protein Cdh1 (APC/C^{Cdh1}) was shown to augment YAP activity and promote G1/S phase transition via destabilization of LATS1/2 during G1 of the cell cycle (W. Kim et al., 2019). And Cdc14A was shown to dephosphorylate Cdh1 and activate APC/C^{Cdh1} (Bembenek & Yu, 2001; Jaspersen et al., 1998, 1999; Kao et al., 2014). These findings suggest that Cdc14A may promote YAP-mediated G1/S transition via its activation of APC/C^{Cdh1}. Cdc14A is a good candidate conduit for the DAPK3-YAP connection as 1) Cdc14A was identified as a binding partner of DAPK3 (Wu et al., 2015), and 2) it was suggested that DAPK3 enzymatic activity regulates Cdc14A-dependent alterations to cell cycle distribution in a context-dependent manner (Hu et al., 2020; Wu et al., 2015). In the subsections that follow, I present the preliminary findings from my examination of Cdc14A as an intermediary molecule for the DAPK3-YAP connection.

3.3.5. DAPK3 Overexpression Altered Cdc14A Subcellular Localization and Decreased Cdc14A Protein Abundance.

Kaiser and colleagues showed that the subcellular distribution of Cdc14A varied, whereas the protein levels and phosphatase activity of Cdc14A changed little during cell cycle progression (Kaiser et al., 2002). To examine the influence that DAPK3 may have on Cdc14A subcellular localization, I transfected HEK293T with GFP-tagged Cdc14A, with or without ectopic expression of HA-tagged DAPK3, then recorded GFP fluorescence in live cells at 24-hour post-transfection. Cdc14A-FLAG-GFP proteins localized to the cytoplasm in most cells (**Figure 22A**), which

suggests that a great fraction of cells was in the G2 or M phase. A small fraction of cells was in G1 or S phase, as indicated by Cdc14A foci that emulated centrosomal staining (**Figure 22A**). However, proof that these Cdc14A-decorated organelles were centrosomes will need to be confirmed by co-localization experiments with γ-tubulin. Interestingly, when HEK293T cells were transfected with both Cdc14A-FLAG-GFP and DAPK3-HA (**Figure 23B, Lane 2**), a dramatic change in cellular distribution for GFP-associated fluorescence was observed (**Figure 22A**). For one, the demarcation of cytoplasm from nucleus by GFP-associated fluorescence in singly transfected HEK293T dissipated in cells overexpressing DAPK3. Secondly, in cells co-transfected with Cdc14A-FLAG-GFP and DAPK3-HA, the GFP-associated fluorescence acquired characteristics of autophagosomes (i.e., punta and ring-like structures). That these punta or ring-like structures are autophagosomes will need to be confirmed by co-localization experiments with LC3.

The sequestration of GFP-tagged Cdc14A in presumed autophagosomes suggests degradation of Cdc14A. Examination of Cdc14A-FLAG-GFP abundance via α-FLAG immunoblot indicated that alongside ectopic expression of HA-tagged DAPK3, levels of Cdc14A-FLAG-GFP decreased (**Figure 22B**). Moreover, endogenous levels of Cdc14A, detected via immunoblotting with Cdc14A monoclonal antibodies, also decreased with ectopic expression of HA-tagged DAPK3. It is important to note that the α-Cdc14A used in this study was produced via the DCS-291 clone that was raised against a recombinant fragment corresponding to the C-terminal residues 343-623 of human Cdc14A. As the parent plasmid used in this study for subcloning contain only residues 1-383 of human Cdc14A, it is unlikely that immunoreactivity from Cdc14A-FLAG-GFP was detected with the α-Cdc14A. To summarize, preliminary immunofluorescence microscopy and

immunoblotting showed that the ectopic expression of HA-tagged DAPK3 induced translocation of Cdc14A to presumed autophagosomes and reduced overall Cdc14A abundance.

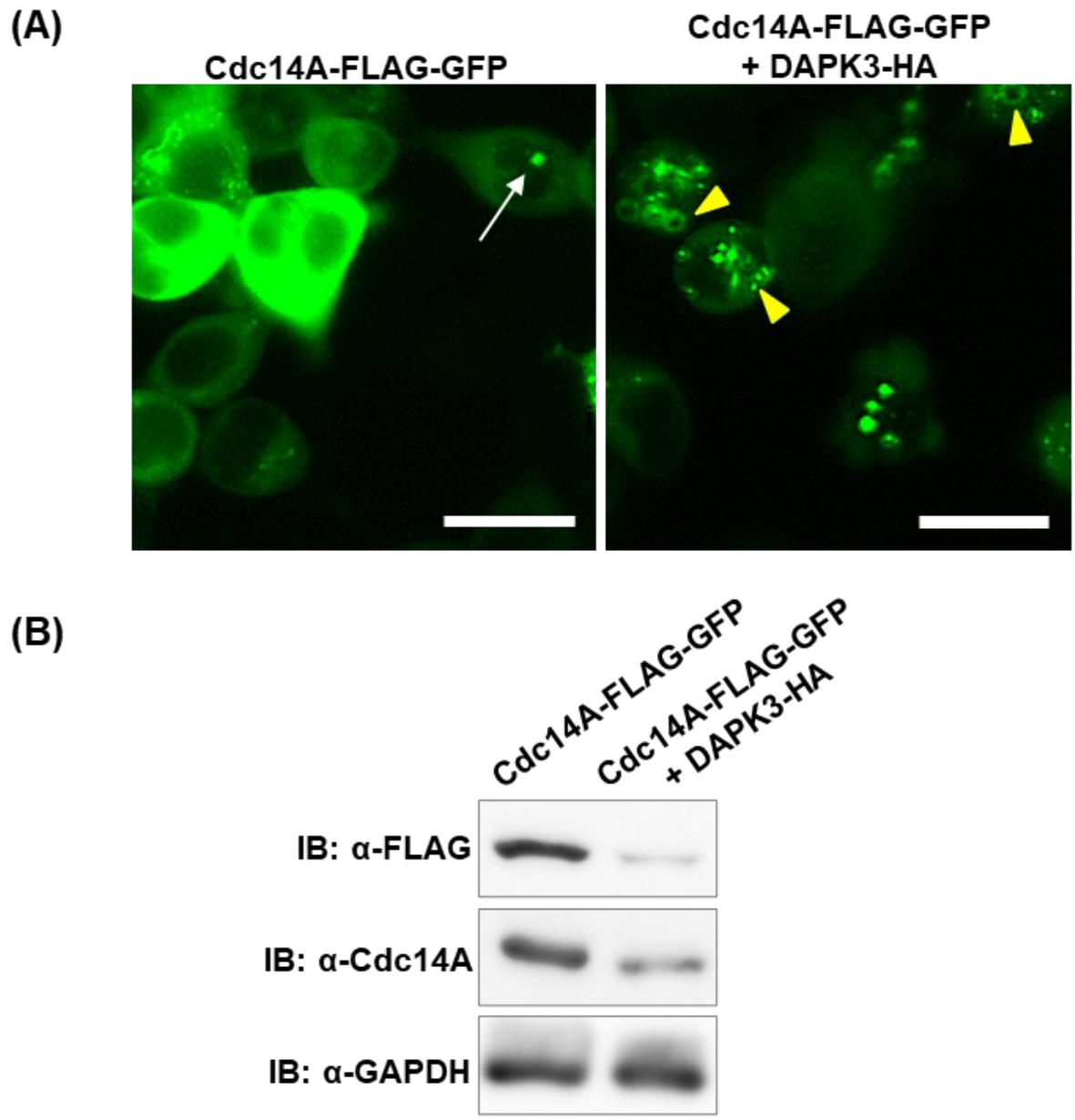

Figure 22. Ectopic expression of HA-tagged DAPK3 altered Cdc14A subcellular localization and decreased Cdc14A protein abundance. (A) GFP-associated fluorescence was recorded in live HEK293T cells expressing Cdc14A-FLAG-GFP with or without DAPK3-HA overexpression at 24-hour post-transfection. White arrow points to presumed centrosome. Yellow arrowhead points to presumed autophagosomes. Scale bars = 20 μm. **(B)** HEK293T cells were transfected with Cdc14A-FLAG-GFP with or without DAPK3-HA. Cdc14A-FLAG-GFP and endogenous Cdc14A protein was analyzed by immunoblotting 24 hours after transfection. GAPDH was used as loading control.

3.3.6. Truncation of Cdc14A near the N-terminus barred DAPK3-induced Translocation of Cdc14A to Presumed Autophagosomes and led to Decreased DAPK3 Recovery in Pull-down Assay.

DAPK3 is known to induce autophagy (**Section 1.13**). Therefore, the translocation of Cdc14A to presumed autophagosomes may be conditioned upon autophagy rather than a functional interplay between DAPK3 and Cdc14A. Nonetheless, given the direct interaction observed between the N-terminus (a.a. 1-348) of Cdc14A and DAPK3 (Wu et al., 2015), the translocation of Cdc14A could be coordinated by DAPK3. The N-terminus of Cdc14A contain two ubiquination sites (K69 and K72). Potentially, ubiquination at K69 and/or K72 on Cdc14A directed Cdc14A to aggrephagy – a form of ubiquitin-dependent selective autophagy (R. H. Chen et al., 2019). And the binding of DAPK3 to Cdc14A facilitated this aggrephagy. If so, then the deletion of K69 and/or K72 on Cdc14A should prevent the translocation of Cdc14A to autophagosomes. Indeed, truncation of Cdc14A at V44, K80, or G100 prevented translocation of Cdc14A from the cytoplasm to presumed autophagosomes (**Figure 23A**). As well, recovery of DAPK3 in pull-down experiment diminished with progressive truncation of the N-terminus of Cdc14A (**Figure 23B**).

(A)

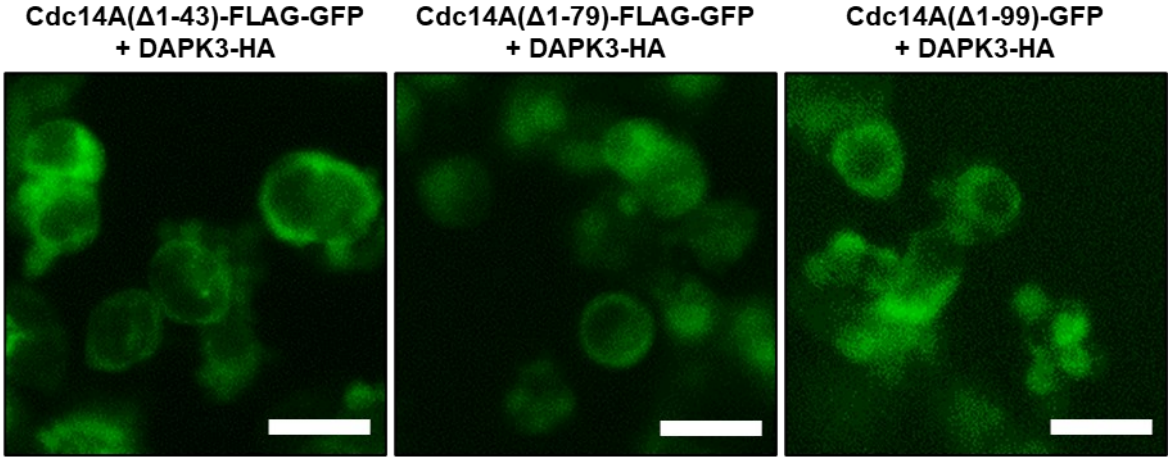
Cdc14A(Δ1-43)-FLAG-GFP
+ DAPK3-HA
Cdc14A(Δ1-79)-FLAG-GFP
+ DAPK3-HA
Cdc14A(Δ1-99)-GFP
+ DAPK3-HA

(B)

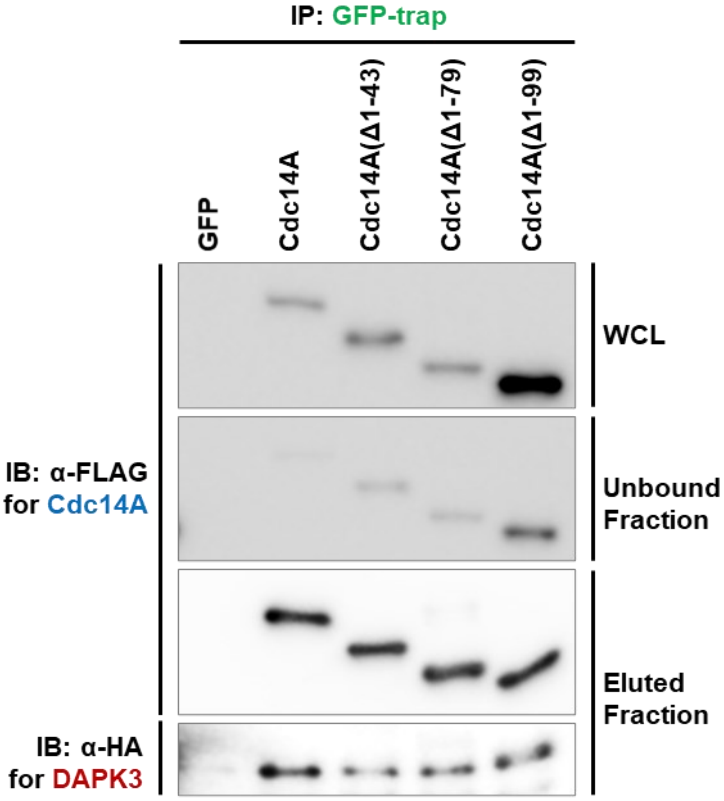
IP: GFP-trap
GFP
Cdc14A
Cdc14A(Δ1-43)
Cdc14A(Δ1-79)
Cdc14A(Δ1-99)
WCL
Unbound
Fraction
Eluted
Fraction
IB: α-FLAG
for Cdc14A
IB: α-HA
for DAPK3

Figure 23. Truncation of Cdc14A near the N-terminus barred DAPK3-induced translocation of Cdc14A to presumed autophagosomes and led to decreased binding affinity to DAPK3. **(A)** GFP-associated fluorescence was recorded in live HEK293T cells co-transfected with truncated Cdc14A-FLAG-GFP and DAPK3-HA at 24-hour post-transfection. Scale bars = 20 μm. **(B)** HEK293T cells were co-transfected with DAPK3-HA and Cdc14A-FLAG-GFP or truncated Cdc14A-FLAG-GFP. At 24-hour post-transfection, GFP-tagged (truncated)Cdc14A were immunoprecipitated via GFP-Trap®_A (Chromotek). Eluted fractions were then analyzed for DAPK3 protein abundance.

3.4. Discussion.

In the bioinformatic chapter of this thesis, DAPK3 was shown to be a potential key factor for UC progression. Given the importance of mucosal healing in reducing the risk of CAD/CAC (**Section 1.7**), and the involvement of DAPK3 in various cellular signaling pathways that trigger cell proliferation, migration, growth, apoptosis, and autophagy (**Section 1.13**), experiments were designed to examine the effects of HS compounds on Caco-2 monolayers. These studies were predicted to reveal the role that DAPK3 may play in IEC wound repair. An advantage of small molecule inhibitors is that they can be titrated to reveal a spectrum of phenotypes. Moreover, the inhibition of enzymatic activity does not necessarily prevent protein-protein interactions. Therefore, the use of small molecule inhibitors presents an opportunity to differentiate between the enzymatic and structural role of a protein. The major argument against the use of small molecule inhibitors is their potential off-target effects. Across the human kinome, the ATP-binding site is highly conserved. Thus, development of selective small molecule inhibitors is beleaguered with unintended kinase targets (Zarrin et al., 2021). Several uncommon features in the ATP-binding pocket of DAPK3 underwrite the high selectivity offered by HS38. An example is the positioning of Lys42, which forms a single hydrogen bond with the thioether of HS38. This hydrogen bond forms part of the DAPK3-ATP interaction that is distinct from other members of the kinome, so this restrictive structural feature provides an avenue to augment the selectivity of HS compounds towards DAPK3 (D. A. Carlson et al., 2018). Nevertheless, HS38 displays high potency towards DAPK1 and the structurally related PIM3 kinase (D. A. Carlson et al., 2013). Whereas DAPK1 is known to regulate DAPK3 via multisite phosphorylation (Shani et al., 2004), no regulatory relationship for DAPK3 has been reported for PIM3. It is thus necessary to consider the off-target influences that DAPK1 and PIM3 may have on IEC wound healing when utilizing

HS38. The PIM3 contribution to wound healing was addressed in this cell study via parallel *in vitro* experiments completed by treatment of Caco-2 cells with HS38, HS56, or HS94. Unfortunately, with regards to DAPK1, all currently available DAPK3 inhibitors showed comparable potency towards both DAPK1 and DAPK3 (Al-Ghabkari et al., 2016; D. A. Carlson et al., 2013, 2018). Thus, the crosstalk between DAPK3 and DAPK1 activities and their overlapping biological functions (**Section 1.12 and 1.13**) will need to be assessed in future studies. This may be completed via introduction of constitutively active ΔCaM mutant DAPK1 (Singh et al., 2016) or following the development of a selective inhibitor that can differentiate between DAPK3 and DAPK1.

Data from the current study showed that DAPK3 inhibition in Caco-2 significantly enhanced wound healing. An analysis of EdU cell proliferation assays suggest that this increased rate of wound closure is owed, in part, to the augmentation of cell proliferation by DAPK3 inhibition. Additionally, detailed inspection of EdU-coupled fluorescence revealed probable effects of DAPK3 inhibition on cell cycle kinetics. Recently, Pereira and colleagues showed that by measuring the fluorescence intensities stemming from the stoichiometric azide-fluorochrome detection of EdU-substituted DNA, one can determine the length of S-phase by pulsing asynchronous cell population with EdU for incremental periods of time (Pereira et al., 2017). Essentially, when the pulsing duration matches the length of S-phase, a cohort of cells would be labeled for the full S-phase and will show maximum intensity. In the current study, all Caco-2 monolayers were exposed to EdU for the same duration of time. As such, the absolute length of S-phase cannot be determined. However, the increased distribution of EdU-positive cells towards maximal-intensity suggests that the altered cell proliferation might be a consequence of accelerated cell cycle progression.

YAP-driven increase in cell proliferation has been proposed to result from the deregulation of S-phase duration (Cabochette et al., 2015) or G1/S transition (W. Kim et al., 2019). As well, stiffness-induced YAP activation is known to connect mechanical stress, transmitted by the ECM, to expression of genes implicated in cell proliferation (**Section 1.8**). And so, YAP activation in 2D culture can be estimated by the evaluation of YAP/F-actin colocalization (Lee et al., 2019). When DAPK3 was inhibited, colocalization of YAP with F-actin increased, particularly so around the perinuclear actin cap, which is essential for of YAP nuclear signaling (Elosegui-Artola et al., 2017; Shiu et al., 2018). The perinuclear actin cap and actin cap-associated focal adhesions (ACAFA) are major elements of the cellular mechanotransduction system, and FAK is a critical component of ACAFA (D.-H. Kim et al., 2012). Attenuation of FAK activity was demonstrated to block YAP nuclear accumulation (N. G. Kim & Gumbiner, 2015; Yamashiro et al., 2020) and previous report of FAK inhibition by the ectopic expression of DAPK3 (Nehru et al., 2013) suggests that the activation of YAP in HS38-treated monolayers may be an effect of unrestrained FAK activation. Interestingly, despite the colocalization of YAP with perinuclear stress fibers in HS38-treated monolayers, the count of cells with nuclear accumulation of YAP did not appear to differ between HS38-treated and control monolayers. This observation might have been corollary to the oscillating nature of YAP activity. Thus, the spatiotemporal dynamics of YAP during injury repair will need to be investigated in future studies.

DAPK3 may regulate YAP-mediated cell proliferation and cell cycle progression via various routes. For one, DAPK3 may exert control on YAP activity through Wnt signaling, as DAPK3 knockdown was shown to reduce β-catenin/TCF4 mediated-transcriptional activities (Togi et al., 2011), and Wnt signaling was demonstrated to induce YAP activity during crypt regeneration (Guillermin et al., 2021). However, it should be noted that DAPK3 activity was not required for

its regulation of Wnt signaling (Togi et al., 2011), and Wnt signaling could induce YAP activity via increased transcription of *YAP* rather than through post-translational regulation of YAP protein localization (Guillermin et al., 2021). Thus, the results presented in this thesis, brought about through DAPK3 inhibition, are unlikely to be facilitated via Wnt signaling.

DAPK3 may promote YAP activity through either the direct phosphorylation of RLC, or the inhibition of MLCP. Actomyosin, composed of F-actin and NM-II, serves as a central mediator between mechanical cues and Hippo/YAP signaling (**Section 1.8**). The disruption of actin polymerization with cytochalasin D or latrunculin A resulted in cytoplasmic retention of YAP. Likewise, inhibition of myosin II ATPase activity with blebbistatin reduced nuclear accumulation of YAP (Wada et al., 2011). NM-II activity is regulated by the phosphorylation of its regulatory light chains (RLC). Monophosphorylation of RLC on Ser19 increases the ATPase activity of NM-II, and diphosphorylation of RLC on both Ser19 and Thr18 further enhance the increase. (Adelstein & Anne Conti, 1975; Craig et al., 1983; Umemoto et al., 1989; Walsh, 2011). NM-II activity is terminated when RLC dephosphorylation of Ser19 and Thr18 is completed by MLCP, the activity of which is attenuated by the phosphorylation of its subunit MYPT1 on Thr697. In both smooth muscle and non-muscle cells, DAPK3 phosphorylates RLC at Ser19/Thr18 (Borman et al., 2002; Moffat et al., 2011; Murata-Hori et al., 1999; Niiro & Ikebe, 2001). DAPK3 was also found to phosphorylate Thr697 on MYPT1 (MacDonald, Borman, et al., 2001) and the activation site (Thr38) of the protein kinase C-activated inhibitor of MLCP (CPI-17) (MacDonald, Eto, et al., 2001). As DAPK3 inhibition ought to attenuate NM-II activity, which should reduce YAP activity, the (de)regulation of NM-II function via DAPK3 inhibition does not explain the outcomes observed in the cell studies conducted for this thesis.

DAPK3 may influence YAP activity through its inhibition of MLCP, independently of NM-II. Merlin/NF2, an upstream regulator of the Hippo pathway, was demonstrated to be a substrate of MYPT1-PP1δ (i.e., MLCP) (H. Jin et al., 2006). And recently, Muñoz-Galván and colleagues showed that the knockdown of *MYPT1* in ovarian cancer cell lines attenuated Merlin/NF2 dephosphorylation to deactivate the Hippo pathway, which led to increased YAP activity (Muñoz-Galván et al., 2020). As DAPK3 inhibition ought to enhance MYPT1 function, thus strengthening the activation of Merlin/NF2 to reduce YAP activity, the (de)regulation of MYPT1 function via DAPK3 inhibition does not explain the outcomes observed in the cell studies conducted for this thesis.

Cdc14A is another phosphatase through which DAPK3 may exert its influence on YAP activity. Cdc14A is a dual-specificity phosphatase that is selective towards phosphorylated serine on substrates of proline-directed kinases such as cyclin-dependent kinases (CDKs) and mitogen-activated protein kinases (MAPKs) (N.-P. Chen et al., 2017; Kaiser et al., 2002). Subcellular localization of Cdc14A is contingent on cell cycle phases. Cdc14A associates with centrosomes during interphase and become dispersed throughout the cell upon mitotic entry (Kaiser et al., 2002). With regards to Hippo/YAP, Chen and colleagues showed that a pool of Cdc14A colocalized with F-actin at the leading edge of cells and stress fibers, where it exerted control over cell migration and cell invasion via the Hippo upstream regulator KIBRA (N.-P. Chen et al., 2016). Cdc14A also controls mitotic exit by dephosphorylating CDK1-phosphorylated YAP, a mechanism that had demonstrated importance in the control of discordant cell proliferation (S. Yang et al., 2015). Moreover, Cdc14A was shown to dephosphorylate the anaphase promoting complex/cyclosome (APC/C) specific activator protein Cdh1 to activate APC/C^{Cdh1} (Bembenek & Yu, 2001; Jaspersen et al., 1998, 1999; Kao et al., 2014). And APC/C^{Cdh1} was shown to augment YAP activity and

promote G1/S phase transition via destabilization of LATS1/2 during G1 of the cell cycle (W. Kim et al., 2019).

Preliminary results obtained in this thesis indicate that DAPK3 overexpression in HEK293T cells reduced Cdc14A abundance. Given that the truncation of Cdc14A near the N-terminus barred DAPK3-induced translocation of Cdc14A to presumed autophagosomes and led to decreased DAPK3 recovery in pull-down assay, the standing hypothesis is that the ubiquination of Cdc14A at K69 and/or K72 directed Cdc14A to aggrephagy, and that the binding of DAPK3 to Cdc14A mediated the ubiquination. Several studies had implicated DAPK3 as a regulator of protein ubiquination state. Ubiquination of the DNA-binding androgen receptor (AR) was partly mediated through the direct phosphorylation of the E3 ligase MDM2 (murine double minute 2) by DAPK3 (Felten et al., 2013), and the ubiquination state of STING (stimulator of interferon genes) was shown to be promoted through direct phosphorylation of E3 ligase LMO7 (LIM domain only 7) by DAPK3 (Takahashi et al., 2021). Takahashi and colleagues identified ~20 candidate E3 ligases as potential targets for direct phosphorylation by DAPK3 within the context of STING ubiquination (Takahashi et al., 2021). DAPK3 as a regulator of Cdc14A ubiquination state is therefore a feasible hypothesis and warrants further investigation.

In summary, results from the current cell studies demonstrate the regulation of intestinal epithelial cell proliferation by DAPK3, post-injury. This effect is in part mediated by the Hippo effector YAP, with Cdc14A as a probable intermediary for the DAPK3-YAP connection.

Chapter 4 . Animal Studies of DAPK3 Contributions to the Resolution of Colitis using the Dextran Sodium Sulfate (DSS) Mouse Model of Acute Intestinal Injury.

4.1. Introduction.

Mucosal healing in UC is essential to reduce the rates of disease relapse, as well as to lower the risk of dysplasia and CAC progression (Boal Carvalho & Cotter, 2017; Carvalho et al., 2016). In **Chapter 3** , DAPK3 inhibition was demonstrated to augment Caco-2 cell proliferation to enhance wound closure; moreover, DAPK3 inhibition increased colocalization of YAP with F-actin. To evaluate the effects of DAPK3 inhibition on wound healing in UC, I utilized the dextran sodium sulfate (DSS) mouse model of colitis to address the following three questions: 1) Does DAPK3 inhibition affect the severity of DSS-induced colitis? 2) How does DAPK3 inhibition affect epithelial cell proliferation post-DSS-induced injury? And 3) How does DAPK3 inhibition affect Hippo signaling in the DSS-model of colitis?

4.1.1. The Mouse Model of Dextran Sodium Sulfate (DSS)-induced UC.

One of the most common animal models of UC is the chemical-induction of colitis by administration of DSS. DSS is a water-soluble, negatively charged, sulfated polysaccharide that is directly toxic to the colonic epithelium. When administered at 2-5% concentration in drinking water for 5-7 days, the 36-50 kDa form of DSS causes crypt destruction that is associated with the loss of surface epithelium, the infiltration of inflammatory cells into the mucosa and submucosa, and edema of the submucosa (Perše & Cerar, 2012). The compromised mucosal barrier allows for the entry of luminal antigens and pathogenic microbes into the mucosa, resulting in the development of colitis (Perše & Cerar, 2012). Clinical manifestation of short-term exposure to

DSS (i.e., 5-7 days) include weight loss, diarrhea, blood in stool, and eventually death. The disruptive effects of DSS on colonic epithelium lends itself to the *in vivo* study of factors that may play a role in the re-establishment of epithelial integrity.

4.2. Methods.

4.2.1. Model of DSS-induced UC with Recovery.

Experimental UC was induced in nine to 11-weeks old male C57BL/6 mice by the addition of 2.5% (w/v) DSS (36-50 kDa, MP Biochemicals) in drinking water for seven days. For recovery, mice were provided regular drinking water for two days post-DSS-acclimatization. After two days of recovery on regular drinking water (DSS+2), animals were euthanized by cervical dislocation after anesthesia by isoflurane inhalation. All animal protocols and use were approved by the Animal Care and Use Committee at the University of Calgary and conform to the guidelines set by the Canadian Council of Animal Care.

To evaluate the effects of DAPK3 inhibition, littermates were randomized into four groups: 1) Water + DMSO, 2) Water + HS38, 3) DSS + DMSO, and 4) DSS + HS38. Daily subcutaneous injection of HS38 (500 μg/kg) began three days prior to the introduction of DSS in drinking water and continued until euthanasia on DSS+2. The HS38 dosage was selected based on *in vitro* binding kinetics (D. A. Carlson et al., 2013), and observations from previous studies of *in vivo* tolerance among treatment animals. An overview of the study design is shown in **Figure 24A**. Body weight was tracked daily then normalized to day one of DSS administration. A disease activity index (DAI) score was estimated based on weight, stool consistency, and blood in feces (J. J. Kim et al., 2012). Criteria for DAI scoring is outlined in **Table 5**. The DAI scores and the relative weight curve was analyzed with two-way ANOVA. Multiple comparison analysis was done *post hoc* with the Šídák

correction method. Macroscopic scoring of colon tissue was performed according to the grading system outlined in **Table 6**. The Mann-Whitney U method was utilized to compare macroscopic scores. Sample size (n) was 10 for vehicle control and 12 for HS38-treated mice.

4.2.2. Histological Examination of Epithelial Damage and Inflammation.

Paraffin-embedded distal-colon tissues sectioned at 5-µm thickness were deparaffinized, rehydrated with gradient ethanol, then stained with hematoxylin and eosin (H&E) for blinded microscopic assessment of UC severity. The grading system considers the degree of epithelial damage and infiltration of inflammatory cells (Hirota et al., 2011), as well as the percentage of involvement. Criteria for scoring is outlined in **Table 7**. The Mann-Whitney U method was utilized to compare histological scores. Sample size was 10 each for vehicle control and HS38-treated mice.

Table 5. Criteria for the scoring of daily activity index.

Parameters	Score			
	0	1	2	3
Weight Change	<=5%	>5%	>10%	>15%
Stool Consistency	Normal	Loose Stool	Diarrhea	
Blood in Stool	Normal	Slight	Gross	

Table 6. Criteria for the macroscopic scoring of colon tissue.

Parameters	Score			
	0	1	2	3
Colon Shortening	<5%	5-15%	15-30%	>30%
Colonic Edema	Normal	>=1 cm	>= 3cm	>= 5 cm
Adhesion	None	Minor	Major	
Inflammation	Normal	Localized hyperemia	Ulceration w/o Hyperemia	Ulceration with Inflammation

Table 7. Criteria for the histological scoring of epithelial damage and inflammation.

Parameters	Score				
	0	1	2	3	4
Epithelial Damage	Normal	Villus Vacuolation/ Bleeding	Loss of Epithelium	Complete Loss of Crypt Architecture	
% Architectural Change	0%	0-30%	30-60%	>60%	
Inflammation	Normal	Increased Inflammatory Cells in the Lamina Propria	Increased Inflammatory Cells in the Submucosa	Dense Inflammatory Cell Mass	Transmural Inflammation
% Inflammation	0%	0-25%	25-50%	50-75%	>75%

4.2.3. Immunohistochemistry.

Deparaffinized tissues were rehydrated with gradient ethanol, then subjected to heat-induced antigen retrieval in 10 mM sodium citrate (pH 6.0). Sections were subsequently washed with PBST, then blocked with 10% normal donkey serum in PBS. Overnight incubation was carried out at 4 °C with Ki-67 (D3B5) rabbit mAb (12202, Cell Signaling) or YAP (D8H1X) XP® rabbit mAb, diluted 1:400 in PBS. The Cy3-conjugated AffiniPure donkey anti-rabbit IgG (711-165-152, Jackson ImmunoResearch) was the secondary antibody utilized, and was applied to samples at 1:200 dilution. 4',6-diamidino-2-phenylindole (DAPI; 62248, Thermo Scientific) was used at 10 μg/mL to mark nuclei. For sections tagged with α-Ki-67, images were taken with the Olympus FV10i confocal microscope on the 60X objective (oil). Ki-67^{+} positive nuclei was manually counted, then expressed as a percentage of total nuclei per crypt. Between 19-30 well-oriented crypts from 2-3 sections were evaluated per animal. Sample size was 3-8 animals per group. For sections tagged with α-YAP, images were taken with Nikon A1R laser scanning confocal microscope on 40X objective (oil) at Nyquist (xy-plane). For image deconvolution, stacks of 10 equidistant (0.5 μm) z-planes were evaluated. Sample size was two animals and four sections per group.

4.2.4. Immunoblotting.

Midsections from murine colon were homogenized with Polytron™ homogenizer. The buffer used contained 20 mM Tris-HCl (pH 8.0), 100 mM NaCl, 0.1% (w/v) SDS, 0.9 mM EDTA, 0.5% (v/v) Triton X-100, 7 mM Na_3VO_4, 50 mM NaF, and cOmplete™ Protease Inhibitor Cocktail. Homogenates were sonicated for 10 minutes at 4 °C, then centrifuged at 14,000 rpm for 10 minutes. Supernatants were then collected for immunoblotting. Proteins were resolved by SDS-PAGE (12%) gel electrophoresis then transferred onto 0.2 μm nitrocellulose membranes. Blocking was done

with 5% (w/v) non-fat milk in TBST, then membranes were incubated overnight in primary antibodies at 4 °C. Primary antibodies used were the Phospho-YAP (Ser127) (D9W2I) rabbit mAb (13008, Cell Signaling), diluted 1:500 in TBST (containing 5% (w/v) BSA), the Phospho-YAP (Ser397) (D1E7Y) rabbit mAb (13619, Cell Signaling), diluted 1:1,000 in TBST (containing 5% (w/v) BSA), the Phospho-MOB1 (Thr35) (D2F10) rabbit mAb (8699, Cell Signaling), diluted 1:1,000 in TBST (containing 5% (w/v) BSA), the DAPK3/ZIPK rabbit Antibody (2928, Cell Signaling), diluted 1:500 in TBST (containing 5% (w/v) BSA), the MST1 rabbit Antibody (3682, Cell Signaling), diluted 1:1,000 in TBST (containing 5% (w/v) BSA), the MST2 rabbit Antibody (3952, Cell Signaling), diluted 1:1,000 in TBST (containing 5% (w/v) BSA), the LATS1 (C66B5) rabbit mAb, (3477, Cell Signaling), diluted 1:500 in TBST (containing 5% (w/v) BSA), the YAP/TAZ (D24E4) rabbit mAb (8418, Cell Signaling), diluted 1:1,000 in TBST (containing 5% (w/v) BSA), the MOB1 (E1N9D) rabbit mAb (13730, Cell Signaling), diluted 1:1,000 in TBST (containing 5% (w/v) BSA), and the GAPDH (14C10) rabbit mAb (2118, Cell Signaling), diluted 1:1,250 in TBST (containing 5% (w/v) BSA). Immunoreactive proteins were visualized using the ChemiDoc Imaging System (Bio-Rad).

4.2.5. Quantitative Real-time Reverse Transcription Polymerase Chain Reaction.

Samples for quantitative real-time polymerase chain reaction (qRT-PCR) were obtained through the University of Calgary Intestinal Inflammation Tissue Bank (Protocol #18142, Ethics #REB14-2430). Consenting patients undergoing endoscopy as part of an investigation into IBD status, or as part of a colonic cancer screen were included. Screening subjects who were found negative for IBD constitute the control group. For this study, biopsy specimens taken from the left colon of healthy individuals (n=7) or the left colon of IBD patients with active inflammation [UC-inflamed (n=9), Crohn's disease (CD)-inflamed (n=9), fibrotic CD-inflamed (n=5)] were utilized. All

samples were stabilized in RNAlater™ (Ambion) and were stored at -80 °C to minimize RNA degradation.

RNA was extracted from biopsies with the TRIzol™ reagent (15596, Invitrogen). Biopsies suspended in RNAlater were thawed on ice, washed with ice-cold PBS, then placed into 500 µL of TRIzol. Stainless steel beads (0.9-2.0 mm diameter; SSB14B-RNA, Next Advance) were added to the biopsies to facilitate homogenization with the Bullet Blender® Homogenizer (Next Advance). Homogenates were transferred to a fresh Eppendorf tube, then incubated for 10 minutes at RT prior to the addition of 100 µL of chloroform. After 10 minutes of incubation at RT, the samples were centrifuged at 12,000 rpm for 15 minutes at 4 °C. RNA isolation was then completed with the addition of 250 µL of isopropanol to the RNA-containing aqueous phase. After 10 minutes of incubation, the samples were centrifuged at 14,000 rpm for 10 minutes at 4 °C. The pellets were then washed with 500 µL of 75% (v/v) ethanol in UltraPure™ DNase/RNase-Free Distilled Water (10977, Invitrogen). Post-wash, the pellets were air-dried then resuspended in 25 µL of UltraPure distilled water (containing 0.1 mM EDTA). After 10 minutes of incubation at 60 °C, RNA yield and quality was determined via a Nanodrop spectrophotometer. Total RNA (1.5 µg) was then prepared into cDNA using the RT^2 First Strand kit (330404, Qiagen) by following procedures outlined in the manufacturer manual. Finally, reverse-transcribed RNA was diluted with the addition of 80 µL nuclease-free water.

The PCR reactions were ran using the CFX96 Touch Real-Time PCR Detection System (Bio-Rad). DAPK3 was amplified with forward primer 5'-CTGGAGTGGAAGCTGCTGGAAG-3' and reverse primer 5'-AACTTGGCTGCGTACTCCTTGC-3', ribosomal protein lateral stalk subunit P0 (RPLP0) was amplified with forward primer 5'-TGGTCATCCAGCAGGTGTTCGA-3' and reverse primer 5'-ACAGACACTGGCAACATTGCGG-3', peptidylprolyl isomerase A (PPIA) was amplified with

forward primer 5'-GGCAAATGCTGGACCCAACACA-3' and reverse primer 5'-TGCTGGTCTTGCCATTCCTGGA-3'. The PCR reaction components were: 20 µL total volume, 2.5 µL of cDNA, 250 nM of each primer, and 10 µL of SsoAdvanced™ Universal SYBR® Green Supermix (1725271, Bio-Rad). The PCR cycling parameters were 95 °C 30 seconds, (95 °C 10 seconds, 61.5 °C 30 seconds) x 40 cycles, melt curve 65 °C to 95 °C (0.5 °C/5 seconds). Melt curves were inspected to rule out amplification of unrelated fragments during PCR. Cycle threshold was determined with the LinRegPCR analysis program (v11.0, https://www.medischebiologie.nl/wp-content/uploads/2018/11/linregpcr.zip). Gene expression was calculated by using the comparative threshold cycle ($2^{-\Delta\Delta Ct}$) method. Briefly, ΔCt was calculated vs. the geometric mean of *RPLP0* and *PPIA*, as these two genes were found stably expressed in IBD (Krzystek-Korpacka et al., 2014). ΔΔCt was calculated against the ΔCt of inter-run calibrator, represented by one of the seven normal, non-inflamed samples. $2^{-\Delta\Delta Ct}$ was then log-transformed to arrive at the relative fold expression for each sample. Statistical analysis for the qRT-PCR experiment was performed using one-way ANOVA with *post hoc* multiple comparisons corrected via the Dunnett method.

4.3. Results.

4.3.1. *In vivo* HS38 Administration Increased Susceptibility to DSS-induced Colitis.

DAPK3 abundance in colon tissues from C57BL/6 mice was evaluated via immunoblotting. After seven days of DSS treatment plus two days of recovery (DSS+2), with or without treatment with the DAPK3 inhibitor HS38, DAPK3 protein levels were significantly downregulated (**Figure 24B**). Interestingly, when treated with the DAPK3 inhibitor HS38, mice showed greater weight loss than their vehicle-control littermates (1.36% of total variation, $p<0.0001$; **Figure 25A**). Moreover, two of the mice that were treated with HS38 had to be removed from the study due to severe weight

loss that exceeded the humane endpoint criteria (weight loss of >15%). Two-way ANOVA of DAI indicated no significant HS38-dependent variation over the course of DSS-induced colitis (**Figure 25B**). However, *post hoc* multiple comparison showed significant elevation of DAI that was HS38-dependent (p=0.0391) during recovery from DSS-induced colitis (**Figure 25B**). While macroscopic scores did not differ between HS38-treated and vehicle-control mice at DSS+2 (**Figure 25C)**, histological analyses revealed a small but significant increase in colitis severity for the HS38-treated mice, per measures of epithelial damage and inflammation (**Figure 25D, E**). These data suggest that DAPK3 plays a protective role in DSS-induced colitis.

4.3.2. *In vivo* HS38 Administration Attenuated IEC proliferation post DSS-induced Injury.

To determine the proliferative fraction of IECs in mice, paraffin-embedded distal-colon tissues were stained with antibodies targeting Ki-67. Mice given regular drinking water showed no significant differences in IEC proliferation regardless of treatment with HS38 or DMSO (**Figure 26A**). In these animals, Ki-67^{+} cells were displayed at the crypt base and encompassed ~25% of total crypt IECs (**Figure 26B**). In response to DSS-induced injury, Ki-67^{+} cells increased to ~57% of total IECs per crypt (**Figure 26A)**. In mice recovering from DSS-induced injury, HS38 treatment decreased the epithelial distribution of proliferating cells to a level similar to uninjured animals (~32%, **Figure 26B**). These data indicate that the lack of DAPK3 activity impeded resolution of intestinal injury after acute DSS colitis and appeared to attenuate epithelial-specific proliferation.

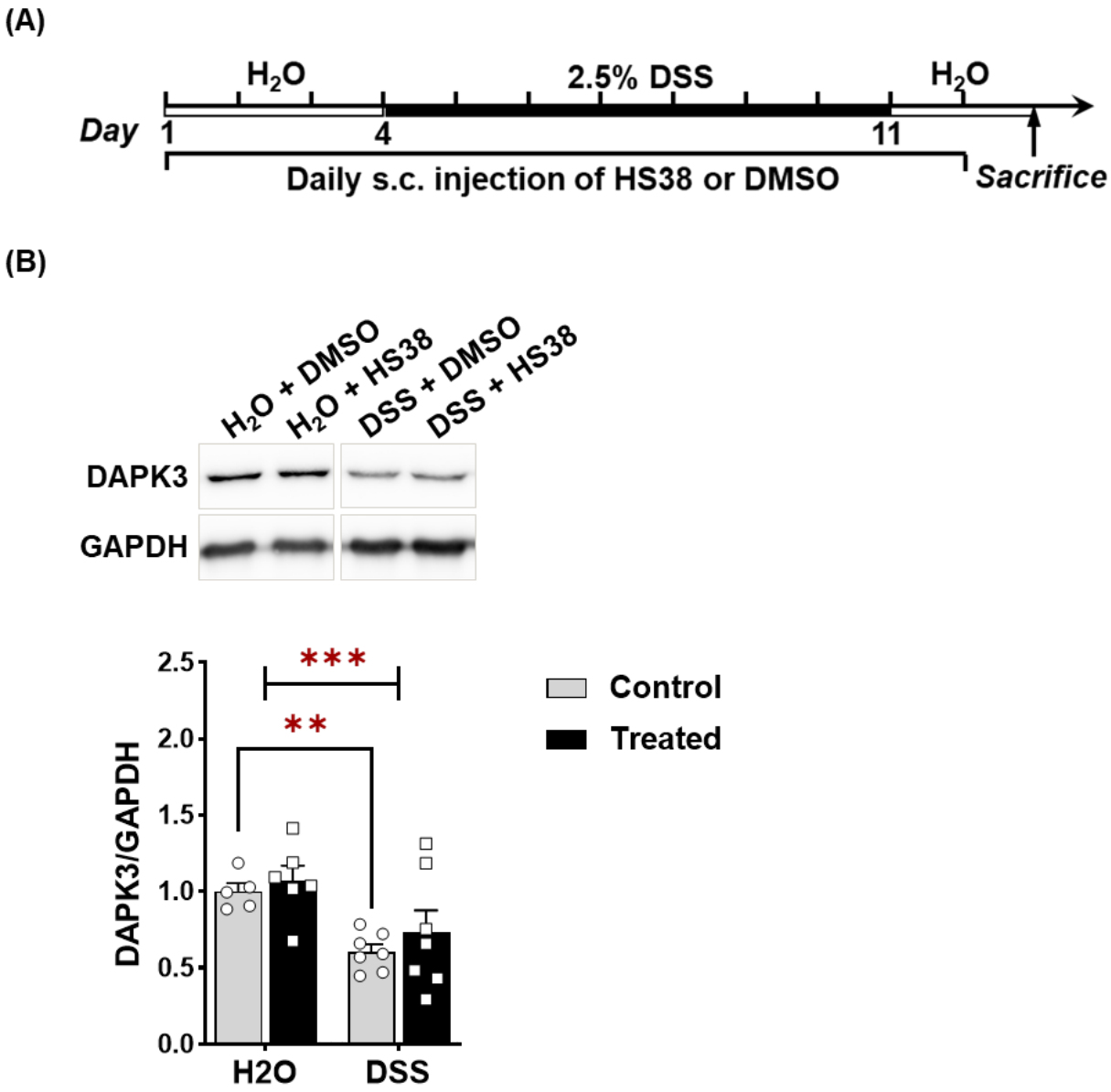

Figure 24. DAPK3 abundance decreased in colon tissue of DSS-treated mice. (A) Diagram showing the procedures that C57BL/6 mice underwent throughout the study. **(B)** Lysates from midsections of murine colon were used for immunoblotting using α-DAPK3, with GAPDH as loading control. Statistical significance was determined via unpaired t-test. ***$p<0.001$. Error bars represent ± SEM. n=5-7.

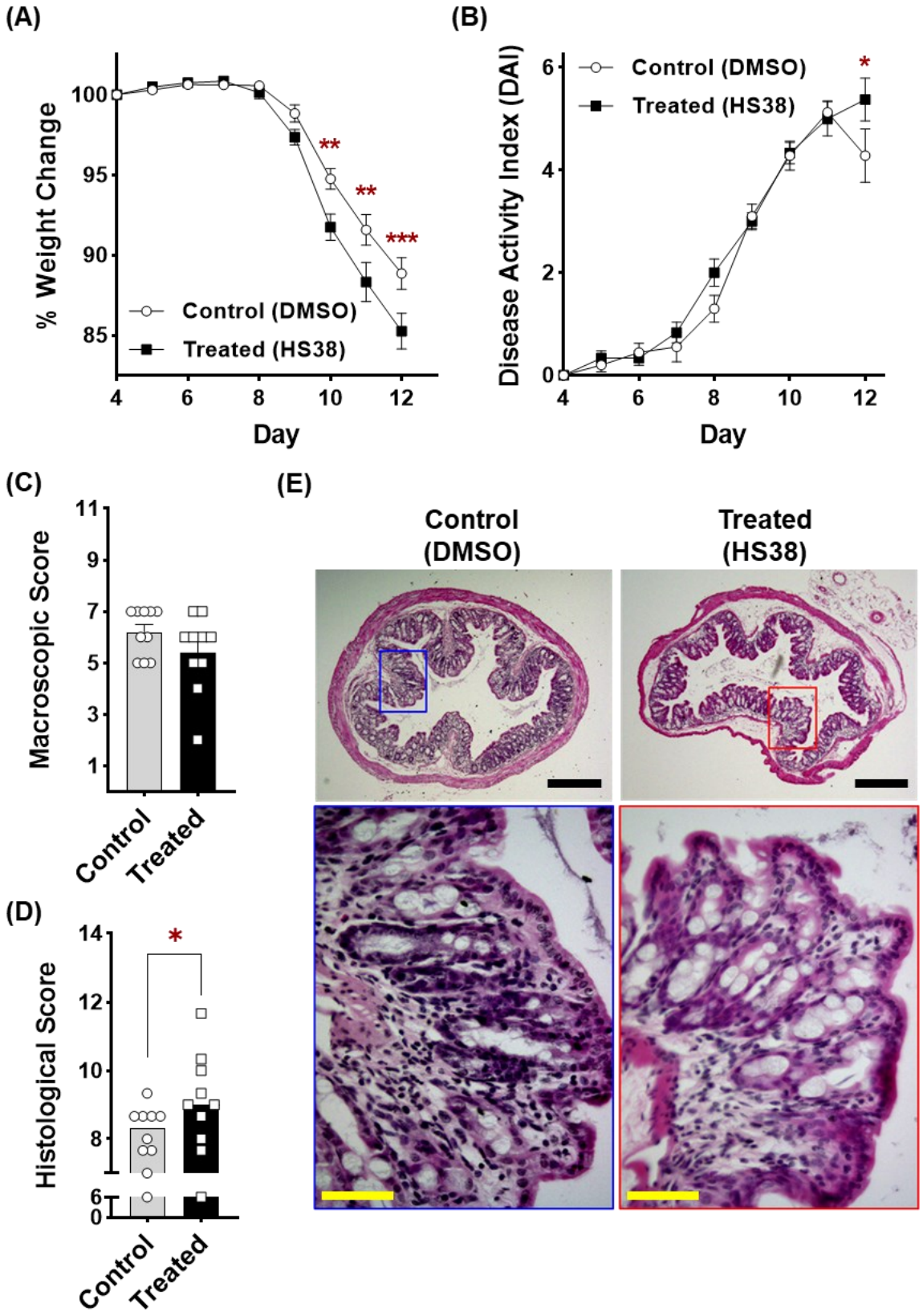
(A)
% Weight Change
100
95
90
85
**
**
***
Control (DMSO)
Treated (HS38)
4
6
8
10
12
Day
(B)
Disease Activity Index (DAI)
6
4
2
0
Control (DMSO)
Treated (HS38)
*
4
6
8
10
12
Day
(C)
Macroscopic Score
11
9
7
5
3
1
Control
Treated
(D)
Histological Score
14
12
10
8
6
0
*
Control
Treated
(E)
Control (DMSO)
Treated (HS38)

Figure 25. *In vivo* administration of HS38 increased susceptibility to DSS-induced colitis. (A) The percentage weight change after introduction of 2.5% DSS in drinking water of mice treated with 500 μg/kg HS38 (n=12) or DMSO (n=10). Statistical significance was determined via multiple comparison analysis after 2way-ANOVA with the Šídák correction method. **(B)** DAI scores, analyzed in the same manner as was done for body weight. **(C)** & **(D)** Macroscopic and histological scores were estimated for HS38-treated (n=10) and vehicle control (n=10) mice at DSS+2. Statistical significance was determined via unpaired Student's t-test. **(E)** Representative H&E staining of the colon of HS38-treated and vehicle control mice. *$p<0.05$, **$p<0.01$, ***$p<0.001$. Error bars represent ± SEM. Scale bars (black) = 300 μm. Scale bars (yellow) = 50 μm.

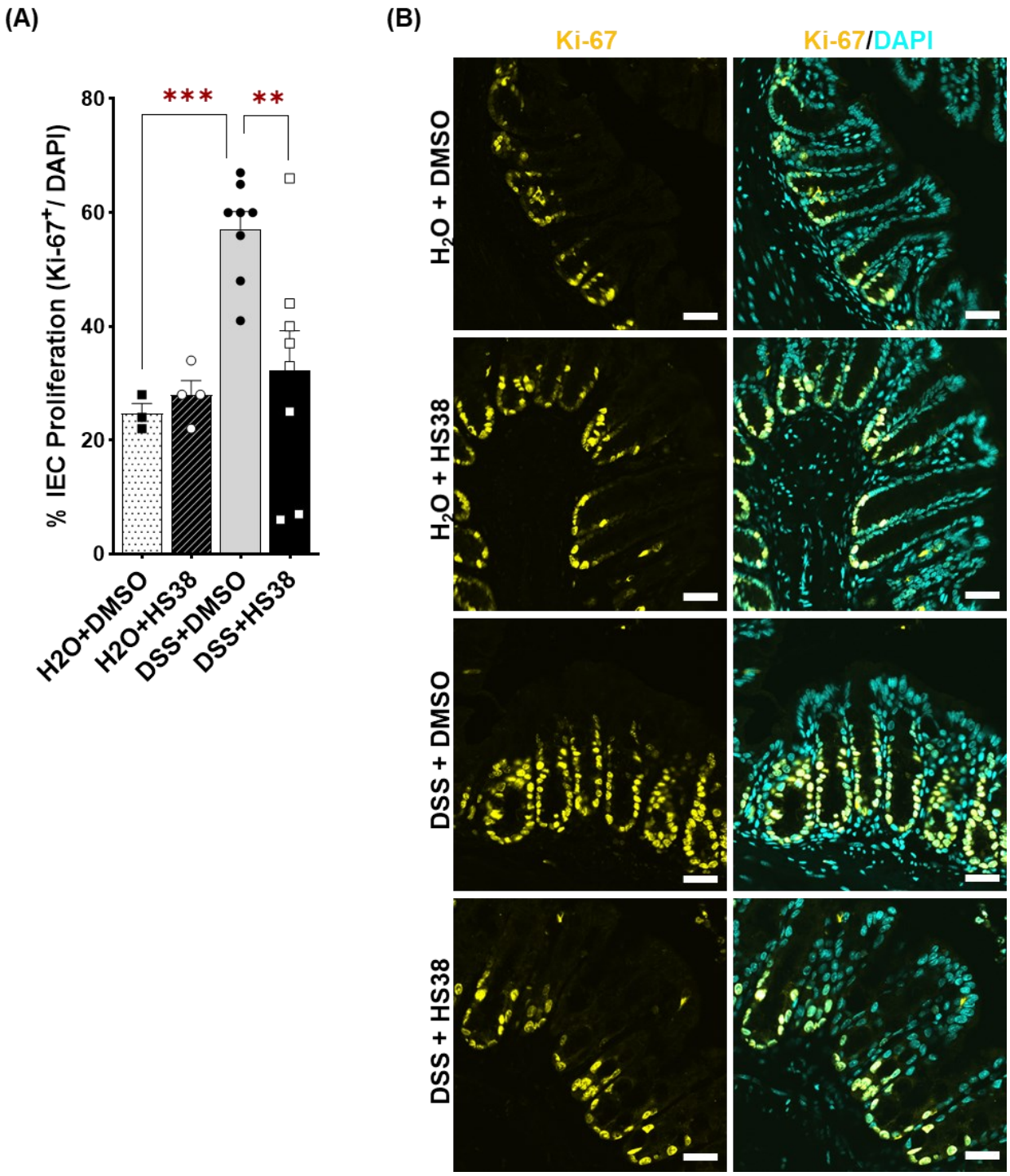
(A)
% IEC Proliferation (Ki-67+/ DAPI)
80
60
40
20
0
***
**
H2O+DMSO
H2O+HS38
DSS+DMSO
DSS+HS38
(B)
Ki-67
Ki-67/DAPI
H2O + DMSO
H2O + HS38
DSS + DMSO
DSS + HS38

Figure 26. *In vivo* HS38 administration attenuated colonic IEC proliferation following recovery from DSS-induced injury. (A) Percent proliferation of IECs, evaluated by the number of Ki-67^{+} cells as percentage of total DAPI^{+} cells per crypt. Statistical significance was determined via unpaired Student's t-test. **p<0.01, ***p<0.001. n=3-8 animals. Error bars represent ± SEM. **(B)** Representative Ki-67 staining of the colon of HS38-treated and vehicle control mice. Scale bars = 50 μm.

4.3.3. HS38 Administration Stimulated YAP Nuclear Accumulation *in vivo*.

The essential role of Hippo signaling on repair from acute intestinal injury has been demonstrated in multiple studies. As the downstream effector of Hippo pathway, the transcriptional regulator YAP has been implicated as an important mediator of mechanotransduction and proliferation during colonic epithelial repair (**Section 1.9**). With regards to DSS-induced colitis, Cai and colleagues showed impaired epithelial regeneration of *Yap*-deficient colonic crypts (J. Cai et al., 2010). And Yui and colleagues found that the colonic epithelium undergoes a YAP-dependent transition to fetal-like state to facilitate repair during recovery from DSS-induced colitis (Yui et al., 2018).

The effects of DAPK3 inhibition on the core Hippo signaling pathway and the cellular localization of YAP was investigated to test whether the change in IEC proliferation, brought about by DAPK3 inhibition, may involve the Hippo pathway. Intriguingly, in >50% of uninjured animals, YAP protein abundance appeared elevated in response to DAPK3 inhibition (**Figure 27A**); however, this difference did not reach statistical significance (**Figure 27B**). DAPK3 inhibition was accompanied with decreased phospho-S127-YAP levels (**Figure 27A**), significantly so in injured animals but not in uninjured animals (**Figure 27C**). However, none of the core Hippo regulators showed significant changes in protein abundance upon DAPK3 inhibition (**Figure 28**).

The phosphorylation of Ser127 specifically primes the binding of YAP to 14-3-3 and leads to its cytoplasmic retention (Zhao et al., 2007). To substantiate the results obtained from $pYAP^{S127}$ immunoblots, paraffin-embedded distal-colon tissues were probed with antibodies targeting total YAP to evaluate its subcellular localization. In animals receiving both DSS and HS38, colonic IECs showed increased nuclear accumulation of YAP when compared to animals receiving DSS and DMSO (**Figure 27D**); this nuclear accumulation of YAP was observed in IECs located at the

crypt base and the crypt apex (**Figure 27D. Insets (iii) and (iv) respectively**). These data suggest that DAPK3 inhibition bypassed the Hippo pathway to activate YAP.

4.3.4. *DAPK3* Expression is Downregulated in Inflamed Colonic Tissues of Patients with Fibrotic CD.

Data from the current cell and animal studies support the primary overarching hypothesis that DAPK3 is an important effector in the reparative epithelium. This suggests that *DAPK3* may be differentially expressed in inflamed tissues of IBD patients vs. non-inflamed tissues of healthy individuals. To investigate, *DAPK3* expression was compared between biopsy specimens collected from healthy controls and IBD patients with active inflammation (UC-inflamed, CD-inflamed, or fibrotic CD-inflamed) by way of qRT-PCR analysis. UC-inflamed tissues showed comparable *DAPK3* expression to non-inflamed tissues from healthy individuals (**Figure 29**). This finding echoes the result obtained from differential gene expression analysis of *DAPK3* in left-sided colitis, that was conducted on the GSE47908 microarray dataset (**Table 2**). Interestingly, whereas CD-inflamed tissues also showed insignificant changes to *DAPK3* expression, inflamed tissues from patients with fibrotic CD displayed significant downregulation of *DAPK3* (**Figure 29**: mean difference=1.8-fold, $p<0.0001$).

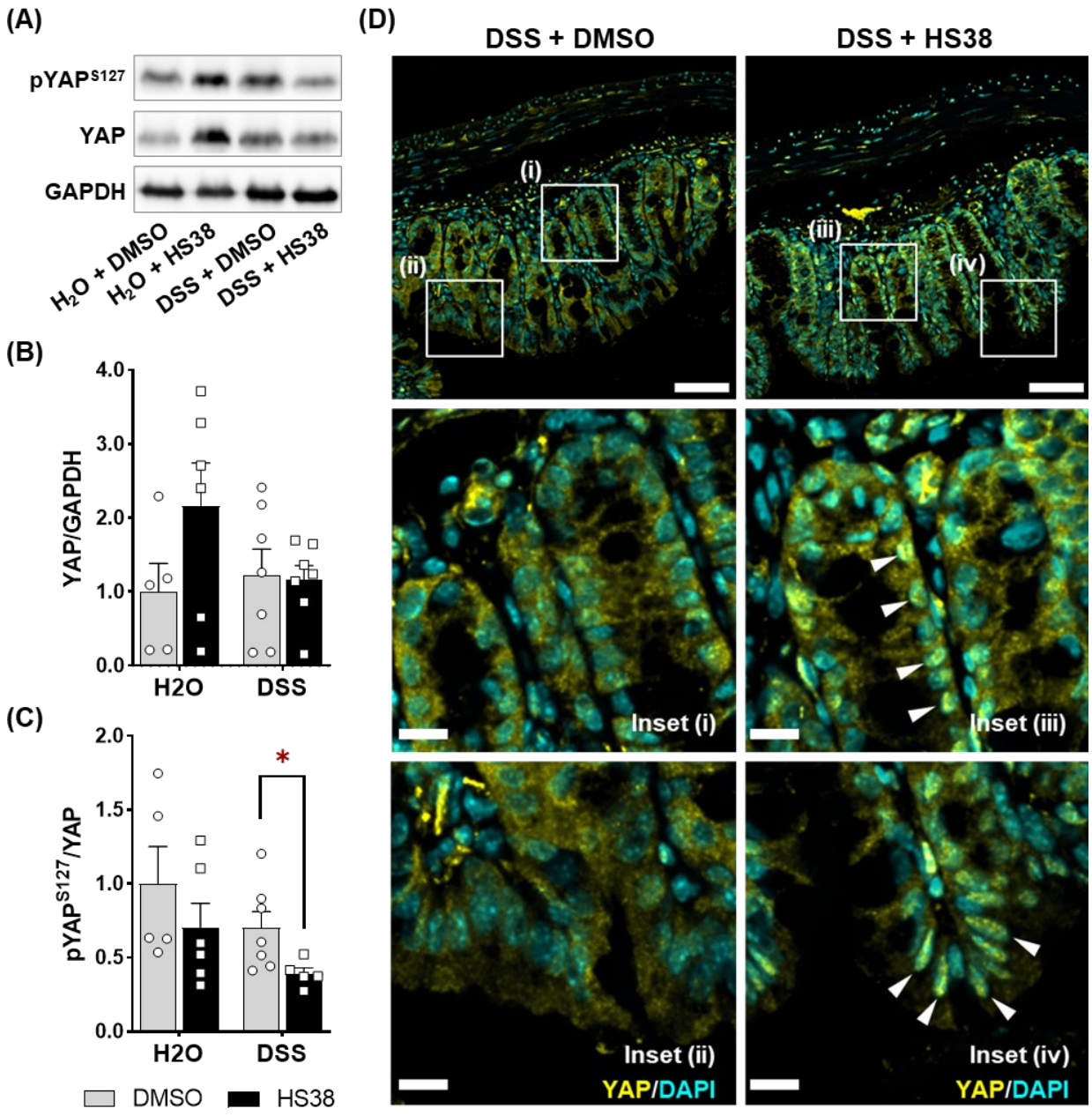
(A)
pYAP^{S127}
YAP
GAPDH
H$_2$O + DMSO
H$_2$O + HS38
DSS + DMSO
DSS + HS38
(B)
YAP/GAPDH
4.0
3.0
2.0
1.0
0.0
H2O
DSS
(C)
pYAP^{S127}/YAP
2.0
1.5
1.0
0.5
0.0
*
H2O
DSS
DMSO
HS38
(D)
DSS + DMSO
DSS + HS38
(i)
(ii)
(iii)
(iv)
Inset (i)
Inset (iii)
Inset (ii)
YAP/DAPI
Inset (iv)
YAP/DAPI

Figure 27. Administration of HS38 stimulated YAP nuclear accumulation in colonic IECs following DSS-induced injury. Lysates obtained from mice colon midsections were immunoblotted for total YAP and phospho-S127 YAP, with GAPDH utilized as loading control **(A)**. Results from densitometric analysis of total YAP vs. GAPDH **(B)** and phospho-S127 YAP vs. total YAP **(C)** are presented as mean normalized protein abundance (n=5-7). Error bars represent ± SEM. Statistical significance was determined via unpaired Student's t-test **$p<0.05$. **(D)** Mouse distal-colon tissue sections were immunostained for YAP (yellow) and DNA (cyan). Arrowheads point toward nuclear accumulation of YAP. Scale bars (main panels) = 100 μm. Scale bars (insets) = 20 μm.

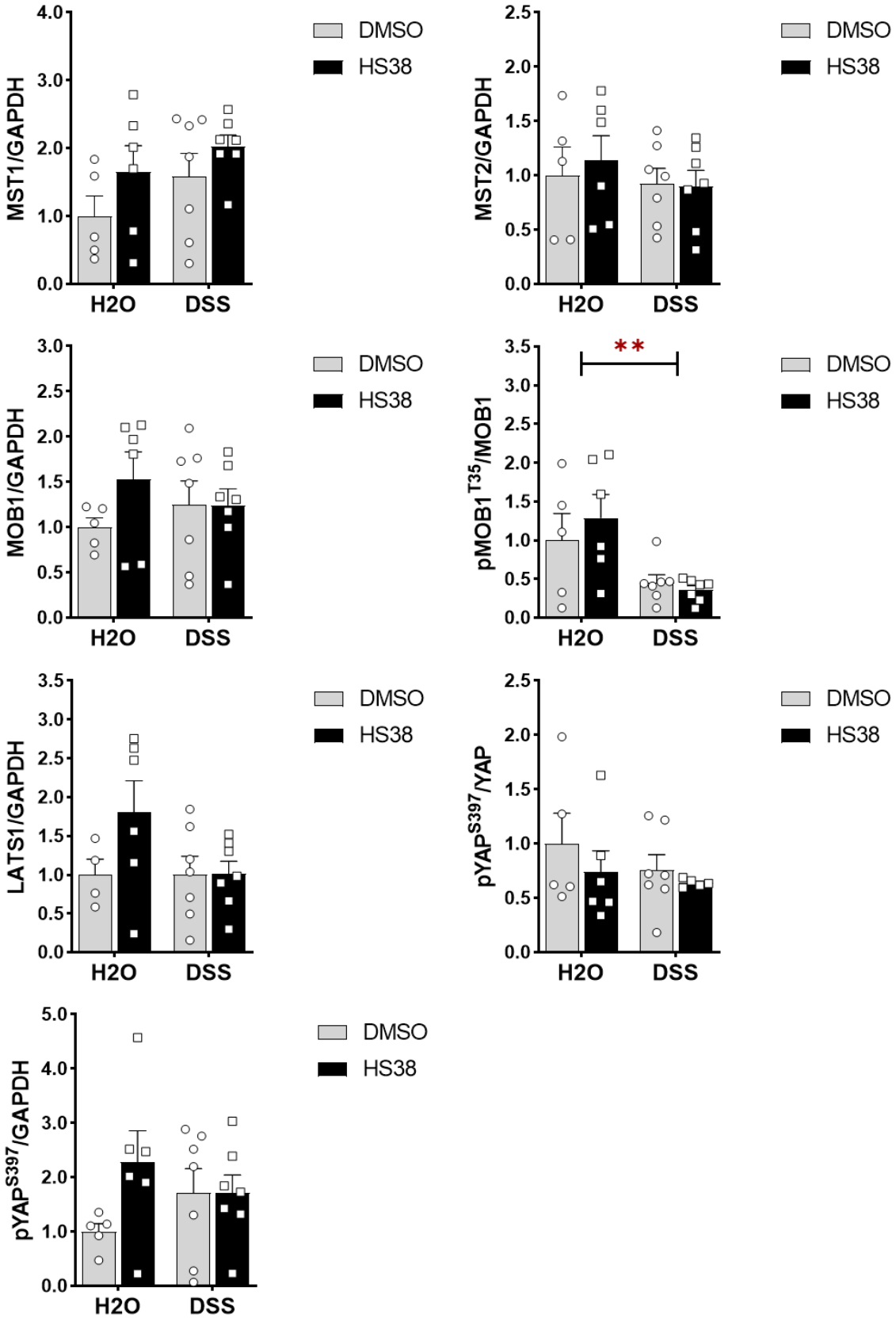
MST1/GAPDH
MST2/GAPDH
MOB1/GAPDH
pMOB1T35/MOB1
LATS1/GAPDH
pYAPS397/YAP
pYAPS397/GAPDH
DMSO
HS38
H2O
DSS
**

Figure 28. Core Hippo regulators showed insignificant changes in protein abundance upon treatment with HS38. Lysates obtained from mice colon midsections were immunoblotted for core regulators of the Hippo pathway. GAPDH was used as loading control. The results represent the mean normalized protein abundance. n=5-7. Error bars represent ± SEM. Statistical significance was determined via unpaired Student's t-test **$p<0.01$.

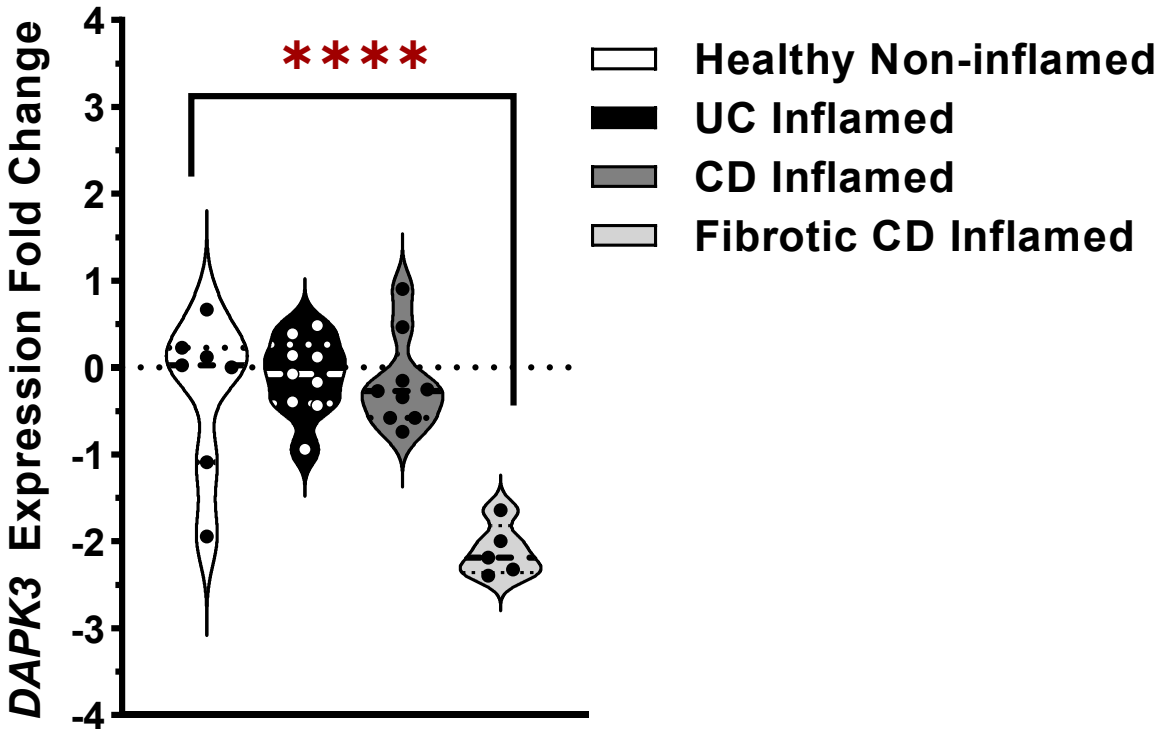

Figure 29. DAPK3 expression is downregulated in inflamed colonic tissues of patients with fibrotic CD. *DAPK3* gene expression is downregulated by 1.8-fold ($p<0.0001$) in inflamed tissues biopsied from the left colon of fibrotic CD patients. Statistical significance was identified by one-way ANOVA with *post hoc* multiple comparisons corrected via the Dunnett method. Data are presented as a violin plot showing the median (dashed line) along with the upper and lower limits of the interquartile range between the 25th and 75th percentile (dotted lines). N=7, 9, 9, and 5 for healthy non-inflamed, UC inflamed, CD inflamed, and fibrotic CD inflamed, respectively.

4.4. Discussion.

In **Chapter 2** of this thesis, DAPK3 and the Hippo pathway were identified as potential key factors for UC progression (**Section 2.4**). In **Chapter 3** , inhibition of DAPK3 via application of HS38 was found to enhance Caco-2 monolayer wound closure (**Section 3.3.1**) via augmentation of cell proliferation (**Section 3.3.2**). Additionally, HS38 treatment was coupled with YAP activation, as indicated by the increased colocalization of YAP with F-actin in monolayers treated with HS38 (**Section 3.3.3**). These results present an intriguing possibility of DAPK3 contributing to UC progression through its regulation of YAP-mediated IEC proliferation. Mucosal healing is crucial for tempering the progression of UC (Boal Carvalho & Cotter, 2017; Carvalho et al., 2016), and YAP activity was suggested to promote mucosal regeneration for UC recovery. Notably, IEC-specific YAP ablation in mice was shown to impede regeneration of colonic crypts, and increased DSS-induced weight loss and tissue damage (J. Cai et al., 2010; Taniguchi et al., 2015). In this Chapter of the thesis, the chemical toxin DSS was used to induce colitis in mice, and the effects of DAPK3 inhibitor HS38 on epithelial repair and YAP activation was investigated post-DSS removal.

In terms of IEC proliferation, no changes were observed between vehicle control and HS38-treated mice at baseline (**Figure 26**). However, in >50% of uninjured mice (i.e., mice receiving H_2O instead of DSS), YAP protein abundance increased in response to treatment with the DAPK3 inhibitor HS38 (**Figure 27A**). As well, a trend was found towards a reduction in phosphorylation of YAP on S127 in uninjured mice treated with HS38 (**Figure 27C**). Given that YAP is largely dispensable in homeostasis, it was not surprising to find a lack of prominent defects in these control animals, despite the alteration of YAP protein abundance and YAP activation by HS38. Unexpectedly, however, the hyperproliferative phenotype of Caco-2 cells treated with HS38 was

not observed in the DSS-model of animal colitis. Instead, animals treated with HS38 displayed a significant decrease in IEC proliferation (**Figure 26**). This anti-proliferative effect of HS38 on IECs likely played a part in the worsening severity of DSS-induced colitis (**Figure 25**). Paradoxically, in mice recovering from DSS-induced injuries, phosphorylation of YAP on S127 decreased significantly in the HS38 treatment group (**Figure 27B**). Further, administration of HS38 stimulated YAP nuclear accumulation in the IECs (**Figure 27C**). These data suggest that the inhibition of DAPK3 via HS38 prompted YAP activation, which ought to have enhanced IEC regeneration. One plausible explanation for such paradoxical phenotype is that the IEC proliferation in mice recovering from DSS-induced injury was depressed by the functioning of YAP in other cell types.

A recent study conducted by Zhou and colleagues suggest that YAP can drive macrophages toward M1 polarization while restricting M2 polarization during UC development (X. Zhou et al., 2019). Macrophages are effector cells of the innate immune system that play an important role in inflammation, wound healing, and fibrosis development (Cosin-Roger et al., 2019; Steinbach & Plevy, 2014). Though highly heterogeneous, macrophages are broadly categorized into two functional groups: the pro-inflammatory M1 macrophages and the anti-inflammatory M2 macrophages. It is maintained that macrophages oscillate between these two functional phenotypes depending on the combination of cytokines and stimulating factors in their microenvironment (Cosin-Roger et al., 2019; Steinbach & Plevy, 2014). For example, M1 macrophages are polarized by IFN-γ and lipopolysaccharides (LPS), and secrete pro-inflammatory cytokines (e.g., TNF-α and IL-6) to promote the differentiation and activation of Th-1 and Th-17 cells. On the other hand, M2 macrophages are polarized by IL-4 and TGF-β, and produce matrix metalloproteases and growth factors to promote wound healing (Cosin-Roger et al., 2019;

Steinbach & Plevy, 2014). Previous studies have demonstrated the protective nature of M2 polarized macrophages during DSS-induced colitis, whereas M1 polarized macrophages were shown to contribute to disease severity (Arranz et al., 2012; Hunter et al., 2010; Weisser et al., 2011).

M2 macrophages act as a source of Wnt3a, a canonical Wnt ligand that is involved in epithelial regeneration after injury (Cosin-Roger et al., 2019; Koch, 2017). Wnt3a-mediated canonical Wnt signaling is inhibited by the non-canonical Wnt ligand Wnt5a (Topol et al., 2003), with its expression in macrophages found to be upregulated in response to IFN-γ, LPS, TNF-α or IL-6 (Shao et al., 2016). While IEC proliferation was not specifically examined, Zhou and colleagues found that myeloid-specific ablation of YAP attenuated the severity of DSS-induced colitis, and that YAP impeded M2 polarization, promoted M1 polarization, and increased production of IL-6 (X. Zhou et al., 2019). Potentially, administration of HS38 brought about YAP activation in macrophages, which could impair M2 polarization to depress IEC proliferation post- DSS-induced injury.

Given that IL-6 signaling can trigger YAP activation via stimulation of gp130-associated Src family kinase Yes (Taniguchi et al., 2015), Zhou and colleagues proposed a positive feedback loop between YAP and IL-6 in macrophages, which may encourage the development of CAC (X. Zhou et al., 2019). With respect to IL-6 signaling, Sato and colleagues demonstrated the induction of DAPK3 activity by leukemia inhibitory factor (N. Sato et al., 2006), an IL-6 like and gp130 utilizing cytokines (Heinrich et al., 2003). Presumably, DAPK3 plays a part in tempering the proposed positive feedback loop between YAP and IL-6. Apart from the IL-6/gp130-Src-YAP axis, the regulation of macrophage programming by DAPK3 was demonstrated by Mukhopadhyay and colleagues (Mukhopadhyay et al., 2008), whose study found that DAPK3 restrained IFN-γ induced

gene expression in macrophages through its phosphorylation of the ribosomal protein L13a. The phosphorylation of L13a activated the IFN-γ-activated inhibitor of translation complex to repress translation of inflammatory genes (Mukhopadhyay et al., 2008). Given their findings, Mukhopadhyay and colleagues proposed that DAPK3 plays an important role in the macrophage "resolution of inflammation" program. DAPK3 may take part of a yet undefined counteracting mechanism that resets the positive feedback loop between YAP and IL-6 in macrophages.

The balancing of macrophage polarization is essential to the success of self-limiting inflammation vs. pathogenic inflammation, which in turn, is necessary for efficient wound repair (Hine & Loke, 2019; Thoo et al., 2019). During the inflammation stage of mucosal wound healing, pro-inflammatory macrophages differentiate from infiltrating monocytes to offer protective responses against pathogens by the secretion of IL-6 and TNF-α (Hine & Loke, 2019; Koh & DiPietro, 2011). During the reparative stage of mucosal wound healing, macrophages transition from pro-inflammatory to reparative phenotype to assist in the resolution of inflammation and tissue regeneration via efferocytosis and the secretion of IL-10 and TGF-β (Hine & Loke, 2019; Koh & DiPietro, 2011). The deregulation of macrophage polarization and/or macrophage dysfunction can promote chronic inflammation and/or the development of intestinal fibrosis (Hine & Loke, 2019; Koh & DiPietro, 2011; Thoo et al., 2019). Although not the focus of this thesis, qRT-PCR analysis of inflamed tissues from patients with fibrotic CD showed significant downregulation of *DAPK3* expression (**Figure 29**). In fibrotic CD, the decrease in *DAPK3* expression could have potentiated deregulation of YAP, whose activity in the epithelial compartment and macrophages was reported to carry relevance in lung, kidney, and liver fibrosis (Feng et al., 2018; Noguchi et al., 2018). While DAPK3 has not been directly linked with fibrosis in intestinal diseases, it was demonstrated to promote epithelial-mesenchymal transition (J. Li et al., 2015), a process that is important for

wound healing, fibrosis and cancer progression. Recently, *DAPK3* expression was also associated with lymphatic invasion and poor prognosis in colon cancer patients (H.-M. Chen & MacDonald, 2021). This evidence suggests that DAPK3 may contribute to the development of fibrosis during UC progression.

Chapter 5 . General Discussion of Key Findings and Significance.

The intestinal epithelial barrier is a dynamic piece of machinery that is required for protection against biological, physical, and chemical insults. The integrity of this barrier may be weakened periodically, but it is restored through mechanisms involving various cell types (e.g., IECs, macrophages, lymphoid cells, innate lymphoid cells, and the commensal microbiota). While inflammation is necessary for epithelial repair, chronic inflammation occurring in and around the epithelium can cause aberrant wound healing behaviour, which has been reported as an underlying cause for UC (**Section 1.5**).

Current approaches in UC therapies largely focus on the dampening of inflammatory response. The American Gastroenterological Association recommends the use of infliximab, adalimumab, golimumab, vedolizumab, tofacitinib and ustekinumab for the induction and maintenance of remission in moderate to severe UC (Feuerstein et al., 2020). Infliximab, adalimumab and golimumab are TNF-α antagonists that reduce inflammatory response (Mitoma et al., 2018). Vedolizumab targets the α4β7 integrin and inhibits lymphocyte trafficking (Feagan et al., 2013). Tofacitinib inhibits the Janus kinase (JAK) family of proteins to downregulate IL-6 and IFN-γ (McInnes et al., 2019). And ustekinumab targets the p40 subunit of IL-12 and IL-23 and prevents the binding of IL-12/23 to their cognate receptors on natural killer and T cells (Benson et al., 2011). Immune-centric therapies have limited efficacy on resolving the chronicity of UC, particularly so in patients with greater disease severity (**Section 1.3**). Over the last 25 years, our comprehension of UC pathophysiology has expanded to encompass the importance of epithelial dysfunction, and the dependence of epithelial repair on actin cytoskeleton remodeling in the genesis and perpetuation of UC. (**Section 1.11**). Given that DAPK3 has been shown to regulate key signaling

pathways that coordinate actin cytoskeleton remodeling and epithelial repair (**Section 1.13**), it is sensible to consider DAPK3 as an effector in epithelial repair and UC progression.

The overarching hypothesis of this thesis was that DAPK3 is an important effector in the reparative intestinal epithelium. Bioinformatic studies conducted for this thesis implicated DAPK3 as a key factor in colitis-dysplasia progression. Furthermore, YAP, a transcriptional co-activator with demonstrated control over UC severity, epithelial repair, and cytoskeleton-related cellular functions was also associated with UC progression. Results presented in this thesis support the notion that actin reorganization is a key determinant for UC progression, a concept that was documented in studies conducted by Kanaan and colleagues (Kanaan et al., 2010), as well as May and colleagues (May et al., 2011). But, to my knowledge, this thesis is the first to employ sophisticated bioinformatic analyses of large patient databases to associate DAPK3 and YAP to UC progression.

Cell studies conducted for this thesis revealed increased IEC proliferation that underwrote the enhanced wound closure observed in monolayers treated with the DAPK3 inhibitor HS38. Additionally, application of HS38 promoted colocalization of YAP with F-actin, which is indicative of YAP activation. In mice recovering from DSS-induced UC, treatment with HS38 also prompted YAP activation. However, administration of HS38 to mice repressed injury-induced IEC hyperproliferation, which elicited worsening of disease severity. These data put forward DAPK3 as a regulator of intestinal epithelial repair and establish a novel linkage between the enzymatic function of DAPK3 and the (in)activation of YAP within the context of UC.

The identification of DAPK3 as a key factor in mending intestinal epithelial defect will assist in the design of UC therapeutics. For one, the regulation of YAP by DAPK3 may be exploited in the development of precision prophylactics for UC patients at high risk for neoplastic progression. To

that end, additional research is required to decipher the full consequence of DAPK3 activation/inhibition on epithelial repair and UC progression.

Chapter 6 . Limitations and Future Studies.

In the bioinformatic chapter of this study, molecular network intersections were examined to decern biological processes and molecules bridging pancolitis to CAD. The progression of UC to CAD occurs through multiple mechanisms involving various cell types. The present analyses were completed on transcriptional profiles of bulk tissues, and genes may demonstrate diverse functions across different cell types. Hence, the gene sets identified from the averaged dataset need to be re-examined in a cell type-specific way (e.g., single cell RNA-Seq) to precisely identify the susceptible cell types and convergent pathways among different cells.

Epithelial wound repair and inflammation are interconnected processes. During these processes, modification of a signaling molecule in one cell type may ameliorate disease severity while the same modification in a different cell type will aggravate the holistic disease phenotype. For example, YAP in IEC was shown to promote epithelial regeneration for attenuation of UC severity (J. Cai et al., 2010; Taniguchi et al., 2015), while YAP in macrophages was demonstrated to aggravate UC severity (X. Zhou et al., 2019). In studies conducted for this thesis, inhibition of DAPK3 via HS38 was found to increase cell proliferation in monocultures of wounded Caco-2 monolayers but decreased IEC proliferation in mice recovering from DSS-induced injury. While this discrepancy may be the consequence of interspecies differences on the regulation of DAPK3 subcellular localization (Weitzel et al., 2011), similar effects of DAPK3 inhibition on YAP activation, observed in both Caco-2 and mice, suggests that the conflict is more likely caused by the functioning of DAPK3 on non-epithelial cell types, such as macrophages (**Section 4.4**). To investigate, co-culture systems can be set up to help dissect the differential effects of DAPK3 inhibition on epithelial cells and macrophages, and to better our understanding of the interaction between these two cell types upon DAPK3 inhibition. The co-culturing of Caco-2 with one or

more immune cell types, described by Leonard and colleagues (Leonard et al., 2010), can be utilized for this purpose. Recently, a primary human macrophage-enteroid co-culture system was described by Noel and colleagues (Noel et al., 2017), and may also be used to substantiate results gathered from immortalized stable human cells lines such as Caco-2.

In the intestinal mucosa, epithelial damage induces a fibrogenic response that include the activation of fibroblasts and the generation of the provisional ECM, that act as a source of growth factors and cytokines for wound healing (Rieder et al., 2007). Dysregulation of signaling pathways that govern ECM remodeling can impair epithelial repair and can incite the formation of ulcers and/or the development of fibrosis (Rieder et al., 2007). In this context, FAK is a key molecule that mediates signal transduction between cells and the ECM (Seong et al., 2013). In the current study, *DAPK3* expression was found downregulated in inflamed tissues of patients with fibrotic CD. Given that 1) the ectopic expression of DAPK3 was shown to inhibit FAK (Nehru et al., 2013), 2) the attenuation of FAK activity was demonstrated to block YAP nuclear accumulation (N. G. Kim & Gumbiner, 2015; Yamashiro et al., 2020), and 3) YAP expression was associated with stenotic CD and YAP knockdown was shown to suppress activation of fibroblast (Ou et al., 2021), the effects of DAPK3 inhibition on epithelial restitution in an epithelial-fibroblast co-culture system is also worthy of investigation.

Mice have a long tradition of use in research. However, *Dapk3* whole-body knockout is embryonically lethal for mice (Kocher et al., 2015). Endothelial-cell specific *Dapk3* knockout is also embryonically lethal (Zhang et al., 2019). Whereas Zhang and colleagues reported success in generating inducible-*Dapk3* whole-body knockout and smooth-muscle specific *Dapk3* knockout lines, Takahashi and colleagues were unable to maintain *Dapk3* knockout lines generated using CRISPR-Cas9 (Takahashi et al., 2021). In consideration of the availability of HS38, a DAPK3

inhibitor that is well-tolerated by mice and offers high potency and selectivity towards DAPK3, the cost and efforts associated with the generation of *Dapk3* knockout in mice may outweigh the benefits. To investigate the *in vivo* role of DAPK3, this study utilized the DAPK3 inhibitor HS38. The limitations associated with the use of HS38 was discussed in **Section 3.4**. For future studies, a genetic approach will likely be necessary to dissect the independent roles that DAPK1 and DAPK3 plays in intestinal epithelial repair and Hippo signaling. Alternatively, additional structure-activity relationship study may be performed to inform the construction of DAPK3 pharmacophores that do not act against DAPK1.

Over the last ten years, various organoid culture methods were developed and have become a popular tool in research into gastrointestinal physiology. For the current study, thoughts were given to the use of intestinal organoids for their closer resemblance to the *in vivo* system. However, organoids can vary greatly from culture to culture (depending on stem cell donor), and between multiple organoids within the same culture (de Souza, 2018). Furthermore, the effect of ECM composition on organoid culture is yet undefined (J. Kim et al., 2020). Lastly, the addition of ROCK inhibitor Y27632 in organoid culture, widely performed during organoid generation to enhance stem cell survival (Kardia et al., 2021; J. Kim et al., 2020), may complicate interpretation of results achieved with DAPK3 inhibition, given the overlapping functions of DAPK3 and ROCK (e.g., regulation of RLC phosphorylation and FAK activation). Cell lines are currently the best option for *in vitro* study of cellular and molecular phenotypes, as reproducibility may be an issue with the use of organoids. It is likely that soon, standardization of strategies for controlling the variability in organoid cultures will permit the reliable use of organoids for future studies of DAPK3.

References

Adelstein, R. S., & Anne Conti, M. (1975). Phosphorylation of platelet myosin increases actin-activated myosin ATPase activity. *Nature*, *256*(5518), 597–598. https://doi.org/10.1038/256597a0

Ahmad, T., Armuzzi, A., Neville, M., Bunce, M., Ling, K. L., Welsh, K. I., Marshall, S. E., & Jewell, D. P. (2003). The contribution of human leucocyte antigen complex genes to disease phenotype in ulcerative colitis. *Tissue Antigens*, *62*(6), 527–535. https://doi.org/10.1046/j.1399-0039.2003.00129.x

Akyol, T. Y. (2019). *RVenn: Set Operations for Many Sets* (R package version 1.1.0.).

Alexa, A., & Rahnenführer, J. (2021). *topGO: Enrichment Analysis for Gene Ontology* (R package version 2.44.0).

Al-Ghabkari, A., Deng, J.-T., McDonald, P. C., Dedhar, S., Alshehri, M., Walsh, M. P., & MacDonald, J. A. (2016). A novel inhibitory effect of oxazol-5-one compounds on ROCKII signaling in human coronary artery vascular smooth muscle cells. *Scientific Reports*, *6*, 32118. https://doi.org/10.1038/srep32118

Allen, A., Hutton, D. A., & Pearson, J. P. (1998). The MUC2 gene product: a human intestinal mucin. *The International Journal of Biochemistry & Cell Biology*, *30*(7), 797–801. https://doi.org/10.1016/S1357-2725(98)00028-4

Ananthakrishnan, A. N., Cagan, A., Cai, T., Gainer, V. S., Shaw, S. Y., Churchill, S., Karlson, E. W., Murphy, S. N., Kohane, I., & Liao, K. P. (2015). Colonoscopy is associated with a reduced risk for colon cancer and mortality in patients with inflammatory bowel diseases. *Clinical Gastroenterology and Hepatology*, *13*(2), 322-329.e1. https://doi.org/10.1016/J.CGH.2014.07.018

Antoni, L., Nuding, S., Wehkamp, J., & Stange, E. F. (2014). Intestinal barrier in inflammatory bowel disease. *World Journal of Gastroenterology*, *20*(5), 1165–1179. https://doi.org/10.3748/wjg.v20.i5.1165

Aragona, M., Panciera, T., Manfrin, A., Giulitti, S., Michielin, F., Elvassore, N., Dupont, S., & Piccolo, S. (2013). A mechanical checkpoint controls multicellular growth through

YAP/TAZ regulation by actin-processing factors. *Cell*, *154*(5), 1047–1059. https://doi.org/10.1016/j.cell.2013.07.042

Arciero, J., & Swigon, D. (2013). Equation-based models of wound healing and collective cell migration. In Y. Vodovotz & G. An (Eds.), *Complex Systems and Computational Biology Approaches to Acute Inflammation* (pp. 185–207). Springer. https://doi.org/10.1007/978-3-030-56510-7_11

Arijs, I., Li, K., Toedter, G., Quintens, R., Van Lommel, L., Van Steen, K., Leemans, P., De Hertogh, G., Lemaire, K., Ferrante, M., Schnitzler, F., Thorrez, L., Ma, K., Song, X. Y. R., Marano, C., Van Assche, G., Vermeire, S., Geboes, K., Schuit, F., … Rutgeerts, P. (2009). Mucosal gene signatures to predict response to infliximab in patients with ulcerative colitis. *Gut*, *58*(12), 1612–1619. https://doi.org/10.1136/gut.2009.178665

Arranz, A., Doxaki, C., Vergadi, E., Martinez de la Torre, Y., Vaporidi, K., Lagoudaki, E., Ieronymaki, E., Androulidaki, A., Venihaki, M., Margioris, A., Stathopoulos, E., Tsichlis, P., & Tsatsanis, C. (2012). Akt1 and Akt2 protein kinases differentially contribute to macrophage polarization. *Proceedings of the National Academy of Sciences of the United States of America*, *109*(24), 9517–9522. https://doi.org/10.1073/pnas.1119038109

Arthur, J. C., Perez-Chanona, E., Mühlbauer, M., Tomkovich, S., Uronis, J. M., Fan, T.-J., Campbell, B. J., Abujamel, T., Dogan, B., Rogers, A. B., Rhodes, J. M., Stintzi, A., Simpson, K. W., Hansen, J. J., Keku, T. O., Fodor, A. A., & Jobin, C. (2012). Intestinal inflammation targets cancer-inducing activity of the microbiota. *Science*, *338*(6103), 120–123. https://doi.org/10.1126/science.1224820

Ayyaz, A., Kumar, S., Sangiorgi, B., Ghoshal, B., Gosio, J., Ouladan, S., Fink, M., Barutcu, S., Trcka, D., Shen, J., Chan, K., Wrana, J. L., & Gregorieff, A. (2019). Single-cell transcriptomes of the regenerating intestine reveal a revival stem cell. *Nature*, *569*(7754), 121–125. https://doi.org/10.1038/s41586-019-1154-y

Baker, A. M., Cross, W., Curtius, K., Al Bakir, I., Choi, C. H. R., Davis, H. L., Temko, D., Biswas, S., Martinez, P., Williams, M. J., Lindsay, J. O., Feakins, R., Vega, R., Hayes, S. J., Tomlinson, I. P. M., McDonald, S. A. C., Moorghen, M., Silver, A., East, J. E., … Graham, T. A. (2019). Evolutionary history of human colitis-associated colorectal cancer. *Gut*, *68*(6), 985–995. https://doi.org/10.1136/gutjnl-2018-316191

Barcelo, A., Claustre, J., Moro, F., Chayvialle, J. A., Cuber, J. C., & Plaisancié, P. (2000). Mucin secretion is modulated by luminal factors in the isolated vascularly perfused rat colon. *Gut*, *46*(2), 218–224. https://doi.org/10.1136/gut.46.2.218

Bayer, K. U., & Schulman, H. (2019). CaM Kinase: Still Inspiring at 40. *Neuron*, *103*(3), 380–394. https://doi.org/10.1016/j.neuron.2019.05.033

Belkaid, Y., & Hand, T. W. (2014). Role of the microbiota in immunity and inflammation. *Cell*, *157*(1), 121–141. https://doi.org/10.1016/j.cell.2014.03.011

Bembenek, J., & Yu, H. (2001). Regulation of the Anaphase-promoting Complex by the Dual Specificity Phosphatase Human Cdc14a. *Journal of Biological Chemistry*, *276*(51), 48237–48242. https://doi.org/10.1074/jbc.M108126200

Bement, W. M., Forscher, P., & Mooseker, M. S. (1993). A novel cytoskeletal structure involved in purse string wound closure and cell polarity maintenance. *Journal of Cell Biology*, *121*(3), 565–578. https://doi.org/10.1083/jcb.121.3.565

Benson, J. M., Peritt, D., Scallon, B. J., Heavner, G. A., Shealy, D. J., Giles-Komar, J. M., & Mascelli, M. A. (2011). Discovery and mechanism of ustekinumab: A human monoclonal antibody targeting interleukin-12 and interleukin-23 for treatment of immune-mediated disorders. *MAbs*, *3*(6), 535–545. https://doi.org/10.4161/mabs.3.6.17815

Bialik, S., & Kimchi, A. (2014). The DAP-kinase interactome. *Apoptosis*, *19*(2), 316–328. https://doi.org/10.1007/s10495-013-0926-3

Bjerrum, J. T., Nielsen, O. H., Riis, L. B., Pittet, V., Mueller, C., Rogler, G., & Olsen, J. (2014). Transcriptional analysis of left-sided colitis, pancolitis, and ulcerative colitis-associated dysplasia. *Inflammatory Bowel Diseases*, *20*(12), 2340–2352. https://doi.org/10.1097/MIB.0000000000000235

Blair, S. A., Kane, S. V., Clayburgh, D. R., & Turner, J. R. (2006). Epithelial myosin light chain kinase expression and activity are upregulated in inflammatory bowel disease. *Laboratory Investigation*, *86*(2), 191–201. https://doi.org/10.1038/labinvest.3700373

Blighe, K., Rana, S., & Lewis, M. (2021). *EnhancedVolcano: Publication-ready volcano plots with enhanced colouring and labeling.* (R package version 1.10.0).

Boal Carvalho, P., & Cotter, J. (2017). Mucosal Healing in Ulcerative Colitis: A Comprehensive Review. *Drugs*, *77*(2), 159–173. https://doi.org/10.1007/s40265-016-0676-y

Bollrath, J., Phesse, T. J., von Burstin, V. A., Putoczki, T., Bennecke, M., Bateman, T., Nebelsiek, T., Lundgren-May, T., Canli, Ö., Schwitalla, S., Matthews, V., Schmid, R. M., Kirchner, T., Arkan, M. C., Ernst, M., & Greten, F. R. (2009). gp130-Mediated Stat3 Activation in Enterocytes Regulates Cell Survival and Cell-Cycle Progression during Colitis-Associated Tumorigenesis. *Cancer Cell*, *15*(2), 91–102. https://doi.org/10.1016/j.ccr.2009.01.002

Borman, M. A., MacDonald, J. A., Murányi, A., Hartshorne, D. J., & Haystead, T. A. J. (2002). Smooth muscle myosin phosphatase-associated kinase induces Ca2+ sensitization via myosin phosphatase inhibition. *Journal of Biological Chemistry*, *277*(26), 23441–23446. https://doi.org/10.1074/jbc.M201597200

Bouma, G., & Strober, W. (2003). The immunological and genetic basis of inflammatory bowel disease. *Nature Reviews Immunology*, *3*(7), 521–533. https://doi.org/10.1038/nri1132

Bouzid, T., Kim, E., Riehl, B. D., Esfahani, A. M., Rosenbohm, J., Yang, R., Duan, B., & Lim, J. Y. (2019). The LINC complex, mechanotransduction, and mesenchymal stem cell function and fate. *Journal of Biological Engineering*, *13*(1), 68. https://doi.org/10.1186/s13036-019-0197-9

Brito, C., & Sousa, S. (2020). Non-Muscle Myosin 2A (NM2A): Structure, Regulation and Function. *Cells*, *9*(7), 1590. https://doi.org/10.3390/cells9071590

Büning, C., Geissler, N., Prager, M., Sturm, A., Baumgart, D. C., Büttner, J., Bühner, S., Haas, V., & Lochs, H. (2012). Increased small intestinal permeability in ulcerative colitis: Rather genetic than environmental and a risk factor for extensive disease? *Inflammatory Bowel Diseases*, *18*(10), 1932–1939. https://doi.org/10.1002/ibd.22909

Cabochette, P., Vega-Lopez, G., Bitard, J., Parain, K., Chemouny, R., Masson, C., Borday, C., Hedderich, M., Henningfeld, K. A., Locker, M., Bronchain, O., & Perron, M. (2015). Yap controls retinal stem cell DNA replication timing and genomic stability. *eLife*, *4*, e08488. https://doi.org/10.7554/eLife.08488

Cai, D., Chen, S. C., Prasad, M., He, L., Wang, X., Choesmel-Cadamuro, V., Sawyer, J. K., Danuser, G., & Montell, D. J. (2014). Mechanical feedback through E-cadherin promotes

direction sensing during collective cell migration. *Cell*, *157*(5), 1146–1159. https://doi.org/10.1016/j.cell.2014.03.045

Cai, J., Zhang, N., Zheng, Y., De Wilde, R. F., Maitra, A., & Pan, D. (2010). The Hippo signaling pathway restricts the oncogenic potential of an intestinal regeneration program. *Genes and Development*, *24*(21), 2383–2388. https://doi.org/10.1101/gad.1978810

Callus, B. A., Verhagen, A. M., & Vaux, D. L. (2006). Association of mammalian sterile twenty kinases, Mst1 and Mst2, with hSalvador via C-terminal coiled-coil domains, leads to its stabilization and phosphorylation. *FEBS Journal*, *273*(18), 4264–4276. https://doi.org/10.1111/j.1742-4658.2006.05427.x

Campellone, K. G., & Welch, M. D. (2010). A nucleator arms race: Cellular control of actin assembly. *Nature Reviews Molecular Cell Biology*, *11*(4), 237–251. https://doi.org/10.1038/nrm2867

Carlson, D. A., Franke, A. S., Weitzel, D. H., Speer, B. L., Hughes, P. F., Hagerty, L., Fortner, C. N., Veal, J. M., Barta, T. E., Zieba, B. J., Somlyo, A. V., Sutherland, C., Deng, J. T., Walsh, M. P., Macdonald, J. A., & Haystead, T. A. J. (2013). Fluorescence linked enzyme chemoproteomic strategy for discovery of a potent and selective DAPK1 and ZIPK inhibitor. *ACS Chemical Biology*, *8*(12), 2715–2723. https://doi.org/10.1021/cb400407c

Carlson, D. A., Singer, M. R., Sutherland, C., Redondo, C., Alexander, L. T., Hughes, P. F., Knapp, S., Gurley, S. B., Sparks, M. A., MacDonald, J. A., & Haystead, T. A. J. (2018). Targeting Pim Kinases and DAPK3 to Control Hypertension. *Cell Chemical Biology*, *25*(10), 1195-1207.e32. https://doi.org/10.1016/j.chembiol.2018.06.006

Carlson, M. (2021). *org.Hs.eg.db: Genome wide annotation for Human* (R package version 3.13.0.).

Carvalho, P. B., De Castro, F. D., Rosa, B., Moreira, M. J., & Cotter, J. (2016). Mucosal healing in ulcerative colitis - when zero is better. *Journal of Crohn's and Colitis*, *10*(1), 20–25. https://doi.org/10.1093/ecco-jcc/jjv180

Chan, E. H. Y., Nousiainen, M., Chalamalasetty, R. B., Schäfer, A., Nigg, E. A., & Sillje, H. H. W. (2005). The Ste20-like kinase Mst2 activates the human large tumor suppressor kinase Lats1. *Oncogene*, *24*(12), 2076–2086. https://doi.org/10.1038/sj.onc.1208445

Chandrasinghe, P., Cereser, B., Moorghen, M., al Bakir, I., Tabassum, N., Hart, A., Stebbing, J., & Warusavitarne, J. (2018). Role of SMAD proteins in colitis-associated cancer: from known to the unknown. *Oncogene*, *37*(1), 1–7. https://doi.org/10.1038/onc.2017.300

Chánez-Paredes, S., Montoya-García, A., Castro-Ochoa, K. F., Cordero, J. G., Cedillo-Barron, L., Shibayama, M., Nava, P., Flemming, S., Schlegel, N., Gautreau, A. M., Vargas Robles, H., Mondragon-Flores, R., & Schnoor, M. (2021). The Arp2/3 inhibitory protein arpin is required for intestinal epithelial barrier integrity. *Frontiers in Cell and Developmental Biology*, *9*, 625719. https://doi.org/10.3389/fcell.2021.625719

Chang, J., Leong, R. W., Wasinger, V. C., Ip, M., Yang, M., & Phan, T. G. (2017). Impaired Intestinal Permeability Contributes to Ongoing Bowel Symptoms in Patients With Inflammatory Bowel Disease and Mucosal Healing. *Gastroenterology*, *153*(3), 723-731.e1. https://doi.org/10.1053/j.gastro.2017.05.056

Chaturvedi, L. S., Marsh, H. M., & Basson, M. D. (2011). Role of RhoA and its effectors ROCK and mDia1 in the modulation of deformation-induced FAK, ERK, p38, and MLC motogenic signals in human Caco-2 intestinal epithelial cells. *American Journal of Physiology. Cell Physiology*, *301*(5), C1224–C1238. https://doi.org/10.1152/ajpcell.00518.2010

Chen, H.-M., & MacDonald, J. A. (2021). Network analysis identifies DAPK3 as a potential biomarker for lymphatic invasion and colon adenocarcinoma prognosis. *iScience*, *24*(8), 102831. https://doi.org/10.1016/j.isci.2021.102831

Chen, N.-P., Uddin, B., Hardt, R., Ding, W., Panic, M., Lucibello, I., Kammerer, P., Ruppert, T., & Schiebel, E. (2017). Human phosphatase CDC14A regulates actin organization through dephosphorylation of epithelial protein lost in neoplasm. *Proceedings of the National Academy of Sciences*, *114*(20), 5201–5206. https://doi.org/10.1073/pnas.1619356114

Chen, N.-P., Uddin, B., Voit, R., & Schiebel, E. (2016). Human phosphatase CDC14A is recruited to the cell leading edge to regulate cell migration and adhesion. *Proceedings of the National Academy of Sciences of the United States of America*, *113*(4), 990–995. https://doi.org/10.1073/pnas.1515605113

Chen, R. H., Chen, Y. H., & Huang, T. Y. (2019). Ubiquitin-mediated regulation of autophagy. *Journal of Biomedical Science*, *26*(1), 1–12. https://doi.org/10.1186/s12929-019-0569-y

Citri, A., Harari, D., Shohat, G., Ramakrishnan, P., Gan, J., Lavi, S., Eisenstein, M., Kimchi, A., Wallach, D., Pietrokovski, S., & Yarden, Y. (2006). Hsp90 recognizes a common surface on client kinases. *Journal of Biological Chemistry*, *281*(20), 14361–14369. https://doi.org/10.1074/jbc.M512613200

Collins, J. W., Keeney, K. M., Crepin, V. F., Rathinam, V. A. K., Fitzgerald, K. A., Finlay, B. B., & Frankel, G. (2014). Citrobacter rodentium: infection, inflammation and the microbiota. *Nature Reviews. Microbiology*, *12*(9), 612–623. https://doi.org/10.1038/nrmicro3315

Cosin-Roger, J., Ortiz-Masià, M. D., & Barrachina, M. D. (2019). Macrophages as an Emerging Source of Wnt Ligands: Relevance in Mucosal Integrity. *Frontiers in Immunology*, *10*, 2297. https://doi.org/10.3389/fimmu.2019.02297

Coward, S., Clement, F., Benchimol, E. I., Bernstein, C. N., Avina-Zubieta, J. A., Bitton, A., Carroll, M. W., Hazlewood, G., Jacobson, K., Jelinski, S., Deardon, R., Jones, J. L., Kuenzig, M. E., Leddin, D., McBrien, K. A., Murthy, S. K., Nguyen, G. C., Otley, A. R., Panaccione, R., … Kaplan, G. G. (2019). Past and Future Burden of Inflammatory Bowel Diseases Based on Modeling of Population-Based Data. *Gastroenterology*, *156*(5), 1345-1353.e4. https://doi.org/10.1053/j.gastro.2019.01.002

Cox, J. H., Kljavin, N. M., Ota, N., Leonard, J., Roose-Girma, M., Diehl, L., Ouyang, W., & Ghilardi, N. (2012). Opposing consequences of IL-23 signaling mediated by innate and adaptive cells in chemically induced colitis in mice. *Mucosal Immunology*, *5*(1), 99–109. https://doi.org/10.1038/mi.2011.54

Craig, R., Smith, R., & Kendrick-Jones, J. (1983). Light-chain phosphorylation controls the conformation of vertebrate non-muscle and smooth muscle myosin molecules. *Nature*, *302*(5907), 436–439. https://doi.org/10.1038/302436a0

Cunningham, K. E., & Turner, J. R. (2012). Myosin light chain kinase: Pulling the strings of epithelial tight junction function. *Annals of the New York Academy of Sciences*, *1258*(1), 34–42. https://doi.org/10.1111/j.1749-6632.2012.06526.x

Danese, S., Rudziński, J., Brandt, W., Dupas, J. L., Peyrin-Biroulet, L., Bouhnik, Y., Kleczkowski, D., Uebel, P., Lukas, M., Knutsson, M., Erlandsson, F., Hansen, M. B., & Keshav, S. (2015). Tralokinumab for moderate-to-severe UC: A randomised, double-blind, placebo-controlled, phase IIa study. *Gut*, *64*(2), 243–249. https://doi.org/10.1136/gutjnl-2014-308004

Dang, B., Mravic, M., Hu, H., Schmidt, N., Mensa, B., & DeGrado, W. F. (2019). SNAC-tag for sequence-specific chemical protein cleavage. *Nature Methods*, *16*(4), 319–322. https://doi.org/10.1038/s41592-019-0357-3

Darling, T. K., & Lamb, T. J. (2019). Emerging Roles for Eph Receptors and Ephrin Ligands in Immunity. *Frontiers in Immunology*, *10*, 1473. https://doi.org/10.3389/fimmu.2019.01473

Das, A., Fischer, R. S., Pan, D., & Waterman, C. M. (2016). YAP nuclear localization in the absence of cell-cell contact is mediated by a filamentous actin-dependent, Myosin II and Phospho-YAP-independent pathway during extracellular matrix mechanosensing. *Journal of Biological Chemistry*, *291*(12), 6096–6110. https://doi.org/10.1074/jbc.M115.708313

Davies, S., Reddy, H., Caivano, M., & Cohen, P. (2000). Specificity and mechanism of action of some commonly used protein kinase inhibitors. *Biochemical Journal*, *351*(Pt 1), 95–105. https://doi.org/10.1042/0264-6021:3510095

Davis, S., & Meltzer, P. S. (2007). GEOquery: A bridge between the Gene Expression Omnibus (GEO) and BioConductor. *Bioinformatics*, *23*(14), 1846–1847. https://doi.org/10.1093/bioinformatics/btm254

de Souza, N. (2018). Organoids. *Nature Methods*, *15*, 23. https://doi.org/10.1038/nmeth.4576

Del Zotto, B., Mumolo, G., Pronio, A. M., Montesani, C., Tersigni, R., & Boirivant, M. (2003). TGF-β1 production in inflammatory bowel disease: Differing production patterns in Crohn's disease and ulcerative colitis. *Clinical and Experimental Immunology*, *134*(1), 120–126. https://doi.org/10.1046/j.1365-2249.2003.02250.x

Deng, F., Peng, L., Li, Z., Tan, G., Liang, E., Chen, S., Zhao, X., & Zhi, F. (2018). YAP triggers the Wnt/β-catenin signalling pathway and promotes enterocyte self-renewal, regeneration and tumorigenesis after DSS-induced injury. *Cell Death and Disease*, *9*(2), 153. https://doi.org/10.1038/s41419-017-0244-8

Deng, Y., Pang, A., & Wang, J. H. (2003). Regulation of mammalian STE20-like kinase 2 (MST2) by protein phosphorylation/dephosphorylation and proteolysis. *Journal of Biological Chemistry*, *278*(14), 11760–11767. https://doi.org/10.1074/jbc.M211085200

Desai, M. S., Seekatz, A. M., Koropatkin, N. M., Kamada, N., Hickey, C. A., Wolter, M., Pudlo, N. A., Kitamoto, S., Terrapon, N., Muller, A., Young, V. B., Henrissat, B., Wilmes, P., Stappenbeck, T. S., Núñez, G., & Martens, E. C. (2016). A Dietary Fiber-Deprived Gut

Microbiota Degrades the Colonic Mucus Barrier and Enhances Pathogen Susceptibility. *Cell*, *167*(5), 1339-1353.e21. https://doi.org/https://doi.org/10.1016/j.cell.2016.10.043

Dignass, A. U., & Podolsky, D. K. (1993). Cytokine modulation of intestinal epithelial cell restitution: Central role of transforming growth factor β. *Gastroenterology*, *105*(5), 1323–1332. https://doi.org/10.1016/0016-5085(93)90136-Z

Driscoll, T. P., Cosgrove, B. D., Heo, S. J., Shurden, Z. E., & Mauck, R. L. (2015). Cytoskeletal to Nuclear Strain Transfer Regulates YAP Signaling in Mesenchymal Stem Cells. *Biophysical Journal*, *108*(12), 2783–2793. https://doi.org/10.1016/j.bpj.2015.05.010

Dulai, P. S., Sandborn, W. J., & Gupta, S. (2016). Colorectal Cancer and Dysplasia in Inflammatory Bowel Disease: A Review of Disease Epidemiology, Pathophysiology, and Management. *Cancer Prevention Research*, *9*(12), 887–894. https://doi.org/10.1158/1940-6207.CAPR-16-0124

Dupont, S., Morsut, L., Aragona, M., Enzo, E., Giulitti, S., Cordenonsi, M., Zanconato, F., Le Digabel, J., Forcato, M., Bicciato, S., Elvassore, N., & Piccolo, S. (2011). Role of YAP/TAZ in mechanotransduction. *Nature*, *474*(7350), 179–184. https://doi.org/10.1038/nature10137

Eaden, J. A., Abrams, K. R., & Mayberry, J. F. (2001). The risk of colorectal cancer in ulcerative colitis: A meta-analysis. *Gut*, *48*(4), 526–535. https://doi.org/10.1136/gut.48.4.526

Elosegui-Artola, A., Andreu, I., Beedle, A. E. M., Lezamiz, A., Uroz, M., Kosmalska, A. J., Oria, R., Kechagia, J. Z., Rico-Lastres, P., Le Roux, A. L., Shanahan, C. M., Trepat, X., Navajas, D., Garcia-Manyes, S., & Roca-Cusachs, P. (2017). Force Triggers YAP Nuclear Entry by Regulating Transport across Nuclear Pores. *Cell*, *171*(6), 1397-1410.e14. https://doi.org/10.1016/j.cell.2017.10.008

Fang, J., Wang, H., Zhou, Y., Zhang, H., Zhou, H., & Zhang, X. (2021). Slimy partners: the mucus barrier and gut microbiome in ulcerative colitis. *Experimental & Molecular Medicine*, *53*(5), 772–787. https://doi.org/10.1038/s12276-021-00617-8

Farag, A. K., & Roh, E. J. (2019). Death-associated protein kinase (DAPK) family modulators: Current and future therapeutic outcomes. *Medicinal Research Reviews*, *39*(1), 349–385. https://doi.org/10.1002/med.21518

Farooqi, A. A., de la Roche, M., Djamgoz, M. B. A., & Siddik, Z. H. (2019). Overview of the oncogenic signaling pathways in colorectal cancer: Mechanistic insights. *Seminars in Cancer Biology*, *58*, 65–79. https://doi.org/10.1016/j.semcancer.2019.01.001

Feagan, B. G., Rutgeerts, P., Sands, B. E., Hanauer, S., Colombel, J. F., Sandborn, W. J., Van Assche, G., Axler, J., Kim, H.-J., Danese, S., Fox, I., Milch, C., Sankoh, S., Wyant, T., Xu, J., Parikh, A., & GEMINI 1 Study Group. (2013). Vedolizumab as induction and maintenance therapy for ulcerative colitis. *The New England Journal of Medicine*, *369*(8), 699–710. https://doi.org/10.1056/NEJMoa1215734

Felten, A., Brinckmann, D., Landsberg, G., & Scheidtmann, K. H. (2013). Zipper-interacting protein kinase is involved in regulation of ubiquitination of the androgen receptor, thereby contributing to dynamic transcription complex assembly. *Oncogene*, *32*(41), 4981–4988. https://doi.org/10.1038/onc.2012.503

Feng, Y., Liang, Y., Zhu, X., Wang, M., Gui, Y., Lu, Q., Gu, M., Xue, X., Sun, X., He, W., Yang, J., Johnson, R. L., & Dai, C. (2018). The signaling protein Wnt5a promotes TGFβ1-mediated macrophage polarization and kidney fibrosis by inducing the transcriptional regulators Yap/Taz. *The Journal of Biological Chemistry*, *293*(50), 19290–19302. https://doi.org/10.1074/jbc.RA118.005457

Feuerstein, J. D., Isaacs, K. L., Schneider, Y., Siddique, S. M., Falck-Ytter, Y., Singh, S., Chachu, K., Day, L., Lebwohl, B., Muniraj, T., Patel, A., Peery, A. F., Shah, R., Sultan, S., Singh, H., Spechler, S., Su, G., Thrift, A. P., Weiss, J. M., … Terdiman, J. (2020). AGA Clinical Practice Guidelines on the Management of Moderate to Severe Ulcerative Colitis. *Gastroenterology*, *158*(5), 1450–1461. https://doi.org/10.1053/j.gastro.2020.01.006

Finch-Edmondson, M. L., Strauss, R. P., Passman, A. M., Sudol, M., Yeoh, G. C., & Callus, B. A. (2015). TAZ protein accumulation is negatively regulated by YAP abundance in mammalian cells. *Journal of Biological Chemistry*, *290*(46), 27928–27938. https://doi.org/10.1074/jbc.M115.692285

Fiocchi, C. (1997). Intestinal inflammation: a complex interplay of immune and nonimmune cell interactions. *American Journal of Physiology. Gastrointestinal and Liver Physiology*, *273*(4), G769–G775. https://doi.org/10.1152/ajpgi.1997.273.4.G769

Ford, A. C., Sandborn, W. J., Khan, K. J., Hanauer, S. B., Talley, N. J., & Moayyedi, P. (2011). Efficacy of biological therapies in inflammatory bowel disease: Systematic review and

meta-analysis. *American Journal of Gastroenterology*, *106*(4), 644–659. https://doi.org/10.1038/ajg.2011.73

Fujiwara, N., Usui, T., Ohama, T., & Sato, K. (2016). Regulation of beclin 1 protein phosphorylation and autophagy by protein phosphatase 2A (PP2A) and death-associated protein kinase 3 (DAPK3). *Journal of Biological Chemistry*, *291*(20), 10858–10866. https://doi.org/10.1074/jbc.M115.704908

Gaudier, E., Jarry, A., Blottière, H. M., De Coppet, P., Buisine, M. P., Aubert, J. P., Laboisse, C., Cherbut, C., & Hoebler, C. (2004). Butyrate specifically modulates MUC gene expression in intestinal epithelial goblet cells deprived of glucose. *American Journal of Physiology. Gastrointestinal and Liver Physiology*, *287*(6), G1168-1174. https://doi.org/10.1152/ajpgi.00219.2004

Geremia, A., & Arancibia-Cárcamo, C. V. (2017). Innate lymphoid cells in intestinal inflammation. *Frontiers in Immunology*, *8*, 1296. https://doi.org/10.3389/fimmu.2017.01296

Gitter, A. H., Wullstein, F., Fromm, M., & Schulzke, J. D. (2001). Epithelial barrier defects in ulcerative colitis: Characterization and quantification by electrophysiological imaging. *Gastroenterology*, *121*(6), 1320–1328. https://doi.org/10.1053/gast.2001.29694

Goyette, P., Boucher, G., Mallon, D., Ellinghaus, E., Jostins, L., Huang, H., Ripke, S., Gusareva, E. S., Annese, V., Hauser, S. L., Oksenberg, J. R., Thomsen, I., Leslie, S., Daly, M. J., Van Steen, K., Duerr, R. H., Barrett, J. C., McGovern, D. P. B., Schumm, L. P., … Zhao, Z. Z. (2015). High-density mapping of the MHC identifies a shared role for HLA-DRB1∗01:03 in inflammatory bowel diseases and heterozygous advantage in ulcerative colitis. *Nature Genetics*, *47*(2), 172–179. https://doi.org/10.1038/ng.3176

Graham, W. V., He, W., Marchiando, A. M., Zha, J., Singh, G., Li, H. S., Biswas, A., Ong, M. L. D. M., Jiang, Z. H., Choi, W., Zuccola, H., Wang, Y., Griffith, J., Wu, J., Rosenberg, H. J., Wang, Y., Snapper, S. B., Ostrov, D., Meredith, S. C., … Turner, J. R. (2019). Intracellular MLCK1 diversion reverses barrier loss to restore mucosal homeostasis. *Nature Medicine*, *25*(4), 690–700. https://doi.org/10.1038/s41591-019-0393-7

Grassie, M. E., Moffat, L. D., Walsh, M. P., & MacDonald, J. A. (2011). The myosin phosphatase targeting protein (MYPT) family: A regulated mechanism for achieving substrate specificity of the catalytic subunit of protein phosphatase type 1δ. *Archives of Biochemistry and Biophysics*, *510*(2), 147–159. https://doi.org/10.1016/j.abb.2011.01.018

Graves, P. R., Winkfield, K. M., & Haystead, T. A. J. (2005). Regulation of Zipper-interacting Protein Kinase Activity in Vitro and in Vivo by Multisite Phosphorylation. *Journal of Biological Chemistry*, *280*(10), 9363–9374. https://doi.org/10.1074/jbc.M412538200

Gregorieff, A., Liu, Y., Inanlou, M. R., Khomchuk, Y., & Wrana, J. L. (2015). Yap-dependent reprogramming of Lgr5+ stem cells drives intestinal regeneration and cancer. *Nature*, *526*(7575), 715–718. https://doi.org/10.1038/nature15382

Grivennikov, S. I. (2013). Inflammation and colorectal cancer: Colitis-associated neoplasia. *Seminars in Immunopathology*, *35*(2), 229–244. https://doi.org/10.1007/s00281-012-0352-6

Grivennikov, S. I., & Cominelli, F. (2016). Colitis-Associated and Sporadic Colon Cancers: Different Diseases, Different Mutations? *Gastroenterology*, *150*(4), 808–810. https://doi.org/10.1053/j.gastro.2016.02.062

Gruber, R., Panayiotou, R., Nye, E., Spencer-Dene, B., Stamp, G., & Behrens, A. (2016). YAP1 and TAZ Control Pancreatic Cancer Initiation in Mice by Direct Up-regulation of JAK–STAT3 Signaling. *Gastroenterology*, *151*(3), 526–539. https://doi.org/10.1053/j.gastro.2016.05.006

Guillermin, O., Angelis, N., Sidor, C. M., Ridgway, R., Baulies, A., Kucharska, A., Antas, P., Rose, M. R., Cordero, J., Sansom, O., Li, V. S. W., & Thompson, B. J. (2021). Wnt and Src signals converge on YAP-TEAD to drive intestinal regeneration. *The EMBO Journal*, *40*(13), e105770. https://doi.org/10.15252/embj.2020105770

Guilluy, C., Osborne, L. D., Van Landeghem, L., Sharek, L., Superfine, R., Garcia-Mata, R., & Burridge, K. (2014). Isolated nuclei adapt to force and reveal a mechanotransduction pathway in the nucleus. *Nature Cell Biology*, *16*(4), 376–381. https://doi.org/10.1038/ncb2927

Haberman, Y., Karns, R., Dexheimer, P. J., Schirmer, M., Somekh, J., Jurickova, I., Braun, T., Novak, E., Bauman, L., Collins, M. H., Mo, A., Rosen, M. J., Bonkowski, E., Gotman, N., Marquis, A., Nistel, M., Rufo, P. A., Baker, S. S., Sauer, C. G., … Denson, L. A. (2019). Ulcerative colitis mucosal transcriptomes reveal mitochondriopathy and personalized mechanisms underlying disease severity and treatment response. *Nature Communications*, *10*(1), 38. https://doi.org/10.1038/s41467-018-07841-3

Hagerty, L., Weitzel, D. H., Chambers, J., Fortner, C. N., Brush, M. H., Loiselle, D., Hosoya, H., & Haystead, T. A. J. (2007). ROCK1 phosphorylates and activates zipper-interacting

protein kinase. *Journal of Biological Chemistry*, *282*(7), 4884–4893. https://doi.org/10.1074/jbc.M609990200

Hao, Y., Chun, A., Cheung, K., Rashidi, B., & Yang, X. (2008). Tumor suppressor LATS1 is a negative regulator of oncogene YAP. *Journal of Biological Chemistry*, *283*(9), 5496–5509. https://doi.org/10.1074/jbc.M709037200

Hein, A. L., Brandquist, N. D., Ouellette, C. Y., Seshacharyulu, P., Enke, C. A., Ouellette, M. M., Batra, S. K., & Yan, Y. (2019). PR55α regulatory subunit of PP2A inhibits the MOB1/LATS cascade and activates YAP in pancreatic cancer cells. *Oncogenesis*, *8*(11), 63. https://doi.org/10.1038/s41389-019-0172-9

Heinrich, P. C., Behrmann, I., Haan, S., Hermanns, H. M., Müller-Newen, G., & Schaper, F. (2003). Principles of interleukin (IL)-6-type cytokine signalling and its regulation. *Biochemical Journal*, *374*(Pt 1), 1–20. https://doi.org/10.1042/BJ20030407

Hicks-Berthet, J., Ning, B., Federico, A., Tilston-Lunel, A., Matschulat, A., Ai, X., Lenburg, M. E., Beane, J., Monti, S., & Varelas, X. (2021). Yap/Taz inhibit goblet cell fate to maintain lung epithelial homeostasis. *Cell Reports*, *36*(2), 109347. https://doi.org/10.1016/j.celrep.2021.109347

Hine, A. M., & Loke, P. (2019). Intestinal Macrophages in Resolving Inflammation. *The Journal of Immunology*, *203*(3), 593–599. https://doi.org/10.4049/jimmunol.1900345

Hirota, S. A., Ng, J., Lueng, A., Khajah, M., Parhar, K., Li, Y., Lam, V., Potentier, M. S., Ng, K., Bawa, M., McCafferty, D.-M., Rioux, K. P., Ghosh, S., Xavier, R. J., Colgan, S. P., Tschopp, J., Muruve, D., MacDonald, J. A., & Beck, P. L. (2011). The NLRP3 inflammasome plays key role in the regulation of intestinal homeostasis. *Inflammatory Bowel Diseases*, *17*(6), 1359–1372. https://doi.org/10.1002/IBD.21478

Holmes, K. C., Popp, D., Gebhard, W., & Kabsch, W. (1990). Atomic model of the actin filament. *Nature*, *347*(6288), 44–49. https://doi.org/10.1038/347044a0

Hosoba, K., Komatsu, S., Ikebe, M., Kotani, M., Wenqin, X., Tachibana, T., Hosoya, H., & Hamao, K. (2015). Phosphorylation of myosin II regulatory light chain by ZIP kinase is responsible for cleavage furrow ingression during cell division in mammalian cultured cells. *Biochemical and Biophysical Research Communications*, *459*(4), 686–691. https://doi.org/10.1016/j.bbrc.2015.03.005

Howe, K. L., Reardon, C., Wang, A., Nazli, A., & Mckay, D. M. (2005). Transforming growth factor-beta regulation of epithelial tight junction proteins enhances barrier function and blocks enterohemorrhagic Escherichia coli O157:H7-induced increased permeability. *The American Journal of Pathology*, *167*(6), 1587–1597. https://doi.org/10.1016/s0002-9440(10)61243-6

Hu, H., Yin, J. H., Shao, D. D., Wang, L. L., He, F., Huang, X. X., Guo, H. L., Xiang, X. N., Zhu, S. S., Zhang, P. H., & Chen, J. S. (2020). The phosphorylation of hCDC14A modulated by ZIPK regulates autophagy of murine pancreatic islet β-TC3 cells upon glucose stimulation. *European Review for Medical and Pharmacological Sciences*, *24*(19), 10028–10035. https://doi.org/10.26355/eurrev_202010_23217

Hunter, M., Wang, A., Parhar, K., Johnston, M., van Rooijen, N., Beck, P. L., & McKay, D. M. (2010). In vitro-derived alternatively activated macrophages reduce colonic inflammation in mice. *Gastroenterology*, *138*(4), 1395–1405. https://doi.org/10.1053/j.gastro.2009.12.041

Hwang, S., Zimmerman, N. P., Agle, K. A., Turner, J. R., Kumar, S. N., & Dwinell, M. B. (2012). E-cadherin is critical for collective sheet migration and is regulated by the chemokine CXCL12 protein during restitution. *Journal of Biological Chemistry*, *287*(26), 22227–22240. https://doi.org/10.1074/jbc.M112.367979

Hyams, J. S., Davis, S., Mack, D. R., Boyle, B., Griffiths, A. M., LeLeiko, N. S., Sauer, C. G., Keljo, D. J., Markowitz, J., Baker, S. S., Rosh, J., Baldassano, R. N., Patel, A., Pfefferkorn, M., Otley, A., Heyman, M., Noe, J., Oliva-Hemker, M., Rufo, P., … Denson, L. A. (2017). Factors associated with early outcomes following standardised therapy in children with ulcerative colitis (PROTECT): a multicentre inception cohort study. *The Lancet. Gastroenterology & Hepatology*, *2*(12), 855–868. https://doi.org/10.1016/S2468-1253(17)30252-2

Ihara, E., & MacDonald, J. A. (2007). The regulation of smooth muscle contractility by zipper-interacting protein kinase. *Canadian Journal of Physiology and Pharmacology*, *85*(1), 79–87. https://doi.org/10.1139/y06-103

Iizuka, M., & Konno, S. (2011). Wound healing of intestinal epithelial cells. *World Journal of Gastroenterology*, *17*(17), 2161–2171. https://doi.org/10.3748/wjg.v17.i17.2161

Imajo, M., Ebisuya, M., & Nishida, E. (2014). Dual role of YAP and TAZ in renewal of the intestinal epithelium. *Nature Cell Biology*, *17*(1), 7–19. https://doi.org/10.1038/NCB3084

Imajo, M., Miyatake, K., Iimura, A., Miyamoto, A., & Nishida, E. (2012). A molecular mechanism that links Hippo signalling to the inhibition of Wnt/β-catenin signalling. *EMBO Journal*, *31*(5), 1109–1122. https://doi.org/10.1038/emboj.2011.487

Ishizaki, T., Uehata, M., Tamechika, I., Keel, J., Nonomura, K., Maekawa, M., & Narumiya, S. (2000). Pharmacological properties of Y-27632, a specific inhibitor of rho-associated kinases. *Molecular Pharmacology*, *57*(5), 976–983.

Issenman, R. M., Jenkins, R. T., & Radoja, C. (1993). Intestinal permeability compared in pediatric and adult patients with inflammatory bowel disease. *Clinical and Investigative Medicine*, *16*(3), 187–196.

Ito, H., Yamashita, Y., Tanaka, T., Takaki, M., Le, M. N., Yoshida, L.-M., & Morimoto, K. (2020). Cigarette smoke induces endoplasmic reticulum stress and suppresses efferocytosis through the activation of RhoA. *Scientific Reports*, *10*(1), 1–11. https://doi.org/10.1038/s41598-020-69610-x

Itzkowitz, S. H., & Yio, X. (2004). Inflammation and Cancer IV. Colorectal cancer in inflammatory bowel disease: the role of inflammation. *American Journal of Physiology. Gastrointestinal and Liver Physiology*, *287*(1), G7–G17. https://doi.org/10.1152/ajpgi.00079.2004

Ivanovska, J., Tregubova, A., Mahadevan, V., Chakilam, S., Gandesiri, M., Benderska, N., Ettle, B., Hartmann, A., Söder, S., Ziesché, E., Fischer, T., Lautscham, L., Fabry, B., Segerer, G., Gohla, A., & Schneider-Stock, R. (2013). Identification of DAPK as a scaffold protein for the LIMK/cofilin complex in TNF-induced apoptosis. *International Journal of Biochemistry and Cell Biology*, *45*(8), 1720–1729. https://doi.org/10.1016/j.biocel.2013.05.013

Jaspersen, S. L., Charles, J. F., & Morgan, D. O. (1999). Inhibitory phosphorylation of the APC regulator Hct1 is controlled by the kinase Cdc28 and the phosphatase Cdc14. *Current Biology*, *9*(5), 227–236. https://doi.org/10.1016/S0960-9822(99)80111-0

Jaspersen, S. L., Charles, J. F., Tinker-Kulberg, R. L., & Morgan, D. O. (1998). A late mitotic regulatory network controlling cyclin destruction in Saccharomyces cerevisiae. *Molecular Biology of the Cell*, *9*(10), 2803–2817. https://doi.org/10.1091/mbc.9.10.2803

Jin, H., Sperka, T., Herrlich, P., & Morrison, H. (2006). Tumorigenic transformation by CPI-17 through inhibition of a merlin phosphatase. *Nature*, *442*(7102), 576–579. https://doi.org/10.1038/nature04856

Jin, Y., & Blikslager, A. T. (2020). The Regulation of Intestinal Mucosal Barrier by Myosin Light Chain Kinase/Rho Kinases. *International Journal of Molecular Sciences*, *21*(10), 3550. https://doi.org/10.3390/ijms21103550

Jochems, P., Garssen, J., van Keulen, A., Masereeuw, R., & Jeurink, P. (2018). Evaluating Human Intestinal Cell Lines for Studying Dietary Protein Absorption. *Nutrients*, *10*(3), 322. https://doi.org/10.3390/nu10030322

Jonkman, J. E. N., Cathcart, J. A., Xu, F., Bartolini, M. E., Amon, J. E., Stevens, K. M., & Colarusso, P. (2014). An introduction to the wound healing assay using live-cell microscopy. *Cell Adhesion and Migration*, *8*(5), 440–451. https://doi.org/10.4161/cam.36224

Jostins, L., Ripke, S., Weersma, R. K., Duerr, R. H., McGovern, D. P., Hui, K. Y., Lee, J. C., Philip Schumm, L., Sharma, Y., Anderson, C. A., Essers, J., Mitrovic, M., Ning, K., Cleynen, I., Theatre, E., Spain, S. L., Raychaudhuri, S., Goyette, P., Wei, Z., … Whittaker, P. (2012). Host-microbe interactions have shaped the genetic architecture of inflammatory bowel disease. *Nature*, *491*(7422), 119–124. https://doi.org/10.1038/nature11582

Kabir, M., Fofaria, R., Arebi, N., Bassett, P., Tozer, P. J., Hart, A. L., Thomas-Gibson, S., Humphries, A., Suzuki, N., Saunders, B., Warusavitarne, J., Faiz, O., & Wilson, A. (2020). Systematic review with meta-analysis: IBD-associated colonic dysplasia prognosis in the videoendoscopic era (1990 to present). *Alimentary Pharmacology & Therapeutics*, *52*(1), 5–19. https://doi.org/10.1111/APT.15778

Kagnoff, M. F. (2014). The intestinal epithelium is an integral component of a communications network. *Journal of Clinical Investigation*, *124*(7), 2841–2843. https://doi.org/10.1172/JCI75225

Kaiko, G. E., Chen, F., Lai, C. W., Chiang, I. L., Perrigoue, J., Stojmirović, A., Li, K., Muegge, B. D., Jain, U., VanDussen, K. L., Goggins, B. J., Keely, S., Weaver, J., Foster, P. S., Lawrence, D. A., Liu, T. C., & Stappenbeck, T. S. (2019). PAI-1 augments mucosal damage in colitis. *Science Translational Medicine*, *11*(482), eaat0852. https://doi.org/10.1126/scitranslmed.aat0852

Kaiser, B. K., Zimmerman, Z. A., Charbonneau, H., & Jackson, P. K. (2002). Disruption of centrosome structure, chromosome segregation, and cytokinesis by misexpression of human Cdc14A phosphatase. *Molecular Biology of the Cell*, *13*(7), 2289–2300. https://doi.org/10.1091/mbc.01-11-0535

Kanaan, Z., Qadan, M., Eichenberger, M. R., & Galandiuk, S. (2010). The actin-cytoskeleton pathway and its potential role in inflammatory bowel disease-associated human colorectal cancer. *Genetic Testing and Molecular Biomarkers*, *14*(3), 347–353. https://doi.org/10.1089/gtmb.2009.0197

Kao, L., Wang, Y. T., Chen, Y. C., Tseng, S. F., Jhang, J. C., Chen, Y. J., & Teng, S. C. (2014). Global analysis of cdc14 dephosphorylation sites reveals essential regulatory role in mitosis and cytokinesis. *Molecular and Cellular Proteomics*, *13*(2), 594–605. https://doi.org/10.1074/mcp.M113.032680

Karayiannakis, A. J., Syrigos, K. N., Efstathiou, J., Valizadeh, A., Noda, M., Playford, R. J., Kmiot, W., & Pignatelli, M. (1998). Expression of catenins and E-cadherin during epithelial restitution in inflammatory bowel disease. *The Journal of Pathology*, *185*(4), 413–418.

Kardia, E., Frese, M., Smertina, E., Strive, T., Zeng, X.-L., Estes, M., & Hall, R. N. (2021). Culture and differentiation of rabbit intestinal organoids and organoid-derived cell monolayers. *Scientific Reports*, *11*(1), 1–12. https://doi.org/10.1038/s41598-021-84774-w

Kassambara, A. (2020). *ggpubr: "ggplot2" Based Publication Ready* (R package version 0.4.0).

Kawai, T., Akira, S., & Reed, J. C. (2003). ZIP kinase triggers apoptosis from nuclear PML oncogenic domains. *Molecular and Cellular Biology*, *23*(17), 6174–6186. https://doi.org/10.1128/mcb.23.17.6174-6186.2003

Kawai, T., Matsumoto, M., Takeda, K., Sanjo, H., & Akira, S. (1998). ZIP kinase, a novel serine/threonine kinase which mediates apoptosis. *Molecular and Cellular Biology*, *18*(3), 1642–1651. https://doi.org/10.1128/MCB.18.3.1642

Kim, D.-H., Khatau, S. B., Feng, Y., Walcott, S., Sun, S. X., Longmore, G. D., & Wirtz, D. (2012). Actin cap associated focal adhesions and their distinct role in cellular mechanosensing. *Scientific Reports*, *2*(1), 1–13. https://doi.org/10.1038/srep00555

Kim, J. J., Shajib, Md. S., Manocha, M. M., & Khan, W. I. (2012). Investigating intestinal inflammation in DSS-induced model of IBD. *Journal of Visualized Experiments*, *60*, 3678. https://doi.org/10.3791/3678

Kim, J., Koo, B.-K., & Knoblich, J. A. (2020). Human organoids: model systems for human biology and medicine. *Nature Reviews. Molecular Cell Biology*, *21*(10), 571–584. https://doi.org/10.1038/s41580-020-0259-3

Kim, M. J., Lee, Y. S., Han, G. Y., Lee, H. N., Ahn, C., & Kim, C. W. (2015). Profilin 2 promotes migration, invasion, and stemness of HT29 human colorectal cancer stem cells. *Bioscience, Biotechnology and Biochemistry*, *79*(9), 1438–1446. https://doi.org/10.1080/09168451.2015.1043118

Kim, N. G., & Gumbiner, B. M. (2015). Adhesion to fibronectin regulates Hippo signaling via the FAK-Src-PI3K pathway. *Journal of Cell Biology*, *210*(3), 503–515. https://doi.org/10.1083/jcb.201501025

Kim, W., Cho, Y. S., Wang, X., Park, O., Ma, X., Kim, H., Gan, W., Jho, E. hoon, Cha, B., Jeung, Y. ji, Zhang, L., Gao, B., Wei, W., Jiang, J., Chung, K. S., & Yang, Y. (2019). Hippo signaling is intrinsically regulated during cell cycle progression by APC/C ^{Cdh1}. *Proceedings of the National Academy of Sciences of the United States of America*, *116*(19), 9423–9432. https://doi.org/10.1073/pnas.1821370116

Kobayashi, T., Okamoto, S., Hisamatsu, T., Kamada, N., Chinen, H., Saito, R., Kitazume, M. T., Nakazawa, A., Sugita, A., Koganei, K., Isobe, K., & Hibi, T. (2008). IL23 differentially regulates the Th1/Th17 balance in ulcerative colitis and Crohn's disease. *Gut*, *57*(12), 1682–1689. https://doi.org/10.1136/gut.2007.135053

Koch, S. (2017). Extrinsic control of Wnt signaling in the intestine. *Differentiation*, *97*, 1–8. https://doi.org/10.1016/j.diff.2017.08.003

Koch, S., & Nusrat, A. (2012). The life and death of epithelia during inflammation: Lessons learned from the gut. *Annual Review of Pathology*, *7*, 35–60. https://doi.org/10.1146/annurev-pathol-011811-120905

Kocher, B. A., White, L. S., & Piwnica-Worms, D. (2015). DAPK3 Suppresses Acini Morphogenesis and is Required for Mouse Development. *Molecular Cancer Research*, *13*(2), 358–367. https://doi.org/10.1158/1541-7786.MCR-14-0333

Kögel, D., Bierbaum, H., Preuss, U., & Scheidtmann, K. H. (1999). C-terminal truncation of Dlk/ZIP kinase leads to abrogation of nuclear transport and high apoptotic activity. *Oncogene*, *18*(51), 7212–7218. https://doi.org/10.1038/sj.onc.1203169

Koh, T. J., & DiPietro, L. A. (2011). Inflammation and wound healing: The role of the macrophage. *Expert Reviews in Molecular Medicine*, *13*, e23. https://doi.org/10.1017/S1462399411001943

Komatsu, S., & Ikebe, M. (2004). ZIP kinase is responsible for the phosphorylation of myosin II and necessary for cell motility in mammalian fibroblasts. *The Journal of Cell Biology*, *165*(2), 243–254. https://doi.org/10.1083/jcb.200309056

Konsavage, W. M., Kyler, S. L., Rennoll, S. A., Jin, G., & Yochum, G. S. (2012). Wnt/β-catenin signaling regulates yes-associated protein (YAP) gene expression in colorectal carcinoma cells. *Journal of Biological Chemistry*, *287*(15), 11730–11739. https://doi.org/10.1074/jbc.M111.327767

Krämer, A., Green, J., Pollard, J., & Tugendreich, S. (2014). Causal analysis approaches in ingenuity pathway analysis. *Bioinformatics*, *30*(4), 523–530. https://doi.org/10.1093/bioinformatics/btt703

Krzystek-Korpacka, M., Diakowska, D., Bania, J., & Gamian, A. (2014). Expression stability of common housekeeping genes is differently affected by bowel inflammation and cancer: implications for finding suitable normalizers for inflammatory bowel disease studies. *Inflammatory Bowel Diseases*, *20*(7), 1147–1156. https://doi.org/10.1097/MIB.0000000000000067

Kuester, D., Guenther, T., Biesold, S., Hartmann, A., Bataille, F., Ruemmele, P., Peters, B., Meyer, F., Schubert, D., Bohr, U. R., Malfertheiner, P., Lippert, H., Silver, A. R. J., Roessner, A., & Schneider-Stock, R. (2010). Aberrant methylation of DAPK in long-standing ulcerative colitis and ulcerative colitis-associated carcinoma. *Pathology Research and Practice*, *206*(9), 616–624. https://doi.org/10.1016/j.prp.2010.05.004

Kuipers, D., Mehonic, A., Kajita, M., Peter, L., Fujita, Y., Duke, T., Charras, G., & Gale, J. E. (2014). Epithelial repair is a two-stage process driven first by dying cells and then by their neighbours. *Journal of Cell Science*, *127*(6), 1229–1241. https://doi.org/10.1242/jcs.138289

Kunovszki, P., Milassin, Á., Gimesi-Országh, J., Takács, P., Szántó, K., Bálint, A., Farkas, K., Borsi, A., Lakatos, P. L., Szamosi, T., & Molnár, T. (2020). Epidemiology, mortality and prevalence of colorectal cancer in ulcerative colitis patients between 2010-2016 in Hungary – a population-based study. *PLoS ONE*, *15*(5), e0233238. https://doi.org/10.1371/journal.pone.0233238

Lai, Y., Wu, B., Chen, L., & Zhao, H. (2004). A statistical method for identifying differential gene-gene co-expression patterns. *Bioinformatics*, *20*(17), 3146–3155. https://doi.org/10.1093/bioinformatics/bth379

Lakatos, L., Mester, G., Erdelyi, Z., David, G., Pandur, T., Balogh, M., Fischer, S., Vargha, P., & Lakatos, P. L. (2006). Risk factors for ulcerative colitis-associated colorectal cancer in a Hungarian cohort of patients with ulcerative colitis: results of a population-based study. *Inflammatory Bowel Diseases*, *12*(3), 205–211. https://doi.org/10.1097/01.MIB.0000217770.21261.ce

Lee, J. Y., Dominguez, A. A., Nam, S., Stowers, R. S., Qi, L. S., & Chaudhuri, O. (2019). Identification of cell context-dependent YAP-associated proteins reveals β1 and β4 integrin mediate YAP translocation independently of cell spreading. *Scientific Reports*, *9*(1), 1–11. https://doi.org/10.1038/s41598-019-53659-4

Lei, Q.-Y., Zhang, H., Zhao, B., Zha, Z.-Y., Bai, F., Pei, X.-H., Zhao, S., Xiong, Y., & Guan, K.-L. (2008). TAZ Promotes Cell Proliferation and Epithelial-Mesenchymal Transition and Is Inhibited by the Hippo Pathway. *Molecular and Cellular Biology*, *28*(7), 2426–2436. https://doi.org/10.1128/mcb.01874-07

Leister, P., Felten, A., Chasan, A. I., & Scheidtmann, K. H. (2008). ZIP kinase plays a crucial role in androgen receptor-mediated transcription. *Oncogene*, *27*(23), 3292–3300. https://doi.org/10.1038/sj.onc.1210995

Leonard, F., Collnot, E.-M., & Lehr, C.-M. (2010). A three-dimensional coculture of enterocytes, monocytes and dendritic cells to model inflamed intestinal mucosa in vitro. *Molecular Pharmaceutics*, *7*(6), 2103–2119. https://doi.org/10.1021/mp1000795

Leoni, G., Neumann, P. A., Sumagin, R., Denning, T. L., & Nusrat, A. (2015). Wound repair: Role of immune-epithelial interactions. *Mucosal Immunology*, *8*(5), 959–968. https://doi.org/10.1038/mi.2015.63

Li, C., Wen, A., Shen, B., Lu, J., Huang, Y., & Chang, Y. (2011). FastCloning: A highly simplified, purification-free, sequence- and ligation-independent PCR cloning method. *BMC Biotechnology*, *11*(1), 1–10. https://doi.org/10.1186/1472-6750-11-92

Li, G. M., Li, L., Li, M. Q., Chen, X., Su, Q., Deng, Z. J., Liu, H. B., Li, B., Zhang, W. H., Jia, Y. X., Wang, W. J., Ma, J. Y., Zhang, H. L., Xie, D., Zhu, X. F., He, Y. L., Guan, X. Y., & Bi, J. (2021). DAPK3 inhibits gastric cancer progression via activation of ULK1-dependent autophagy. *Cell Death and Differentiation*, *28*(3), 952–967. https://doi.org/10.1038/s41418-020-00627-5

Li, J., Deng, Z., Wang, Z., Wang, D., Zhang, L., Su, Q., Lai, Y., Li, B., Luo, Z., Chen, X., Chen, Y., Huang, X., Ma, J., Wang, W., Bi, J., & Guan, X. (2015). Zipper-interacting protein kinase promotes epithelial-mesenchymal transition, invasion and metastasis through AKT and NF-kB signaling and is associated with metastasis and poor prognosis in gastric cancer patients. *Oncotarget*, *6*(10), 8323–8338. https://doi.org/10.18632/oncotarget.3200

Li, K.-X., Du, Q., Wang, H.-P., & Sun, H.-J. (2019). Death-associated protein kinase 3 deficiency alleviates vascular calcification via AMPK-mediated inhibition of endoplasmic reticulum stress. *European Journal of Pharmacology*, *852*, 90–98. https://doi.org/10.1016/j.ejphar.2019.03.007

Liu, C. Y., Zha, Z. Y., Zhou, X., Zhang, H., Huang, W., Zhao, D., Li, T., Chan, S. W., Lim, C. J., Hong, W., Zhao, S., Xiong, Y., Lei, Q. Y., & Guan, K. L. (2010). The hippo tumor pathway promotes TAZ degradation by phosphorylating a phosphodegron and recruiting the SCFβ-TrCP E3 ligase. *Journal of Biological Chemistry*, *285*(48), 37159–37169. https://doi.org/10.1074/jbc.M110.152942

Liu, W., Xie, Y., Ma, J., Luo, X., Nie, P., Zuo, Z., Lahrmann, U., Zhao, Q., Zheng, Y., Zhao, Y., Xue, Y., & Ren, J. (2015). IBS: an illustrator for the presentation and visualization of biological sequences. *Bioinformatics*, *31*(20), 3359–3361. https://doi.org/10.1093/bioinformatics/btv362

Lopes, F., Keita, Å. V., Saxena, A., Reyes, J. L., Mancini, N. L., Al Rajabi, A., Wang, A., Baggio, C. H., Dicay, M., Van Dalen, R., Ahn, Y., Carneiro, M. B. H., Peters, N. C., Rho, J. M., MacNaughton, W. K., Girardin, S. E., Jijon, H., Philpott, D. J., Söderholm, J. D., & McKay, D. M. (2018). ER-stress mobilization of death-associated protein kinase-1-dependent xenophagy counteracts mitochondria stress-induced epithelial barrier dysfunction. *Journal of Biological Chemistry*, *293*(9), 3073–3087. https://doi.org/10.1074/jbc.RA117.000809

Lutgens, M. W. M. D., van Oijen, M. G. H., van der Heijden, G. J. M. G., Vleggaar, F. P., Siersema, P. D., & Oldenburg, B. (2013). Declining risk of colorectal cancer in inflammatory bowel disease: an updated meta-analysis of population-based cohort studies. *Inflammatory Bowel Diseases*, *19*(4), 789–799. https://doi.org/10.1097/MIB.0b013e31828029c0

MacDonald, J. A., Borman, M. A., Muranyi, A., Somlyo, A. V., Hartshorne, D. J., & Haystead, T. A. J. (2001). Identification of the endogenous smooth muscle myosin phosphatase-

associated kinase. *Proceedings of the National Academy of Sciences*, *98*(5), 2419–2424. https://doi.org/10.1073/pnas.041331498

MacDonald, J. A., Eto, M., Borman, M. A., Brautigan, D. L., & Haystead, T. A. J. (2001). Dual Ser and Thr phosphorylation of CPI-17, an inhibitor of myosin phosphatase, by MYPT-associated kinase. *FEBS Letters*, *493*(2–3), 91–94. https://doi.org/10.1016/S0014-5793(01)02277-3

MacDonald, J. A., & Walsh, M. P. (2018). Regulation of Smooth Muscle Myosin Light Chain Phosphatase by Multisite Phosphorylation of the Myosin Targeting Subunit, MYPT1. *Cardiovascular & Hematological Disorders-Drug Targets*, *18*(1), 4–13. https://doi.org/10.2174/1871529x18666180326120638

Madill-Thomsen, K., Withecomb, S., Parkes, M., Jovanovic, V., Venner, J., Fedorak, R., Halloran, P., & Halloran, B. P. (2018). Molecular archetype heterogeneity in ulcerative colitis biopsies. *Journal of the Canadian Association of Gastroenterology*, *1*(S2), 110–111. https://doi.org/10.1093/jcag/gwy009.070

Mahler, M., Bogdanos, D. P., Pavlidis, P., Fritzler, M. J., Csernok, E., Damoiseaux, J., Bentow, C., Shums, Z., Forbes, A., & Norman, G. L. (2013). PR3-ANCA: A promising biomarker for ulcerative colitis with extensive disease. *Clinica Chimica Acta*, *424*, 267–273. https://doi.org/10.1016/j.cca.2013.06.005

Manders, E. M. M., Verbeek, F. J., & Aten, J. A. (1993). Measurement of co-localization of objects in dual-colour confocal images. *Journal of Microscopy*, *169*(3), 375–382. https://doi.org/10.1111/j.1365-2818.1993.tb03313.x

May, D., Pan, S., Crispin, D. A., Lai, K., Bronner, M. P., Hogan, J., Hockenbery, D. M., McIntosh, M., Brentnall, T. A., & Chen, R. (2011). Investigating neoplastic progression of ulcerative colitis with label-free comparative proteomics. *Journal of Proteome Research*, *10*(1), 200–209. https://doi.org/10.1021/pr100574p

McInnes, I. B., Byers, N. L., Higgs, R. E., Lee, J., Macias, W. L., Na, S., Ortmann, R. A., Rocha, G., Rooney, T. P., Wehrman, T., Zhang, X., Zuckerman, S. H., & Taylor, P. C. (2019). Comparison of baricitinib, upadacitinib, and tofacitinib mediated regulation of cytokine signaling in human leukocyte subpopulations. *Arthritis Research & Therapy*, *21*(1), 183. https://doi.org/10.1186/S13075-019-1964-1

McKenzie, A. T., Katsyv, I., Song, W. M., Wang, M., & Zhang, B. (2016). DGCA: A comprehensive R package for Differential Gene Correlation Analysis. *BMC Systems Biology*, *10*(1), 1–25. https://doi.org/10.1186/s12918-016-0349-1

McQuin, C., Goodman, A., Chernyshev, V., Kamentsky, L., Cimini, B. A., Karhohs, K. W., Doan, M., Ding, L., Rafelski, S. M., Thirstrup, D., Wiegraebe, W., Singh, S., Becker, T., Caicedo, J. C., & Carpenter, A. E. (2018). CellProfiler 3.0: Next-generation image processing for biology. *PLoS Biology*, *16*(7), e2005970. https://doi.org/10.1371/journal.pbio.2005970

Medeiros, N. A., Burnette, D. T., & Forscher, P. (2006). Myosin II functions in actin-bundle turnover in neuronal growth cones. *Nature Cell Biology*, *8*(3), 215–226. https://doi.org/10.1038/ncb1367

Merino, F., Pospich, S., & Raunser, S. (2020). Towards a structural understanding of the remodeling of the actin cytoskeleton. *Seminars in Cell and Developmental Biology*, *102*, 51–64. https://doi.org/10.1016/j.semcdb.2019.11.018

Mitoma, H., Horiuchi, T., Tsukamoto, H., & Ueda, N. (2018). Molecular mechanisms of action of anti-TNF-α agents – Comparison among therapeutic TNF-α antagonists. *Cytokine*, *101*, 56–63. https://doi.org/10.1016/j.cyto.2016.08.014

Miyoshi, H., Ajima, R., Luo, C. T., Yamaguchi, T. P., & Stappenbeck, T. S. (2012). Wnt5a potentiates TGF-β signaling to promote colonic crypt regeneration after tissue injury. *Science*, *338*(6103), 108–113. https://doi.org/10.1126/science.1223821

Moffat, L. D., Brown, S. B. A., Grassie, M. E., Ulke-Lemée, A., Williamson, L. M., Walsh, M. P., & MacDonald, J. A. (2011). Chemical Genetics of Zipper-interacting Protein Kinase Reveal Myosin Light Chain as a *Bona Fide* Substrate in Permeabilized Arterial Smooth Muscle. *Journal of Biological Chemistry*, *286*(42), 36978–36991. https://doi.org/10.1074/jbc.M111.257949

Monteleone, G., Mann, J., Monteleone, I., Vavassori, P., Bremner, R., Fantini, M., Del Vecchio Blanco, G., Tersigni, R., Alessandroni, L., Mann, D., Pallone, F., & MacDonald, T. T. (2004). A Failure of Transforming Growth Factor-β1 Negative Regulation Maintains Sustained NF-κB Activation in Gut Inflammation. *Journal of Biological Chemistry*, *279*(6), 3925–3932. https://doi.org/10.1074/jbc.M303654200

Moparthi, L., & Koch, S. (2019). Wnt signaling in intestinal inflammation. *Differentiation*, *108*, 24–32. https://doi.org/10.1016/j.diff.2019.01.002

Moriyama, K., Iida, K., & Yahara, I. (1996). Phosphorylation of Ser-3 of cofilin regulates its essential function on actin. *Genes to Cells*, *1*(1), 73–86. https://doi.org/10.1046/j.1365-2443.1996.05005.x

Moyer, R. A., Wendt, M. K., Johanesen, P. A., Turner, J. R., & Dwinell, M. B. (2007). Rho activation regulates CXCL12 chemokine stimulated actin rearrangement and restitution in model intestinal epithelia. *Laboratory Investigation*, *87*(8), 807–817. https://doi.org/10.1038/labinvest.3700595

Mukhopadhyay, R., Ray, P. S., Arif, A., Brady, A. K., Kinter, M., & Fox, P. L. (2008). DAPK-ZIPK-L13a axis constitutes a negative-feedback module regulating inflammatory gene expression. *Molecular Cell*, *32*(3), 371–382. https://doi.org/10.1016/j.molcel.2008.09.019

Muller, M., Hansmannel, F., Arnone, D., Choukour, M., Ndiaye, N. C., Kokten, T., Houlgatte, R., & Peyrin-Biroulet, L. (2020). Genomic and molecular alterations in human inflammatory bowel disease-associated colorectal cancer. *United European Gastroenterology Journal*, *8*(6), 675. https://doi.org/10.1177/2050640620919254

Muñoz-Galván, S., Felipe-Abrio, B., Verdugo-Sivianes, E. M., Perez, M., Jiménez-García, M. P., Suarez-Martinez, E., Estevez-Garcia, P., & Carnero, A. (2020). Downregulation of MYPT1 increases tumor resistance in ovarian cancer by targeting the Hippo pathway and increasing the stemness. *Molecular Cancer*, *19*(1), 7. https://doi.org/10.1186/s12943-020-1130-z

Murata-Hori, M., Suizu, F., Iwasaki, T., Kikuchi, A., & Hosoya, H. (1999). ZIP kinase identified as a novel myosin regulatory light chain kinase in HeLa cells. *FEBS Letters*, *451*(1), 81–84. https://doi.org/10.1016/S0014-5793(99)00550-5

Nagumo, Y., Han, J., Bellila, A., Isoda, H., & Tanaka, T. (2008). Cofilin mediates tight-junction opening by redistributing actin and tight-junction proteins. *Biochemical and Biophysical Research Communications*, *377*(3), 921–925. https://doi.org/10.1016/j.bbrc.2008.10.071

Nalleweg, N., Chiriac, M. T., Podstawa, E., Lehmann, C., Rau, T. T., Atreya, R., Krauss, E., Hundorfean, G., Fichtner-Feigl, S., Hartmann, A., Becker, C., & Mudter, J. (2015). IL-9 and its receptor are predominantly involved in the pathogenesis of UC. *Gut*, *64*(5), 743–755. https://doi.org/10.1136/gutjnl-2013-305947

Natoli, M., Leoni, B. D., D'Agnano, I., Zucco, F., & Felsani, A. (2012). Good Caco-2 Cell Culture Practices. *Toxicology in Vitro*, *26*(8), 1243–1246. https://doi.org/10.1016/j.tiv.2012.03.009

Nehru, V., Almeida, F. N., & Aspenström, P. (2013). Interaction of RhoD and ZIP kinase modulates actin filament assembly and focal adhesion dynamics. *Biochemical and Biophysical Research Communications*, *433*(2), 163–169. https://doi.org/10.1016/j.bbrc.2013.02.046

Newell-Litwa, K. A., Horwitz, R., & Lamers, M. L. (2015). Non-muscle myosin II in disease: mechanisms and therapeutic opportunities. *Disease Models & Mechanisms*, *8*(12), 1495–1515. https://doi.org/10.1242/dmm.022103

Ng, K. M., Ferreyra, J. A., Higginbottom, S. K., Lynch, J. B., Kashyap, P. C., Gopinath, S., Naidu, N., Choudhury, B., Weimer, B. C., Monack, D. M., & Sonnenburg, J. L. (2013). Microbiota-liberated host sugars facilitate post-antibiotic expansion of enteric pathogens. *Nature*, *502*(7469), 96–99. https://doi.org/10.1038/nature12503

Ng, S. C., Shi, H. Y., Hamidi, N., Underwood, F. E., Tang, W., Benchimol, E. I., Panaccione, R., Ghosh, S., Wu, J. C. Y., Chan, F. K. L., Sung, J. J. Y., & Kaplan, G. G. (2017). Worldwide incidence and prevalence of inflammatory bowel disease in the 21st century: a systematic review of population-based studies. *The Lancet*. https://doi.org/10.1016/S0140-6736(17)32448-0

Nguyen, P. M., Putoczki, T. L., & Ernst, M. (2015). STAT3-activating cytokines: A therapeutic opportunity for inflammatory bowel disease? *Journal of Interferon and Cytokine Research*, *35*(5), 340–350. https://doi.org/10.1089/jir.2014.0225

Nigdelioglu, R., Hamanaka, R. B., Meliton, A. Y., O'Leary, E., Witt, L. J., Cho, T., Sun, K., Bonham, C., Wu, D., Woods, P. S., Husain, A. N., Wolfgeher, D., Dulin, N. O., Chandel, N. S., & Mutlu, G. M. (2016). Transforming Growth Factor (TGF)-β promotes de novo serine synthesis for collagen production. *Journal of Biological Chemistry*, *291*(53), 27239–27251. https://doi.org/10.1074/jbc.M116.756247

Niiro, N., & Ikebe, M. (2001). Zipper-interacting Protein Kinase Induces Ca^{2+}-free Smooth Muscle Contraction via Myosin Light Chain Phosphorylation. *Journal of Biological Chemistry*, *276*(31), 29567–29574. https://doi.org/10.1074/jbc.M102753200

Noel, G., Baetz, N. W., Staab, J. F., Donowitz, M., Kovbasnjuk, O., Pasetti, M. F., & Zachos, N. C. (2017). A primary human macrophage-enteroid co-culture model to investigate mucosal gut physiology and host-pathogen interactions. *Scientific Reports*, *7*, 45270. https://doi.org/10.1038/srep45270

Noguchi, S., Saito, A., & Nagase, T. (2018). YAP/TAZ Signaling as a Molecular Link between Fibrosis and Cancer. *International Journal of Molecular Sciences*, *19*(11), 3674. https://doi.org/10.3390/IJMS19113674

Nterma, P., Panopoulou, E., Papadaki-Petrou, E., & Assimakopoulou, M. (2020). Immunohistochemical Profile of Tumor Suppressor Proteins RASSF1A and LATS1/2 in Relation to p73 and YAP Expression, of Human Inflammatory Bowel Disease and Normal Intestine. *Pathology and Oncology Research*, *26*(1), 567–574. https://doi.org/10.1007/s12253-018-00575-z

Nusrat, A., Delp, C., & Madara, J. L. (1992). Intestinal epithelial restitution characterization of a cell culture model and mapping of cytoskeletal elements in migrating cells. *Journal of Clinical Investigation*, *89*(5), 1501–1511. https://doi.org/10.1172/JCI115741

Okamoto, M., Takayama, K., Shimizu, T., Ishida, K., Takahashi, O., & Furuya, T. (2009). Identification of death-associated protein kinases inhibitors using structure-based virtual screening. *Journal of Medicinal Chemistry*, *52*(22), 7323–7327. https://doi.org/10.1021/JM901191Q

Oliphant, K., & Allen-Vercoe, E. (2019). Macronutrient metabolism by the human gut microbiome: major fermentation by-products and their impact on host health. *Microbiome*, *7*(1), 91. https://doi.org/10.1186/S40168-019-0704-8

Ono, T., Terada, F., Okumura, M., Chihara, T., & Hamao, K. (2020). Impairment of cytokinesis by cancer-associated DAPK3 mutations. *Biochemical and Biophysical Research Communications*, *533*(4), 1095–1101. https://doi.org/10.1016/j.bbrc.2020.09.078

Ou, W., Xu, W., Liu, F., Guo, Y., Huang, Z., Feng, T., Liu, C.-Y., & Du, P. (2021). Increased expression of yes-associated protein/YAP and transcriptional coactivator with PDZ-binding motif/TAZ activates intestinal fibroblasts to promote intestinal obstruction in Crohn's disease. *EBioMedicine*, *69*, 103452. https://doi.org/10.1016/j.ebiom.2021.103452

Ouahed, J., Gordon, W., Canavan, J. B., Zhou, H., Du, S., von Schack, D., Phillips, K., Wang, L., Augustine Dunn, W., Field, M., Friel, S., Griffith, A., Evans, S., Tollefson, S., Carrellas,

M., Cao, B., Merker, A., Bousvaros, A., Shouval, D. S., … Makrauer, F. (2018). Mucosal gene expression in pediatric and adult patients with ulcerative colitis permits modeling of ideal biopsy collection strategy for transcriptomic analysis. *Inflammatory Bowel Diseases*, *24*(12), 2565–2578. https://doi.org/10.1093/ibd/izy242

Owen, K. A., Abshire, M. Y., Tilghman, R. W., Casanova, J. E., & Bouton, A. H. (2011). FAK regulates intestinal epithelial cell survival and proliferation during mucosal wound healing. *PLoS ONE*, *6*(8), e23123. https://doi.org/10.1371/journal.pone.0023123

Page, G., Kögel, D., Rangnekar, V., & Scheidtmann, K. H. (1999). Interaction partners of Dlk/ZIP kinase: co-expression of Dlk/ZIP kinase and Par-4 results in cytoplasmic retention and apoptosis. *Oncogene*, *18*(51), 7265–7273. https://doi.org/10.1038/sj.onc.1203170

Panciera, T., Azzolin, L., Cordenonsi, M., & Piccolo, S. (2017). Mechanobiology of YAP and TAZ in physiology and disease. *Nature Reviews Molecular Cell Biology*, *18*(12), 758–770. https://doi.org/10.1038/nrm.2017.87

Pang, Y., Ruan, H., Wu, D., Lang, Y., Sun, K., & Xu, C. (2020). Assessment of clinical activity and severity using serum ANCA and ASCA antibodies in patients with ulcerative colitis. *Allergy, Asthma and Clinical Immunology*, *16*, 37. https://doi.org/10.1186/s13223-020-00433-1

Park, H. W., Kim, Y. C., Yu, B., Moroishi, T., Mo, J. S., Plouffe, S. W., Meng, Z., Lin, K. C., Yu, F. X., Alexander, C. M., Wang, C. Y., & Guan, K. L. (2015). Alternative Wnt Signaling Activates YAP/TAZ. *Cell*, *162*(4), 780–794. https://doi.org/10.1016/j.cell.2015.07.013

Pastorelli, L., Salvo, C. De, Mercado, J. R., Vecchi, M., & Pizarro, T. T. (2013). Central role of the gut epithelial barrier in the pathogenesis of chronic intestinal inflammation: Lessons learned from animal models and human genetics. *Frontiers in Immunology*, *4*, 280. https://doi.org/10.3389/fimmu.2013.00280

Pavlidis, S., Monast, C., Loza, M. J., Branigan, P., Chung, K. F., Adcock, I. M., Guo, Y., Rowe, A., & Baribaud, F. (2019). I_MDS: an inflammatory bowel disease molecular activity score to classify patients with differing disease-driving pathways and therapeutic response to anti-TNF treatment. *PLoS Computational Biology*, *15*(4), e1006951. https://doi.org/10.1371/journal.pcbi.1006951

Pereira, P. D., Serra-Caetano, A., Cabrita, M., Bekman, E., Braga, J., Rino, J., Santus, R., Filipe, P. L., Sousa, A. E., & Ferreira, J. A. (2017). Quantification of cell cycle kinetics by EdU (5-

ethynyl-2'- deoxyuridine)-coupled-fluorescence-intensity analysis. *Oncotarget*, *8*(25), 40514–40532. https://doi.org/10.18632/oncotarget.17121

Perez White, B., & Getsios, S. (2014). Eph receptor and ephrin function in breast, gut, and skin epithelia. *Cell Adhesion & Migration*, *8*(4), 327–338. https://doi.org/10.4161/19336918.2014.970012

Perše, M., & Cerar, A. (2012). Dextran sodium sulphate colitis mouse model: Traps and tricks. *Journal of Biomedicine and Biotechnology*, *2012*, 718617. https://doi.org/10.1155/2012/718617

Peterson, L. W., & Artis, D. (2014). Intestinal epithelial cells: Regulators of barrier function and immune homeostasis. *Nature Reviews Immunology*, *14*(3), 141–153. https://doi.org/10.1038/nri3608

Piccolo, S., Dupont, S., & Cordenonsi, M. (2014). The biology of YAP/TAZ: Hippo signaling and beyond. *Physiological Reviews*, *94*(4), 1287–1312. https://doi.org/10.1152/physrev.00005.2014

Pittayanon, R., Lau, J. T., Leontiadis, G. I., Tse, F., Yuan, Y., Surette, M., & Moayyedi, P. (2020). Differences in Gut Microbiota in Patients With vs Without Inflammatory Bowel Diseases: A Systematic Review. *Gastroenterology*, *158*(4), 930-946.e1. https://doi.org/10.1053/j.gastro.2019.11.294

Planell, N., Lozano, J. J., Mora-Buch, R., Masamunt, M. C., Jimeno, M., Ordás, I., Esteller, M., Ricart, E., Piqué, J. M., Panés, J., & Salas, A. (2013). Transcriptional analysis of the intestinal mucosa of patients with ulcerative colitis in remission reveals lasting epithelial cell alterations. *Gut*, *62*(7), 967–976. https://doi.org/10.1136/gutjnl-2012-303333

Plouffe, S. W., Lin, K. C., Moore, J. L., Tan, F. E., Ma, S., Ye, Z., Qiu, Y., Ren, B., & Guan, K. L. (2018). The Hippo pathway effector proteins YAP and TAZ have both distinct and overlapping functions in the cell. *Journal of Biological Chemistry*, *293*(28), 11230–11240. https://doi.org/10.1074/jbc.RA118.002715

Porter, R. J., Kalla, R., & Ho, G.-T. (2020). Ulcerative colitis: Recent advances in the understanding of disease pathogenesis. *F1000Research*, *9*, F1000 Faculty Rev-294. https://doi.org/10.12688/f1000research.20805.1

Praskova, M., Khoklatchev, A., Ortiz-Vega, S., & Avruch, J. (2004). Regulation of the MST1 kinase by autophosphorylation, by the growth inhibitory proteins, RASSF1 and NORE1, and by Ras. *Biochemical Journal*, *381*(2), 453–462. https://doi.org/10.1042/BJ20040025

Praskova, M., Xia, F., & Avruch, J. (2008). MOBKL1A/MOBKL1B Phosphorylation by MST1 and MST2 Inhibits Cell Proliferation. *Current Biology*, *18*(5), 311–321. https://doi.org/10.1016/j.cub.2008.02.006

Qiao, Y., Chen, J., Lim, Y. B., Finch-Edmondson, M. L., Seshachalam, V. P., Qin, L., Jiang, T., Low, B. C., Singh, H., Lim, C. T., & Sudol, M. (2017). YAP Regulates Actin Dynamics through ARHGAP29 and Promotes Metastasis. *Cell Reports*, *19*(8), 1495–1502. https://doi.org/10.1016/j.celrep.2017.04.075

Qin, Z., Xia, W., Fisher, G. J., Voorhees, J. J., & Quan, T. (2018). YAP/TAZ regulates TGF-β/Smad3 signaling by induction of Smad7 via AP-1 in human skin dermal fibroblasts. *Cell Communication and Signaling*, *16*(1), 18. https://doi.org/10.1186/s12964-018-0232-3

Reinisch, W., Panés, J., Khurana, S., Toth, G., Hua, F., Comer, G. M., Hinz, M., Page, K., O'Toole, M., Moorehead, T. M. D., Zhu, H., Sun, Y. H., & Cataldi, F. (2015). Anrukinzumab, an anti-interleukin 13 monoclonal antibody, in active UC: Efficacy and safety from a phase IIa randomised multicentre study. *Gut*, *64*(6), 894–900. https://doi.org/10.1136/gutjnl-2014-308337

Rieder, F., Brenmoehl, J., Leeb, S., Schölmerich, J., & Rogler, G. (2007). Wound healing and fibrosis in intestinal disease. *Gut*, *56*(1), 130. https://doi.org/10.1136/gut.2006.090456

Rinninella, E., Raoul, P., Cintoni, M., Franceschi, F., Miggiano, G. A. D., Gasbarrini, A., & Mele, M. C. (2019). What is the Healthy Gut Microbiota Composition? A Changing Ecosystem across Age, Environment, Diet, and Diseases. *Microorganisms*, *7*(1), 14. https://doi.org/10.3390/microorganisms7010014

Ritchie, M. E., Phipson, B., Wu, D., Hu, Y., Law, C. W., Shi, W., & Smyth, G. K. (2015). Limma powers differential expression analyses for RNA-sequencing and microarray studies. *Nucleic Acids Research*, *43*(7), e47. https://doi.org/10.1093/nar/gkv007

Robles, A. I., Traverso, G., Zhang, M., Roberts, N. J., Khan, M. A., Joseph, C., Lauwers, G. Y., Selaru, F. M., Popoli, M., Pittman, M. E., Ke, X., Hruban, R. H., Meltzer, S. J., Kinzler, K. W., Vogelstein, B., Harris, C. C., & Papadopoulos, N. (2016). Whole-Exome Sequencing

Analyses of Inflammatory Bowel Disease-Associated Colorectal Cancers. *Gastroenterology*, *150*(4), 931–943. https://doi.org/10.1053/j.gastro.2015.12.036

Rocchi, A., Benchimol, E. I., Bernstein, C. N., Bitton, A., Feagan, B., Panaccione, R., Glasgow, K. W., Fernandes, A., & Ghosh, S. (2012). Inflammatory bowel disease: a Canadian burden of illness review. *Canadian Journal of Gastroenterology*, *26*(11), 811–817. https://doi.org/10.1155/2012/984575

Romberg-Camps, M. J. L., Dagnelie, P. C., Kester, A. D. M., Hesselink-Van De Kruijs, M. A. M., Cilissen, M., Engels, L. G. J. B., Van Deursen, C., Hameeteman, W. H. A., Wolters, F. L., Russel, M. G. V. M., & Stockbrügger, R. W. (2009). Influence of phenotype at diagnosis and of other potential prognostic factors on the course of inflammatory bowel disease. *American Journal of Gastroenterology*, *104*(2), 371–383. https://doi.org/10.1038/ajg.2008.38

Rosenblatt, J., Raff, M. C., & Cramer, L. P. (2001). An epithelial cell destined for apoptosis signals its neighbors to extrude it by an actin- and myosin-dependent mechanism. *Current Biology*, *11*(23), 1847–1857. https://doi.org/10.1016/S0960-9822(01)00587-5

Rottner, K., Faix, J., Bogdan, S., Linder, S., & Kerkhoff, E. (2017). Actin assembly mechanisms at a glance. *Journal of Cell Science*, *130*(20), 3427–3435. https://doi.org/10.1242/jcs.206433

Russo, J. M., Florian, P., Shen, L., Graham, W. V., Tretiakova, M. S., Gitter, A. H., Mrsny, R. J., & Turner, J. R. (2005). Distinct temporal-spatial roles for rho kinase and myosin light chain kinase in epithelial purse-string wound closure. *Gastroenterology*, *128*(4), 987–1001. https://doi.org/10.1053/j.gastro.2005.01.004

Safroneeva, E., Vavricka, S., Fournier, N., Seibold, F., Mottet, C., Nydegger, A., Ezri, J., Straumann, A., Rogler, G., & Schoepfer, A. M. (2015). Systematic analysis of factors associated with progression and regression of ulcerative colitis in 918 patients. *Alimentary Pharmacology and Therapeutics*, *42*(5), 540–548. https://doi.org/10.1111/apt.13307

Saito, T., Ohira, M., Hayashi, A., Kozuma, S., Hattori, A., Hori, T., & Seki, N. (1998). Assignment of the ZIP kinase gene to human chromosome 19p13.3 by somatic hybrid analysis and fluorescence in-situ hybridization. *Journal of Human Genetics*, *43*(3), 209–211. https://doi.org/10.1007/s100380050073

Sandborn, W. J., Ferrante, M., Bhandari, B. R., Berliba, E., Feagan, B. G., Hibi, T., Tuttle, J. L., Klekotka, P., Friedrich, S., Durante, M., Morgan-Cox, M. A., Laskowski, J., Schmitz, J., & D'Haens, G. R. (2020). Efficacy and Safety of Mirikizumab in a Randomized Phase 2 Study of Patients With Ulcerative Colitis. *Gastroenterology*, *158*(3), 537–549.e10. https://doi.org/10.1053/j.gastro.2019.08.043

Sands, B. E., Sandborn, W. J., Panaccione, R., O'Brien, C. D., Zhang, H., Johanns, J., Adedokun, O. J., Li, K., Peyrin-Biroulet, L., Van Assche, G., Danese, S., Targan, S., Abreu, M. T., Hisamatsu, T., Szapary, P., Marano, C., & UNIFI Study Group. (2019). Ustekinumab as Induction and Maintenance Therapy for Ulcerative Colitis. *New England Journal of Medicine*, *381*(13), 1201–1214. https://doi.org/10.1056/nejmoa1900750

Santhanam, S., Rajamanickam, S., Motamarry, A., Ramakrishna, B. S., Amirtharaj, J. G., Ramachandran, A., Pulimood, A., & Venkatraman, A. (2012). Mitochondrial electron transport chain complex dysfunction in the colonic mucosa in ulcerative colitis. *Inflammatory Bowel Diseases*, *18*(11), 2158–2168. https://doi.org/10.1002/ibd.22926

Sato, A., Kayama, H., Shojima, K., Matsumoto, S., Koyama, H., Minami, Y., Nojima, S., Morii, E., Honda, H., Takeda, K., & Kikuchi, A. (2015). The Wnt5a-Ror2 axis promotes the signaling circuit between interleukin-12 and interferon-γ in colitis. *Scientific Reports*, *5*(1), 1–16. https://doi.org/10.1038/srep10536

Sato, N., Kamada, N., Muromoto, R., Kawai, T., Sugiyama, K., Watanabe, T., Imoto, S., Sekine, Y., Ohbayashi, N., Ishida, M., Akira, S., & Matsuda, T. (2006). Phosphorylation of threonine-265 in Zipper-interacting protein kinase plays an important role in its activity and is induced by IL-6 family cytokines. *Immunology Letters*, *103*(2), 127–134. https://doi.org/10.1016/j.imlet.2005.10.015

Sato, N., Kawai, T., Sugiyama, K., Muromoto, R., Imoto, S., Sekine, Y., Ishida, M., Akira, S., & Matsuda, T. (2005). Physical and functional interactions between STAT3 and ZIP kinase. *International Immunology*, *17*(12), 1543–1552. https://doi.org/10.1093/intimm/dxh331

Schepers, A. G., Vries, R., Van Den Born, M., Van De Wetering, M., & Clevers, H. (2011). Lgr5 intestinal stem cells have high telomerase activity and randomly segregate their chromosomes. *EMBO Journal*, *30*(6), 1104–1109. https://doi.org/10.1038/emboj.2011.26

Schindelin, J., Arganda-Carreras, I., Frise, E., Kaynig, V., Longair, M., Pietzsch, T., Preibisch, S., Rueden, C., Saalfeld, S., Schmid, B., Tinevez, J. Y., White, D. J., Hartenstein, V., Eliceiri, K., Tomancak, P., & Cardona, A. (2012). Fiji: An open-source platform for

biological-image analysis. *Nature Methods*, *9*(7), 676–682. https://doi.org/10.1038/nmeth.2019

Schlegelmilch, K., Mohseni, M., Kirak, O., Pruszak, J., Rodriguez, J. R., Zhou, D., Kreger, B. T., Vasioukhin, V., Avruch, J., Brummelkamp, T. R., & Camargo, F. D. (2011). Yap1 acts downstream of α-Catenin to control epidermal proliferation. *Cell*, *144*(5), 782–795. https://doi.org/10.1016/j.cell.2011.02.031

Schroeder, B. O. (2019). Fight them or feed them: how the intestinal mucus layer manages the gut microbiota. *Gastroenterology Report*, *7*(1), 3–12. https://doi.org/10.1093/gastro/goy052

Schultz, B. M., Salazar, G. A., Paduro, C. A., Pardo-Roa, C., Pizarro, D. P., Salazar-Echegarai, F. J., Torres, J., Riedel, C. A., Kalergis, A. M., Álvarez-Lobos, M. M., & Bueno, S. M. (2018). Persistent Salmonella enterica serovar Typhimurium infection increases the susceptibility of mice to develop intestinal inflammation. *Frontiers in Immunology*, *9*, 1166. https://doi.org/10.3389/fimmu.2018.01166

Schwayer, C., Sikora, M., Slováková, J., Kardos, R., & Heisenberg, C. P. (2016). Actin Rings of Power. *Developmental Cell*, *37*(6), 493–506. https://doi.org/10.1016/j.devcel.2016.05.024

Seeler, J.-S., & Dejean, A. (1999). The PML nuclear bodies: actors or extras? *Current Opinion in Genetics & Development*, *9*(3), 362–367. https://doi.org/10.1016/S0959-437X(99)80054-9

Selden, L. A., Kinosian, H. J., Estes, J. E., & Gershman, L. C. (1999). Impact of profilin on actin-bound nucleotide exchange and actin polymerization dynamics. *Biochemistry*, *38*(9), 2769–2778. https://doi.org/10.1021/bi981543c

Seo, Y., Park, S. Y., Kim, H. S., & Nam, J. S. (2020). The Hippo-YAP Signaling as Guardian in the Pool of Intestinal Stem Cells. *Biomedicines*, *8*(12), 560. https://doi.org/10.3390/biomedicines8120560

Seong, J., Tajik, A., Sun, J., Guan, J.-L., Humphries, M. J., Craig, S. E., Shekaran, A., García, A. J., Lu, S., Lin, M. Z., Wang, N., & Wang, Y. (2013). Distinct biophysical mechanisms of focal adhesion kinase mechanoactivation by different extracellular matrix proteins. *Proceedings of the National Academy of Sciences of the United States of America*, *110*(48), 19372–19377. https://doi.org/10.1073/pnas.1307405110

Shani, G., Marash, L., Gozuacik, D., Bialik, S., Teitelbaum, L., Shohat, G., & Kimchi, A. (2004). Death-associated protein kinase phosphorylates ZIP kinase, forming a unique kinase

hierarchy to activate its cell death functions. *Molecular and Cellular Biology*, *24*(19), 8611–8626. https://doi.org/10.1128/MCB.24.19.8611-8626.2004

Shannon, P., Markiel, A., Ozier, O., Baliga, N., Wang, J., Ramage, D., Amin, N., Schwikowski, B., & Ideker, T. (2003). Cytoscape: a software environment for integrated models of biomolecular interaction networks. *Genome Research*, *13*(11), 2498–2504. https://doi.org/10.1101/gr.1239303

Shao, Y., Zheng, Q., Wang, W., Xin, N., Song, X., & Zhao, C. (2016). Biological functions of macrophage-derived Wnt5a, and its roles in human diseases. *Oncotarget*, *7*(41), 67674–67684. https://doi.org/10.18632/oncotarget.11874

Shenoy, A. K., Fisher, R. C., Butterworth, E. A., Pi, L., Chang, L.-J., Appelman, H. D., Chang, M., Scott, E. W., & Huang, E. H. (2012). Transition from colitis to cancer: high Wnt activity sustains the tumor-initiating potential of colon cancer stem cell precursors. *Cancer Research*, *72*(19), 5091–5100. https://doi.org/10.1158/0008-5472.CAN-12-1806

Shiu, J., Aires, L., Lin, Z., & Vogel, V. (2018). Nanopillar force measurements reveal actin-cap-mediated YAP mechanotransduction. *Nature Cell Biology*, *20*(3), 262–271. https://doi.org/10.1038/S41556-017-0030-Y

Shoval, Y., Pietrokovski, S., & Kimchi, A. (2007). ZIPK: a unique case of murine-specific divergence of a conserved vertebrate gene. *PLoS Genetics*, *3*(10), 1884–1893. https://doi.org/10.1371/journal.pgen.0030180

Sifroni, K. G., Damiani, C. R., Stoffel, C., Cardoso, M. R., Ferreira, G. K., Jeremias, I. C., Rezin, G. T., Scaini, G., Schuck, P. F., Dal-Pizzol, F., & Streck, E. L. (2010). Mitochondrial respiratory chain in the colonic mucosal of patients with ulcerative colitis. *Molecular and Cellular Biochemistry*, *342*(1–2), 111–115. https://doi.org/10.1007/s11010-010-0474-x

Silverberg, M. S., Mirea, L., Bull, S. B., Murphy, J. E., Steinhart, A. H., Greenberg, G. R., McLeod, R. S., Cohen, Z., Wade, J. A., & Siminovitch, K. A. (2003). A population- and family-based study of Canadian families reveals association of HLA DRB1*0103 with colonic involvement in inflammatory bowel disease. *Inflammatory Bowel Diseases*, *9*(1), 1–9. https://doi.org/10.1097/00054725-200301000-00001

Singh, P., Ravanan, P., & Talwar, P. (2016). Death Associated Protein Kinase 1 (DAPK1): A Regulator of Apoptosis and Autophagy. *Frontiers in Molecular Neuroscience*, *9*, 46. https://doi.org/10.3389/fnmol.2016.00046

Small, J. V. (1988). The actin cytoskeleton. *Electron Microscopy Reviews*, *1*(1), 155–174. https://doi.org/10.1016/S0892-0354(98)90010-7

Smith, P. J., Levine, A. P., Dunne, J., Guilhamon, P., Turmaine, M., Sewell, G. W., O'Shea, N. R., Vega, R., Paterson, J. C., Oukrif, D., Beck, S., Bloom, S. L., Novelli, M., Rodriguez-Justo, M., Smith, A. M., & Segal, A. W. (2014). Mucosal transcriptomics implicates under expression of BRINP3 in the pathogenesis of ulcerative colitis. *Inflammatory Bowel Diseases*, *20*(10), 1802–1812. https://doi.org/10.1097/MIB.0000000000000169

Sommer, F., Anderson, J. M., Bharti, R., Raes, J., & Rosenstiel, P. (2017). The resilience of the intestinal microbiota influences health and disease. *Nature Reviews. Microbiology*, *15*(10), 630–638. https://doi.org/10.1038/nrmicro.2017.58

Steinbach, E. C., & Plevy, S. E. (2014). The role of macrophages and dendritic cells in the initiation of inflammation in IBD. *Inflammatory Bowel Diseases*, *20*(1), 166–175. https://doi.org/10.1097/MIB.0b013e3182a69dca

Strober, W., & Fuss, I. J. (2011). Proinflammatory cytokines in the pathogenesis of inflammatory bowel diseases. *Gastroenterology*, *140*(6), 1756–1767. https://doi.org/10.1053/j.gastro.2011.02.016

Syamaladevi, D. P., Spudich, J. A., & Sowdhamini, R. (2012). Structural and functional insights on the Myosin superfamily. *Bioinformatics and Biology Insights*, *6*, 11–21. https://doi.org/10.4137/BBI.S8451

Takahashi, M., Lio, C. W. J., Campeau, A., Steger, M., Ay, F., Mann, M., Gonzalez, D. J., Jain, M., & Sharma, S. (2021). The tumor suppressor kinase DAPK3 drives tumor-intrinsic immunity through the STING–IFN-β pathway. *Nature Immunology*, *22*(4), 485–496. https://doi.org/10.1038/s41590-021-00896-3

Tang, H.-W., Wang, Y.-B., Wang, S.-L., Wu, M.-H., Lin, S.-Y., & Chen, G.-C. (2011). Atg1-mediated myosin II activation regulates autophagosome formation during starvation-induced autophagy. *The EMBO Journal*, *30*(4), 636–651. https://doi.org/10.1038/emboj.2010.338

Taniguchi, K., Wu, L. W., Grivennikov, S. I., De Jong, P. R., Lian, I., Yu, F. X., Wang, K., Ho, S. B., Boland, B. S., Chang, J. T., Sandborn, W. J., Hardiman, G., Raz, E., Maehara, Y., Yoshimura, A., Zucman-Rossi, J., Guan, K. L., & Karin, M. (2015). A gp130-Src-YAP

module links inflammation to epithelial regeneration. *Nature*, *519*(7541), 57–62. https://doi.org/10.1038/nature14228

Thoo, L., Noti, M., & Krebs, P. (2019). Keep calm: the intestinal barrier at the interface of peace and war. *Cell Death & Disease*, *10*(11), 849. https://doi.org/10.1038/s41419-019-2086-z

Togi, S., Ikeda, O., Kamitani, S., Nakasuji, M., Sekine, Y., Muromoto, R., Nanbo, A., Oritani, K., Kawai, T., Akira, S., & Matsuda, T. (2011). Zipper-interacting protein kinase (ZIPK) modulates canonical Wnt/β-catenin signaling through interaction with nemo-like kinase and T-cell factor 4 (NLK/TCF4). *Journal of Biological Chemistry*, *286*(21), 19170–19177. https://doi.org/10.1074/jbc.M110.189829

Tomasetti, C., & Bozic, I. (2015). The (not so) immortal strand hypothesis. *Stem Cell Research*, *14*(2), 238–241. https://doi.org/10.1016/j.scr.2015.01.005

Topol, L., Jiang, X., Choi, H., Garrett-Beal, L., Carolan, P., & Yang, Y. (2003). Wnt-5a inhibits the canonical Wnt pathway by promoting GSK-3-independent beta-catenin degradation. *The Journal of Cell Biology*, *162*(5), 899–908. https://doi.org/10.1083/jcb.200303158

Torres, J., & Colombel, J. F. (2016). Genetics and phenotypes in inflammatory bowel disease. *The Lancet*, *387*(10014), 98–100. https://doi.org/10.1016/S0140-6736(15)00464-X

Troncone, E., Marafini, I., Stolfi, C., & Monteleone, G. (2018). Transforming growth factor-β1/Smad7 in intestinal immunity, inflammation, and cancer. *Frontiers in Immunology*, *9*, 1408. https://doi.org/10.3389/fimmu.2018.01407

Turner, J. R. (2009). Intestinal mucosal barrier function in health and disease. *Nature Reviews. Immunology*, *9*(11), 799–809. https://doi.org/10.1038/nri2653

Turner, J. R., Rill, B. K., Carlson, S. L., Carnes, D., Kerner, R., Mrsny, R. J., & Madara, J. L. (1997). Physiological regulation of epithelial tight junctions is associated with myosin light-chain phosphorylation. *The American Journal of Physiology*, *273*(4), C1378–C1385. https://doi.org/10.1152/ajpcell.1997.273.4.C1378

Ulke-Lemée, A., & MacDonald, J. A. (2010). Opportunities to Target Specific Contractile Abnormalities with Smooth Muscle Protein Kinase Inhibitors. *Pharmaceuticals*, *3*(6), 1739–1760. https://doi.org/10.3390/ph3061739

Ullman, T., Odze, R., & Farraye, F. A. (2009). Diagnosis and management of dysplasia in patients with ulcerative colitis and Crohn's disease of the colon. *Inflammatory Bowel Diseases*, *15*(4), 630–638. https://doi.org/10.1002/ibd.20766

Umemoto, S., Bengur, A. R., & Sellers, J. R. (1989). Effect of multiple phosphorylations of smooth muscle and cytoplasmic myosins on movement in an in vitro motility assay. *Journal of Biological Chemistry*, *264*(3), 1431–1436. https://doi.org/10.1016/s0021-9258(18)94205-5

Van Der Kraak, L., Gros, P., & Beauchemin, N. (2015). Colitis-associated colon cancer: Is it in your genes? *World Journal of Gastroenterology*, *21*(41), 11688–11699. https://doi.org/10.3748/wjg.v21.i41.11688

Varelas, X. (2014). The hippo pathway effectors TAZ and YAP in development, homeostasis and disease. *Development*, *141*(8), 1614–1626. https://doi.org/10.1242/dev.102376

Venegas, D. P., De La Fuente, M. K., Landskron, G., González, M. J., Quera, R., Dijkstra, G., Harmsen, H. J. M., Faber, K. N., & Hermoso, M. A. (2019). Short Chain Fatty Acids (SCFAs)-Mediated Gut Epithelial and Immune Regulation and Its Relevance for Inflammatory Bowel Diseases. *Frontiers in Immunology*, *10*, 277. https://doi.org/10.3389/fimmu.2019.00277

Villalta, J. I., Galli, S., Iacaruso, M. F., Arciuch, V. G. A., Poderoso, J. J., Jares-Erijman, E. A., & Pietrasanta, L. I. (2011). New algorithm to determine true colocalization in combination with image restoration and time-lapse confocal microscopy to map Kinases in mitochondria. *PLoS ONE*, *6*(4), 19031. https://doi.org/10.1371/journal.pone.0019031

Vinayaga-Pavan, M., Frampton, M., Pontikos, N., Levine, A. P., Smith, P. J., Jonasson, J. G., Björnsson, E. S., Segal, A. W., & Smith, A. M. (2019). Elevation in Cell Cycle and Protein Metabolism Gene Transcription in Inactive Colonic Tissue from Icelandic Patients with Ulcerative Colitis. *Inflammatory Bowel Diseases*, *25*(2), 317–327. https://doi.org/10.1093/ibd/izy350

Visser-Grieve, S., Zhou, Z., She, Y. M., Huang, H., Cyr, T. D., Xu, T., & Yang, X. (2011). LATS1 tumor suppressor is a novel actin-binding protein and negative regulator of actin polymerization. *Cell Research*, *21*(10), 1513–1516. https://doi.org/10.1038/cr.2011.122

Wada, K. I., Itoga, K., Okano, T., Yonemura, S., & Sasaki, H. (2011). Hippo pathway regulation by cell morphology and stress fibers. *Development*, *138*(18), 3907–3914. https://doi.org/10.1242/dev.070987

Walsh, M. P. (2011). Vascular Smooth muscle myosin light chain diphosphorylation: Mechanism, function, and pathological implications. *IUBMB Life*, *63*(11), 987–1000. https://doi.org/10.1002/iub.527

Weisser, S., Brugger, H., Voglmaier, N., McLarren, K., van Rooijen, N., & Sly, L. (2011). SHIP-deficient, alternatively activated macrophages protect mice during DSS-induced colitis. *Journal of Leukocyte Biology*, *90*(3), 483–492. https://doi.org/10.1189/jlb.0311124

Weitzel, D. H., Chambers, J., & Haystead, T. A. J. (2011). Phosphorylation-dependent control of ZIPK nuclear import is species specific. *Cellular Signalling*, *23*(1), 297–303. https://doi.org/10.1016/j.cellsig.2010.09.016

Willemsen, L. E. M., Koetsier, M. A., van Deventer, S. J. H., & van Tol, E. A. F. (2003). Short chain fatty acids stimulate epithelial mucin 2 expression through differential effects on prostaglandin E(1) and E(2) production by intestinal myofibroblasts. *Gut*, *52*(10), 1442–1447. https://doi.org/10.1136/gut.52.10.1442

Wu, W., Hu, H., Ye, Z., Leong, M., He, M., Li, Q., Hu, R., & Zhang, S. (2015). Zipper-interacting protein kinase interacts with human cell division cycle 14A phosphatase. *Molecular Medicine Reports*, *11*(4), 2775–2780. https://doi.org/10.3892/mmr.2014.3067

Xie, Z., Wang, Y., Yang, G., Han, J., Zhu, L., Li, L., & Zhang, S. (2021). The role of the Hippo pathway in the pathogenesis of inflammatory bowel disease. *Cell Death and Disease*, *12*(1), 79. https://doi.org/10.1038/s41419-021-03395-3

Xu, X., Wang, X., Todd, E. M., Jaeger, E. R., Vella, J. L., Mooren, O. L., Feng, Y., Hu, J., Cooper, J. A., Morley, S. C., & Huang, Y. H. (2016). Mst1 Kinase Regulates the Actin-Bundling Protein L-Plastin To Promote T Cell Migration. *Journal of Immunology*, *197*(5), 1683–1691. https://doi.org/10.4049/jimmunol.1600874

Yamada, S., Yoshino, T., Matsuura, M., Minami, N., Toyonaga, T., Honzawa, Y., Tsuji, Y., & Nakase, H. (2014). Long-term efficacy of infliximab for refractory ulcerative colitis: results from a single center experience. *BMC Gastroenterology*, *14*(1), 80. https://doi.org/10.1186/1471-230X-14-80

Yamashiro, Y., Thang, B., Ramirez, K., Shin, S., Kohata, T., Ohata, S., Nguyen, T., Ohtsuki, S., Nagayama, K., & Yanagisawa, H. (2020). Matrix mechanotransduction mediated by thrombospondin-1/integrin/YAP in the vascular remodeling. *Proceedings of the National Academy of Sciences of the United States of America*, *117*(18), 9896–9905. https://doi.org/10.1073/pnas.1919702117

Yang, H., Rotter, J. I., Toyoda, H., Landers, C., Tyan, D., McElree, C. K., & Targan, S. R. (1993). Ulcerative colitis: A genetically heterogeneous disorder defined by genetic (HLA class II) and subclinical (antineutrophil cytoplasmic antibodies) markers. *Journal of Clinical Investigation*, *92*(2), 1080–1084. https://doi.org/10.1172/JCI116613

Yang, N., Higuchi, O., Ohashi, K., Nagata, K., Wada, A., Kangawa, K., Nishida, E., & Mizuno, K. (1998). Cofilin phosphorylation by LIM-kinase 1 and its role in Rac-mediated actin reorganization. *Nature*, *393*(6687), 809–812. https://doi.org/10.1038/31735

Yang, S., Zhang, L., Chen, X., Chen, Y., & Dong, J. (2015). Oncoprotein YAP regulates the spindle checkpoint activation in a mitotic phosphorylation-dependent manner through up-regulation of BubR1. *Journal of Biological Chemistry*, *290*(10), 6191–6202. https://doi.org/10.1074/jbc.M114.624411

Yu, F. X., Zhao, B., Panupinthu, N., Jewell, J. L., Lian, I., Wang, L. H., Zhao, J., Yuan, H., Tumaneng, K., Li, H., Fu, X. D., Mills, G. B., & Guan, K. L. (2012). Regulation of the Hippo-YAP pathway by G-protein-coupled receptor signaling. *Cell*, *150*(4), 780–791. https://doi.org/10.1016/j.cell.2012.06.037

Yuhan, R., Koutsouris, A., Savkovlc, S. D., & Hecht, G. (1997). Enteropathogenic Escherichia coli-induced myosin light chain phosphorylation alters intestinal epithelial permeability. *Gastroenterology*, *113*(6), 1873–1882. https://doi.org/10.1016/S0016-5085(97)70006-4

Yui, S., Azzolin, L., Maimets, M., Pedersen, M. T., Fordham, R. P., Hansen, S. L., Larsen, H. L., Guiu, J., Alves, M. R. P., Rundsten, C. F., Johansen, J. V., Li, Y., Madsen, C. D., Nakamura, T., Watanabe, M., Nielsen, O. H., Schweiger, P. J., Piccolo, S., & Jensen, K. B. (2018). YAP/TAZ-Dependent Reprogramming of Colonic Epithelium Links ECM Remodeling to Tissue Regeneration. *Cell Stem Cell*, *22*(1), 35-49.e7. https://doi.org/10.1016/j.stem.2017.11.001

Zarrin, A. A., Bao, K., Lupardus, P., & Vucic, D. (2021). Kinase inhibition in autoimmunity and inflammation. *Nature Reviews. Drug Discovery*, *20*(1), 39–63. https://doi.org/10.1038/s41573-020-0082-8

Zhang, Y., Zhang, C., Zhang, H., Zeng, W., Li, S., Chen, C., Song, X., Sun, J., Sun, Z., Cui, C., Cao, X., Zheng, L., Wang, P., Zhao, W., Zhang, Z., Xu, Y., Zhu, M., & Chen, H. (2019). ZIPK mediates endothelial cell contraction through myosin light chain phosphorylation and is required for ischemic-reperfusion injury. *FASEB Journal*, *33*(8), 9062–9074. https://doi.org/10.1096/fj.201802052RRR

Zhao, B., Li, L., Tumaneng, K., Wang, C. Y., & Guan, K. L. (2010). A coordinated phosphorylation by Lats and CK1 regulates YAP stability through SCFβ-TRCP. *Genes and Development*, *24*(1), 72–85. https://doi.org/10.1101/gad.1843810

Zhao, B., Li, L., Wang, L., Wang, C. Y., Yu, J., & Guan, K. L. (2012). Cell detachment activates the Hippo pathway via cytoskeleton reorganization to induce anoikis. *Genes and Development*, *26*(1), 54–68. https://doi.org/10.1101/gad.173435.111

Zhao, B., Wei, X., Li, W., Udan, R. S., Yang, Q., Kim, J., Xie, J., Ikenoue, T., Yu, J., Li, L., Zheng, P., Ye, K., Chinnaiyan, A., Halder, G., Lai, Z. C., & Guan, K. L. (2007). Inactivation of YAP oncoprotein by the Hippo pathway is involved in cell contact inhibition and tissue growth control. *Genes and Development*, *21*(21), 2747–2761. https://doi.org/10.1101/gad.1602907

Zhou, D., Zhang, Y., Wu, H., Barryg, E., Yin, Y., Lawrence, E., Dawson, D., Willis, J. E., Markowitz, S. D., Camargo, F. D., & Avruch, J. (2011). Mst1 and Mst2 protein kinases restrain intestinal stem cell proliferation and colonic tumorigenesis by inhibition of Yes-associated protein (Yap) overabundance. *Proceedings of the National Academy of Sciences of the United States of America*, *108*(49), E1312–E1320. https://doi.org/10.1073/pnas.1110428108

Zhou, K., Muroyama, A., Underwood, J., Leylek, R., Ray, S., Soderling, S. H., & Lechler, T. (2013). Actin-related protein2/3 complex regulates tight junctions and terminal differentiation to promote epidermal barrier formation. *Proceedings of the National Academy of Sciences of the United States of America*, *110*(40), E3820–E3829. https://doi.org/10.1073/pnas.1308419110

Zhou, Q., Shen, Z. F., Wu, B. S., Xu, C. B., He, Z. Q., Chen, T., Shang, H. T., Xie, C. F., Huang, S. Y., Chen, Y. G., Chen, H. B., & Han, S. T. (2019). Risk of Colorectal Cancer in Ulcerative Colitis Patients: A Systematic Review and Meta-Analysis. *Gastroenterology Research and Practice*, *2019*, 5363261. https://doi.org/10.1155/2019/5363261

Zhou, X., Wang, S., Zhang, P., Wang, Q., Xiao, J., Zhang, C., Zheng, X., Xu, X., Xue, S., Hui, L., Ji, H., Wei, B., & Wang, H. (2019). YAP Aggravates Inflammatory Bowel Disease by Regulating M1/M2 Macrophage Polarization and Gut Microbial Homeostasis. *Cell Reports*, *27*(4), 1176-1189.e5. https://doi.org/10.1016/j.celrep.2019.03.028

Appendix A. Gene lists for Venn Diagram.

Appendix A. These gene lists compliment the Venn diagram depicted in **Figure 5**.

Pancolitis ∩ Left-sided colitis

Common Up-regulation (Count = 465)

ABCC1, ACKR1, ACPP, ACVR1, ADA, ADAMTS9, ADGRF5, ADGRG5, ADGRG6, ADGRL4, ADM, AGPAT4, AJUBA, ALDH1A2, ALDH1A3, ANGPT2, ANXA1, ANXA5, ANXA6, APIP, APOBEC3G, APOL1, APOL2, AREG, ARFGAP3, ARHGAP29, ARHGEF3, ARL4C, ARMCX2, ARNTL2, ART3, ASAP1, ASPHD2, ASRGL1, ASS1, ATP11A, ATP2C1, B9D1, BACE2, BAG2, BGN, BHLHA15, BIRC3, BNC2, BNIP3, BRD3OS, BTN3A3, C1orf216, C2, C2CD4A, C3, C4A/C4B, C4BPA, C4BPB, CADM1, CALD1, CARD16, CARD6, CARD8, CASP1, CASP17P, CASP4, CAV2, CBR3, CBX4, CCDC69, CCL20, CCL24, CCN2, CCN4, CD38, CD3D, CD44, CD55, CDC25B, CDH3, CDH5, CEACAM6, CEBPB, CEBPD, CEP128, CEP135, CFB, CFI, CHI3L1, CHST2, CIITA, CLDN1, CLEC4A, COL4A1, COL6A3, COTL1, CPEB4, CR1, CREB3L2, CSF2RB, CSGALNACT1, CSGALNACT2, CTHRC1, CTLA4, CTSK, CXCL1, CXCL11, CXCL2, CXCL3, CXCL6, CXCL8, CXCR2, CYP4X1, CYTOR, CYYR1, DAPP1, DCPS, DDIT4, DEFA5, DEFA6, DEFB4A/DEFB4B, DEGS1, DERL3, DMBT1, DNAJB9, DOC2B, DOK3, DRAM1, DUOX2, DUOXA2, DUSP10, DUSP6, ECSCR, EHD3, EIF5A2, ELK3, ELL2, ENG, ENTPD1, EOGT, EPHA2, ERO1A, F2R, F3, FADS1, FAM167B, FAM241A, FAM30A, FAM92A, FBXO16, FBXO6, FCGR3A/FCGR3B, FCN1, FCRL5, FERMT2, FFAR2, FKBP11, FLJ32255, FOXQ1, FSCN1, FSTL1, FUT8, FUT8-AS1, GABRP, GAL, GALNT2, GALNT6, GBP1, GBP2, GBP5, GIMAP2, GIMAP6, GIMAP8, GLCCI1, GMPR, GNA15, GNB5, GPR171, GPR176, GPX7, GPX8, GREM1, GRHL1, GUCY1A1, GUCY1B1, GZMB, HCAR3, HEG1, HLA-DMA, HS3ST1, HS6ST2, IDO1, IFITM1, IFITM2, IFITM3, IFNG, IGFBP5, IGFBP7, IGFLR1, IGHG3, IGLL1/IGLL5, IKBIP, IL12RB1, IL15RA, IL1B, IL1RN, IL33, INHBA, INSC, IRAK3, IRF1, ISG20, ITGA5, ITGAL, ITGAX, ITK, ITPR1, JAZF1, KCND3, KCNE3, KCNN3, KDELR3, KIAA0895, KIF14, KLF2, KLF7, KLHL29, KLHL5, KRT6B, KYNU, LAG3, LATS2, LAX1, LBH, LCN2, LCP2, LDB2, LDLRAD3, LINC-PINT, LINC00888, LIPG, LIX1L, LMO2, LOC101928100, LPCAT1, LPGAT1, LPIN1, LRP8, LRRC8C, LST1, LYN, MADCAM1, MAFF, MAP3K20, MAP3K8, MAP4K1, MAP9, MCAM, MCUB, MDM2, ME1, MEI1, MEOX1, MFNG, MGP, MIAT, MICB, MIR3142HG, MMP10, MMP3, MMP7, MMP9, MMRN1, MNDA, MR1, MRGPRF, MSN, MTCL1, MUC1, MYEOV, MYO1F, MZB1, NCF1, NCOA7, NFKBIZ, NLRC5, NOS2, NUCB2, NXPE3, ODF3B, OLFM1, OLFM4, ORAI2, OSBPL3, P2RY13, PACC1, PALM2AKAP2, PALMD, PAPLN, PARP14, PARP8, PARP9, PARVG, PCDH17, PCDH7, PDE4B, PDZK1IP1, PEA15, PECAM1, PF4, PFKFB3, PGM2L1, PHLDA1, PI3, PIK3R3, PIM2, PIM3, PITPNC1, PLA1A, PLAAT4, PLAUR, PLEKHO1, PLN, PLS3, PMAIP1, PNOC, PODXL, PPM1K, PPP1R16B, PRDM1, PRDX4, PRKAR2B, PROK2, PRRX1, PSAT1, PSMB8-AS1, PSMB9, PTAFR, PTPN22, PTPRG, RAB29, RAB31, RAB8B, RAC2, RAMP3, RASA4B, RASGRP1, RASSF5, RBPMS, RCBTB1, RCN1, RECQL, REG1A, REG1B, REG3A, REG4, RGCC, RGS5, RILPL2, RIPOR3, RNF183, RNF213, ROBO1, RPL22L1, RPS6KA2, RTEL1-TNFRSF6B, S100A11, S100A8, S100A9, S100P, SAA2, SAA4, SACS, SAMD9L, SAMSN1, SASH3, SCD, SEC11C, SEC14L1, SEC24D, SELENOM, SELP, SELPLG, SEMA4D, SEPTIN6, SERPINA1, SERPINA3, SERPING1, SGMS1, SHCBP1, SHFL, SIK1/SIK1B, SLA, SLC16A14, SLC16A3, SLC25A37, SLC28A3, SLC2A3, SLC41A1, SLC6A14, SLC6A20, SLC6A6, SLC7A11, SLC7A5, SLC8A1, SLC9A7, SLCO4A1, SLFN5, SLPI, SNX20, SOCS1, SOCS3, SORD, SP110, SPCS3, SPIDR, SPNS2, SPON2, SRD5A3, SSR3, ST3GAL1, ST3GAL5, STOM, STRIP2, STS, SULF1, SYTL1, TACSTD2, TAGAP, TAP1, TAP2, TCIM, TCN1, TEK, TESC, TGM2, THEMIS2, TIMP1, TMC6, TMEM158, TMTC1, TNFRSF1B, TNFRSF6B, TNIP3, TPK1, TPRG1, TPST2, TRERF1, TRIB2, TRIM22, TRIM29, TSTA3, TTC7B, TUBB6, TWSG1, TYMP, UBE2L6, UNC5CL, VAMP5, VNN1, VSIG1, VWA1, VWF, WARS1, ZBP1, ZC3H12A, ZEB1, ZFPM2, ZG16B.

Common Down-regulation (Count = 159)

A1CF, ABCB1, ABCG2, ACAA2, ACAT1, ACOT8, ACOX1, ACSF2, ADGRA3, ADH1A, ADH1C, ADIRF, AKAP1, AMACR, AMN, ANK3, ANXA13, APOBEC3B, AQP8, ARHGAP42, ARHGAP44, B4GALNT2, BCAT2, BMP3, BRINP3, C11orf52, C11orf54, C9orf24, CA1, CA7, CAMK1D, CAPN13, CDHR1, CDKL1, CES2, CHP2, CHRNA1, CLDN8, CLYBL, CNNM2, CWH43, CYP2S1, CYP4F2, CYP4F3, DEPDC7, DHRS11, DPP10-AS1, EFNA5, EPHX2, ESPN, ETFDH, FAM120AOS, FAM189A1, FGF9, FGFR2, GABRA2, GBA3, GCNT2, GPR160, GUCA2A, GXYLT2, HAGLR, HIGD1A, HMGA2, HMGCS2, HNF4A, HOXA5, HSD3B2, HSDL2, HSPB3, IL1R2, IMPA2, LINC02023, LYRM7, MAOA, MATN2, MEP1B, METTL7A, MTMR11, NAAA, NAPEPLD, NDUFC1, NHEJ1, NPY1R, NSF, NWD2, OSBPL1A, OTC, PADI2, PAG1, PANK3, PBLD, PCK1, PDE6A, PDK2, PEX11A, PHGR1, PHLPP2, PLA2G12B, PLCD1, PLCE1, PPARG, PPARGC1A, PRDX6, PRXL2A, PSD3, PTGDR, PTGR1, PXMP2, RAPGEFL1, RETSAT, RHOU, RMDN2, RNASE1, RUNDC3B, SATB2, SATB2-AS1, SCIN, SCUBE2, SELENBP1, SEMA5A, SLC13A2, SLC16A9, SLC17A4, SLC26A2, SLC26A3, SLC36A1, SLC39A5, SLC44A1, SMIM14, SMPDL3B, SRI, SSTR1, SUGCT, TEX11, TINAG, TLCD4, TMCC3, TMED6, TMEM171,

TMEM63C, TMEM72, TMEM98, TRABD2A, TSPAN7, UGP2, UGT1A1, UGT1A3, UGT1A6, UGT2A3, UGT2B28, UNC5C, VLDLR, VLDLR-AS1, VSTM2A, YBX2, ZDHHC11, ZNF704, ZNF91.

Contra-regulated (Count = 1)

PIK3AP1.

Pancolitis ∩ CAD

Common Up-regulation (Count = 209)

AASDH, AASS, AHCYL1, AKNA, ANKRD11, ANKRD36B, AP1S1, AP3D1, APP, ARAP1, ARID1B, ARL15, ARMCX3, ATF5, ATF6B, ATP6V0E1, ATRX, ATXN1-AS1, B2M, BBS4, BPTF, BRD4, C1RL, CBX3, CD47, CDC27, CDC42BPB, CEP295, CHD9, CLASP1, COA1, COPG1, CORO1B, CRIM1-DT, CSAD, CSNK1E, CSNK1G2, CTSZ, CTTN, DARS1, DCAF16, DHTKD1, DIP2A, DNAJC7, EHBP1, EHBP1L1, EI24, EIF5B, ENAH, EP300, EPC1, EPG5, ERC1, ERGIC1, ERGIC2, ERICH1, EVI5, FAT4, FBXL17, FGFR1, FKBP10, FOXC1, FOXO1, GABPB1, GOLGA8A/GOLGA8B, GPATCH2, H4C3, HCFC1R1, HCG11, HCG18, HNRNPA0, HNRNPL, HOXB8, IDS, IFT80, ITGB5, ITPRIPL2, JADE1, JMY, JPX, KAT2B, KATNBL1, KDSR, KIF13A, KIF21A, KIF3A, KIZ, KPNA6, LAMB1, LLGL1, LMO4, LRCH3, LUC7L3, MAFG, MAP4, MARCHF2, MED31, MEF2A, MIB1, MIDN, MINDY2, MINK1, MLEC, MMP14, MPHOSPH9, MPRIP, MTA1, MTDH, MYO1C, MZF1, N4BP2L2, NASP, NCOR2, NDUFB8, NFIB, NFIC, NPEPL1, NPIPB4 (includes others), NPTN-IT1, NR2F2, NSUN6, NUMB, NUTF2, OBSL1, PABPN1, PARP10, PBX2, PCED1A, PCSK5, PDXDC1, PDZRN3, PGGHG, PHF3, PIAS3, PPM1F, PPP3CA, PPP3R1, PRRC2C, PTCD3, PTPN1, PURA, PURB, RAB12, RAB24, RAPGEF6, RASL11A, RBM26, RBM3, RBM4, RBM43, RDH11, REX1BD, RLF, RNF24, RPL32P3, RPS10, RTN4, SAV1, SBF1, SDHA, SFXN3, SKI, SLC39A7, SLCO3A1, SMARCC1, SMC3, SMIM27, SOX4, SP3, SPG7, SRGAP2B, SRRM2, SSPN, STK4, TAF1D, TECPR1, THRAP3, TK2, TMEM154, TMEM223, TNPO3, TNRC6A, TRIM14, TRIM4, TRIM8, TSPAN18, TUT7, USF1, USP4, USP42, WASF2, WNT6, XXYLT1, YIF1B, YPEL3, YWHAB, ZBED1, ZBED6, ZBTB1, ZBTB20, ZBTB7A, ZC2HC1A, ZMYM5, ZNF117, ZNF281, ZNF37A, ZNF654, ZNF785, ZNF827.

Common Down-regulation (Count = 985)

ABCA5, ABCC4, ABCD3, ABCF2, ABHD10, ABHD11, ABHD12, ABHD17B, ABHD5, ABHD6, ACAP2, ACER3, ACO2, ACOT11, ACSL5, ACTR2, ADAM10, AFDN, AFF4, AGFG1, AGO2, AGPS, AHCYL2, AHNAK, AIFM1, AK2, AKAP13, AKIRIN1, ALDH1B1, ALDH6A1, ALG5, AMD1, AMMECR1, ANAPC5, ANKEF1, ANKFY1, ANKHD1/ANKHD1-EIF4EBP3, ANKS4B, AP1AR, AP1G1, AP2A1, AP3B1, AP5M1, APC, API5, APLP2, ARF1, ARF6, ARFGEF1, ARFGEF2, ARFIP1, ARHGAP21, ARHGAP27, ARHGAP5, ARHGEF7, ARHGEF9, ARID1A, ARID2, ARIH1, ARPC5, ASAH1, ASAH2B, ASXL2, ATAD2B, ATE1, ATF1, ATF2, ATG16L1, ATG5, ATL2, ATOH1, ATP13A3, ATP1B3, ATP2A2, ATP2A3, ATP6V0A1, ATP6V1A, ATP6V1C1, ATP7A, ATP8A1, AVL9, AZIN1, B3GALNT2, B3GNT5, B3GNT6, B4GALT1, BACH1, BANF1, BCL2L1, BCL2L13, BCL2L2, BCLAF1, BLOC1S6, BMP5, BRD3, BROX, BTBD7, BUB1, BZW1, C12orf49, C12orf66, C17orf80, C1orf56, C1S, C2orf49, C5orf22, C5orf24, C6orf62, CAB39, CALM1 (includes others), CAMK2D, CAMKK2, CANT1, CANX, CAPN5, CAPN7, CAPRIN1, CAPZA1, CARMIL1, CARNMT1, CASK, CASP8, CBX5, CCDC126, CCDC186, CCDC6, CCDC91, CCND2, CCNE2, CCNG2, CCNT2, CCT2, CD164, CD24, CD46, CD74, CDC25A, CDC40, CDC42, CDC42SE2, CDC5L, CDCP1, CDH1, CDHR5, CDK13, CDK17, CDK2, CDK6, CDK8, CDV3, CEACAM7, CEBPZOS, CELF1, CEP350, CEP70, CEPT1, CERS6, CFL1, CFTR, CGGBP1, CHD1L, CHM, CHMP1B, CHN2, CITED2, CKAP5, CLIC4, CLIC5, CLINT1, CLN8, CLPTM1, CMAS, CMTM4, CNOT1, CNOT6L, CNOT8, CNST, CNTNAP2, COCH, COG3, COPA, COQ7, COX15, CP, CPD, CPNE3, CPNE8, CREB1, CREBL2, CRLS1, CSNK1A1, CSNK2A1, CTDSPL2, CTNNA1, CTNND1, CTTNBP2NL, CUL4B, CXADR, CYB5R3, CYP51A1, CYTH1, DAB2, DAPK3, DAZAP2, DBT, DCAF11, DCTN4, DCTN5, DCUN1D1, DCUN1D4, DDAH1, DDC, DDX39B, DDX3X, DDX42, DENND11, DENND1B, DENR, DEPDC1, DGKA, DHX15, DHX35, DHX9, DIAPH2, DICER1, DLAT, DLD, DLG1, DNAJA4, DNAJB1, DNAJC11, DNAJC3, DNMBP, DOCK1, DOCK5, DSC2, DSG2, DSG2-AS1, DTL, DYNC1H1, DYNC1LI2, EBP, EDN3, EEA1, EEF1D, EFCAB14, EFNB2, EHF, EIF4A2, EIF4B, EIF4E3, ELAVL1, ELK4, ELP3, EME1, EMILIN3, EML4, ENSA, ENTPD4, EPAS1, EPB41L4B, EPHX1, EPRS1, EPS8L2, ERBB2, ERI3, ERLIN1, ESRP1, ESYT2, ETNK1, ETV6, EXD2, EXOC4, EXOC5, EXOC6, EZR, F11R, F2RL1, FA2H, FAF1, FAM126B, FAM199X, FAM76A, FAM76B, FANCF, FANCI, FAR1, FAR2, FARP2, FBXO28, FBXO38, FBXO45, FBXW11, FCF1, FGD4, FGD6, FHL1, FIGNL1, FKBP1A, FKBP5, FKBP8, FLNB, FLOT2, FNDC3A, FNIP1, FOPNL, FOXA1, FOXJ3, FOXN3, FOXO3B, FPR3, FRYL, FUS, FYTTD1, G3BP1, G3BP2, GAB1, GABPA, GALC, GALNT4, GART, GAS2L3, GASK1B, GATM, GDAP2, GDE1, GDI2, GFM1, GFM2, GFPT1, GHITM, GLE1, GM2A, GMFB, GNA13, GNAS, GNRH1, GNS, GOLGA7, GOPC, GPC6, GPD2, GPR39, GPSM2, GRPEL2, GSN, GSPT1, GTDC1, GTF2H2, GTF2I, GTF3C2, GTPBP2, GUF1, HACD3, HAUS6, HERC4, HIPK1, HIPK2, HIPK3, HMGCS1, HNF4G, HNMT, HNRNPH1, HNRNPU, HP1BP3, HPS3, HSP90AA1, HSP90AB1, HSP90B1, HSPA14, HSPA4, HSPA8, HSPD1, HSPH1, HTATSF1, IAH1, ICE2, IDH3A, IFNGR1, IGIP, IKBKB, IKZF5, IL2RG, IL32, IL6R, IL6ST, INO80D, INPP5A, IPO5, IPO8, IPP, IRF6, ITCH, ITGA6, ITGB1, ITGB4, ITPRID2, JAK1, JMJD1C, JUND, KANSL1L, KBTBD2, KBTBD4, KCTD20, KCTD5, KDM1B, KDM4C, KDM6A, KHDC4, KIAA1109, KIAA1217, KIAA1324, KIF22, KIF5B, KIFAP3, KITLG, KLF3, KLHDC10, KLHDC3,

KLHL12, KLHL20, KMT2A, KMT5A, KPNA1, KPNA4, KRAS, KRIT1, L2HGDH, L3MBTL2, LACC1, LAD1, LANCL1, LAPTM4B, LARP1B, LARP4, LARP4B, LARS1, LIG4, LIMK2, LIN7C, LMAN1, LMBR1, LNPEP, LPAR5, LPP, LRATD1, LSS, MACC1, MAML2, MAN1A1, MAP3K12, MAP3K13, MAP3K2, MAP3K7, MAP4K5, MAP7, MAPK1, MAPK14, MAPK1IP1L, MAPKAP1, MAPRE1, MAPRE3, MARCHF6, MARS2, MAT2A, MAT2B, MATR3, MAX, MAZ, MBD1, MBNL1, MBNL2, MBP, MBTPS1, MCCC2, MCL1, MCM3AP, MCM4, ME2, MED20, MED23, MED6, MEF2C, MET, METTL9, MEX3C, MFAP3, MFN1, MFN2, MFSD14C, MGA, MGAT4A, MIA3, MICAL2, MIER1, MIS18A, MKRN2, MLX, MLXIP, MOSPD1, MPP5, MPP7, MPZL1, MPZL2, MRPL30, MRPL38, MRPS15, MSANTD4, MSH3, MSH6, MTCH2, MTMR1, MTMR2, MTPAP, MTUS1, MXD1, MYL12A, MYO6, MYSM1, NAA15, NAA50, NAB1, NADK, NAPA, NAV1, NBR1, NCKAP1, NCOA2, NEAT1, NECTIN2, NEK2, NEMP1, NFE2L2, NFIA, NFS1, NFX1, NFYA, NGEF, NHLRC3, NHSL1, NIPAL2, NIPBL, NKAPD1, NMD3, NME7, NMNAT1, NNT, NOLC1, NOM1, NONO, NOTCH2, NOX1, NPEPPS, NR1D2, NR2F6, NRAS, NRIP1, NSD2, NSMAF, NUBPL, NUCB1, NUCKS1, NUDT21, NUDT3, NUMA1, NUP160, NUP58, NXT2, OCRL, OGA, OGDH, ORC5, OSBP, OXR1, P4HB, PACSIN2, PAFAH1B1, PAFAH2, PAK1, PAPOLA, PARL, PATL1, PAWR, PBRM1, PCGF1, PCGF5, PCIF1, PCNP, PDE3A, PDE4DIP, PDE5A, PDE7A, PDE8A, PDGFD, PDK4, PDLIM5, PDS5B, PEX1, PGGT1B, PGK1, PGRMC1, PHTF2, PIAS2, PICALM, PIGR, PIK3C2A, PIK3CB, PIK3R1, PIP4K2A, PKN2, PKP2, PKP3, PLD1, PLEC, PLEKHA1, PLEKHB2, PLEKHF2, PLEKHH1, PLK1, PLLP, PLPP3, PLXNC1, PNN, PNRC2, POF1B, POLDIP3, PPARA, PPFIA1, PPM1A, PPP1CB, PPP1R10, PPP1R21, PPP1R3B, PPP2R1A, PPP2R1B, PPP4R3A, PPP4R3B, PPTC7, PRELID3B, PRIM2, PRKAA1, PRKAB1, PRKAB2, PRKACB, PRKAR1A, PRKCI, PRKCSH, PROX1, PRPF31, PRPF4, PRPF4B, PRPS2, PRUNE1, PSEN1, PSME3, PSME4, PSPC1, PTAR1, PTBP1, PTBP3, PTENP1, PTGER4, PTK2, PTPN11, PTPN12, PTPN9, PTPRD, PTPRS, PUS10, PWWP3A, PXK, QSER1, R3HCC1L, RAB11B, RAB18, RAB1A, RAB2A, RAB35, RAB5A, RAB6A, RABEP1, RAD21, RALB, RALGAPA2, RANBP2, RAP1GDS1, RAP2A, RAP2B, RAPGEF2, RASA2, RASEF, RASSF3, RASSF6, RBL2, RBM14, RBM22, RBM47, RBM48, RBM5, RBM6, RBMX, RC3H1, RC3H2, RCAN1, RCC1L, RDH13, REEP3, REPIN1, REPS2, RERE, RFC3, RFC5, RHEB, RHOB, RIF1, RIOK3, RIPK1, RIPK4, RIT1, RMND1, RNASEH1, RNF14, RNF146, RNF6, RNFT1, RNGTT, RO60, ROCK2, RPAP3, RPEL1, RPRD1A, RPS27A, RPS6KA3, RRM1, RRN3P1, RTN4IP1, RUFY3, RXRB, SAE1, SAFB, SAMD12, SAMD5, SAR1B, SARAF, SBF2, SC5D, SCAMP1, SCARB2, SCOC, SCRN3, SCYL2, SDHC, SEC22B, SEC23A, SEC61A1, SECISBP2L, SELENOP, SENP1, SEPTIN10, SEPTIN11, SEPTIN2, SERBP1, SET, SETD5, SETX, SF3B1, SGCB, SGPP1, SH3D19, SHC1, SIKE1, SKP2, SLAIN2, SLC1A1, SLC20A1, SLC25A13, SLC25A36, SLC2A13, SLC30A5, SLC35A2, SLC35A3, SLC35D1, SLC37A4, SLC39A14, SLC39A8, SLC39A9, SLC44A4, SLC4A7, SLC5A3, SLIT2, SLMAP, SMAD5, SMARCA2, SMCHD1, SMCR8, SNAP23, SNX13, SNX27, SOCS4, SOCS6, SORT1, SOS2, SP1, SPAG9, SPAST, SPIN1, SPON1, SPOPL, SPRED1, SPRED2, SPRYD7, SPTAN1, SPTBN1, SPTLC1, SPTLC2, SQLE, SRFBP1, SRPK1, SRPRA, SRRT, SRSF1, SRSF10, SRSF11, SRSF3, SRSF5, SS18, ST6GAL1, STAG2, STIP1, STK26, STK38, STX16, STX17, STX3, STXBP2, STYX, SUPT16H, SYNRG, SYPL1, SYTL2, TAB2, TAF9B, TALAM1, TAOK1, TASOR2, TCF7L2, TENT2, TES, TFAM, TFCP2, TFG, TFRC, TGFBR2, THBS1, TIA1, TJP1, TLDC2, TLE4, TM9SF3, TMED4, TMEM168, TMEM192, TMEM245, TMEM259, TMEM260, TMEM267, TMEM30A, TMEM33, TMEM87B, TMEM97, TMOD3, TMPO, TMPRSS2, TMX1, TNIK, TNKS2, TNRC6B, TOB2, TOX4, TP53, TPD52, TPH1, TPP1, TPP2, TPR, TRA2B, TRAM1, TRAPPC1, TRAPPC11, TRIM23, TRIM59, TRIP10, TRMT1L, TRMT2B, TRNT1, TRRAP, TRUB1, TSN, TTC22, TTC37, TTN-AS1, TUBGCP2, TUBGCP3, TUBGCP4, TWF1, TXNIP, UBAP2L, UBE3B, UBE3C, UBE4B, UBXN4, UBXN7, UEVLD, UGCG, UGT8, UHMK1, UNC93B1, UQCC1, UQCRC1, USO1, USP10, USP33, USP34, USP38, USP47, USP9X, UTP23, UTRN, VAMP3, VDAC1, VDAC3, VKORC1L1, VMP1, VPS26C, VPS35, VPS50, VPS8, VTA1, WAC, WAPL, WASHC4, WASL, WDR1, WSB1, WTAP, WWP2, XIAP, XPNPEP1, XPO7, XRN2, YBX3, YME1L1, YOD1, YTHDF3, YWHAE, YWHAZ, ZBTB26, ZBTB38, ZC3H14, ZDHHC20, ZDHHC21, ZFP36L2, ZMAT3, ZMYM2, ZMYND11, ZNF12, ZNF124, ZNF146, ZNF148, ZNF24, ZNF252P, ZNF253, ZNF317, ZNF33B, ZNF398, ZNF41, ZNF43, ZNF493, ZNF638, ZNF644, ZNF649, ZNF652, ZNF672, ZWILCH, ZYG11B

Contra-regulated (Count = 30)

AFG3L2, AKIRIN2, ALG13, BBX, CALR, DHFR, EGFR, FMNL2, GNAQ, HMBOX1, ILRUN, KLHL24, KMT2C, LOC202181, MALAT1, MCPH1, MED13L, NUP50, RSBN1, SFSWAP, SMG7, SREK1IP1, STAT3, TCAF1, TPM1, TTC3, UBE2G2, VCAN, WASHC1, ZNF160.

Left-sided colitis ∩ CAD

Contra-regulated (Count = 7)

DNAJC10, GPCPD1, JAK2, MYOCD, PKM, RDH5, RRM2.

Left-sided colitis ∩ Pancolitis ∩ CAD

Common Up-regulation (Count = 15)

AMOTL2, BTN3A1, CAV1, CKLF, GABBR1, MSI2, OSBPL8, PALLD, PMEPA1, RASA4, RORA, SPATS2, SSR1, TCIRG1, TXNDC15.

Common Down-regulation (Count = 57)

ABCB11, ADH6, ALDH18A1, ANKH, BSG, CA12, CDKN2B, CHP1, CNTN4, DPP10, DYRK2, EDIL3, ELAVL2, ENTPD5, EXPH5, FAM13A, FMO5, GLS, GSTM4, HADHA, HAVCR1, HHLA2, HMGCR, MAP7D2, MARCKS, MIER3, NBEAL1, NDRG2, NR5A2, OCLN, P2RY1, PAQR5, PDK3, PPID, PPP2R3A, PRKG2, PTP4A1, RMND5A, RPS6KA6, RRAS2, SEMA6A, SEMA6D, SLC16A1, SLC19A3, SLC25A33, SLC38A4, SLC4A4, SLC9A2, SUCLG2, SYNE2, TMEM38B, TRAK2, UGT1A8 (includes others), USP30, VAV3, WDR78, ZBTB7C.

Contra-regulated (Count = 20)

ABHD2, ADAM9, ANP32E, AP1S3, ASPH, BHLHE40, CALU, CBFB, DPY19L1, ECT2, FNDC3B, GLYR1, MAGI1, PDP1, RAB23, SEC24A, SKIL, SLC39A6, STAT1, TPM4.

DEGs found only in CAD.

Up-regulated (Count = 151)

ADAM33, ADAMTSL1, AFDN-DT, AGO4, ALOX15B, ANAPC16, APPBP2, ASB8, ATG16L2, BAIAP2-DT, BNIP3L, BRAP, BRD7, BRI3, BTBD18, CC2D1A, CCDC183, CCDC191, CDC42BPA, CDK10, CDRT4, CEP57, CHD4, CHDH, CMTM8, CPPED1, CRACR2B, CTSS, CYTH3, DHFR2, DNAJC21, DNAJC4, DNMT3A, DVL2, EWSR1, FAM168A, FBXL16, FRG1HP, GALNT5, GAS6, GATAD2B, GKAP1, GMDS-DT, GPALPP1, H1-10, HLA-F-AS1, HOXA6, IGF2BP2, ILF3, INSR, IQSEC1, KIF26A, KLF13, LENG8, LIN7B, LINC00339, LINC00899, LINC00937, LINC01002, LINC01949, LINC02256, LOC101927151, LOC101928143, LOC105379655, LRRK1, LRRN4, LTB4R, MAP3K3, MEGF6, MEIOC, MEX3D, MINDY1, MIR29B2CHG, MKNK2, MORN3, MPHOSPH8, MXD4, NATD1, NFAT5, NIT1, NOL3, NPIPA1 (includes others), NSL1, OIP5-AS1, ORAI3, P3H4, PARVA, PAXIP1-AS2, PCGF2, PDE4A, PDGFA, PFKFB4, PHF20, PIAS1, PIK3C3, PITPNA-AS1, PKD1P1, PKD1P6, PLD6, POGLUT1, POLR2J4, PPIG, PPP1R37, PPP1R3E, PRDM2, PRR14L, PTCD1, RAB26, RAD51-AS1, RBBP6, RCN3, RGS8, RPL23AP32, RPS10P2, RSF1, SDAD1, SLC22A3, SNHG7, SREK1, SRPK2, SUGP2, SUN1, TCP11L2, TGOLN2, THAP6, THOC2, THRA, TIAM2, TMEM129, TMEM43, TRAF3IP2, TRIM73/TRIM74, TRMT10B, TSNAX, TSPAN14, TTC9C, UBE2O, UBN1, VPS13D, WNK4, XRCC2, ZC3H6, ZCRB1, ZFHX3, ZNF134, ZNF254, ZNF329, ZNF417/ZNF587, ZNF467, ZNF688, ZNRF1.

Down-regulated (Count = 368)

ABCE1, ACTR1A, ADGRL3, ADIPOR2, ADORA2B, ADPGK, AGO3, AGPAT3, AKAP10, ANGEL2, ANKRD13C, ANLN, AP2B1, AP2M1, ARHGDIA, ARL8B, ASB7, ATAD2, ATP11B, ATP1B1, ATP6V0A2, ATP6V1D, ATXN7, B4GALT6, BARD1, BAZ2A, BORA, C12orf29, C12orf4, C16orf72, C1orf112, C1orf116, C4orf46, CAPZB, CAST, CCNA2, CCNB1, CCNYL1, CDC6, CDCA2, CDK1, CDK11A, CDT1, CEACAM1, CENPA, CENPH, CENPW, CEP120, CEP76, CHEK1, CHMP2B, CHORDC1, CLCC1, CLCN3, CLK4, CNN3, CNPPD1, COBLL1, COG5, CORO1C, CPEB2, CPSF6, CSE1L, CTPS1, DAGLB, DARS2, DCAF15, DDA1, DDI2, DDX11, DDX18, DDX54, DERL1, DHCR7, DHRS9, DKC1, DLG3, DNAJA1, DNAJB4, DNAJC1, DNAJC5, DNM1L, DSCC1, DST, DUSP3, E2F3, ECE1, ECHDC1, EEF1AKNMT, EGLN1, EHD4, EIF2S1, EIF4E2, ENTPD7, EPB41L2, EPPK1, EPS8, ERAP1, ERCC8, EXO1, FAM118B, FAM83D, FARSA, FARSB, FASTKD2, FBXO22, FDPS, FEM1B, FEN1, FNTB, FOSL2, FRS2, FUT4, G2E3, G6PC3, GALK2, GK, GK3P, GNAI3, GNB1, GOSR2, GPATCH11, GPRC5A, GPT2, GRK2, GTPBP4, GYG1, HDAC8, HEATR1, HELLS, HHIP, HINT3, HNRNPA3, HNRNPF, HUS1, ID1, IDE, IDI1, IER3IP1, IMPAD1, IPO7, IQGAP3, ITGB6, JAG1, KCTD10, KDM7A, KIF23, KIF2A, KIF2C, KLHL7, KMT2D, KPNA2, KRT18, LGALS8, LGR4, LIG3, LINS1, LMBRD2, LONP2, LPAR1, LRRC58, LRRC59, LRSAM1, MACROH2A2, MAN1A2, MAP2K4, MAPKAPK3, MARCHF7, MARK2, MCM10, MCM7, MCM8, MCMBP, METTL15, MFSD9, MGAT2, MKI67, MKLN1, MLLT10, MMAA, MOB4, MREG, MRPL42, MRPL44, MRPS16, MTFR1, MTPN, MUC13, MYO1E, NADK2, NAPG, NCBP1, NCBP2, NCOA3, NDC1, NDE1, NDFIP2, NDUFA9, NEDD1, NFE2L3, NIBAN2, NIN, NOL11, NUDCD2, NUDT4B, NUP88, NUP98, NUS1, NUS1P3, ODC1, OGFOD1, OSGIN2, PAICS, PAK2, PCYT1A, PDE12, PDE4D, PDIA6, PDS5A, PDSS1, PLEK2, PLK4, PNO1, PNP, PNPT1, POLE2, POMGNT1, POT1, PPHLN1, PPIL1, PRC1, PREPL, PRNP, PRPF38A, PRR14, PRRC1, PSMD1, PSMD11, PSMD12, PTPN21, PVR, RAB10, RAB27A, RABL3, RAD18, RALGPS2, RAN, RANBP1, RANGAP1, RAPH1, RBBP9, RCC1, RFFL, RFK, RGPD4 (includes others), RNA45SN5, RNF114, RNF38, RPE, RPL27A, RRS1, RSAD2, RSPH10B/RSPH10B2, SAP30L, SDE2, SEC23IP, SEH1L, SEL1L, SELENOI, SEPSECS, SEPTIN8, SERPINB8, SFN, SGMS2, SH3GLB2, SHMT1, SLC11A2, SLC30A1, SLC33A1, SLC41A2, SLC4A2, SLC7A6, SLCO2B1, SMC2, SMC4, SMPD1, SMURF1, SNIP1, SNX14, SPEN, SQOR, SRR, SRSF2, SSX2IP, STAM2, STK17A, STOML2, STRN, SUMO3, SURF4, SUV39H2, SYNCRIP, SYNJ1, TAB3, TANK,

TBCD, TCP1, TDP1, TFDP1, TGFBR1, THADA, THUMPD3, TIMM10B, TM9SF1, TM9SF4, TMBIM6, TMED5, TMED7, TMEM170A, TMEM19, TMEM265, TMEM50B, TNFRSF10B, TOMM70, TPX2, TRIQK, TSR1, TUBB, TXLNG, UBA1, UBA6, UBE2J1, UBE2L3, UBE2N, UBE2T, UBR1, UBTF, UFM1, USP24, USP25, UTP14A, UTP15, UTP18, UTP4, VANGL1, VRK1, VTI1A, WDHD1, WDR48, WDR5, WDR76, WDR77, WDR89, XPO5, XRCC5, YAP1, YKT6, YTHDC2, ZBTB8A, ZDHHC3, ZDHHC5, ZER1, ZFR, ZNF322, ZNF330, ZNF451, ZNF621, ZWINT.

DEGs found only in Pancolitis.

Up-regulated (Count = 676)

ABCG5, ABI2, ACAP1, ACKR3, ACKR4, ACTN1, ADAM8, ADAMTS1, ADAMTS2, ADAMTS5, ADCY7, ADGRA2, ADPRH, AEBP1, AFAP1L1, AFAP1L2, AGRN, AGT, AGTRAP, AHI1, AHNAK2, AKT3, ALAS2, ALDH1L2, ALDOB, ALOX5, ANGPTL2, ANKDD1A, ANKRD12, ANKRD36, ANKRD36BP2, ANKRD44, ANOS1, ANTXR1, ANXA10, AOPEP, APBA2, APCDD1, APLNR, APOBEC1, APOLD1, ARFGAP1, ARHGAP24, ARHGAP28, ARHGAP32, ARHGAP4, ARHGAP6, ARHGAP9, ARHGEF6, ARID3A, ARL3, ARL6, ARSA, ASXL1, ATF3, ATOX1, ATP8B2, BAG5, BAX, BCL2A1, BDNF, BHLHE22, BICC1, BICD1, BICD2, BISPR, BMP2, BNIP2, BOC, BOK, BTN3A2, C11orf96, C1GALT1, C1QTNF5, C20orf194, CACNA2D1, CALHM6, CARD8-AS1, CARMN, CAVIN1, CAVIN2, CAVIN3, CCDC167, CCDC88A, CCL11, CCM2L, CCN1, CCNI, CCNO, CCP110, CD109, CD1D, CD68, CD82, CD93, CDC42SE1, CDH11, CDK14, CDKN1C, CELF2, CELSR1, CEP164, CEP170, CEP19, CEP85L, CHAC1, CHRDL2, CHROMR, CHST3, CHSY1, CLCN4, CLDN11, CLDN2, CLEC11A, CLEC7A, CLIC3, CLIP4, CLMP, COL12A1, COL15A1, COL16A1, COL18A1, COL1A1, COL1A2, COL23A1, COL27A1, COL3A1, COL4A2, COL5A2, COL5A3, COL6A1, COL7A1, COL8A1, COL9A2, COPG2, COX7A1, CPLX1, CPT1B, CPXM1, CREBZF, CRISPLD1, CRNDE, CSRP2, CST7, CTNNB1, CX3CL1, CXCL12, CXorf38, CYBC1, CYGB, CYP39A1, CYP7B1, CYSLTR1, CYTH4, DBN1, DCHS1, DDB2, DEF6, DENND5A, DEPP1, DGKZ, DKK3, DLGAP4, DNAAF4, DNM3, DNM3OS, DOCK4, DOCK8, DPEP2, DPYSL3, DSEL, DTX3, DUSP14, DUSP4, DZIP1, EBF1, EDNRA, EFEMP2, EFHC1, EFS, EGFL6, EGR1, EGR2, EGR3, EHD2, ELMO1, EMCN, EMILIN1, EML1, ENO2, ENTPD3, EPHX4, EPS8L1, ERG, ERLEC1, ERO1B, ERP27, ESAM, ETV7, EVL, EXOC3L4, F2RL2, FAM126A, FAM155A, FAM160B1, FAM171B, FAM20A, FAM20C, FAM219A, FAM89A, FAP, FBLN1, FBLN2, FBN1, FBXW7, FER1L4, FES, FGD2, FGD3, FGFR1OP2, FGR, FIBIN, FILIP1, FKBP14, FKBP7, FLRT2, FLT3LG, FOXF1, FRY, FTX, FUT11, FZD2, GABRE, GALNT18, GAS1, GCLM, GIMAP1, GIMAP7, GJC1, GLI3, GLMP, GLT8D2, GNAI2, GNG11, GPR155, GPRC5B, GRAMD2A, GRIN3A, GRK5, GSDME, GTSE1, GUCY1A2, GUK1, H2AC11, H2AC18/H2AC19, H2BC4, HCP5, HCST, HDAC9, HECTD1, HECTD2, HES1, HIP1, HKDC1, HLA-F, HOOK3, HPSE, HSH2D, HSPA12B, HSPA6, HSPB11, HSPG2, HTRA1, ICOS, ID2, IDH2, IFFO1, IFI6, IFIT3, IFIT5, IFNAR2, IGDCC4, IGSF6, IKZF4, IL10RA, IL15, IL18, IL18R1, IL26, IL27RA, INMT, INPP4A, INPP4B, INPP5D, IPW, IRF1-AS1, ISG15, ITGA8, ITGAV, ITGB2-AS1, JAK3, JAM2, JCAD, KATNAL1, KCNE4, KCNJ8, KCNK6, KCNT2, KCTD11, KDR, KIAA0930, KIRREL1, KISS1R, KLC2, KLHL3, KLK10, KRT7, KSR1, LAIR2, LAMA4, LAMA5, LAMB2, LARP6, LCAT, LEF1, LEPR, LHFPL6, LHX6, LIF, LILRA5, LILRB1, LILRB2, LIMCH1, LINC00467, LINC01503, LINC01943, LMCD1, LMNB1, LMNTD2-AS1, LOC100506123, LOC100507516, LOC100996740, LOC101928000, LOC102606465, LOC284454, LOC728392, LOXL1-AS1, LOXL2, LPL, LRCH2, LRG1, LRRC8E, LRRFIP1, LRRK2, LRRN4CL, LSAMP, LTBP2, LUM, LY9, MAGED4/MAGED4B, MAP3K6, MAP4K4, MAP7D1, MCC, MDK, MEG3, MEIS2, MELTF, MIA, MICAL1, MICALL1, MICU3, mir-142, MIR100HG, MIR210HG, MITF, MMP1, MMP2, MMRN2, MN1, MORC4, MPDZ, MRPL52, MSANTD3, MSC-AS1, MSL1, MSRB3, MTMR9LP, MXRA5, MYO5A, NAIP, NAP1L5, NBEAL2, NDST2, NEBL, NEXN, NFATC2, NHSL2, NIBAN1, NME5, NOD2, NOTCH3, NR2F1, NR4A2, NRN1, NRROS, NRXN3, NUAK1, NUB1, NUP210, OLFML2B, OR7E37P, OSMR, OSTM1, P2RX7, P2RY14, PABPC1L, PAOX, PARVB, PBX3, PCDH18, PCED1B, PCOLCE, PCSK9, PDE10A, PDGFRB, PDK1, PDLIM4, PDPN, PER1, PEX13, PHACTR2, PHF21A, PHLDB2, PIEZO1, PITX1, PKD2, PKIA, PLAAT3, PLCB1, PLEKHG2, PLEKHH2, PLEKHS1, PLOD1, PLPP5, PLXNA1, PLXNA3, PLXND1, PML, PNISR, POU2F2, PPM1M, PPP1R18, PPP2R5C, PRKD1, PROCR, PRR16, PRUNE2, PRXL2C, PSENEN, PTGDS, PTP4A3, PTPN13, PTPN14, PTPRCAP, PTPRM, PVT1, PXDC1, PXDN, QKI, QSOX1, RAB34, RAB39B, RAB43, RAI2, RAP2C, RAPGEF3, RAPGEF4, RASGRF2, RASL12, RASSF1, RBIS, RBMS1, RBMS3, RBP7, REL, RERG, RFLNB, RFX7, RGS14, RGS16, RGS19, RHBDF2, RHOBTB1, RHOQ, RIPOR1, RNF145, RNF166, ROBO4, ROR1, RPL39L, RPS24, RPS27L, RSPO3, RTEL1, RUFY2, RUNX1T1, RUNX3, RUSC1-AS1, RWDD2A, S100A13, S100A2, S100A4, S100A6, S100B, S1PR3, SAMD9, SAMHD1, SDC3, SDK1, SEC16B, SEC31A, SELENON, SELENOO, SEMG1, SEPTIN9, SERPINI1, SF3A2, SGCD, SGO2, SH2D3C, SH3PXD2A-AS1, SH3PXD2B, SH3RF3, SHANK3, SHE, SIRPA, SLAMF8, SLC16A4, SLC16A6, SLC17A9, SLC24A3, SLC2A6, SLC38A7, SLC45A4, SLC4A11, SLCO1B3, SLCO2A1, SLFN12, SLFN13, SMARCA1, SNHG12, SNHG9, SNN, SNRNP200, SNTB2, SOBP, SPAG4, SPARC, SPINK4, SPOP, SRM, SRPX2, SSR4, STAT2, STAT5A, STEAP4, STK3, STMN3, STON1, STOX2, STX11, STXBP1, STXBP6, SULF2, SUN2, SYT11, TACC1, TAF10, TAF4B, TASOR, TBC1D10C, TBC1D16, TCEAL7, TCF4, TFAP2C, TFE3, TFF1, TFPI, TGFB1I1, TGS1, THBS2, THEM4, THSD7A, THY1, TIE1, TIMP2, TIMP3, TLNRD1, TM4SF18, TMC8, TMEFF2, TMEM106A, TMEM231, TMEM273, TMEM45A, TMF1, TMPRSS3,

TMTC2, TNC, TNFAIP2, TNFRSF25, TNFRSF4, TNFSF15, TNFSF9, TNK2, TNS1, TOR1AIP2, TOX2, TP53INP1, TP73-AS1, TPM2, TPST1, TRAF3IP3, TRAM2, TRIM7, TRNP1, TRPC1, TSHZ3, TSPAN11, TSPAN2, TSPAN5, TTBK2, TUBA1A, TWIST1, TWIST2, TYK2, UBASH3B, UBE2E2, UBLCP1, UCP2, UROS, USP48, VAMP1, VASN, VEGFC, VGLL3, VPS13C, VPS9D1, VSIR, WASF1, WDR19, WDR54, WFS1, WNT5A, WWC1, WWC3, WWTR1, XAF1, XRN1, YPEL2, ZBTB4, ZBTB46, ZBTB47, ZC3HAV1, ZCCHC24, ZEB2, ZFP36L1, ZFYVE28, ZNF25, ZNF503, ZNF512B, ZNF521, ZNF532, ZNF536, ZSWIM8.

Down-regulated (Count = 241)

ACSM3, ACTB, ACVR1C, ADD3, AGO1, AGPAT5, ALDH3A2, ALG14, ANO10, ANO5, APPL2, ARFRP1, ARNTL, ARSD, ATP5MC3, ATP6V0D2, ATP9A, ATPAF1, B3GNT2, BBIP1, BEST2, BLOC1S5, BRCC3, BTF3L4, C1orf43, C8orf44-SGK3/SGK3, CAMK2N1, CARS1, CASD1, CASP6, CAT, CBFA2T2, CHKA, CMAHP, CMTM6, COBL, COX20, CPA6, CPM, CPT1A, CRK, CRYZL1, CTH, CYB5B, CYP2J2, CYP4F12, DGKH, DHX40, DNAJA3, DPP4, DRAIC, DSP, DSTYK, DUSP16, ECH1, EDEM3, EIF2S3, EIF3CL, EIF4EBP2, ELF1, EMC7, EPB41L3, EPB41L5, EPHA4, EPHB2, ERBB3, ERMP1, FAM83B, FAS, FH, FOXO3, FOXP1, FRZB, FSIP1, FUT6, GALNT12, GATD3A/GATD3B, GAU1, GBA2, GLIPR2, GLUL, GMCL2, GNG4, GNPTAB, GOLIM4, GOT1, GPBP1L1, GPHN, GPR15, GPX3, GRAMD2B, GSR, GTF2A2, HADH, HAPLN1, HES5, HIBCH, HMGCL, HOTTIP, IDH3B, IFT57, IGF1R, IL13RA1, IRF2BP2, KCTD12, KIAA1324L, KIAA2026, KLF4, LAMP1, LGR5, LIMD1, LITAFD, LNPK, LOC100190986, LOC100287497, LOC105379173, LPCAT3, MACROH2A1, MAVS, MBOAT2, MCOLN2, MDM4, METTL16, MFSD4A, MFSD6, MICALCL, MIR570HG, MRPL35, MRTFB, MSH2, MUC12, MYO1A, NDUFA10, NEK3, NEK9, NEO1, NEPRO, NF1, NKTR, NOTCH2NLA/NOTCH2NLB, NREP, NSD3, NT5E, NTRK2, NXPE1, P2RX4, PANX1, PAPOLG, PAPSS2, PAXBP1, PDCD4, PDCD6IP, PDE3B, PGM1, PID1, PLCD3, PLPBP, PNLIPRP2, POGK, PPA2, PPIF, PPP2R5E, PRPF40A, PRR5L, PRSS12, PSG3, PTER, PTPN3, RAB30-DT, RAB4A, RABGAP1L, RB1, RBM39, RDX, RHOA, RPP14, RPS23, RREB1, RSPH3, RSRP1, RYBP, SCAF4, SEMA3C, SERINC3, SF1, SFPQ, SH3BGRL2, SIAE, SKAP2, SLC17A5, SLC25A6, SLC6A19, SLC7A8, SLC9A3, SMAD3, SMG1, SNRPA1, SOCS2, SORL1, SPPL2A, SRGAP1, SRSF4, STBD1, STXBP5, SYNJ2BP, SYTL5, TCAIM, TCTE3, TDP2, TLR4, TMED2, TMEM230, TMEM9B, TMTC4, TOB1, TRIB1, TRIM2, TRPM6, TSPAN6, UBE2I, UQCRC2, VIL1, VIPAS39, VTI1B, WLS, YY1, ZBTB10, ZKSCAN1, ZNF207, ZNF264, ZNF292, ZNF320, ZNF397, ZNF431, ZNF548, ZNF551, ZNF675, ZNF702P, ZNF814, ZNF93, ZRANB2.

DEGs found only in Left-sided Colitis.

Up-regulated (Count = 108)

ABCA12, ANGPTL4, ANO6, ANXA3, APOL3, AQP3, AQP9, ARHGDIB, ATM, ATP10D, BLVRA, CALCRL, CD274, CD40, CEP112, CEP55, CFL2, CFLAR, CHST11, CHST12, CPNE5, CRELD2, CRIP2, CXCL5, CXCL9, CXCR6, CYB5R2, DUSP7, EMB, ENPP2, ERRFI1, FAIM2, FAM49A, FLI1, GBP4, GIMAP4, GIMAP5, GLRX, GOLT1B, GSAP, HHEX, HIF1A, HLA-DRB6, HSPA13, IGKV1-17, IGLJ3, IGLV3-25, IL13RA2, IL17A, IL21R, IL23A, IL2RA, KAZN, LAMC2, LINC00869, LYSMD2, LYZ, MCFD2, MMP12, MTHFD1L, MTHFD2, NCF2, NKG7, NLRP7, NQO2, NT5DC2, PASK, PCSK1, PDIA4, PDLIM3, PGM3, PHF19, PHTF1, PIR, PLAU, PRF1, PRKCH, PSME2, S100A7, SDR16C5, SELL, SEPTIN1, SERPINB5, SETD7, SFMBT2, SH2D1A, SIGLEC10, SIRPG, SLC2A14, SLC38A5, SLC5A1, SNX10, SP140, TBXAS1, TENT5C, TIFA, TMC5, TMEM173, TMEM263, TNFRSF9, TNFSF13, TNFSF13B, TRIM69, TTC9, VSNL1, WDR44, XBP1, ZHX2.

Down-regulated (Count = 184)

ABAT, ABCA8, ACADS, ACVR2A, AKAP9, ALPI, ANKRD9, ANPEP, AP3S2, ASAP3, ASPA, ATP23, ATP5PB, AUH, AVIL, B3GNT8, BEST4, C1orf115, C2orf88, C5orf63, C7orf31, CCNJL, CDC14A, CDK3, CDKN2B-AS1, CFD, CHAD, CHPT1, CIPC, CLCN2, CLDN15, CNGA1, CNIH4, CNKSR3, CNTN3, CPEB3, CPT2, CROT, CRYL1, CTSA, CYCS, CYP27A1, CYP2B6, DDAH2, DEFB1, DMAC2L, EDN1, ENPP1, EPB41L1, FAM162A, FCGRT, FGFR3, FMO4, FOXD2, FTH1, GATA6-AS1, GDPD2, GJB1, GLB1L2, GLTP, GNA11, GRAMD1C, GUCA2B, GULP1, HOXA3, HOXD4, HSD17B11, HSD17B2, ID2-AS1, IGSF9, IPO5P1, ITPKA, KCNG1, KCNJ2, KCNK5, KLB, LAMA1, LANCL3, LDHD, LEAP2, LINC01224, LINC02535, LOC101929340, LOC102724156, LOC105369890, MAGI2, 43892, MAST2, MEP1A, MESP1, METTL7B, MGAT4B, MOCS1, MPC2, MROCKI, MST1L, MT1E, MT1F, MT1G, MT1H, MT1HL1, MT1M, MT1X, MYO1D, NAALADL1, NAT8B, NBPF1 (includes others), NEURL1B, NLN, NPY, NR1H4, NRARP, NUAK2, NVL, OAF, OPN3, PCK2, PDZD3, PHYH, PIGZ, PKDCC, PKIB, PLA2G12A, PLXDC2, PLXNA2, PMM1, PNPLA4, PPP1R36, PRAG1, PRAP1, PRR15, PRR26, RAB40B, RALGPS1, RAVER2, RBKS, SCN9A, SERF1A/SERF1B, SERPINA6, SGK2, SH3RF1, SLC20A2, SLC22A23, SLC22A4, SLC22A5, SLC23A1, SLC23A3, SLC25A23, SLC25A25-AS1, SLC25A34, SLC30A10, SLC35G1, SLC3A1, SLC51A, SMIM32, SOWAHA, SPINK2, SPINT1, SPINT1-AS1, STAP2, SULT1A1, SULT1A2, SVOPL, SYT17, TEF, TLE2, TLN2, TM4SF5, TMEM59, TP53INP2, TP53TG1, TRIM13, TRIM36, TSTD1, TUBAL3, UNC5B, VDR, VIPR1, VSIG10, WSCD1, ZDHHC23, ZFP3, ZNF575, ZNRF3.

Appendix B. Gene lists for gene ontology (GO) terms enriched at the intersection of Pancolitis ∩ Left-sided colitis.

Appendix B. These gene lists compliment the GO term bar graph depicted in **Figure 6** that summarize the enrichment of GO terms by DEGs at the intersection of Pancolitis ∩ Left-sided colitis. The degree of enrichment was reported as the odds ratio (OR), where I_A = # DEGs annotated with the GO term, I_B = # background genes annotated with the GO term, and OR = (I_A/size of DEG list) / (I_B/size of background gene list).

GO.ID	GO. Term	I_B	I_A	List of DEGs Annotated with GO Term	*p*	OR
GO:0060334	Regulation of IFN-gamma mediated signaling pathways	22	7	*IFNG, NLRC5, PARP14, PARP9, PPARG, SOCS1, SOCS3.*	9.7E-06	8.6
GO:0061844	Antimicrobial humoral immune response mediated by AMP	55	13	*CXCL1, CXCL11, CXCL2, CXCL3, CXCL6, CXCL8, DEFA5, DEFA6, PF4, REG1A, REG1B, REG3A, S100A9.*	7.5E-08	6.4
GO:0006953	Acute-phase response	45	10	*APOL2, ASS1, CEBPB, IL1B, REG3A, SAA2, SAA4, SERPINA1, SERPINA3, UGT1A1.*	4.4E-06	6.0
GO:0070098	Chemokine-mediated signaling pathway	68	12	*CCL20, CCL24, CXCL1, CXCL11, CXCL2, CXCL3, CXCL6, CXCL8, CXCR2, PADI2, PF4, ROBO1.*	6.5E-06	4.8
GO:0030593	Neutrophil chemotaxis	93	16	*CCL20, CCL24, CXCL1, CXCL11, CXCL2, CXCL3, CXCL6, CXCL8, CXCR2, IL1B, IL1RN, PDE4B, PF4, RAC2, S100A8, S100A9.*	2.7E-07	4.6
GO:0071222	Cellular response to lipopolysaccharide	171	23	*ASS1, CARD16, CARD8, CASP1, CD55, CEBPB, CXCL1, CXCL6, CXCL8, DEFA5, IL1B, IL1RN, LCN2, LYN, NOS2, PDE4B, PF4, PPARGC1A, PTAFR, PTPN22, SGMS1, TNFRSF1B, ZC3H12A.*	3.6E-06	3.6
GO:0051607	Defense response to virus	198	24	*APOBEC3B, APOBEC3G, BIRC3, BNIP3, DDIT4, DMBT1, GBP1, IFITM1, IFITM2, IFITM3, IFNG, IL12RB1, IL1B, IL33, IRF1, ISG20, MICB, NLRC5, PARP9, PMAIP1, SEC14L1, SPON2, TRIM22, ZC3H12A.*	7.7E-06	3.3
GO:0006954	Inflammatory response	652	79	*ABCC1, ACKR1, ACVR1, ADA, ADM, ANXA1, APOL2, ASS1, BACE2, BIRC3, C2CD4A, C3, CAMK1D, CASP4, CCL20, CCL24, CCN4, CD44, CDH5, CEBPB, CHI3L1, CHST2, CIITA, CXCL1, CXCL11, CXCL2, CXCL3, CXCL6, CXCL8, CXCR2, DUOXA2, DUSP10, EPHA2, EPHX2, F2R, F3, FFAR2, GAL, GBP5, IDO1, IFNG, IL1B, IL1R2, IL1RN, IL33, ITGAL, LYN, MEP1B, MMP3, MMP9, NAPEPLD, NFKBIZ, PF4, PIK3AP1, PPARG, PROK2, PTAFR, PTGDR, RASGRP1, REG3A, S100A8, S100A9, SAA2, SAA4, SELP, SERPINA1, SERPINA3, SGMS1, SMPDL3B, SOCS3, TEK,*	3.2E-10	3.3

GO.ID	GO. Term	I_B	I_A	List of DEGs Annotated with GO Term	*p*	OR
				TGM2, THEMIS2, TIMP1, TNFRSF1B, TNIP3, UGT1A1, VNN1, ZC3H12A.		
GO:0045087	Innate immune response	724	74	*ANXA1, APOBEC3B, APOBEC3G, APOL1, ASS1, BIRC3, C2, C3, C4BPA, C4BPB, CADM1, CASP1, CASP4, CCL20, CCL24, CD44, CD55, CFB, CFI, CIITA, CLDN1, CLEC4A, CR1, DEFA5, DMBT1, DUSP10, FCN1, FFAR2, GBP1, GBP2, GBP5, GZMB, IFITM1, IFITM2, IFITM3, IFNG, IGHG3, IL12RB1, IRAK3, IRF1, ISG20, KYNU, LAG3, LCN2, LRP8, LYN, MICB, MR1, MUC1, NCF1, NLRC5, NOS2, PARP14, PARP9, PPARG, PRDM1, PSMB9, PTAFR, PTPN22, RASGRP1, S100A8, S100A9, SEC14L1, SERPING1, SHFL, SLPI, SMPDL3B, SOCS1, SOCS3, SPON2, TRIM22, TRIM29, VNN1, ZBP1.*	6.6E-07	2.8
GO:0043312	Neutrophil degranulation	458	42	*ACPP, ATP11A, C3, CD44, CD55, CEACAM6, CHI3L1, COTL1, CR1, CXCL1, CXCR2, DEGS1, DOK3, FCN1, ITGAL, ITGAX, LCN2, LPCAT1, METTL7A, MMP9, MNDA, OLFM4, PADI2, PECAM1, PLAUR, PRDX4, PRDX6, PTAFR, RAB31, S100A11, S100A8, S100A9, S100P, SERPINA1, SERPINA3, SLC2A3, SLPI, STOM, TCN1, TMC6, TNFRSF1B, VNN1.*	5.9E-08	2.5

Appendix C. Gene lists for gene ontology (GO) terms enriched at the intersection of Pancolitis ∩ CAD.

Appendix C. These gene lists compliment the GO term bar graph depicted in **Figure 6** that summarize the enrichment of GO terms by DEGs at the intersection of Pancolitis ∩ CAD. The degree of enrichment was reported as the odds ratio (OR), where I_A = # DEGs annotated with the GO term, I_B = # background genes annotated with the GO term, and OR = (I_A/size of DEG list) / (I_B/size of background gene list).

GO.ID	GO. Term	I_B	I_A	List of DEGs Annotated with GO Term	*p*	OR
GO:0030033	Microvillus assembly	15	7	*EZR, PLD1, RAP2A, RAPGEF2, RAPGEF6, STK26, TNIK.*	4.6E-05	6.3
GO:0006893	Golgi to plasma membrane transport	61	14	*ARF1, ARFGEF2, CNST, EXOC4, EXOC5, EXOC6, GOLGA7, GOPC, KIF13A, LLGL1, RABEP1, SPTBN1, TRIM23, VAMP3.*	0.00012	3.1
GO:0031532	Actin cytoskeleton reorganization	74	16	*ARAP1, CDC42BPB, CTTN, CXADR, DAPK3, EZR, FARP2, GAB1, GSN, MINK1, NOTCH2, PAK1, PTPN1, RAP2A, SHC1, TNIK.*	8.4E-05	2.9
GO:0019058	Viral life cycle	304	48	*ATG16L1, ATG5, BANF1, CD46, CD74, CDC42, CHMP1B, CXADR, DDX3X, EEA1, EFNB2, EGFR, F11R, GSN, HACD3, HSP90AB1, HTATSF1, ITCH, ITGB1, ITGB5, KPNA1, KPNA6, NECTIN2, NFIA, NUCKS1, NUP160, NUP50, NUP58, P4HB, PARP10, PCSK5, PKN2, PROX1, RAB1A, RAB5A, RANBP2, ROCK2, RPS27A, SCARB2, SMC3, SRPK1, TFRC, TMPRSS2, TPR, TRIM59, TRIM8, VTA1, WWP2.*	0.00005	2.1
GO:0016032	Viral process	779	109	*AP1G1, AP2A1, ARF1, ATG16L1, ATG5, B2M, BANF1, BCL2L1, BRD4, BUB1, CASP8, CBX5, CCNT2, CD46, CD74, CDC42, CDK13, CFL1, CHMP1B, CREB1, CXADR, DDX3X, DHX9, DLG1, EEA1, EFNB2, EGFR, EIF4A2, EP300, F11R, FKBP8, G3BP1, G3BP2, GSN, HACD3, HIPK2, HSP90AB1, HSPA8, HSPD1, HTATSF1, IKBKB, IL2RG, IL6ST, IPO5, ITCH, ITGB1, ITGB5, KAT2B, KCTD5, KPNA1, KPNA4, KPNA6, LIG4, MAP3K7, MAPK1, MSH6, NCKAP1, NECTIN2, NFE2L2, NFIA, NFX1, NUCKS1, NUP160, NUP50, NUP58, OGA, P4HB, PABPN1, PARP10, PCSK5, PIK3R1, PKN2, PROX1, RAB1A, RAB5A, RAB6A, RANBP2, RIPK1, RNGTT, ROCK2, RPS10, RPS27A, SCARB2, SET, SHC1, SKP2, SMC3, SP1, SRPK1, STAT3, TFRC, TMPRSS2, TP53, TPR, TRAM1, TRIM14, TRIM23, TRIM59, TRIM8, USF1, VDAC1, VPS35, VTA1, WAPL, WASF2, WWP2, YWHAB, YWHAE, ZMYND11.*	5.3E-05	1.9

GO.ID	GO. Term	I_B	I_A	List of DEGs Annotated with GO Term	*p*	OR
GO:0007265	Ras protein signal transduction	411	57	*AKAP13, ARF6, ARFGEF1, ARFGEF2, ARHGAP5, ARHGEF7, ARHGEF9, CDC42, CDC42SE2, CDK2, CFL1, CYTH1, DNMBP, EPS8L2, F2RL1, FARP2, FGD4, FGD6, G3BP1, G3BP2, GNA13, GPSM2, HACD3, ITGB1, KITLG, KRAS, MAPK14, MAPKAP1, MET, MFN2, NCKAP1, NGEF, NOTCH2, NRAS, PLD1, RAB11B, RAB12, RAB18, RAB1A, RAB24, RAB2A, RAB35, RAB5A, RAB6A, RALB, RAP2A, RAP2B, RAPGEF2, RAPGEF6, RASA2, RHOB, RIT1, ROCK2, SHC1, SOS2, TP53, WASF2.*	3.1E-06	1.9
GO:0030335	Positive regulation of cell migration	445	56	*ADAM10, AGO2, AKIRIN1, APC, ARF6, ARHGEF7, ATP7A, ATP8A1, CALR, CAPN7, CARMIL1, CD74, CLASP1, CPNE3, DAB2, DAPK3, DOCK1, DOCK5, EDN3, EGFR, ELP3, F2RL1, FGFR1, GAB1, IL6R, ITGA6, ITGB1, KITLG, LAMB1, MAPK1, MAPK14, MAPRE1, MAZ, MIA3, MMP14, MYO1C, NFE2L2, NUMB, PAK1, PDGFD, PIK3R1, PLPP3, PPM1F, PPP3CA, PROX1, PTK2, RHOB, ROCK2, RTN4, RUFY3, SP1, SPAG9, STAT3, TGFBR2, THBS1, WASHC1.*	6.5E-05	1.7
GO:0006886	Intracellular protein transport	1069	133	*AGFG1, AGPS, AHCYL1, AP1G1, AP1S1, AP2A1, AP3B1, AP3D1, ARF1, ARF6, ARFIP1, CALR, CASP8, CD24, CD74, CDC40, CDH1, CHM, COG3, COPA, COPG1, CTTN, DDX39B, ERBB2, EVI5, EXOC4, FYTTD1, GLE1, GOLGA7, GRPEL2, HNRNPU, HSP90AA1, HSP90B1, HSPA4, HSPA8, HSPD1, IFT80, IPO5, IPO8, KIF13A, KIF3A, KIF5B, KIFAP3, KPNA1, KPNA4, KPNA6, LARS1, MAPK1, MAPK14, MBTPS1, MCM3AP, MFN2, MYO1C, MYO6, NAPA, NMD3, NOLC1, NUP160, NUP50, NUP58, NUTF2, NXT2, PABPN1, PAK1, PARL, PEX1, PIK3R1, POLDIP3, PPM1A, PPP1R10, PPP3CA, PRKAA1, PRKCI, PSEN1, PTPN1, PTPN11, PURA, RAB11B, RAB12, RAB18, RAB1A, RAB24, RAB2A, RAB35, RAB5A, RAB6A, RANBP2, RBM22, RHOB, RPS10, RPS27A, RUFY3, SAR1B, SCARB2, SEC23A, SEC61A1, SMG7, SNX13, SNX27, SRPRA, SRSF1, SRSF11, SRSF3, SRSF5, STAT3, STX16, STX17, STX3, STYX, SYNRG, SYTL2, TCAF1, TCF7L2, TMED4, TNPO3, TP53, TPR, TRAM1, TRIM23, TXNIP, UHMK1, UNC93B1, USO1, USP9X, VPS26C, VPS35, XPO7, YOD1, YWHAB, YWHAE, YWHAZ, ZDHHC20, ZDHHC21.*	1.3E-05	1.7
GO:0061024	Membrane organization	693	86	*ACTR2, AFG3L2, ANKFY1, AP2A1, AP3B1, AP3D1, ARF1, ARPC5, ATP2A2, ATP8A1, BANF1, BCL2L1, CALR, CASP8, CD24, CDC42, CFTR, CHMP1B, CLN8, CNTNAP2, CTSZ, CTTN, DAB2, DLG1, DNAJC11, DOCK1, EEA1, EGFR, F2RL1, FA2H, FAT4, GSN, HSP90AA1, HSPA4, HSPA8, KIF5B, KLHL12, LAPTM4B, LMAN1, MBP, MFN2, MIA3, MPP5, NAPA, NECTIN2, NOX1, PACSIN2, PAFAH1B1, PICALM, PIK3C2A, PLK1, PPP2R1A, PRKCI, PTPRD, RAB1A, RAB5A, RABEP1, REEP3, REPS2, RPS27A, RTN4, SAR1B, SCARB2, SEC22B, SEC23A, SNAP23, SPAST, SPG7, SPTBN1, STAT3, STX16, STX17, STX3, TFG, TFRC, THBS1, TMEM30A, TP53, TRIP10, USO1, VAMP3, VPS8, WASL, YWHAB, YWHAE, YWHAZ.*	5.6E-05	1.7

GO.ID	GO. Term	I_B	I_A	List of DEGs Annotated with GO Term	*p*	OR
GO:0045944	Positive regulation of transcription by RNA polymerase II	1089	115	*ACTR2, AGO2, AKNA, APP, ASXL2, ATAD2B, ATF1, ATF2, ATF5, ATF6B, ATOH1, ATRX, BACH1, BMP5, BPTF, BRD4, CASK, CCNT2, CDC5L, CDK13, CDK8, CITED2, CREB1, DDX3X, DHX9, EGFR, EHF, ELK4, EP300, EPAS1, EPC1, ERLIN1, ETV6, F2RL1, FOXA1, FOXC1, FOXJ3, FOXO1, GABPA, GABPB1, HIPK2, HNF4G, HNRNPU, IKBKB, IKZF5, IRF6, ITGA6, JUND, KAT2B, KMT2A, KMT2C, KPNA6, LMO4, MACC1, MAFG, MAML2, MAPK14, MAX, MED6, MEF2A, MEF2C, MET, MGA, MICAL2, MLX, MLXIP, MOSPD1, MYO6, MYSM1, MZF1, NCOA2, NFE2L2, NFIA, NFIB, NFIC, NIPBL, NR1D2, NRIP1, NUCKS1, PCGF5, PIK3R1, PPARA, PPP3CA, PPP3R1, PROX1, RBM14, RBMX, RIPK1, RLF, RPS27A, RXRB, SAFB, SENP1, SETX, SKI, SMAD5, SMARCA2, SMARCC1, SOX4, SP1, SP3, SS18, STAT3, SUPT16H, TAF9B, TCF7L2, THRAP3, TP53, USF1, WASL, WWP2, ZBED1, ZBTB38, ZNF148, ZNF649.*	5.6E-05	1.4

Appendix D. Comparison of Hippo pathway analyses conducted on UC-subtype DEGs.

Appendix D. Scheme of the Hippo pathway was overlaid with expression log ratios from the Left-sided colitis vs. HC datasets **(A)**, the Pancolitis vs. HC datasets **(B)**, and the CAD vs. HC datasets **(C)**. Colored molecules (red, green, grey) represent genes/proteins that appeared in the datasets. Canonical pathway analyses were completed with the IPA software. DEGs were distinguished by the combined application of FDR ($q < 0.001$) and fold change threshold ($|\log2FC| > 0.75$).

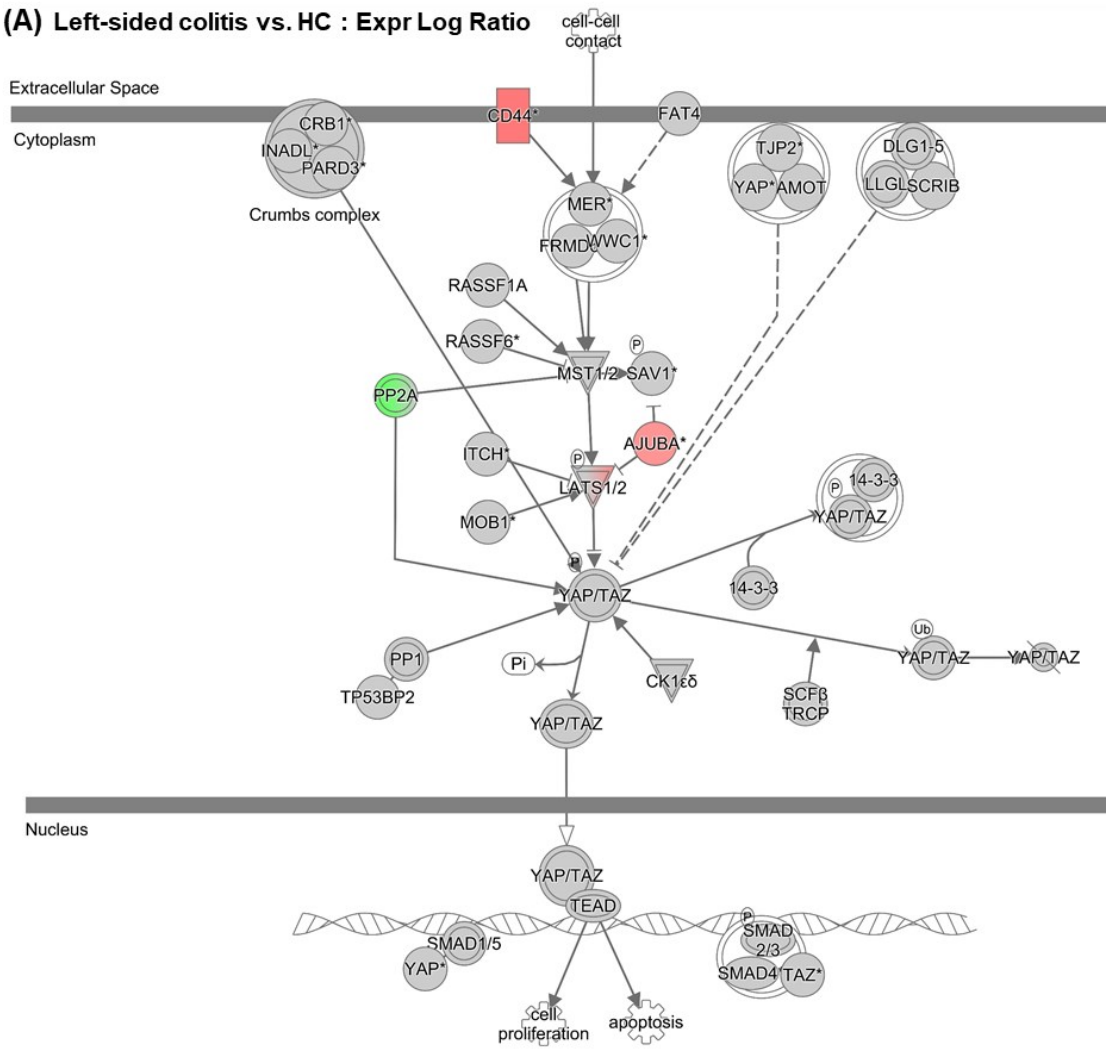
(A) Left-sided colitis vs. HC : Expr Log Ratio
cell-cell contact
Extracellular Space
Cytoplasm
CD44*
FAT4
CRB1*
INADL*
PARD3*
Crumbs complex
TJP2*
YAP*
AMOT
DLG1-5
LLGL
SCRIB
MER*
FRMD
WWC1*
RASSF1A
RASSF6*
MST1/2
SAV1*
PP2A
AJUBA*
ITCH*
LATS1/2
MOB1*
14-3-3
YAP/TAZ
PP1
TP53BP2
Pi
CK1εδ
SCFβ TRCP
Ub
YAP/TAZ
Nucleus
TEAD
SMAD1/5
YAP*
SMAD 2/3
SMAD4
TAZ*
cell proliferation
apoptosis

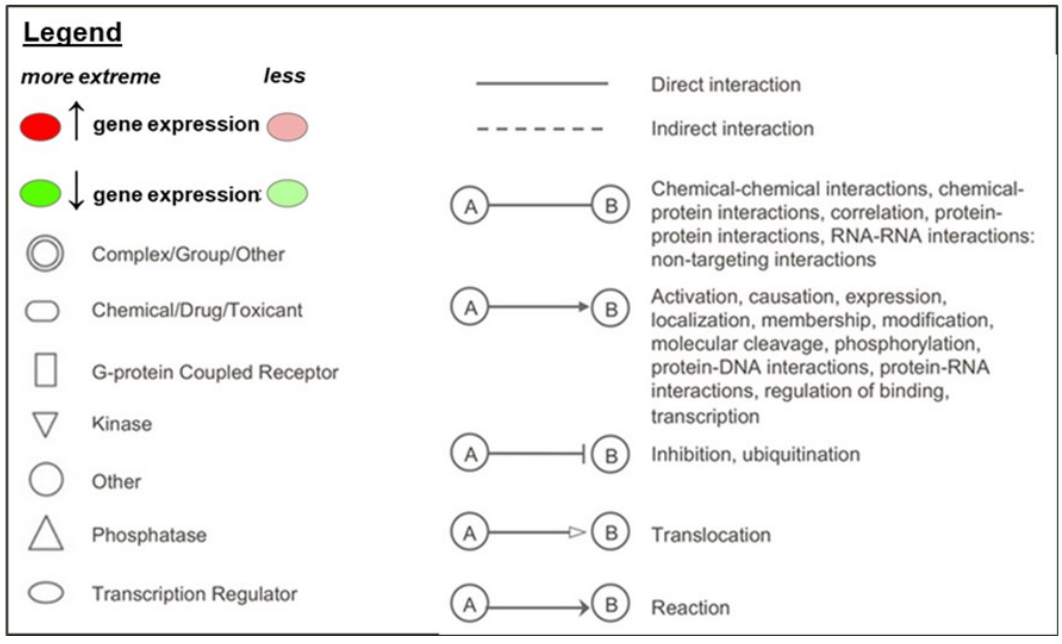
Legend
more extreme
less
gene expression
gene expression
Complex/Group/Other
Chemical/Drug/Toxicant
G-protein Coupled Receptor
Kinase
Other
Phosphatase
Transcription Regulator
Direct interaction
Indirect interaction
A
B
Chemical-chemical interactions, chemical-protein interactions, correlation, protein-protein interactions, RNA-RNA interactions: non-targeting interactions
Activation, causation, expression, localization, membership, modification, molecular cleavage, phosphorylation, protein-DNA interactions, protein-RNA interactions, regulation of binding, transcription
Inhibition, ubiquitination
Translocation
Reaction

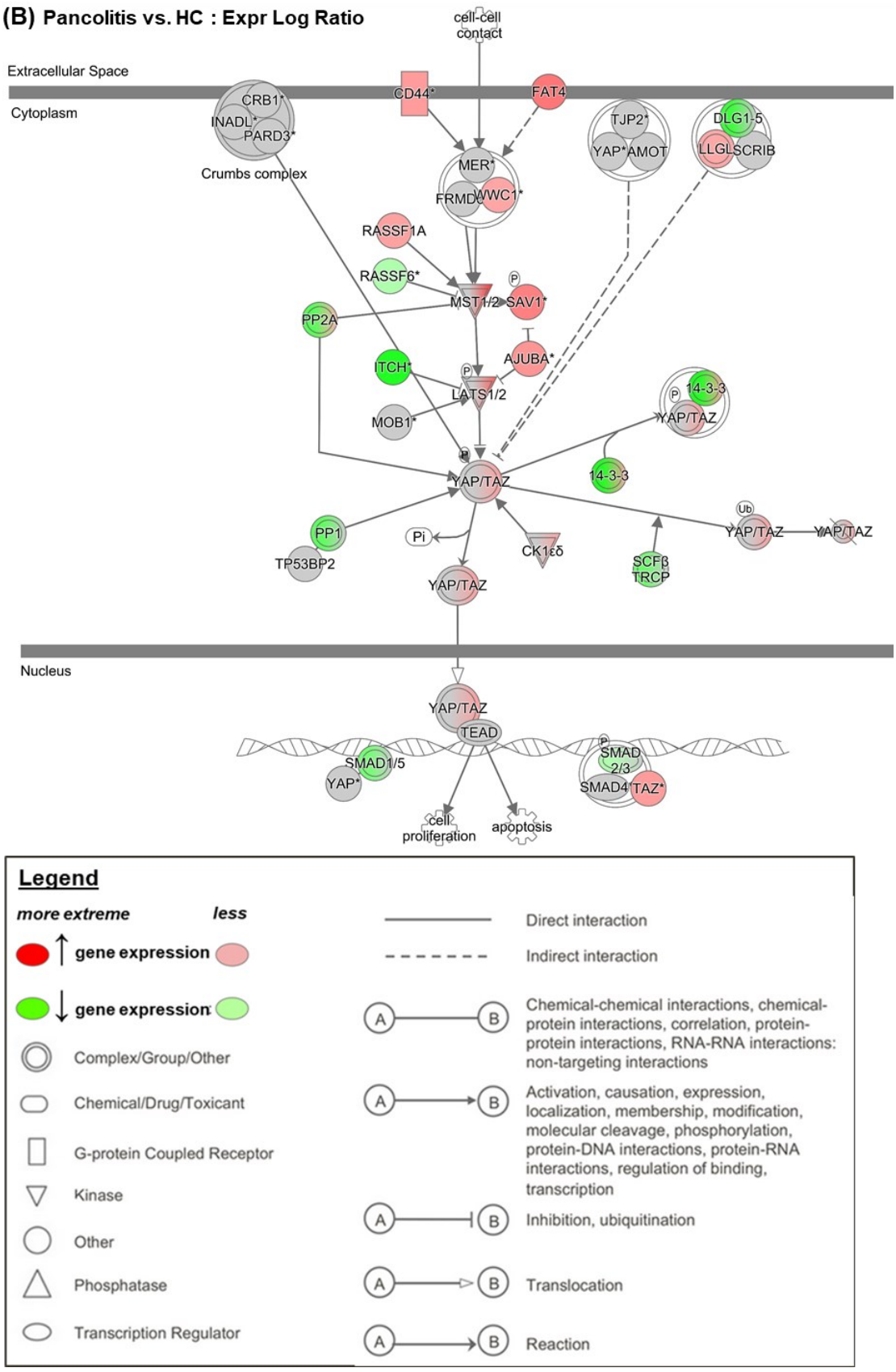
(B) Pancolitis vs. HC : Expr Log Ratio
cell-cell contact
Extracellular Space
Cytoplasm
CRB1*
INADL*
PARD3*
Crumbs complex
CD44*
FAT4
TJP2*
YAP*
AMOT
DLG1-5
LLGL
SCRIB
MER*
FRMD
WWC1*
RASSF1A
RASSF6*
MST1/2
SAV1*
PP2A
ITCH*
AJUBA*
LATS1/2
MOB1*
14-3-3
YAP/TAZ
PP1
TP53BP2
Pi
CK1εδ
SCFβ TRCP
Ub
YAP/TAZ
Nucleus
TEAD
SMAD1/5
YAP*
SMAD 2/3
SMAD4
TAZ*
cell proliferation
apoptosis
Legend
more extreme
less
gene expression
Complex/Group/Other
Chemical/Drug/Toxicant
G-protein Coupled Receptor
Kinase
Other
Phosphatase
Transcription Regulator
Direct interaction
Indirect interaction
Chemical-chemical interactions, chemical-protein interactions, correlation, protein-protein interactions, RNA-RNA interactions: non-targeting interactions
Activation, causation, expression, localization, membership, modification, molecular cleavage, phosphorylation, protein-DNA interactions, protein-RNA interactions, regulation of binding, transcription
Inhibition, ubiquitination
Translocation
Reaction

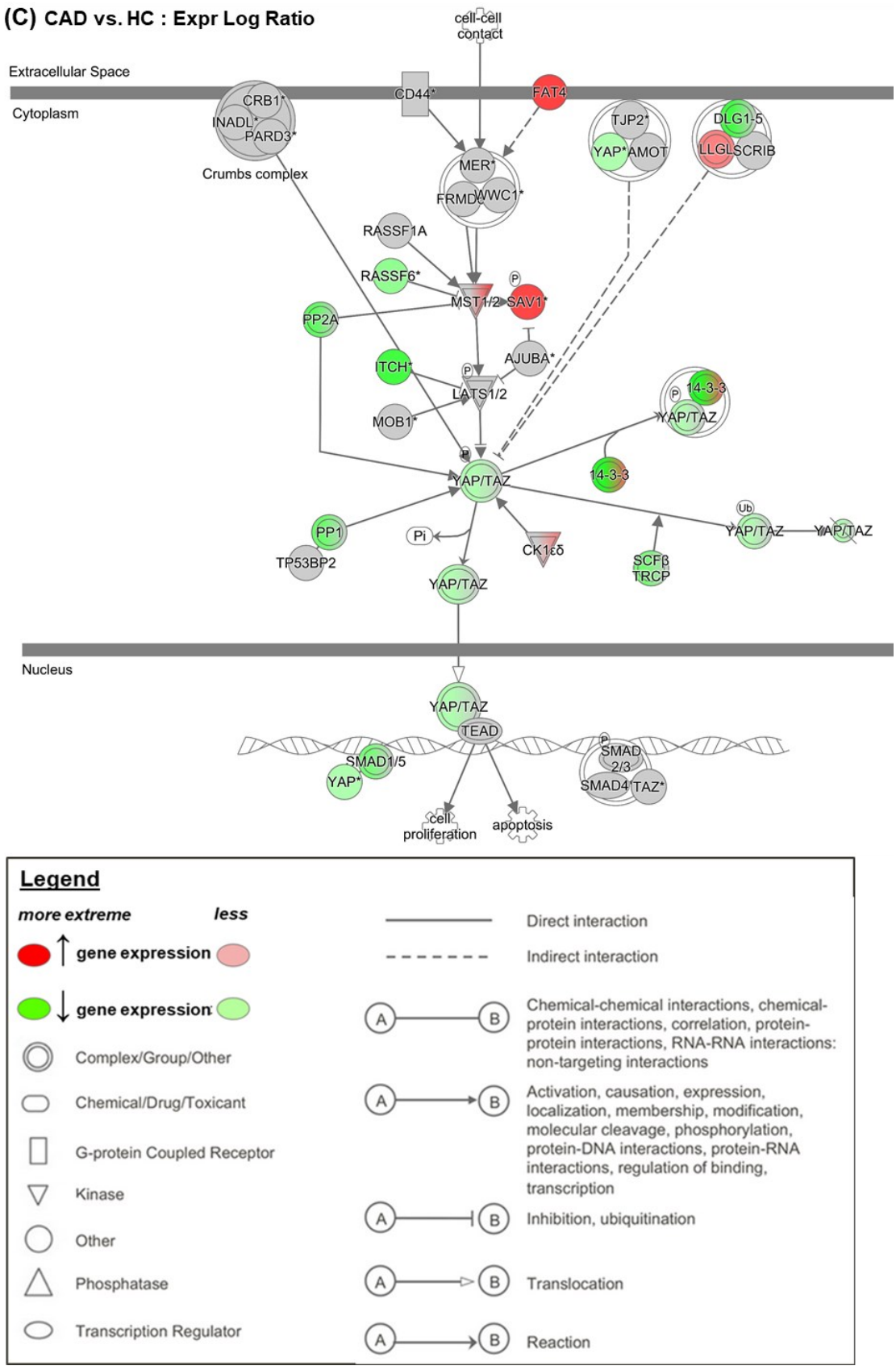
(C) CAD vs. HC : Expr Log Ratio
cell-cell contact
Extracellular Space
Cytoplasm
CRB1*
INADL*
PARD3*
Crumbs complex
CD44*
FAT4
TJP2*
YAP*
AMOT
DLG1-5
LLGL
SCRIB
MER*
FRMD
WWC1*
RASSF1A
RASSF6*
MST1/2
SAV1*
PP2A
ITCH*
AJUBA*
LATS1/2
MOB1*
14-3-3
YAP/TAZ
PP1
TP53BP2
Pi
CK1εδ
SCFβ TRCP
Ub
Nucleus
TEAD
SMAD1/5
YAP*
SMAD 2/3
SMAD4
TAZ*
cell proliferation
apoptosis
Legend
more extreme
less
gene expression
Complex/Group/Other
Chemical/Drug/Toxicant
G-protein Coupled Receptor
Kinase
Other
Phosphatase
Transcription Regulator
Direct interaction
Indirect interaction
Chemical-chemical interactions, chemical-protein interactions, correlation, protein-protein interactions, RNA-RNA interactions: non-targeting interactions
Activation, causation, expression, localization, membership, modification, molecular cleavage, phosphorylation, protein-DNA interactions, protein-RNA interactions, regulation of binding, transcription
Inhibition, ubiquitination
Translocation
Reaction

Appendix E. Comparison of Ephrin receptor pathway analyses conducted on UC-subtype DEGs.

Appendix E. Scheme of the Ephrin receptor pathway was overlaid with expression log ratios from the Left-sided colitis vs. HC datasets **(A)**, the Pancolitis vs. HC datasets **(B)**, and the CAD vs. HC datasets **(C)**. Colored molecules (red, green, grey) represent genes/proteins that appeared in the datasets. Canonical pathway analyses were completed with the IPA software. DEGs were distinguished by the combined application of FDR ($q < 0.001$) and fold change threshold ($|log2FC| > 0.75$).

(A) Left-sided colitis vs. HC : Expr Log Ratio

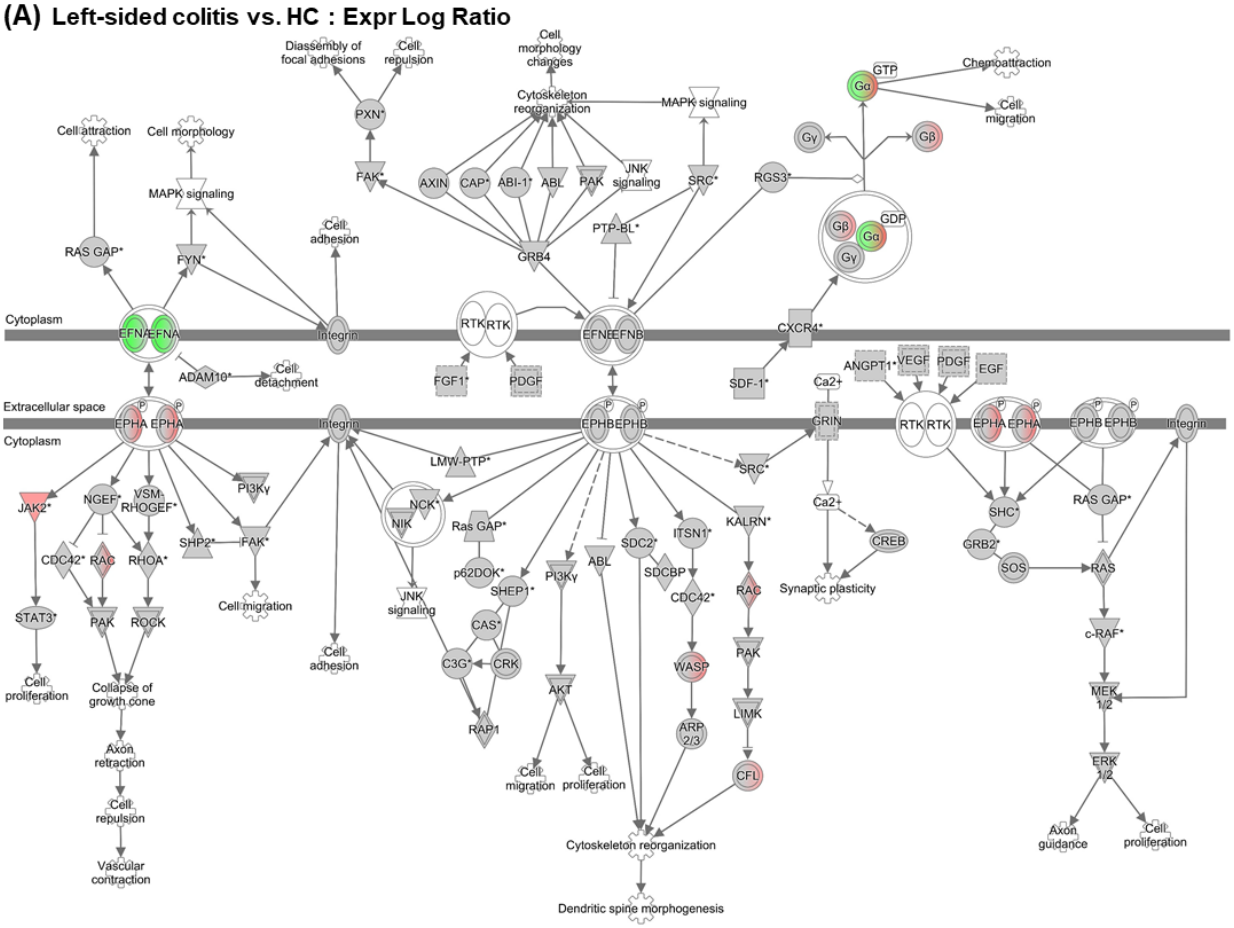

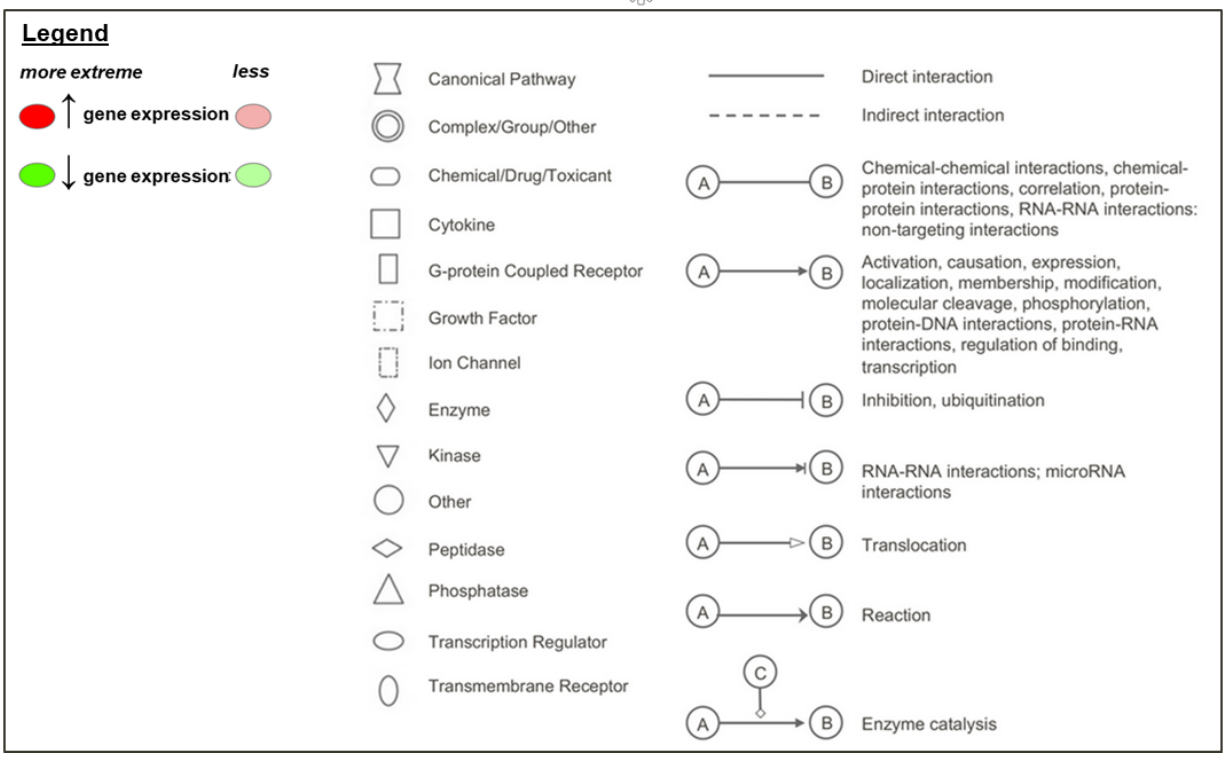

(B) Pancolitis vs. HC : Expr Log Ratio

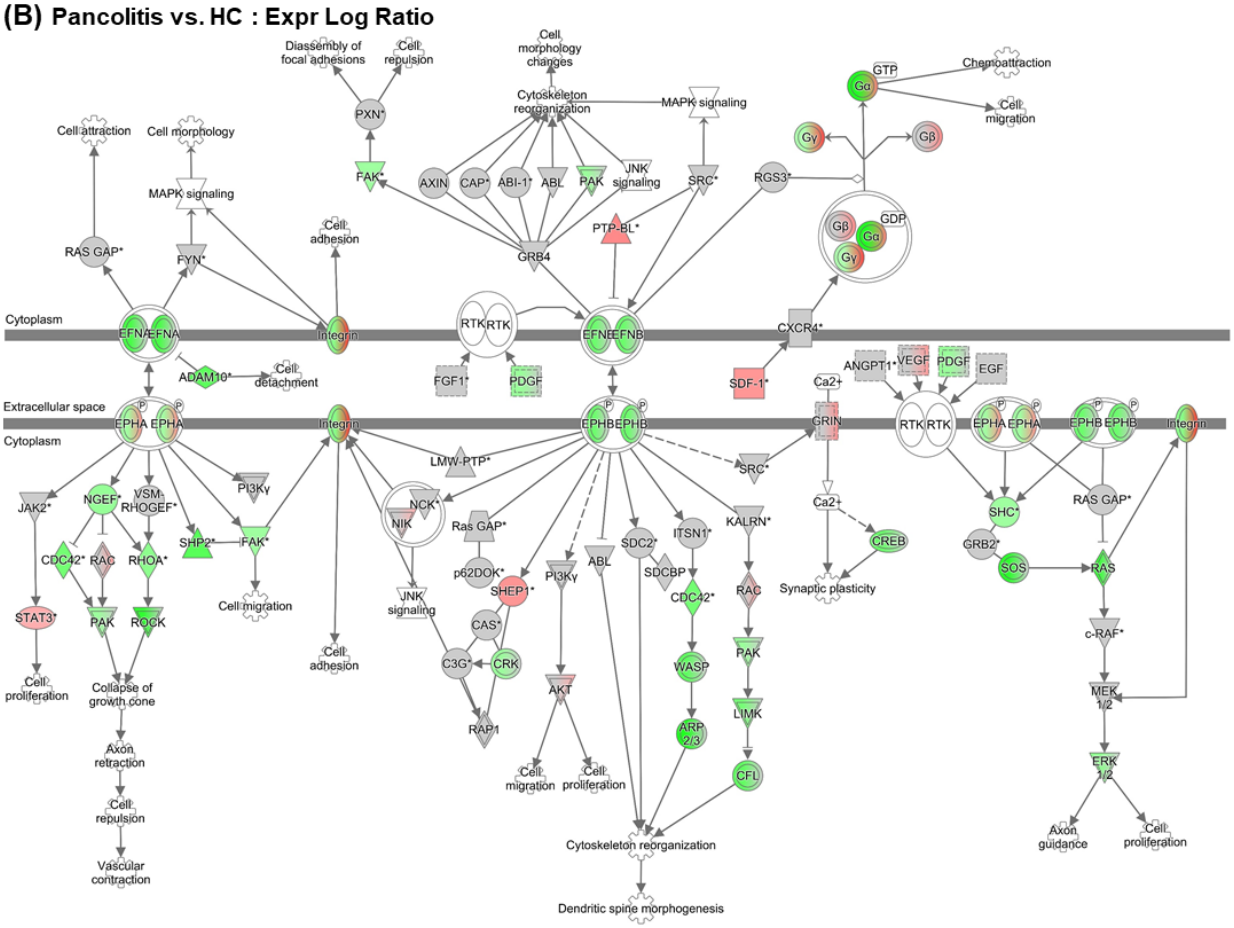

Legend

more extreme *less*

↑ gene expression

↓ gene expression

- Canonical Pathway
- Complex/Group/Other
- Chemical/Drug/Toxicant
- Cytokine
- G-protein Coupled Receptor
- Growth Factor
- Ion Channel
- Enzyme
- Kinase
- Other
- Peptidase
- Phosphatase
- Transcription Regulator
- Transmembrane Receptor

- Direct interaction
- Indirect interaction
- A — B: Chemical-chemical interactions, chemical-protein interactions, correlation, protein-protein interactions, RNA-RNA interactions: non-targeting interactions
- A → B: Activation, causation, expression, localization, membership, modification, molecular cleavage, phosphorylation, protein-DNA interactions, protein-RNA interactions, regulation of binding, transcription
- A ⊣ B: Inhibition, ubiquitination
- A → B: RNA-RNA interactions; microRNA interactions
- A → B: Translocation
- A → B: Reaction
- C, A → B: Enzyme catalysis

(C) CAD vs. HC : Expr Log Ratio

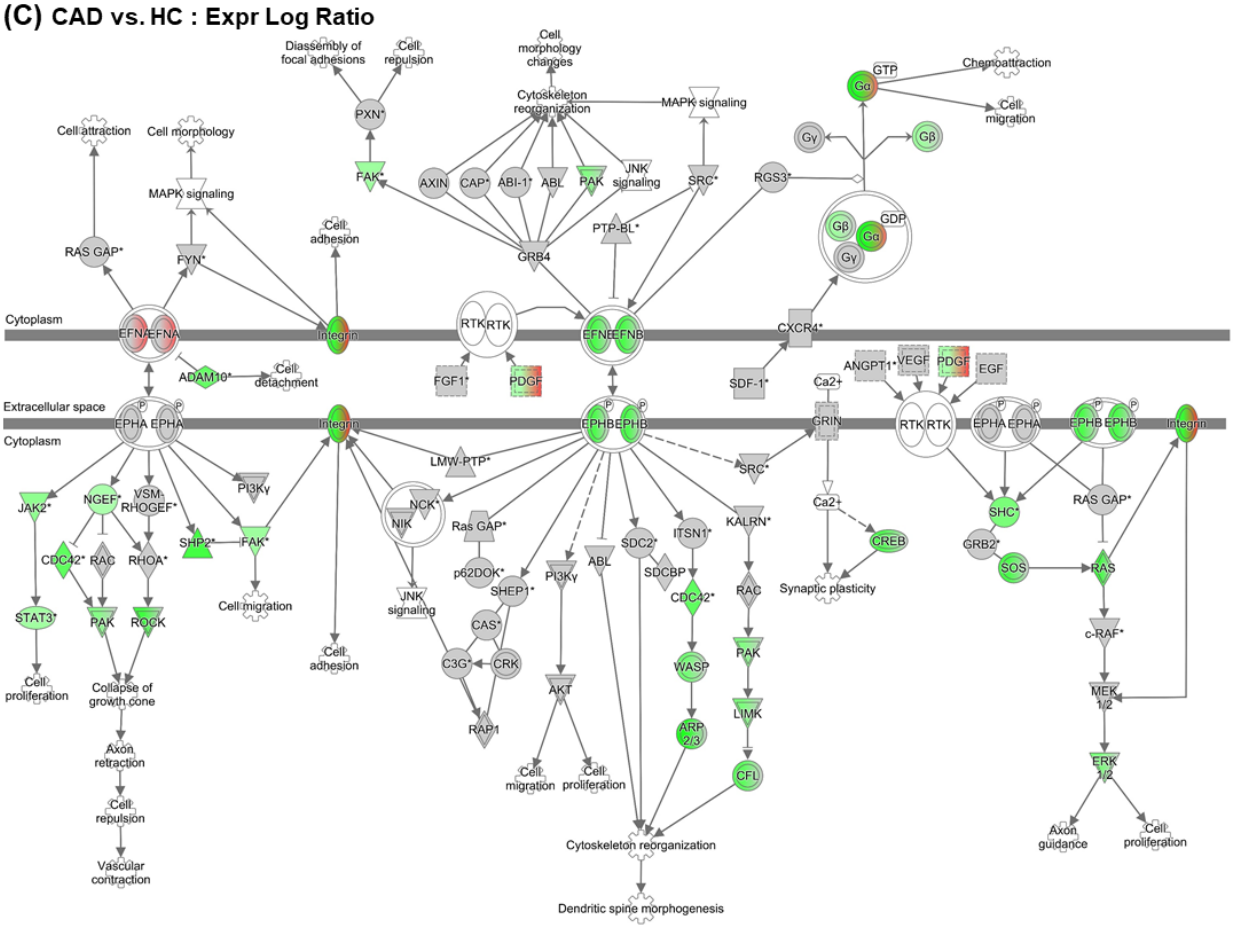

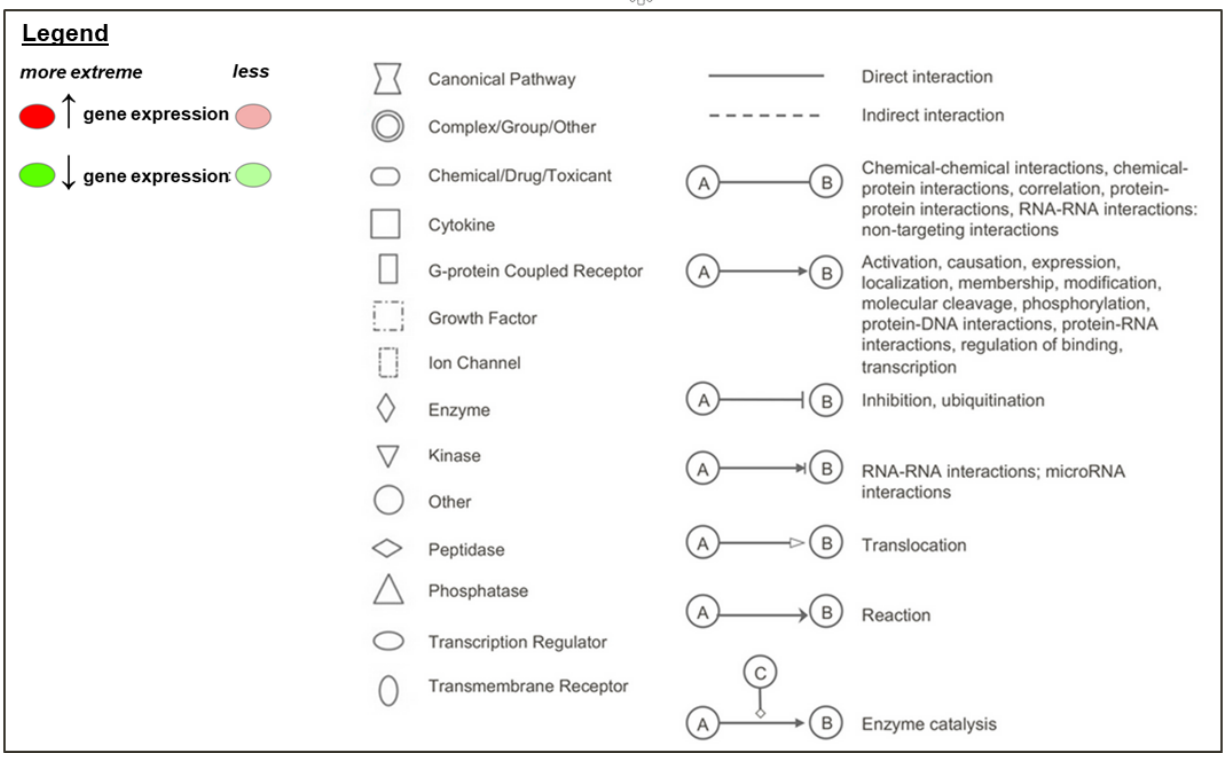

Appendix F. The shortest paths connecting genes situated at the intersection of Pancolitis network 15 and CAD network 1 to UC.

Appendix F. Shortest paths from the 13 focus molecules listed on **Table 2** to the disease *Ulcerative Colitis* were established using the IPA Path Explorer tool. The 13 focus molecules (highlighted in yellow) were used as the starting point for the generation of biological networks based on their connectivity as established in the Ingenuity Knowledge Base (IKB). Allowing for findings from experimentally observed/highly predicted confidence levels and direct/indirect interactions, the IPA Path Explorer tool built 88 shortest paths to connect focus molecules through a minimum of one IPA-derived intermediate molecules to the disease *Ulcerative Colitis*. All probable shortest paths by which the focus molecules were connected to the disease *Ulcerative Colitis* required at least one interconnecting gene product [i.e., none of the lines originating from any of the focus molecules (colored in light blue) connect directly to the disease *Ulcerative Colitis*]. For the majority of indirect connections, gene products CTNNB1 (β-catenin), CDH1 (E-Cadherin), and TNF (Tumor Necrosis Factor) exist as the IPA-derived intermediate molecules.

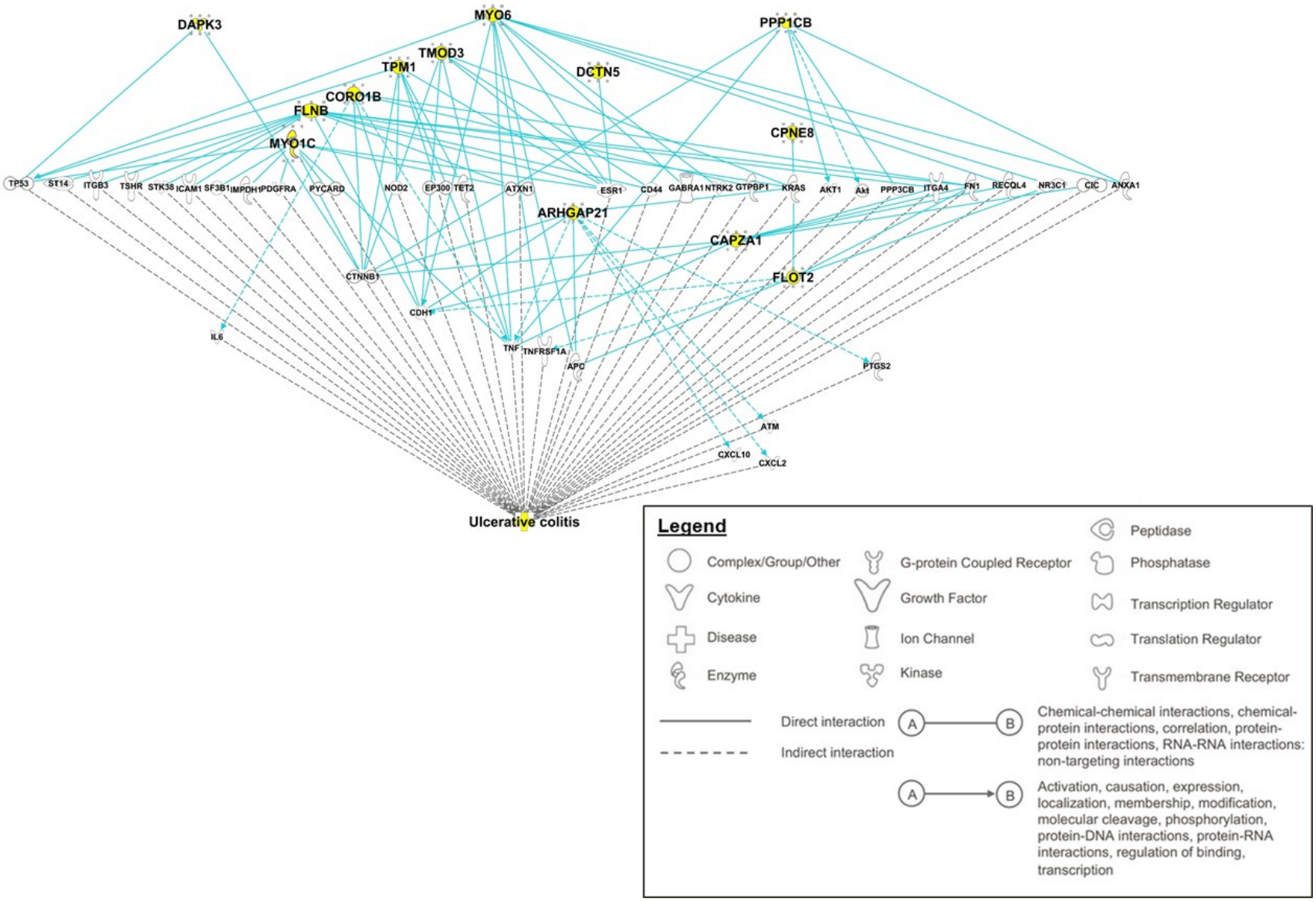
DAPK3
MYO6
PPP1CB
TMOD3
TPM1
DCTN5
CORO1B
FLNB
CPNE8
MYO1C
TP53
ST14
ITGB3
TSHR
STK38
ICAM1
SF3B1
IMPDH1
PDGFRA
PYCARD
NOD2
EP300
TET2
ATXN1
ESR1
CD44
GABRA1
NTRK2
GTPBP1
KRAS
AKT1
Akt
PPP3CB
ITGA4
FN1
RECQL4
NR3C1
CIC
ANXA1
ARHGAP21
CAPZA1
CTNNB1
FLOT2
CDH1
IL6
TNF
TNFRSF1A
APC
PTGS2
ATM
CXCL10
CXCL2
Ulcerative colitis
Legend
Complex/Group/Other
Cytokine
Disease
Enzyme
G-protein Coupled Receptor
Growth Factor
Ion Channel
Kinase
Peptidase
Phosphatase
Transcription Regulator
Translation Regulator
Transmembrane Receptor
Direct interaction
Indirect interaction
A
B
Chemical-chemical interactions, chemical-protein interactions, correlation, protein-protein interactions, RNA-RNA interactions: non-targeting interactions
Activation, causation, expression, localization, membership, modification, molecular cleavage, phosphorylation, protein-DNA interactions, protein-RNA interactions, regulation of binding, transcription